UNIVERSITÀ DEGLI STUDI DI PADOVA

Dipartimento dei Beni Culturali:
Archeologia, Storia dell'Arte, del Cinema e della Musica

SCUOLA DI DOTTORATO DI RICERCA IN:

Studio e Conservazione dei Beni Archeologici ed Architettonici
XXVII Ciclo

Evolution of ornamental vitreous materials in Italy from the Middle Bronze Age to the Iron Age: case studies from Lipari and from the Veneto region

DIRETTORE DELLA SCUOLA: Ch.mo Prof. Giuseppe Salemi
SUPERVISORE: Ch.mo Prof. Gianmario Molin

DOTTORANDO: Giulia Olmeda

CONTENTS

4. ANALYTICAL THECNIQUES

5. RESULTS

6. DISCUSSION

ABSTRACT

The research focused on the chemical and mineralogical study of ornamental vitreous materials belonging to different archaeological sites of south and north Italy, dated from the Middle Bronze Age to the Iron Age. Composition, texture and morphological characteristics of glass beads are investigated in order to shed light on the different types of raw materials used and on the evolution of the production techniques in the within the examined period.

The ornamental vitreous materials dated to the Bronze Age come from Lipari and Salina (Southern Italy), two islands strategically located in the Aeolian archipelago and characterized by important commercial trading with the Mediterranean area throughout the Bronze Age. The vitreous materials are composed by 66 beads of different color and typology from Lipari – Acropolis and Piazza Monfalcone cemetery – and Salina – Villaggio di Portella – dated between the Middle Bronze and the Final Bronze Ages. The Iron Age ornaments come from Padova (Piovego cemetery) and Villa di Villa (Cordignano, Treviso), two important contexts located in the North Eastern Italy. Both sites are positioned in the north – Adriatic area which played a very important role in the connection between the eastern Mediterranean area and continental Europe. Moreover, they are the first archaeometric data of Iron Age ornamental vitreous materials from North-East Italy. From the Piovego Necropolis cremation graves come 38 glass beads dated between the second half of the 6th century and the end of the 5th century B.C. The 8 ornaments from Villa di Villa site are very different for typologies and ages, covering a time span ranging from the Final Bronze Age to the Late Roman Age.

The ornaments were sampled from the bodies and the decorations to obtain 130 micro-samples of different kind of glass. The samples were incorporated in epoxy resin, surface-polished and analyzed by SEM-EDS and EPMA, whereas non – invasive X-Ray Diffraction was performed on the beads. Some samples were also studied by means of Single Crystal X-Ray Diffraction and Micro – Raman Spectroscopy to identify nano – crystalline inclusions.

The analyzed glasses from Lipari and Salina, dated from the Middle Bronze Age (MBA) to the Final Bronze Age (FBA), were obtained using two different fluxes: soda – rich plant ashes (HMG glasses) and mixed alkali plant ashes (LMHK glasses). The MBA samples from Lipari and Salina show a HMG composition, which is present in the whole Italian peninsula in that period. The only MBA1-2 glass is from Lipari Acropolis and it is a HMG amber glass colored

by a Fe-S complex produced in a reducing atmosphere. The MBA3 samples are all from Salina and show a HMG composition. They are mostly blue colored by Co associated to Cu even though a few amber glasses and one white glass are present. Different cobalt sources were hypothesized suggesting the use of different raw materials and, probable, provenance from different production centers. Interestingly, the only analyzed white glass seems to be the early presence in Italy of Ca antimonates to obtain an opaque white glass, while this technology is well known in the same period in Egypt.

The samples dated to the Final Bronze Age (FBA) are all from Lipari (Piazza Monfalcone cemetery and Acropolis) and belong to 2 compositional groups: 15 samples are HMG glasses while 50 are LMHK glasses, produced with mixed alkali ashes as flux. Additional 2 glasses have a particular high content of potash, like a subclass of LMHK glasses (LMHK –K class) identified in Northern Italy. The HMG glasses are mostly blue all colored by low amounts of copper, even though also a few amber and black glasses are present. The LMHK glasses are blue, colored by Cu (sometimes associated to Sn and/or Sb) or by Co associated to Cu, Ni and As, as found in the coeval cobalt blue North Italian glasses. Nine FBA LMHK white glasses from the decorations of the beads were also analyzed. They are opacified by silicates phases (Ca silicates with variable stoichiometry and/or Quartz) as attested in some coeval north Italian and European glasses. The presence of LMHK glasses in south Italy during the FBA is relevant because testify a circulation of these materials from north Italy, where is well known the local production of mixed alkali glasses, to south Italy. Morover, the persistence of HMG glasses, which are not attested in the Italian peninsula during the FBA, underline the importance of Lipari as trade center with the Aegean/Middle East area.

Conversely, all the Iron Age ornaments are LMG glasses, obtained using *natron* as flux, according to the few data of the coeval Italian glasses present in the literature. Only one sample from the Piovego Necropolis is a HMG glass, perfectly comparable with both typical Na – rich ashes glasses of the MBA3 – RBA and with those that still persist during the Early Iron Age. No mixed alkali glasses are present in the analyzed Iron Age samples, even if LMHK glasses have been found, although rarely, in the Early Iron Age materials, specifically in some beads from Golasecca (9^{th} century B.C.) and Bologna (8^{th} century B.C.). The typologies of the 8 Villa di Villa ornaments are variable but their chemical composition is perfectly comparable with coeval data in the literature for similar materials. Two of the three blue glass bracelets

unearthed in the site, have a particular composition with high contents of K_2O that at, has no comparison with coeval celtic arm rings to date.

Chemical composition in both Piovego Necropoli and Villa di Villa samples has a large variability depending on the color and opacity/transparency of the glass. Different materials and coloring techniques were identified: Ca antimonates are present in white and opaque pale blue glasses, Fe is the main chromophore in transparent yellow/amber glasses, while Pb antimonates are used to color and opacify the only analyzed opaque yellow glass from Villa di Villa. The blue color is poorly present and mostly with dark shades due to Co, while Cu – coloring glasses are extremely rare. The identified trace elements related to Co are not the same in all the samples suggesting the use of Co-colorant with different origins. High Fe and Mn amount, in two cases associated with high Pb in the glass matrix (PbO up to 20% wt), characterize some opaque black glasses. Several glasses exhibit a higher content of Al and Fe, although the ratio is variable, as described in the literature for some coeval materials.

The chemical composition and the morphology observed in the Iron Age ornaments reflect the variability of the materials: most of the samples has a heterogeneous texture with metallic and mineral inclusions due to unreacted raw materials and/or newly formed crystals, more similar to Bronze Age *glassy faience* than actual glasses.

An interesting aspect is the complete change of raw materials and production technologies during the transition from the Final Bronze to the Iron Age. The Iron Age glasses show a very high compositional variability, correlated to different raw materials used and to the wide range of production techniques adopted (in particular for the glasses coloring). This variability does not seem related to the different chronological phases of the ornaments, but in several cases shows a connection with the typology of the beads. The data in the literature for this chronological phase (half of the 6^{th} and the end of the 5^{th} century B.C.) and specific typology are numerically scarce and therefore, at present, is not possible to identify the production areas of the ornaments.

This study allows to clarify several aspects of glass production during the period from the Bronze to the Iron Ages, when the vitreous materials are extremely varied in composition, typology and, probably, origin.

RIASSUNTO

La presente ricerca è focalizzata sullo studio chimico e mineralogico di materiali vetrosi per ornamenti appartenenti a diversi siti archeologici del sud e del nord Italia e datati dal Bronzo Medio alla piena Età del Ferro. Le caratteristiche chimiche, tessiturali e mineralogiche dei materiali sono studiate al fine di investigare i diversi tipi di materie prime utilizzate e l'evoluzione delle tecniche di produzione nell'arco cronologico considerato.

I materiali vetrosi ornamentali risalenti all'Età del Bronzo provengono da Lipari e Salina, due isole situate nell'arcipelago eoliano e interessate da importanti traffici commerciali con l'area del Mediterraneo durante tutta l'Età del Bronzo. I materiali vetrosi sono composti da 66 vaghi di colore e tipologia diversa da Lipari -Acropoli e Necropoli di Piazza Monfalcone - e Salina - Villaggio di Portella – e datati tra il Bronzo Medio e il Bronzo Finale.

Gli ornamenti dell'Età del Ferro provengono da Padova (Necropoli del Piovego) e Villa di Villa (Cordignano, Treviso) due importanti contesti del Veneto. Entrambi i siti sono situati in prossimità dell'area nord adriatica, importante anello di collegamento tra l'area del Mediterraneo orientale e l'Europa continentale. Inoltre, le analisi di questi reperti costituiscono i primi dati archeometrici per reperti ornamentali in materiale vetroso provenienti dal Nord-Est Italia. Dalle tombe a cremazione della necropoli del Piovego di Padova provengono 38 vaghi databili tra la seconda metà del VI secolo e la fine del V secolo a.C. Gli 8 ornamenti dal sito di Villa di Villa, invece, sono molto diversi per tipologia ed età, e coprono un arco temporale che compreso tra l'età del Bronzo finale e la tarda Età Romana.

Gli ornamenti sono stati prelevati sia dai corpi che dalle decorazioni dei vaghi, ove possibile, e sono stati micro campionati 130 tipi diversi di vetro. I campioni sono stati incorporati in resina epossidica, lucidati, grafitati e analizzati mediante SEM-EDS e EPMA, mentre l'analisi in diffrazione di raggi X è stata eseguita direttamente sui vaghi in maniera non invasiva. Alcuni campioni sono stati anche studiati mediante diffrazione di raggi X a cristallo singolo e spettroscopia micro Raman per identificare la natura delle inclusioni cristalline disperse nella matrice vetrosa.

I materiali vetrosi da Lipari e Salina, datati dal Bronzo Medio (BM) al Bronzo finale (BF), sono stati prodotti utilizzando due diversi fondenti: ceneri di piante sodiche (vetri HMG) e ceneri di piante ad alcali misti (vetri LMHK). I campioni di BM provenienti da Lipari e Salina

presentano una composizione HMG, presente in tutta la penisola italiana in quel periodo. L'unico vetro di BM1-2 proviene dall'Acropoli di Lipari ed è un vetro color ambra di composizione HMG colorato molto probabilmente dal complesso Fe-S prodotto in atmosfera riducente. I campioni di BM3 sono tutti da Salina e hanno una composizione HMG. Sono per lo più di colore blu colorati da Co associato a Cu. Oltre ai vetri blu sono presenti anche pochi esemplari di colore ambra e un vetro bianco. Diverse fonti di cobalto sembrano essere state impiegate nella produzione dei vetri blu da Salina, suggerendo l'uso di materie prime diverse e, probabilmente, la provenienza da diversi centri di produzione. È interessante notare che l'unico vetro bianco analizzato di BM3 sembra costituire la prima evidenza in Italia dell'uso di antimoniati Ca per ottenere un vetro bianco opaco, mentre questa tecnologia è ben nota nello stesso periodo in Egitto.

I campioni risalenti al Bronzo finale (BF) sono tutti da Lipari (Necropoli e Acropoli di Piazza Monfalcone) e appartengono a due gruppi composizionali: 15 campioni sono vetri HMG mentre 50 sono di tipo LMHK. Due vetri blu hanno una particolare composizione ad alto contenuto di potassio, come già identificato in una sottoclasse di vetri LMHK (LMHK - classe K) provenienti dal nord Italia. I vetri HMG di BF sono per lo più blu colorati da piccole quantità di rame, ma sono presenti anche vetri ambra e un vetro nero. I vetri LMHK sono blu, colorati da Cu (talvolta associato a Sn e / o Sb) o Co associato a Cu, Ni e As, come nei vetri blu al cobalto dal Nord Italia. Nove vetri bianchi LMHK di BF dalle decorazioni dei vaghi sono stati analizzati. Essi sono opacizzati da fasi silicatiche (silicati Ca con stechiometria variabile e / o quarzo), come attestato in alcuni vetri bianchi nord italiani ed europei. La presenza di vetri a composizione LMHK nel sud Italia durante il BF è rilevante perché testimonia una circolazione di questi materiali dal nord Italia, dove è ben nota la produzione locale di vetri ad alcali misti, al Sud Italia. Inoltre, la persistenza di vetri HMG, che non sono attestati nella penisola italiana nel corso del BF, sottolinea l'importanza di Lipari quale luogo di circolazione di materiali provenienti dall'area Egea / Medio Orientale.

Tutti gli ornamenti della piena età del Ferro, invece, sono di tipo LMG, ottenuti utilizzando natron come fondente. Solo un campione dalla necropoli del Piovego è di tipo HMG, ed ha composizione perfettamente comparabile sia coi vetri HMG di BM3 - BR sia con quelli che ancora persistono durante la prima età del ferro. Non sono invece presenti vetri ad alcali misti che in alcuni casi invece persistono, anche se raramente, nei materiali della prima età del Ferro,

in particolare in alcuni vaghi della cultura di Golasecca (IX secolo a.C.) e da Bologna (VIII secolo a.C.).

I vetri di Villa di Villa, aventi tipologie ed età molto differenti fra loro, hanno composizioni comparabili con i dati coevi di materiali simili presenti in letteratura. È interessante notare che due dei tre bracciali di vetro blu rinvenuti nel sito, hanno una particolare composizione ad alto contenuto di K_2O che non trova invece riscontro, almeno per il momento, con i coevi dati disponibili per i bracciali celtici.

La composizione chimica dei materiali dal Piovego e da Villa di Villa ha una grande variabilità in funzione del colore e dell'opacità / trasparenza del vetro. Materiali e tecniche di colorazione differenti sono state identificate: gli antimoniati di Ca sono presenti nei vetri turchesi e bianco opaco; il Fe è l'elemento cromoforo principale nei vetri trasparenti giallo / ambra, mentre gli antimoniati di Pb vengono utilizzati per colorare e opacizzare l'unico vetro giallo opaco analizzato, proveniente da Villa di Villa. Il colore blu è poco presente e nella maggior parte dei materiali con tonalità scure per la presenza di Co, mentre i vetri colorati al Cu sono estremamente rari. Gli elementi associati al Co non sono gli stessi in tutti i campioni suggerendo l'uso di fonti di cobalto di diversa origine e, quindi, una provenienza diversa dei materiali. Alti tenori di Fe e Mn, in due casi associati ad alto Pb nella matrice vetrosa (PbO fino al 20% in peso), caratterizzano alcuni vetri blu e marrone opaco. Diversi vetri presentano un alto contenuto di Al e Fe, anche se il rapporto è variabile, come riscontrato in letteratura per alcuni materiali coevi.

La variabilità chimica e morfologica osservata negli ornamenti dell'età del Ferro riflettere le diverse tessiture dei materiali: la maggior parte dei campioni ha una tessitura eterogenea con inclusioni metalliche e minerali dovute a relitti di materie prime non reagite e / o a cristalli di nuova formazione, e più paragonabili a *faïence* dell'età del Bronzo che a vetri veri e propri.

Un aspetto interessante è il cambiamento completo delle materie prime e tecnologie di produzione durante il passaggio dal Bronzo Finale all'età del Ferro. I vetri dell'età del Ferro mostrano una elevata variabilità composizionale, correlata a diverse materie prime utilizzate e alla vasta gamma di tecniche di produzione adottate (in particolare per la colorazione dei vetri). Questa variabilità non sembra correlata alle diverse fasi cronologiche degli ornamenti, ma in molti casi alla diversa tipologia dei vaghi. I dati in letteratura per questa specifica fase cronologica (metà del VI e fine del V secolo a.C.) e tipologie di materiali sono numericamente

scarsi e quindi, allo stato attuale, non è possibile identificare le zone di produzione e/o provenienza dei reperti. Tuttavia, questa ricerca permette di chiarire alcuni aspetti della produzione del vetro nel periodo compreso tra l'età del Bronzo Medio e la piena età del Ferro, in cui i materiali vetrosi sono evidentemente caratterizzati da una estrema variabilità in termini di composizione, tipologia e, probabilmente, origine.

CHAPTER 1

INTRODUCTION

The thesis was carried on thanks to the co – supervision of Dr. Ivana Angelini (Geosciences Department, Padova University) and Prof. Michele Cupitò (Department of Cultural Heritage, Padova University).

1.1 Project origin

The research focused on the chemical and mineralogical study of ornamental vitreous materials belonging to different archaeological sites of southern and northern Italy, and dated from the Middle Bronze Age to the Iron Age. A large number of archaeometric studies on Italian vitreous materials have been carried out over the years, covering periods ranging from the Early Bronze Age to the Late Iron Age (Angelini et al. 2004, 2005, 2006, 2010a and b, 2011; Arletti et al. 2010a, 2011a, 2012; Artioli et al. 2008; Biavati et al. 1989; Brill 1992; Henderson 1988; Santopadre e Verità 2000; Tite et al. 2008a, b and c; Towle et al. 2001). The results show that there are different compositional classes of glass, sometimes with peculiar textures, associated with specific ages, typologies and provenances. In the transition between the Final Bronze Age to the Iron Age, variations in typology and important chemico-compositional changes occurred in the production of glass (Angelini et al. 2011; Arletti et al. 2010, 2011a; Artioli et al. 2013; Polla et al. 2011; Tite et al. 2008), both associated with the main trade networks of the different periods. In this light, the selected finds belong to two archaeological contexts, differing in age and geographic position:

1) Lipari (Acropolis and Piazza Monfalcone cemetery) and Salina (Villaggio di Portella), Southern Italy. They are important sites characterized by a widespread trade network with the entire Mediterranean throughout the Bronze Age and, therefore, a significant location to study the circulation routes of the different glass productions. The project is part of an earlier study started in 2006 in collaboration with the Geosciences Department of Padova University (Dr. Ivana Angelini and Prof. Gilberto Artioli), the Soprintendenza of Trento (Paolo Bellintani) and the Istituto Italiano di Preistoria e Protostoria. The studied materials cover a chronological range from the Middle Bronze Age 1-2 to the Final Bronze Age 2-3.

2) Padova (Piovego cemetery) and Villa di Villa (Villa di Villa site, Cordigano, Treviso), North-Eastern Italy. The sites are both located in the Veneto region and more generally in the north-Adriatic area, which plays a very important role in the connection between the eastern Mediterranean and continental Europe, because of its geographic location. Furthermore, the analyzed finds represent the first archaeometrical data on Iron Age ornaments from North-East Italy. The project has been developed in cooperation with the Cultural Heritage Department of Padova University (Prof. Giovanni Leonardi, Prof. Michele Cupitò, Dr. Benedetta Prosdocimi, Dr. Stefano Boaro).

The glass beads form the Piovego cemetery of Padova are dated to the second half of the 6th century and the end of the 5th century B.C. (second Iron Age). The ornaments from Villa di Villa are very different both in typologies and ages, covering a wide chronological range from the Final Bronze Age to the Late Roman Age.

1.1 The aim of the research

Composition, texture and morphological characteristics of vitreous material ornaments are investigated in order to shed light on the different types of raw materials used and on the evolution of the production techniques within the examined period, especially for the production of ornaments. In particular, for Lipari and Salina the relationship with coeval Mediterranean and Near Eastern glass productions will be considered, in order to evaluate the trade routes according to the ornaments' circulation. Furthermore, southern Italy materials will be compared with those of northern Italy in order to evaluate any possible spreading of the production techniques and/or objects in the Italian peninsula. While for the Bronze Age there are numerous and detailed archaeometric studies on Italian vitreous materials, for the Iron Age data are more fragmentary. In this line, the study of the vitreous materials from the Veneto region will be interesting to define any possible new compositional classes with respect to the Bronze Age tradition, and to study the evolution of materials and production techniques in the transitional phase from the Final Bronze Age to the Iron Age. Comparisons between Italian Iron Age materials and coeval European glass productions will also be considered.

The analyses' results are explained in Chapter 5, while Chapter 6 presents the discussion and the comparison with coeval Italian and European/Mediterranean glass productions.

CHAPTER 2

ARCHAEOLOGICAL CONTEXTS

The materials analyzed in this research belong to two well distinct chronological phases of the Italian protohistory – the period between the Middle Bronze Age and the Final Bronze Age on one hand and the second Iron Age on the other hand – and to important archaeological sites located in two different parts of Italy (Fig. 2.1). The finds dated to the Bronze Age come from Lipari and Salina, two islands of the Aeolian archipelago (Sicily region, southern Italy). The Iron Age ornaments come from Padova and Villa di Villa di Cordignano, near Treviso, both in the Veneto region (north-eastern Italy).

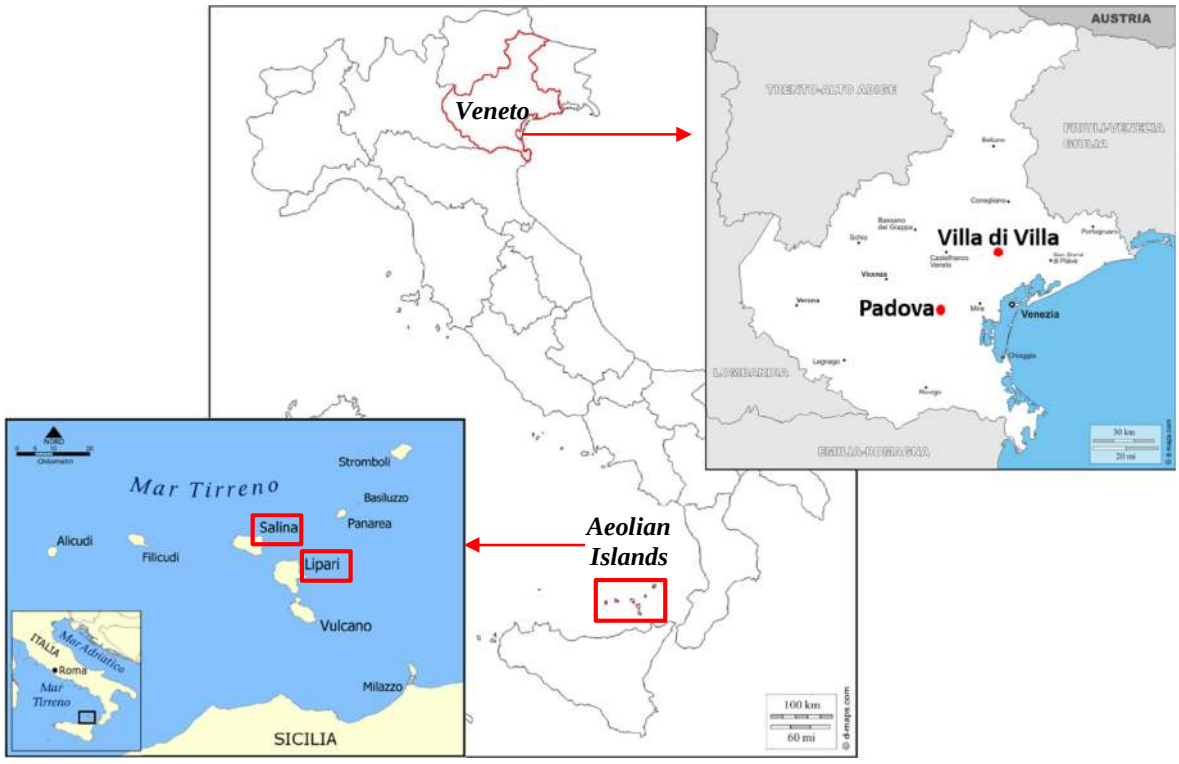

Fig. 2.1: Map of Italy. The two areas of provenance of the studies materials are highlighted in red. Detailed maps of the Veneto region and the Aeolian Islands are also reported.

2.1 Lipari and Salina

Lipari and Salina are two islands in the Aeolian archipelago located in the lower Tirreno See in front of the north-east point of Sicily. They are the first and the second largest islands in the archipelago, respectively, followed by other 5 minor islands (Panarea, Alicudi, Filicudi, Stromboli and Vulcano). The knowledge on the prehistory and protohistory of these islands is due to the exceptional research activities carried out since the half of the 20th century by Luigi Bernabò Brea, one of the most important Italian archaeologists of all time.

In the Aeolian Islands the first phases of the Middle Bronze Age (MBA 1-2) correspond to the second phase of the Capo Graziano culture (17th-15th century B.C.). The name of this culture derives from the Montagnola of Capo Graziano site, in the island of Filicudi. The last phase of the Middle Bronze Age (MBA3) corresponds to the Milazzese culture (14th century B.C.) from the name of a promontory in the nearby Panarea Island, where a site related to this period was identified and excavated. The excavations of the Aeolian Islands highlighted the presence of archaeological evidences related to the Subapennine culture, typical of the Recent Bronze Age (RBA, end of 14th – first half 12th century B.C.) of continental Italy, above the levels of the Milazzese culture; traces of this archaeological aspect, which in the Aeolian Islands is called Ausonio I, also appeared in north-eastern Sicily. This cultural, and probably ethnic, changes correspond to what is reported by the literature sources – Thucydides, Dionysius of Halicarnassus, Diodorus Siculus – about one or more invasions of the Aeolian Islands and Sicily by populations coming from the Italian peninsula – the Ausones, led by King Auson - around the 13th century B.C. According to a legend told by Diodorus Siculus, the son of Auson was Liparus, from whom the Lipari Islands derive their name. The Final Bronze Age (FBA, second half 12th - 10th century B.C.) corresponds in the Aeolian Islands to the Ausonio II culture.

The correlation between the Aeolian phases and the Italian sequence of the Bronze Age are based on the research of Peroni and coauthors (Carancini et al. 1996) while absolute datings of each phase are based on the research of Pacciarelli 2001.

Salina Island – Village of Portella

The glass beads from Salina Island analyzed in this research belong to Villaggio di Portella, a typical site of the Milazzese culture, and are dated to MBA3. The village, discovered in 1955 in Portella, on the eastern coast of the island, was excavated by Luigi Bernabò Brea. It was located in proximity of the sea, surrounded by steep rock faces in an extremely difficult position to reach. The village was composed by 25 circular huts composed of a single space with dry stone walls and perishable material covering. The huts were destroyed by a fire. At present, the village of Portella is an archaeological park open to the public.

The glass beads analyzed all come from the site's *Capanna F* (Fig. 1a), a hut located in the northern part of the settlement, near another similar structure, *Capanna F1* (Fig. 1b); however, this hut seems to date earlier than *Capanna F*. The unearthed finds are composed by several Milazzese culture vessels, stones tools and glass and cornelian ornaments (see below); interestingly, there are also some Apennine and Mycenaean pottery fragments (Bernabò Brea et al. 1968). In fact, the Milazzese culture shows the highest concentration of Mycenaean evidence together with typical aspects of the eastern Mediterranean, particularly Cyprus.

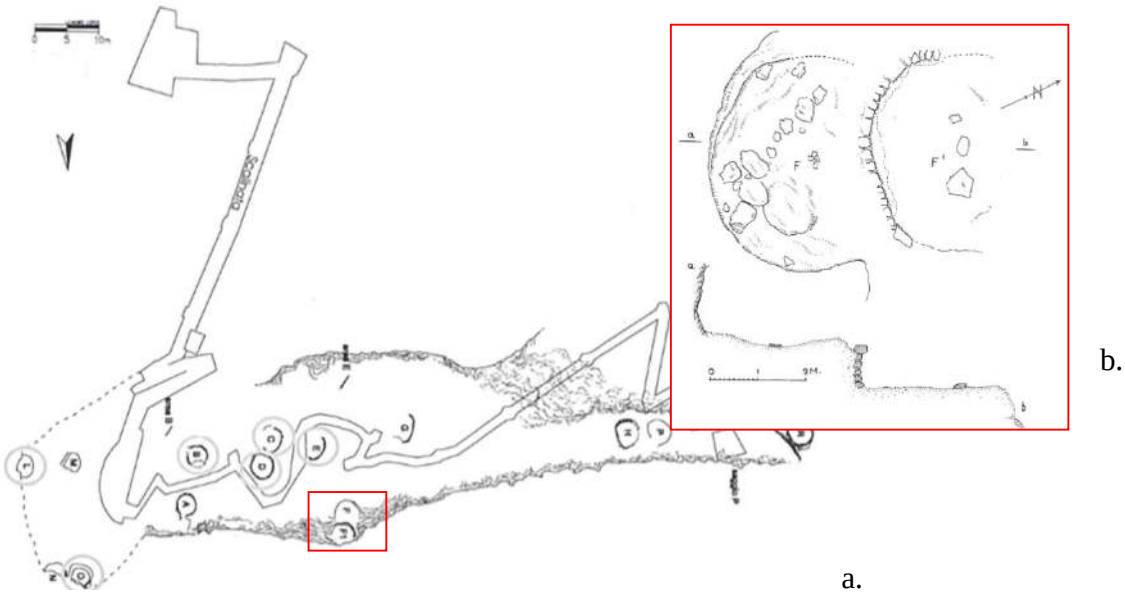

b.

a.

Fig. 1. a. Salina – Villaggio di Portella (from from Martinelli 2005). b. detail of Capanna F and F1 (from Bernabò Brea et al. 1968).

Lipari Island – Acropolis Village and cemetery of Piazza Monfalcone

The materials from Lipari analyzed in this work come from different settlement levels of the Acropolis, attributed to Capo Graziano, Ausonio I and Ausonio II phases – dated to the MBA 1-2, RBA and FBA , respectively–, and from the Ausonio II cemetery of Piazza Monfalcone – dated to the FBA.

Lipari – Acropolis Village

The Acropolis of Lipari Island was excavated by Luigi Bernabò Brea, in different steps, from 1950 to 1970. It was a natural fortress in a difficult position to reach and not particularly large, about 31,000 m^2, oval-shaped. The Bronze Age settlement located in this area was characterized by numerous huts with different shapes according to the various phases – from circular to oval and to sub-quadrangular – and a single fireside inside. They were built with wood and the floor, made of stones or gravel covered by clay, was at a lower level with respect to the soil. The village, developed without interruption from the Capo Graziano phase (MBA1-2) to the Ausonio II phase (FBA), was destroyed by a fire (Bernabò Brea 1958; Bernabò Brea et al. 1980).

The four glass beads analyzed from the Lipari Acropolis settlement come from structures belonging to different levels; in particular (fig. 2): Capanna δ XXI (Capo Graziano culture, MBA 1-2, 17th-15th century B.C.); Capanna O grave III (Ausonio I culture, RBA, end of 14th-first half 12th century B.C); Capanna α VII and Capanna β V (Ausonio II culture, FBA 2-3, 11th-10th century B.C.

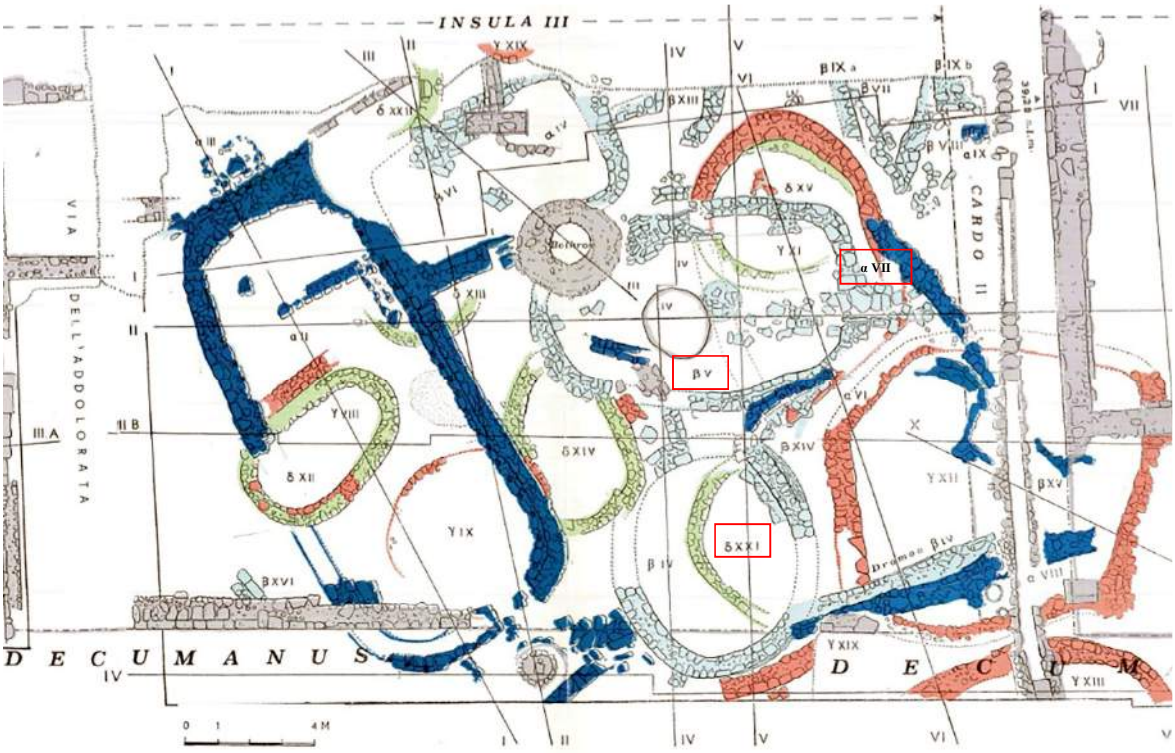

Fig. 2: Plan of the Acropolis excavations (from Bernabò Brea et al. 1980). The red squares show the settlement of origin of the beads analyzed in this work.

Lipari – Piazza Monfalcone cemetery

The Piazza Monfalcone cemetery was discovered in 1954 and the excavations, direct by Luigi Bernabò Brea, unearthed about fifty graves. The cemetery is dated to the initial phase of the Ausonio II, corresponding to the FBA 1-2 phase of peninsular chronological sequence, corresponding to the second half of the 12th-11th century B.C. (Bernabò Brea et al. 1960). Some graves, generally the most ancient ones, are *enchytrismos* graves, with the skeleton crouched into a *pithos* lying horizontally, similarly to other graves of the Middle Bronze Age (Bernabò Brea 1958) and often characterized by rich grave goods. The others are cremation graves, with the bones ashes inside a *situla*, lying horizontally and closed by a large stone (Bernabò Brea 1958; Bernabò Brea et al 1960).

The 53 glass beads selected from the Piazza Monfalcone cemetery belong to graves 18 and 31 (fig. 3). Some beads exhibited at the Archaeological Museum of Lipari and analyzed in this work are indicated as belonging to grave 12. However, it does not correspond to the excavation report (Bernabò Brea et al. 1960). On the contrary, these beads could possibly be a part of the goods of grave 18 (personal communication by P. Bellintani).

Grave 18 is an *enchytrismos* grave with a *pithos* lying down with the opening oriented to the East. A bronze fibula, a bronze rod, numerous vitreous material beads (see Ch. 3.2.1) and three amber beads compose the grave goods.

Grave 31 is an *enchytrismos* grave with a big *pithos* (detail in the red square, fig. 3) horizontally lying with the opening oriented to the East. The grave goods of this inhumation are particularly rich and composed, above all, by numerous ornaments. Among them: a bottle, with spheroidal body and cylindrical neck with flat rim and vertical handle, from body to rim and a chestnut polished paste; two armrings in thick cylindrical gold rod with hooked ends; a small bronze dagger with flat handle melted with the blade, shrinking at the center and widening on the end, with a slightly curved pierced edge, the handle is rather thicker than the blade; six clasps or perhaps ornaments from a large belt, composed by a central ring with a cross, with an oval ring clasp on one end, and with a T clasp on the other; two large bronze brooches with one rod, bent in a large 8 shape on one end; a quadrangular rod brooch with 6-spoke wheel pinhead, broken in three fragments; a cylinder formed by a spiral winding of a thin bronze thread; a fibula with an elongated lowered arch, formed by a bronze band tapered on the ends; two bronze band

digital rings, with loose ends; a digital ring composed of four spiral windings of a thin bronze thread; an earring formed by an incomplete hoop in thin bronze thread; nineteen big amber beads, numerous necklace beads of different dimensions and materials (vitreous material, amber, rock crystal, stones, bronze). Focusing on the glass beads, they are 36 large beads and about 600 small annular beads mostly blue-colored (with different shades). The glass beads were assembled in a copper filament that probably wrapped the arms and the legs of the dead (Bernabò Brea et al. 1960).

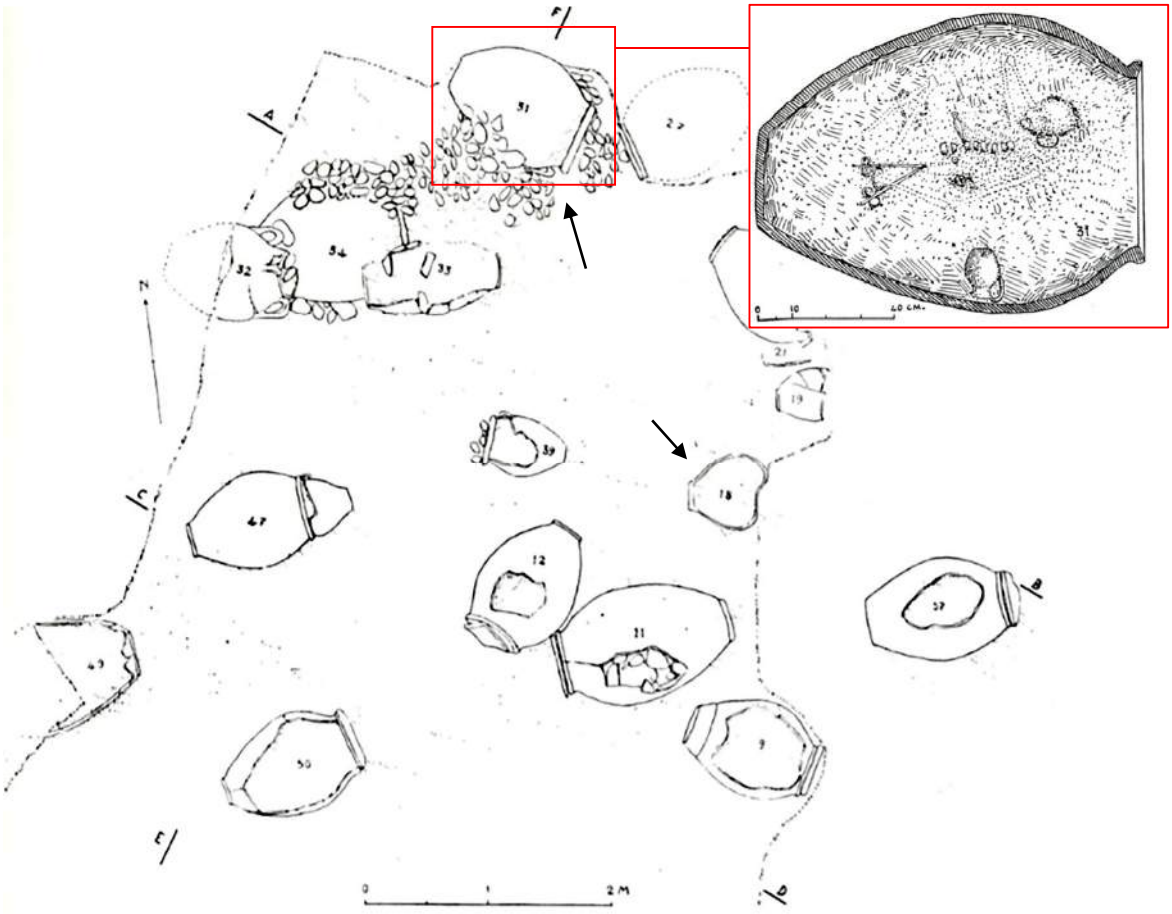

Fig. 3: Plan of the Piazza Monfalcone cemetery – Ausonio phase. Black arrows indicate graves 18 and 31 from which come the analyzed finds; the red square reports a detail of grave 31 (from Bernabò Brea et al. 1960).

2.2 Piovego Cemetery

In the first half of the 6th century B.C. the protourban center of Padova, founded between the end of the 9th and the beginning of the 8th century B.C., was affected by important changes: as other protourban Veneto centers, it developed a urban structure and became a city-state, acquiring an important role in the relationship with the Hallstatt culture and Greek traders in the Adriatic See.

A consequence of this transformation was the reorganization of spaces by building new orthogonal streets and canals together with the new adjustment of the funerary area. In this light, the foundation of the new large Piovego cemetery was particularly significant (Fig. 2.2.1, red circle).

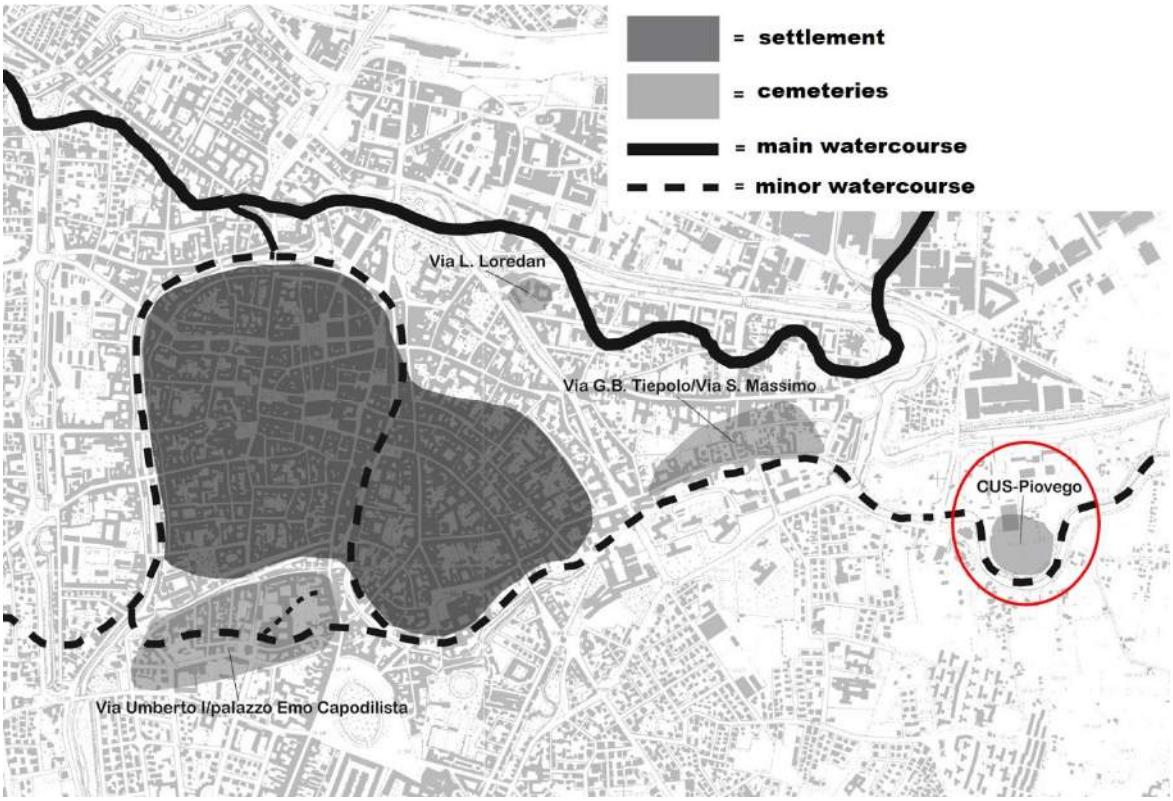

Fig. 2.2.1: Map of the pre – Roman Padova center. In the red circle, the Piovego cemetery is reported (image courtesy of Prof. Michele Cupitò, University of Padova).

The Piovego cemetery was excavated between 1975-77 and 1986-89 by the Institute of Archaeology of the Padova University, under the direction of Loredana Capuis and Elena di Filippo Balestrazzi, followed by Giovanni Leonardi. It is located in the eastern periphery of the pre-Roman center of Padova, between the Roncaiette watercourse (the ancient *Meduacus*/Brenta river) and the medieval Piovego canal. The cemetery is perfectly aligned with other eastern protohistoric funerary areas of Padova (via Tiepolo/via San Massimo and via Ognissanti) all located along the northern bank of the ancient *Meduacus/*Brenta river (Fig. 2.2.1). Two cemeteries were also found in via Loredan and via Umberto I/Palazzo Emo Capodilista, located at north and south of the centre of Padova, respectively (Fig. 2.2.1).

The cemetery was characterized by bi-ritualism but cremation – with graves in circular pits with wooden walls and in large storage vessels (so-called "dolii", fig. 2.2.2) – was predominant with respect to inhumations – with graves in simple pits. Cremation graves usually had grave goods – very rich in a number of cases – composed by pottery and bronze vessels; bronze, iron, gold, amber, coral and glass ornaments; bronze and iron tools and, rarely, iron weapons; inhumations normally had no grave goods. As it often happened in Iron Age cemeteries in the Veneto region, horses were buried and an exceptional double burial with a man and a horse was found. About 4,000 m^2 of the Piovego cemetery were excavated, unearthing 150 cremation graves, 30 inhumation graves, 6 horses graves; however, the total number of graves was probably higher, but agriculture and building works after the Roman age destroyed the archaeological stratification. Inside the cemetery, the space was perfectly organized with sepultures allocated in various groups, differing in the density and richness of the grave goods; however, unlike other coeval Padova cemeteries, the sepulture groups do not create accumulation structures forming a "tumulus".

The cemetery was founded in the first half of the 6th century and was used until the first half of the 4th century B.C. It was probably used by a new large aristocratic group, perhaps of foreign origin, as suggested by the Celtic root of the name *Tival-Bellen* inscribed in the pebble – probably dedicated to the founder – unearthed in the ritual area of the center of the cemetery (Calzavara Capuis and Leonardi 1979; Cupitò 2013; Cupitò 1997; Leonardi et al. 1989; Leonardi 2004; Marinetti 2013; Paltineri 2013).

The Piovego cemetery case study is going to be published in the Progetto di Eccellenza Cariparo “PATAVNOS-Padova città-stato protostorica. Lo studio di caso della necropoli del CUS-Piovego (VI-IV sec. a.C.)”, edited by Giovanni Leonardi and Michele Cupitò.

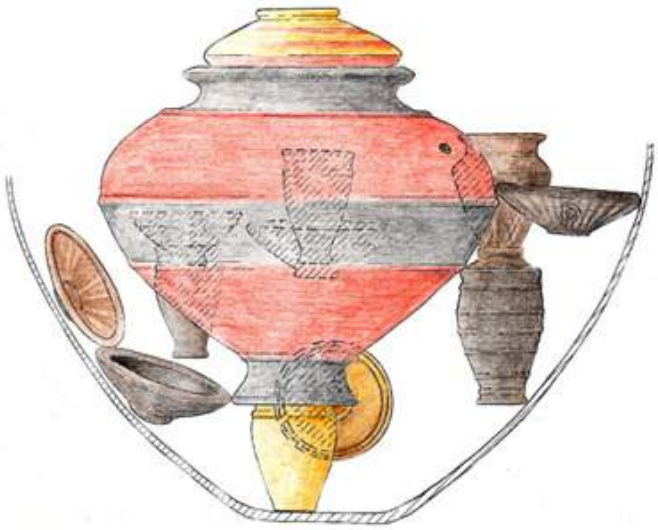

Fig. 2.2.2: Example of a cremation grave enclosed in a “dolio” (image courtesy of prof. Giovanni Leonardi, University of Paodva).

2.3 Villa di Villa site

The Villa di Villa site is part of a plateau located on the southern side of Colle Castelir (353 m, Fig. 2.3.1a-b), a strategic position characterized by the presence of the Meschio river to the west and the Livenza river to the east, near the boundary line between the Veneto and Friuli-Venezia Giulia regions (Northeast Italy).

a)

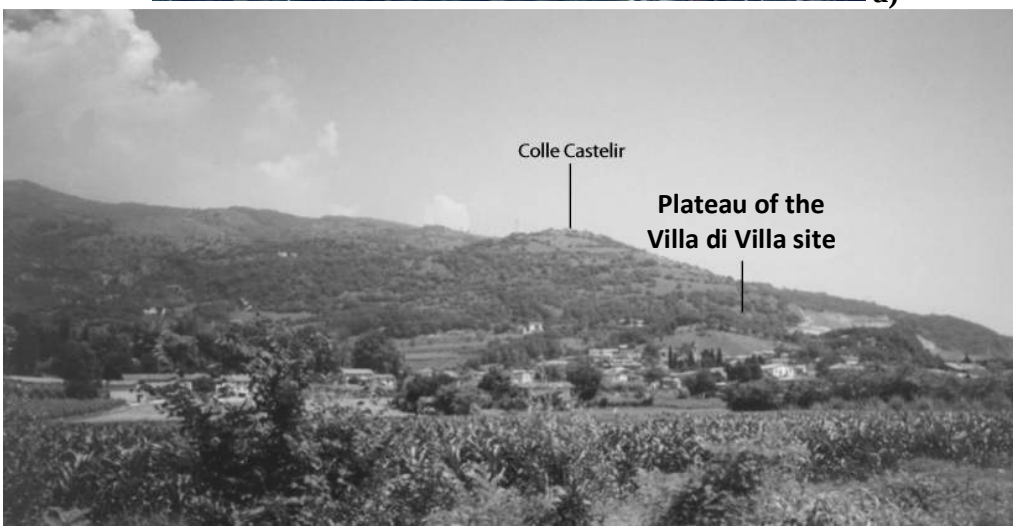

b)

Fig. 2.3.1: a) Air photo of the Colle Catelir; b) Image of the position of the site in the plateau (Images courtesy of Stefano Boaro).

The site was inhabited since the Late Bronze Age (14^{th} – 13^{th} to the 12^{th} century B.C.), then there was a very intensive occupation of the southern side of the hill between the 10^{th} and the beginning of the 8^{th} century B.C. As for the 7^{th} century B.C. the inhabitation of the site is very poor but, in the late 6^{th} century B.C. the hill gained a very important role as a cultual area, becoming a Sanctuary. The Sanctuary activity took place from the 6^{th} century B.C. to the 4^{th} century A.D., even though the excavation finds attested periods of fragmentary use. The site has been excavated since 1976, unveiling the presence of cultual evidences; starting from 2004 it has become the object of annual micro stratigraphic studies by the University of Padova. At present, the unearthed area only involves the Romanization and Early Imperial phases. However, the excavations have also confirmed the presence of layers related to the protohistoric sanctuary, in the whole area below the Romanization and Early Imperial phases, as revealed by the discovery of pottery, metal finds (i.e. rings, fibula, pendants) and glass ornaments (analyzed in this work with other vitreous materials) dated to 6^{th}-4^{th} century B.C. Only a few "stratigraphic windows" of the primary protohistoric deposit have been excavated to date and the work is still in progress.

The 2010 campaign improved the contextualization of the chronology and the definition of the phasing of the structures of the Romanization and Early Imperial period in the previously investigated cult area. The results, although leaving some problems unresolved, have partially modified the hypotheses proposed at the end of the 2008 campaign (Leonardi et al. 2009). In fact, it was ascertained that the structures' remains were not related to a single phase with several structures, as initially supposed, but to two construction phases (from http://www.fastionline.org.):

Building phase 1: 2^{nd} – 1^{st} half of the 1^{st} century B.C.

This was the earliest life phase of the Romanization period, characterized by the use of brick/tile as construction materials. The remains of a first *sacred structure* are razed foundations with a north-west/south-east alignment. The votive finds belonging to this phase were all found in a secondary deposition and are constituted by jars with 'brushed' surfaces and/or high everted rim, grey pottery bowls, a full-casting bronze figurine, silver coins and glass objects (including the three arm rings analyzed in this work).

Building phase 2

Between the end of the 1st century B.C. and the beginning of the 1st century A.D. the area underwent a radical restructuring, involving the demolition of the phase 1 *structure* and the moving back of the cult structures to an area defined by a containing wall downhill.

The alignment of the cult structures in this phase and the dating of the votives seem to indicate the existence of two sub-phases that were very close or perhaps overlapping in date.

Building phase 2 A: end of the 1st century B.C.-beginning of the 1st century A.D.

A small square structure containing the votive deposit named US 16, dates to this phase. It overlay the area of the phase 1 structure on the same alignment and reproduced its simple square plan on a smaller scale. This structure may be considered a reconsecration, within the new spatial organization, of the preceding structure and perhaps of the votives related to its previous phase of use, including bronze votive laminae, a full-casting bronze figurine, numerous fragments of jars for cultual use, a glass rod fragment with a semicircular section (analyzed in this work) and a large numbers of animals bones (burnt or not).

Building phase 2 B: 1st half of the 1st century A.D.

Phase 2B presents a second structure, only visible in the flattened foundation trenches, southwards opened and on a strictly north-south alignment.

The overall plan suggests greater monumentalization, with the cult structures situated on a raised platform with respect to the access route.

Unfortunately, nineteenth century disturbance has caused the almost total loss of phase 2B votives; the dating is proved by impasto jars and sigillata pottery, some of which stamped, found in residual levels.

The vitreous materials analyzed in this work came from 2004, 2008 and 2010 excavations and belong to secondary deposition layers. A complete report of the excavations is not published to date, but preliminary data can be found in Leonardi et al. 2009 (with previous references) and in http://www.fastionline.org.

CHAPTER 3

MATERIALS

3.1 Samples selection

In this study, 130 vitreous material slivers were sampled from the beads for the chemical, textural and mineralogical analysis. The sampling was carried out by means of a scalpel and under the optical microscope (OM, see par. 4.1) to choose the less invasive and not weathered areas. The slivers (about 200-500μm^2) were sampled from the body and, when possible, from the decorations of the beads in order to have all the different types of glass. The sampling methodology and the analytical protocol used have been validated in several previous works (Angelini et al. 2002; Artioli et al. 2008).

The selection of the materials was performed considering the age, the provenance contexts and the typologies of the objects. The different properties of the glasses were also considered, such as color/opacity, conservation state and the material characteristics (porosity, inclusions, fractures, etc.).

3.2 Samples description

3.2.1 Lipari and Salina

The total beads selected for this study are 9 from Salina (Villaggio di Portella) and 57 from Lipari (Acropolis and Piazza Monfalcone cemetery), from which 10 and 66 vitreous materials samples were selected, respectively. The Salina ornaments are composed by 4 fragments with uncertain typologies and 5 half annular beads; the Lipari beads are 36 annular, 1 double annular, 7 globular (one with spiral and one with eyes decoration), 3 barrel-shaped with spiral decoration, 6 fragments, 2 cylindrical with spiral decoration, 1 bead with 4 eyes decoration and 1 trunk-conic bead.

Salina – Villaggio di Portella

The unearthed beads are constituted by different typologies and materials and they were assembled in one or more necklaces (Fig. 2a.). There are 54 carnelian annular and globular beads, with a central larger oval-shaped and faceted one, and numerous vitreous material beads with varying typologies (Bernabò Brea et al. 1968; Martinelli 2005); the segmented typologies comparable with Mycenaean segmented beads are particularly interesting (Nightingale 1994). However, the glass beads analyzed in this work come from a plate of broken beads preserved in the Archaeological Museum of Lipari, together with some copper fragments (Fig. 2b.).
The complete details (dimension, weight, NCS – see Ch. 4 – color etc.) and images of the materials are collected in Table 1 and Figures 3-11, respectively.

a. b.

Fig. 2. a. Necklaces of carnelian (the smaller red one) and vitreous material beads. b. Broken glass beads with copper fragments, Archaeological Museum of Lipari. The analyzed samples come from this group.

Below is a summary of the samples' labels of the beads fragments selected for the analysis and the main characteristics of the finds, grouped by typology:

- **SALFA1, SALFA2, SALFA3 and SALFA4** are three half-annular blue-colored beads, characterized by a brown/yellow weathering (fig. 3-6).
- **SALFAS** is a half-annular blue bead with a spiral decoration (not preserved) and a brown/yellow weathering (fig. 7).

- **SALFFR, SALCFR1 and SALCFR3** are three blue fragments with an irregular shape and a brown/yellow weathering (fig. 8-10).
- **SALCFR4B-Bi** is a blue fragment with a white decoration and a brown/yellow weathering (fig. 11).

Samples	Age	Provenance	Typology	Dimensions (cm)	Color	NCS color	Weight (g)
SALFA1	Milazzese MBA3 14th century B.C.	Capanna F, broken beads plate	Annular	d = 0.3; L = 0.5; h = 0.3	Blue	n.d.	<1
SALFA2	Milazzese MBA3 14th century B.C.	Capanna F, broken beads plate	Annular	d = 0.2; L = 0.6; h =0.3	Blue	n.d.	<1
SALFA3	Milazzese MBA3 14th century B.C.	Capanna F, broken beads plate	Annular	d = 0.3; L = 0.6; h = 0.3	Blue	n.d.	<1
SALFA4	Milazzese MBA3 14th century B.C.	Capanna F, broken beads plate	Annular	d = 0.5; L = 0.6; h = 0.3	Blue	n.d.	<1
SALFAS	Milazzese MBA3 14th century B.C.	Capanna F, broken beads plate	Annular with spiral	d = 0.2; L = 0,6; h = 0.2	Blue	n.d.	<1
SALFFR	Milazzese MBA3 14th century B.C.	Capanna F, broken beads plate	Fragment with irregular shape	th. = 0.2; L = 0.6	Blue	n.d.	<1
SALCFR1	Milazzese MBA3 14th century B.C.	Capanna F, broken beads plate	Fragment with irregular shape	L = 0.3; d = 0.2; h = 0.26	Blue	n.d.	<1
SALCFR3	Milazzese MBA3 14th century B.C.	Capanna F, broken beads plate	Fragment with irregular shape	L = 0.5; th. = 0.3	Blue	n.d.	<1
SALCFR4B-Bi	Milazzese MBA3 14th century B.C.	Capanna F, broken beads plate	Fragment with a white decoration	L = 0.3; th. = 0.2	Blue and white	n.d.	<1

Table 3.2.1: Glass beads from Salina – Villaggio di Portella, Capanna F, analyzed in this work. (L = mean width; h = mean height; d. = mean diameter; th. = thickness; n.d. = not determined). The finds are sampled from the broken beads plate (fig. 2b).

***Figures 3-11**: Optical microscope (OM) images of the glass beads from Capanna F in Salina – Villaggio di Portella, analyzed in this work. In the scale, 1 space corresponds to 1 mm.*

Fig. 3. SALFA1.

Fig. 4. SALFA2.

Fig. 5. SALFA3.

Fig. 6. SALFA4.

Fig. 7. SALFAS.

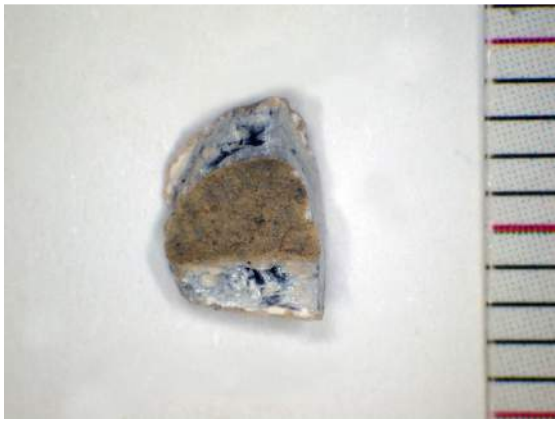

Fig. 8. SALFFR.

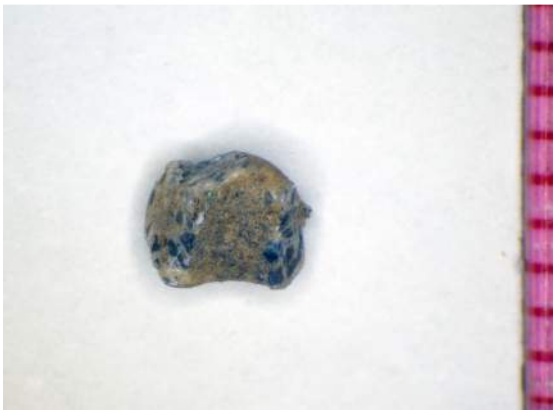

Fig. 9. SALFFR1.

Fig. 10. SALFFR3.

Fig. 11. SALFFR4B-Bi.

Lipari – Acropolis

The analyzed beads typologies are 1 globular, 1 fragment and 2 annular dated to the MBA 1-2 (17^{th}-15^{th} century B.C.), RBA (end of 14^{th} - first half 12^{th} century B.C.) and FBA 2-3 (11^{th}-10^{th} century B.C., respectively.

The complete details (dimension, weight, NCS color etc.) and images of the materials are collected in Table 2 and Figures 13-16, respectively.

Below is a summary of the samples' labels and the main characteristics of each find:

- **LC21M** is a globular transparent yellow/brown bead from Capanna δ XXI, Capo Graziano phase, MBA 1-2, 17^{th}-15^{th} century B.C. (Bernabò Brea 1958, Bernabò Brea et al. 1980). The surface of the bead presents a white weathered layer (fig. 13). The bead was found in the settlement in association with some Mycenaean pottery fragments (Bernabò Brea et al. 1980).
- **LOIIIG** is a fragment with a white/yellow color due to the weathering of the bead (fig. 14). It belongs to grave III located in the ground of Capanna O (Bernabò Brea et al. 1960) Ausonio I phase, RBA, end of 14^{th} - first half 12^{th} century B.C. (Bernabò Brea 1958). It is a cremation grave with a ribbed *situla* (a bucket-shaped vessel) in vertical position (Bernabò Brea et al. 1960 pg. 162).
- **Lβ5AG** is an annular transparent yellow bead from Capanna β V, Ausonio II phase, FB 2-3, 11^{th}-10^{th} century B.C. (Bernabò Brea 1958, Bernabò Brea et al. 1980). Its surface is characterized by an opalescent white weathering layer (fig. 15).
- **Lα7AA** is an annular pale blue bead from Capanna α VII, Ausonio II phase, FB 2-3, 11^{th}-10^{th} century B.C. (Bernabò Brea 1958, Bernabò Brea et al. 1980). A white/gray weathering layer covers the surface of the bead (fig. 16).

Table 3.2.2: Glass beads from the Lipari Acropolis analyzed in this work. (T = grave; Inv. = inventory number assigned to the find; L = mean width; h = mean height; d. = mean hole diameter; int. = internal glass; est. = external layer).

Samples	**Age**	**Provenance**	**Typology**	**Dim. (cm)**	**Color**	**NCS color**	**Wt. (g)**
LC2IM	Capo Graziano MBA1-2 17th-15th century B.C.	Capanna δ XXI, Inv. 7758	Globular	L = 1; h = 0.7; d = 0.5	Yellow/ brown	Est.: S0502-G50Y; Int.: S8020-Y70R	<1
LOIIIG	Ausonio I RBA End 14th-first half of 12th century B.C.	Capanna O, T. III.	Fragment (possibly annular or globular)	L = 0.9; h = 0.8	White/ yellow	S0502-Y50R	<1
Lβ5AG	Ausonio I FBA2-3 11th-10th century B.C.	Capanna β V, Inv. 10629, BH19	Annular	L = 0.7; h = 0.3; d = 0.4	Yellow	Est.: S0505-Y; Int.: S3050-Y10R	<1
Lα7AA	Ausonio I FBA2-3 11th-10th century B.C.	Capanna α VII, Inv. 10630, B58	Annular	L = 1; h = 0.7; d = 0.4	Pale blue	Est.: S0505-Y; Int.: S1050-B10G	<1

***Figures 13-16**: Optical microscope (OM) images of the glass beads from the Lipari Acropolis analyzed in this work. For each figure, labels, provenance and inventory number of the samples are reported. In the scale, 1 space corresponds to 1 mm.*

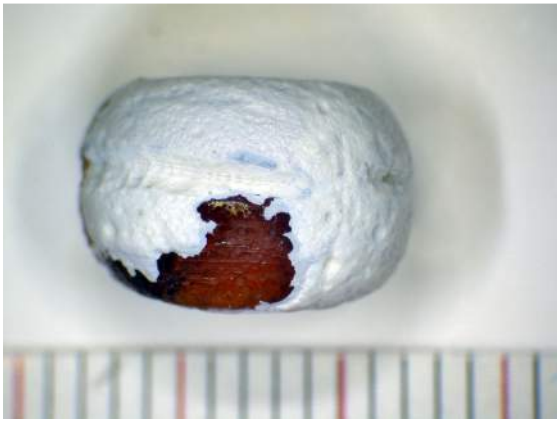

Fig. 13. LC21M, Capanna δ XXI, Inv. 7758.

Fig. 14. LOIIIG, Capanna O, T. III.

Fig. 15. Lβ5AG, Capanna β V, Inv. 10629, BH19.

Fig. 16. Lα7AA, Capanna α VII, Inv. 10630, B58.

Lipari – Piazza Monfalcone cemetery

The ornaments selected for this study are composed of 15 beads belonging to grave 18 and 38 belonging to grave 31. The materials from grave 31 were sampled both from the large necklace (fig. 18a) and from broken beads in plates 1, 2 and 4 (fig. 18b-d) preserved in the Archaeological Museum of Lipari.
The complete details (dimension, weight, NCS color etc.) and images of the materials are collected in Table 3 and Figures 19-45, respectively.
Below is a summary of the samples labels and the main characteristics of the finds, grouped by grave and typology:

Grave 18:

- **L12SM, L12V1, L12V2, L12VA, L12AN1, L12AN2, L12CO, L18AA2, L12AA1, L12AA2, L18CO and L18AA1** are twelve small annular beads with different shades: blue/green (L12SM, V1, V2, VA), dark blue (L12AN1 and AN2), blue (L12CO and L18CO) and pale blue (L12AA1 and AA2, L18AA1 and AA2). Some representative images are reported in fig. 19-21.
- **L12BOTA-B** is a barrel shaped bead with a blue body (A) and a white spiral decoration (B) (fig. 22).
- **L12GA** is a globular blue/green bead (fig. 23).
- **L12DA** is a dark blue double annular bead (fig. 24).

Grave 31:

Necklace:

- **L31CAA1, L31CAA2 and L31CAA3** are three big annular beads, blue and pale blue colored (fig. 25).
- **L31CB2B-A and L31CB1B-A** are two blue (L31CB2A and 1A) barrel shaped beads with a white (L31CB2B and 1B) spiral decoration (fig. 26).
- **L31CCR and L31CSB** are two cylindrical beads with a white spiral decoration. L31CCR (fig. 27) has a brown body while L31CSB (fig. 28) has a blue one. In both

case, the white decoration were not sampled in order to avoid damage to the well preserved surface of the bead.

- **L31CGB-A** is a blue (A) globular bead with a white (B) decoration (fig. 29).
- **L31CTA** is a trunk-conic blue bead (L31COB) (fig. 30).
- **L31COA-B** is a globular dark blue bead (L31COA), with traces of white decoration (L31COB) and possibly remains of eyes decoration (fig. 31).

Plate 1:

- **L311AB1, L311AB2, L311AN1, L311AA1 and L311AA2** are five small annular beads with different shades: pale blue (L311AB1 and B2), black (L311AN1) and blue/green (L311AA1 and AA2). Some representative images are reported in fig. 32-34.
- **L311O1A** is a blue bead with a non-preserved eyes decoration (fig. 35).
- **L311O2B-A, L311O3A-B, L311O4A-B** are three blue (L311O2A, 3A and 4A) bead fragments with a white (L311O2B, 3B and 4B) decoration, possibly eyes (fig. 36).
- **L311FR2 and FR1** are two pale blue (FR2) and blue (FR1) bead fragments with unknown typologies (fig. 37).
- **L311GM1** is a brown globular bead (fig. 38).
- **L311SPA-B** is a blue (A) globular bead with a white (B) spiral decoration (fig. 39).

Plate 2:

- **L312AA1, L312AA2, L312AA3, L312AN1 and L312AN2** are five small annular beads pale blue- (L312AA1, AA2 and AA3) and dark blue- (L312AN1 and AN2) colored (fig. 40-41).

Plate 4:

- **L314AZ1, L314AZ2, L314AA1, L314AA2, L314AN1, L314AN2, L314CO1, L314CO2, L314XA** are nine small annular beads with different blue shades: pale blue (L314AZ1, AZ2, AA1 and AA2), dark blue (L314AN1, AN2, XA) and blue (L314CO1 and CO2). Some representative images are reported in fig. 42-44.
- **L314GA** is a blue globular bead (fig. 45).

a. Necklace

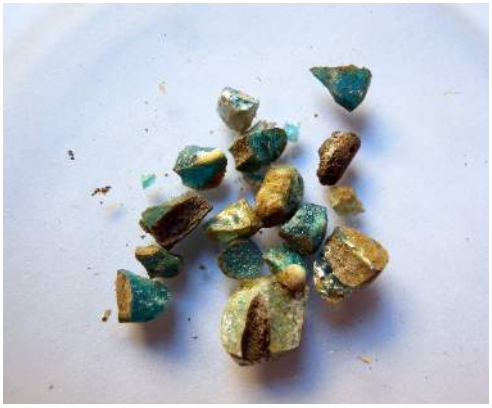

b. Plate 1

c. Plate 2

d. Plate 4

Fig. 18. a: Glass beads from grave 31 of Piazza Monfalcone cemetery, analyzed in this work. a: necklace composed by 36 beads of different typologies; b: broken beads, plate 1; c: broken beads with some metal filaments, plate 2; d: annular beads of different blue shades, plate 4.

Table 3.2.3: Glass beads from Lipari – Piazza Monfalcone cemetery analyzed in this work (typ. = typology; g. = grave; L = mean width; h = mean height; d. = mean hole diameter).

Samples	Age	Provenance	Typology	Dim. (cm)	Color	NCS color	Wt. (g)
L12SM	Ausonio II FBA1-2 second half of 12th-11th century B.C.	g. 18	Annular	L = 0.5; h = 0.2; d = 0.3	Blue/ green	S4040-B60G	<1
L12V1	Ausonio II FBA1-2 second half of 12th-11th century B.C.	g. 18	Annular	L = 0.5; h = 0.3; d = 0.3	Blue/ green	S6030-B30G	<1
L12V2	Ausonio II FBA1-2 second half of 12th-11th century B.C.	g. 18	Annular	L = 0.5; h = 0.3; d = 0.3	Blue/ green	S6030-B30G	<1
L12VA	Ausonio II FBA1-2 second half of 12th-11th century B.C.	g. 18	Annular	L = 0.5; h = 0.2; d = 0.3	Blue/ green	S4040-B30G	<1
L12AN1	Ausonio II FBA1-2 second half of 12th-11th century B.C.	g. 18	Annular	L = 0.6; h = 0.3; d = 0.3	Dark blue	S7020-B	<1
L12AN2	Ausonio II FBA1-2 second half of 12th-11th century B.C.	g. 18	Annular	L = 0.4; h = 0.2; d = 0.2	Dark blue	S7020-B	<1
L12CO	Ausonio II FBA1-2 second half of 12th-11th century B.C.	g. 18	Annular	L = 0.5; h = 0.2; d = 0.3	Blue	S5540-R90B	<1
L18AA2	Ausonio II FBA1-2 second half of 12th-11th century B.C.	g. 18	Annular	L = 0.7; h = 0.4; d = 0.4	Pale blue	S5040-B20G	<1
L12AA1	Ausonio II FBA1-2 second half of 12th-11th century B.C.	g. 18	Annular	L = 0.5; h = 0.3; d = 0.3	Pale blue	S2065-B	<1
L12AA2	Ausonio II FBA1-2 second half of 12th-11th century B.C.	g. 18	Annular	L = 0.7; h = 0.4; d = 0.3	Pale blue	S2065-B	<1
L18CO	Ausonio II FBA1-2 second half of 12th-11th century B.C.	g. 18	Annular	L = 0.5; h = 0.2; d = 0.2	Blue	S4055-B	<1
L18AA1	Ausonio II FBA1-2 second half of 12th-11th century B.C.	g. 18	Annular	L = 0.6; h = 0.2; d = 0.3	Pale blue	S1565-B	<1
L12BOTA	Ausonio II FBA1-2 second half of 12th-11th century B.C.	g. 18	Barrel shaped with spiral decoration	L = 0.2; h = 0.1; d = 0.4	Blue body	S4050-R80B	1÷2
L12BOTB					White spiral	S0510-Y10R	

L12GA	Ausonio II FBA1-2 second half of 12th-11th century B.C.	g. 18	Globular	L= 0.5; h = 0.3; d = 0.2	Blue/ green	S3560-G10Y	<1
L18DA	Ausonio II FBA1-2 second half of 12th-11th century B.C.	g. 18	Double annular	L = 0.6; h = 0.6; d = 0.4	Dark blue	S7020-B	<1
L31CAA1	Ausonio II FBA1-2 second half of 12th-11th century B.C.	g. 31, large necklace	Annular		Pale blue	S2050-B20G	1
L31CAA2	Ausonio II FBA1-2 second half of 12th-11th century B.C.	g. 31, large necklace	Annular		Pale blue	S2555-B40G	1
L31CAA3	Ausonio II FBA1-2 second half of 12th-11th century B.C.	g. 31, large necklace	Annular		Blue	S4040-R10G	1
L31CB2B	Ausonio II FBA1-2 second half of 12th-11th century B.C.	g. 31, large necklace	Barrel shaped with spiral decoration		White spiral	S1000N	1
L31CB2A					Blue body	S4040-B10G	
L31CB1B	Ausonio II FBA1-2 second half of 12th-11th century B.C.	g. 31, large necklace	Barrel shaped with spiral decoration		White spiral	S1000-N	2
L31CB1A	Ausonio II FBA1-2 second half of 12th-11th century B.C.				Blue body	S4050-B10G	
L31CCR	Ausonio II FBA1-2 second half of 12th-11th century B.C.	g. 31, large necklace	Circular with spiral decoration		Brown body	S7020-R	2
					White spiral	S1502-Y50R	
L31CSB	Ausonio II FBA1-2 second half of 12th-11th century B.C.	g. 31, large necklace	Circular with spiral decoration		Blue body	S4030-B10G	1
					White spiral	S1010-Y20R	
L31CGB	Ausonio II FBA1-2 second half of 12th-11th century B.C.	g. 31, large necklace	Globular with spiral decoration		White spiral	S1000N	2
L31CGA					Blue body	S6030-B	
L31CTA	Ausonio II FBA1-2 second half of 12th-11th century B.C.	g. 31, large necklace	Trunk – conic		Pale blue	B4040-B30G	2
L31COA	Ausonio II FBA1-2 second half of 12th-11th century B.C.	g. 31, large necklace	Globular with irregular shape and white decoration (probably eyes)		Blue body	S3050-B10G	2
L31COB					White eyes	S1010-Y	

L311AB1	Ausonio II FBA1-2 second half of 12th-11th century B.C.	g. 31, plate 1	Annular		Pale blue	S3020-B	<1
L311AB2	Ausonio II FBA1-2 second half of 12th-11th century B.C.	g. 31, plate 1	Annular		Pale blue	S2030-B104G	<1
L311AN1	Ausonio II FBA1-2 second half of 12th-11th century B.C.	g. 31, plate 1	Annular	L= 0.1; h = 0.6; d = 0.2	Black	S6030-B	~ 1
L311AA1	Ausonio II FBA1-2 second half of 12th-11th century B.C.	g. 31, plate 1	Annular	L = 0.5; h = 0.2; d = 0.2	Blue/ green	S6030-B50G	<1
L311AA2	Ausonio II FBA1-2 second half of 12th-11th century B.C.	g. 31, plate 1	Annular	Irregular shape	Blue/ green	S3040-B40G	<1
L311O1A	Ausonio II FBA1-2 second half of 12th-11th century B.C.	g. 31, plate 1	Bead with 4 white decorations (possibly eyes)	L = 0.1; h = 0.7; d = 0.3	Blue/ green	S4050-B50G	<1
L311O2B	Ausonio II FBA1-2 second half of 12th-11th century B.C.	g. 31, plate 1	Decorated fragment of eyes bead	Irregular shape	White dec.	S0520-Y10R	<1
L311O2A					Blue body	S2040-B20G	
L311O3A	Ausonio II FBA1-2 second half of 12th-11th century B.C.	g. 31, plate 1	Decorated fragment of eyes bead	Irregular shape	Blue body	S2040-B20G	<1
L311O3B					White dec.	S0520-Y10R	
L311FR2	Ausonio II FBA1-2 second half of 12th-11th century B.C.	g. 31, plate 1	Fragment with irregular shape	L = 0.1; h =7.4; d = 0.2	Pale blue	S1040-B	<1
L311FR1	Ausonio II FBA1-2 second half of 12th-11th century B.C.	g. 31, plate 1	Fragment with irregular shape	L = 0.6; h = 0.5 d = 0.3	Blue	S2555-B30G	<1
L311GM1	Ausonio II FBA1-2 second half of 12th-11th century B.C.	g. 31, plate 1	Globular	L= 0.7; h = 0.7; d = 0.2	Yellow/ brown	S5020-Y60R	<1
L311O4A	Ausonio II FBA1-2 second half of 12th-11th century B.C.	g. 31, plate 1	Decorated fragment of eyes bead	Irregular shape	Blue body	S2040-B20G	<1
L311O4B					White dec.	S0520-Y10R	
L311SPA	Ausonio II FBA1-2 second half of 12th-11th century B.C.	g. 31, plate 1	Globular with spiral decoration	L = 0.7; h = 0.5; d = 0.2	Blue body	S3020-B	<1
L311SPB					White spiral	S1030-Y10R	
L312AA1	Ausonio II FBA1-2 second half of 12th-11th century B.C.	g. 31, plate 2	Annular	L= 0.6; h = 0.3. d = 0.2	Pale Blue	S3050-B40G	<1

L312AA2	Ausonio II FBA1-2 second half of 12th-11th century B.C.	g. 31, plate 2	Annular	L = 0.6; h = 0.3; d= 0.3	Pale Blue	S3050-B40G	<1
L312AA3	Ausonio II FBA1-2 second half of 12th-11th century B.C.	g. 31, plate 2	Annular	L = 0.7; h = 0.3. d = 0.4	Pale Blue	S3050-B40G	<1
L312AN1	Ausonio II FBA1-2 second half of 12th-11th century B.C.	g. 31, plate 2	Annular	L = 0.6; h = 0.3. d = 3.5	Dark blue	S7020-B	<1
L312AN2	Ausonio II FBA1-2 second half of 12th-11th century B.C.	g. 31, plate 2	Annular	L = 0.5; h = 0.3; d = 0.2	Dark blue	S7020-B	<1
L314AZ1	Ausonio II FBA1-2 second half of 12th-11th century B.C.	g. 31, plate 4	Annular	L= 0.6; h = 0.2. d = 0.4	Pale blue	S1565-B	<1
L314AZ2	Ausonio II FBA1-2 second half of 12th-11th century B.C.	g. 31, plate 4	Annular	L = 0.6; h = 0.2; d = 0.4	Pale blue	S1565-B	<1
L314AA1	Ausonio II FBA1-2 second half of 12th-11th century B.C.	g. 31, plate 4	Annular	L = 0.5; h = 0.2; d = 0.4	Pale blue	S1565-B	<1
L314AA2	Ausonio II FBA1-2 second half of 12th-11th century B.C.	g. 31, plate 4	Annular		Pale blue	S1565-B	<1
L314AN1	Ausonio II FBA1-2 second half of 12th-11th century B.C.	g. 31, plate 4	Annular	L = 0.6; h = 0.2; d = 0.4	Dark blue	S7020-B	<1
L314AN2	Ausonio II FBA1-2 second half of 12th-11th century B.C.	g. 31, plate 4	Annular	L = 0.6; h = 0; d = 0.4	Dark blue	S7020-B	<1
L314CO1	Ausonio II FBA1-2 second half of 12th-11th century B.C.	g. 31, plate 4	Annular	L = 0.5; h = 0.2; d = 0.2	Blue	S5540-R90B	<1
L314CO2	Ausonio II FBA1-2 second half of 12th-11th century B.C.	g. 31, plate 4	Annular	L= 0.6; h = 0.2; d = 0.3	Blue	S5540-R90B	<1
L314XA	Ausonio II FBA1-2 second half of 12th-11th century B.C.	g. 31, plate 4	Annular	L = 0.6; h = 0.4; d = 0.3	Dark blue	S7020-B	<1
L314GA	Ausonio II FBA1-2 second half of 12th-11th century B.C.	g. 31, plate 4	Globular	L= 0.6; h = 0.4; d = 0.2	Blue	S3060-B	<1

***Figures 19-45**: Optical microscope (OM) images of the glass beads from Lipari – Piazza Monfalcone cemetery analyzed in this work. In each figure, labels and provenance of the samples are reported. In the scale, 1 space corresponds to 1 mm.*

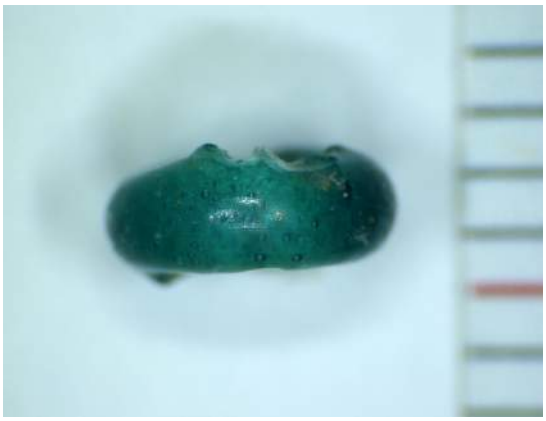

Fig. 19. L12SM, Grave 18.

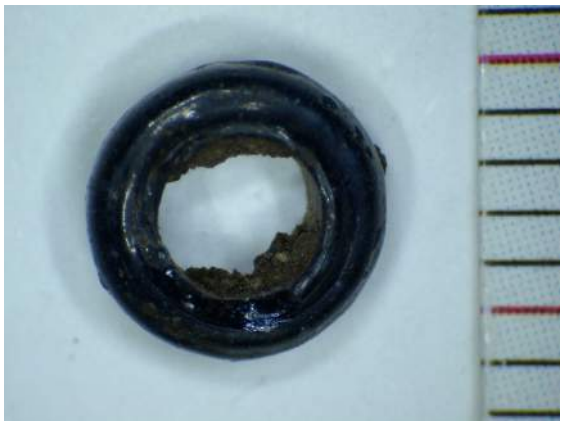

Fig. 20. L12AN1, Grave 18.

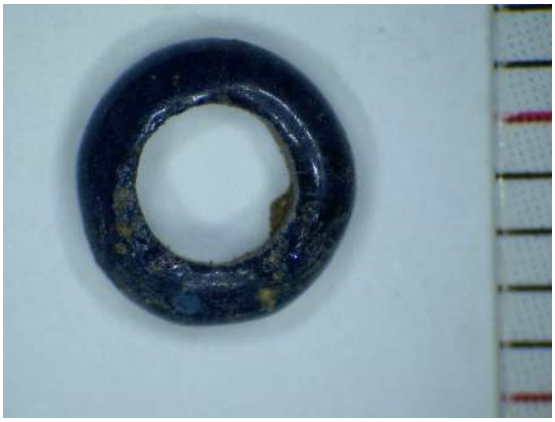

Fig. 21. L12CO, Grave 18.

Fig. 22. L12BOTA-B, Grave 18.

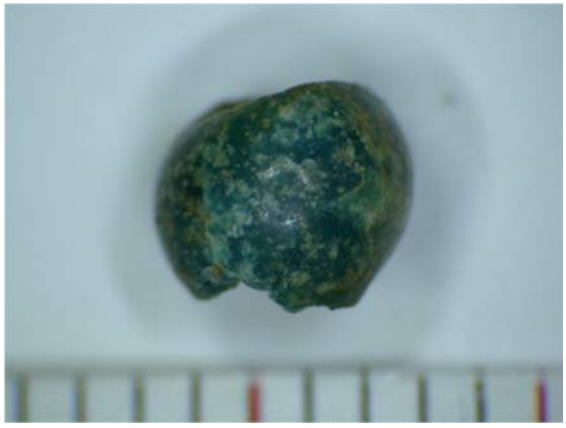

Fig. 23. L12GA, Grave 18.

Fig. 24. L18DA, Grave 18.

Fig. 25. L31CAA2, Grave 31, necklace.

Fig. 26. L31CB1, Grave 31, necklace.

Fig. 27. L31CCR, Grave 31, necklace.

Fig. 28. L31CSB, Grave 31, necklace.

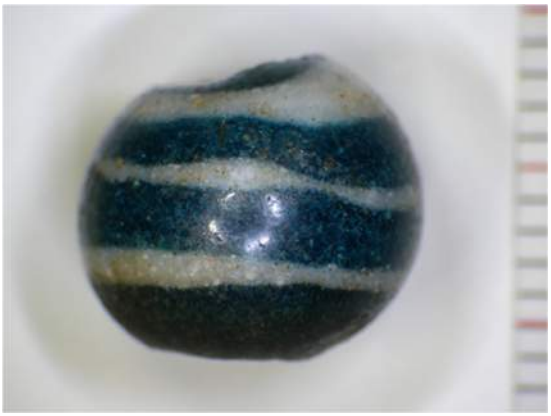

Fig. 29. L31CGBA, Grave 31, necklace.

Fig. 30. L31CTA, Grave 31, necklace.

Fig. 31. L31COAB, Grave 31, necklace.

Fig. 32. L311AB2, Grave 31, plate 1.

Fig. 33. L311AN1, Grave 31, plate 1.

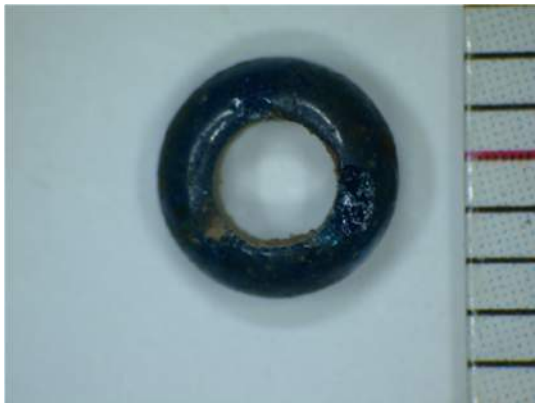

Fig. 34. L311AA1, Grave 31, plate 1.

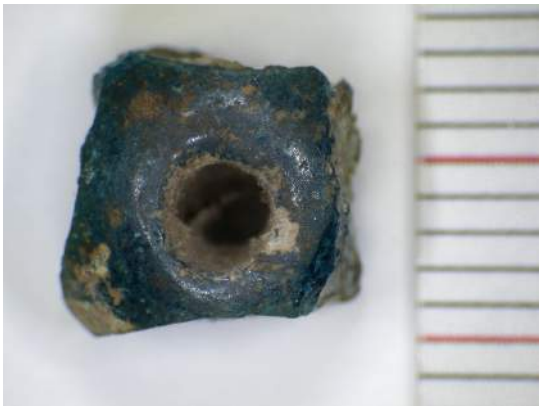

Fig. 35. L311O1A, Grave 31, plate 1.

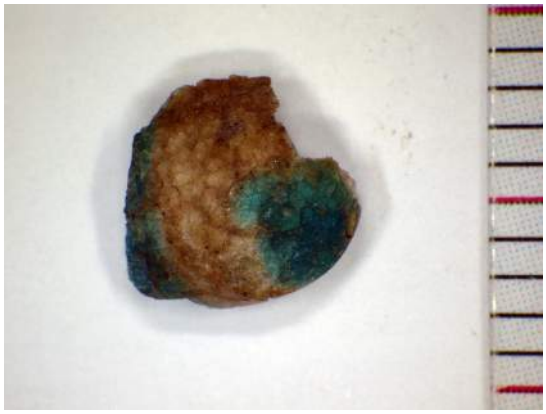

Fig. 36. L311O2BA, Grave 31, plate 1.

Fig. 37. L311FR1, Grave 31, plate 1.

Fig. 38. L311GM1, Grave 31, plate 1.

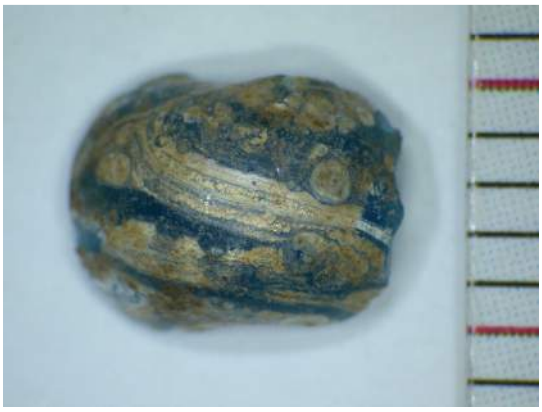

Fig. 39. L311SPAB, Grave 31, plate 1.

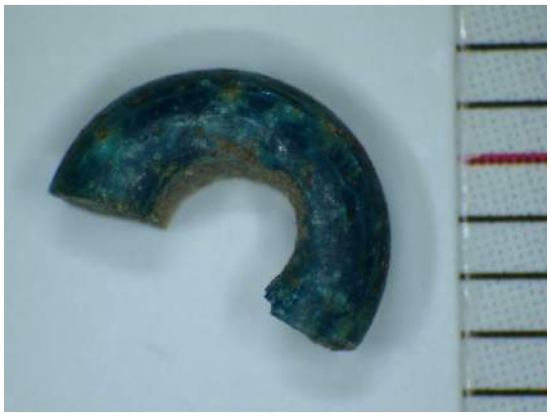

Fig. 403. L312AA2, Grave 31, plate 2.

Fig. 41. L312AN1, Grave 31, plate 2.

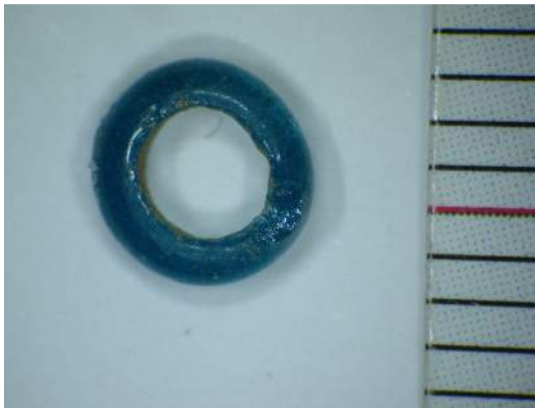

Fig. 42. L314AA1, Grave 31, plate 4.

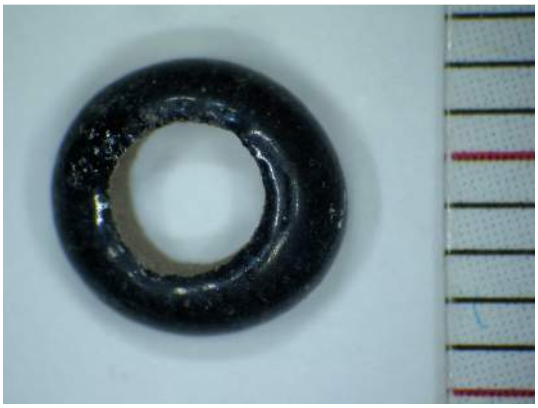

Fig. 43. L314AN2, Grave 31, plate 4.

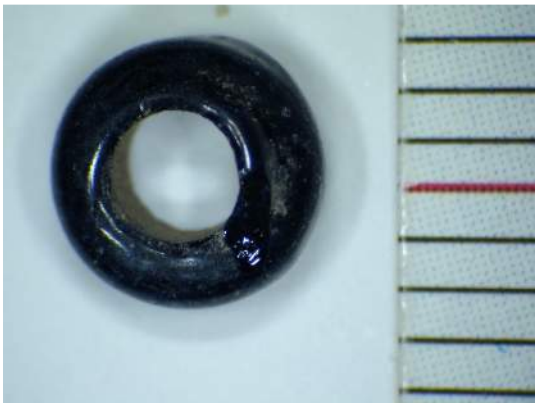

Fig. 44. L314CO2, Grave 31, plate 4.

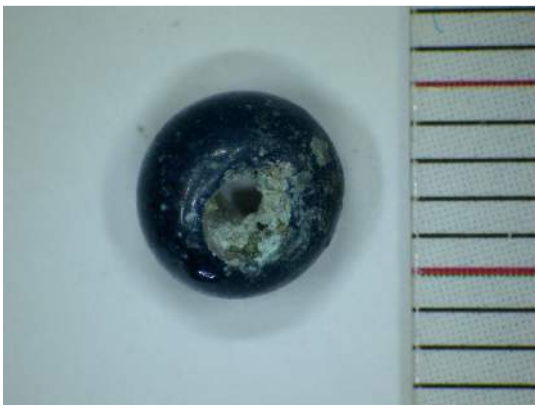

Fig. 45. L314GA, Grave 31, plate 4.

3.2.2 Piovego cemetery

The Archaeological study

The archaeological study of the vitreous material beads of the Piovego cemetery was carried out by B. Prosdocimi, M. Cupitò and G. Leonardi. of the Department of Cultural Heritage of the Padova University; a short paper on this topic was presented in XLVIII Riunione Scientifica dell'Istituto Italiano di Preistoria e Protostoria, Padova, 2013 (Olmeda et al. in press).

The sample of vitreous material beads found in the cemetery is composed by 31 beads with a diameter between 0.8 and 2 cm and 49 particularly small beads with a diameter below 0.5 cm; all items have been found in 16 cremation graves and may be dated between the second half of the 6th century and the end of the 5th century B.C.

The Piovego cemetery beads were most likely used as pendants assembled in fibula rather than in necklaces, as suggested by the frequently found bronze clips. An exception is given by the 47 small annular beads and some bead fragments found in grave 127, all in blue glass, probably associated into a complex jewel.

Most of the samples analyzed in this research belong to simple typologies, such as annular (fig. 1.5), small annular and globular beads with different dimensions (for the typologies nomenclature, see Gambacurta 1987, p. 193). Specific typological considerations can be made on more particular typologies, such as the disc-shaped blue bead with 5 horns (Fig. 1.1) from grave 108 (dated to the last quarter of the 6th century B.C.), which is comparable to similar beads found in later contexts from Este (Padova), even though the number of horns is variable and the colors are different (the Este beads have yellow shades). The most representative examples from Este for this typology are the so-called "Grave of Nerka" (Casa di Ricovero 23/1984) and the nearby grave n. 36/1984, both dated to the beginning of the 3rd century B.C. (Chieco Bianchi 1987, fig. 17.23, 30-31 and fig. 45.3). Two samples were also found in the Benvenuti 123 grave *(Este II*, table 154.72-73) dated between the half of the 3rd and the beginning of the 1st century B.C. Outside Italy, a bead with similar chronology, color and typology was found in grave 121 of tumulus 48 of Stična in Slovenia (Gabrovec 2006, tav. 71.15).

The biconical bead with ribbed edges from grave 1 bis (fig. 1.13), dated to the beginning of the 5th century B.C., has a well attested typology in several graves from Este of the same chronology as Piovego, as in grave 254 of the cemetery Casa Muletti Prosdocimi (*Este* I, table 245.23c) and graves 93, 103, 296 of the cemetery Villa Benvenuti (*Este II*, tables 84.13, 102.25, 215.23b). However, the biconical beads from Este are not yellow/brown-colored as the Piovego one. Indeed, the same color characterizes a biconical bead from Stična, Slovenia, which has a slightly different shape, as it has horn applied on the body (Gabrovec 2006, grave 8 of tumulus 48, table 3.8). This typology, with or without horns applied, is well attested also in amber beads from Este (*Este I*, grave 13 of Casa Alfonsi cemetery, table 264.21f; *Este II*, grave 95 of the Villa Benvenuti cemetery, table 89.2) and Altino, Treviso (Gambacurta 1987, fig. 12); consequently, the brown glass bead could be a copy of the amber objects.

When decorated, the beads of the Piovego cemetery present eyes (black, blue, white), both simple (Gambacurta 1987, type F) and stratified (Gambacurta 1987, type E); anyway, in the literature it is difficult to find eyes beads with the same color, morphology and dimensions of the Piovego ones. The black and white eyes of the annular bead from grave 47 (black narrow in fig. 1.6) are, to date, unusual, unlike the white and blue eyes decoration of the globular bead from grave 106 (fig. 1.10). Two particularly large globular beads (about 2 cm) in black and brown glass with white eyes were found in graves 15 (fig. 1.4) and 86 (fig. 1.3). Beads of the same size are attested in Este from the cemeteries Casa di Ricovero grave 149, Casa Muletti Prosdocimi graves 254 and 258 (*Este I*, tables 43.29, 243.22 and 248.15, respectively) and Villa Benvenuti graves 78 and 126 (*Este II*, tables 49.13 and 184.80). Other examples come from the cemetery of Ca' Cima (Adria), grave 16/93 (Towle et al. 2001, fig. 9.80) and Reggio Emilia area (Damiani et al. 1992, tables XCII.1467). Beads with the same typologies but different colors were found in Hallstatt sites dated from the last quarter of the 7th century B.C. and the middle of the 5th century B.C., as in graves 2363 from S. Lucia di Tolmino (Teržan et al. 1985, table 143A.7) and grave 40 of tumulus 2 from Magdalenska Gora (Tecco-Hvala et al. 2004, table 37B.7), both located in Slovenia.

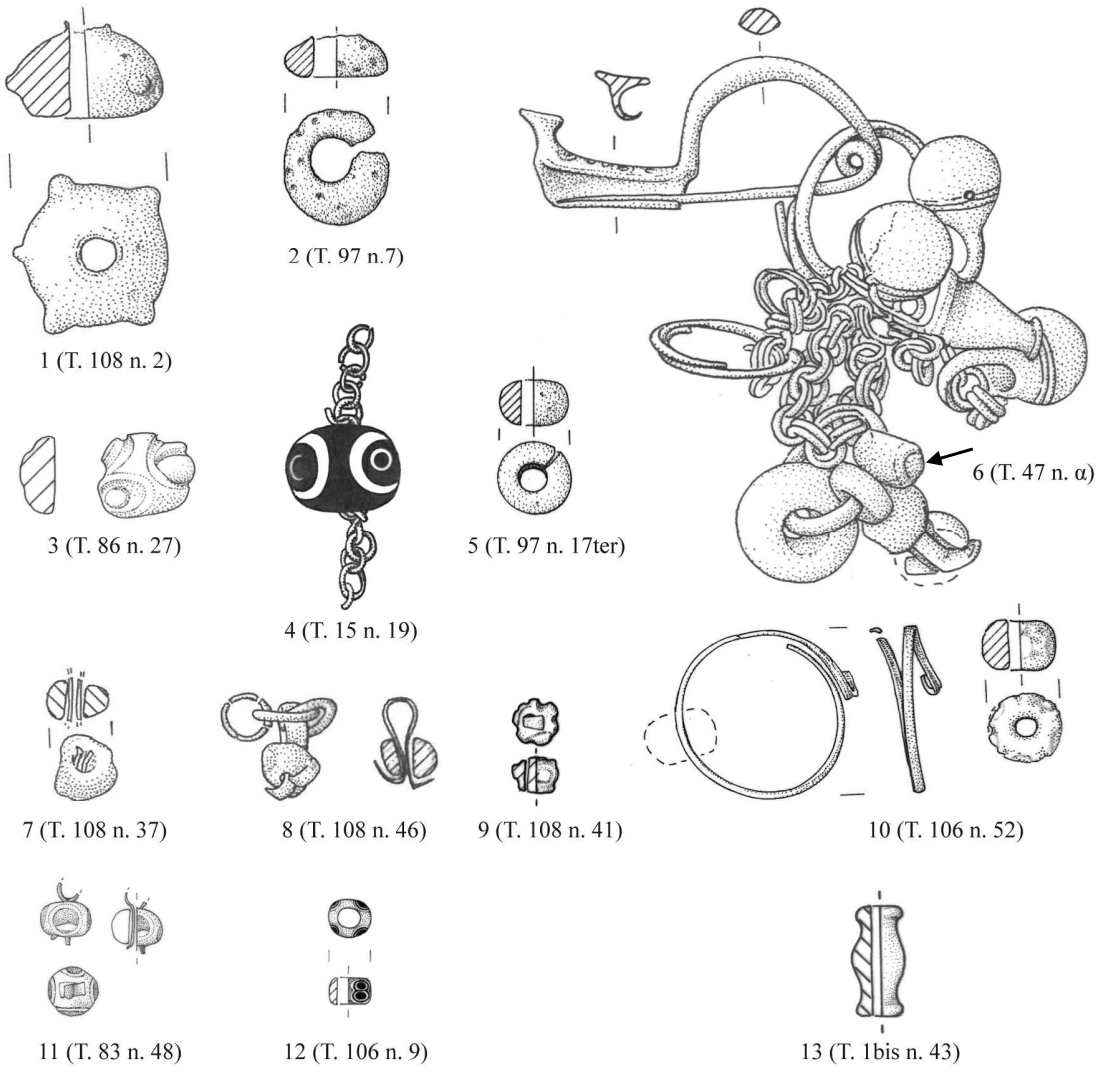

Fig. 1. Vitreous material beads from the Piovego cemetery, Padova (scale 1:1; drawings courtesy of G. Penello and S. Tinazzo, Department of Cultural Heritage, University of Padova).

Beads with stratified eyes decoration are attested in the Piovego cemetery in globular (fig. 1.11) or annular typologies and in one case, not analyzed in the present research for conservative purposes, with double eyes (fig. 1.12). The opaque pale blue bead with blue and white stratified eyes found in grave 83 (fig. 1.11) is very common in Veneto and, in general, in the Po Valley. Indeed, beads with the same typology and colors were found in Altino (Gambacurta 1987, fig. 12), Montebelluna (Manessi et al. 2003, table 57.33b), Adria (Towle et al. 2001, fig. 9.88-89), Bologna (Macellari 2002, table 38), near Modena (Pizzirani 2009,

table 28.12) and in Forcello di Bagnolo San Vito (De Marinis et al. 2005, fig. 111). Similar objects also come from S. Lucia di Tolomino (Teržan et al. 1985, table 143A.7) and Magdalenska Gora (Tecco-Hvala et al. 2004, table 37B.7), Slovenia.
The Piovego cemetery does not present the opaque yellow bead typology with white and/or blue eyes, which was very common in Italy during the Iron Age (Gambacurta 1987).
Concerning the type of ornaments, the Piovego cemetery beads were used more probably as pendants assembled in fibula rather than in necklaces, as suggested by the bronze clips frequently found. An exception is given by the 47 small annular beads and some bead fragments found in grave 127, all in blue glass, probably associated into a complex jewel.

Samples description

For this study 42 different samples of glass were selected from the body and the decoration (where possible) of 38 beads belonging to 16 cremation graves: numbers 1bis, 5, 7, 14, 15, 22, 47, 67, 83, 86, 89, 97, 106, 108, 121, 127. As for typology, the analyzed sample is composed by 9 globular and 13 annular beads – with or without eyes decoration – 3 beads with particular shapes and 13 fragments with no definable shape.
The complete details (dimension, weight, NCS color etc.) and images of the materials are collected in Table 1 and Figures 2-22, respectively. Below is a summary of the samples' labels and the main characteristics of the finds, grouped by typology. The relative and absolute dating for each analyzed object are based on the chronology elaborated by Renato Peroni and other authors in 1975 for the Este cemeteries (Peroni et al. 1975).

<u>Beads fragments</u>:

- **PG-FVA1, FVA5, FVA7, FVA22, FVA67 an**d **FVA97** (Tab. 1.2-3-4-8-13-21) are six transparent green-blue beads fragments belonging to different graves 1bis, 5, 7, 22, 67, 97, respectively; all graves may be dated to the Este IIIC phase (575-525 B.C.) and Este IIID1 phase (525-450 B.C.). In fig. 2 the image of fragment PG-FVA67 is reported, as a representative example.

- **PG-FGi8** (Tab. 1.27) is a transparent yellow bead fragment from grave 108 dated to the transition Este III C/Este D1 phases, around 525 B.C. It is similar to PG-FGi (see below).
- **PG-FGi** (Tab. 1.12) is a transparent yellow bead fragment from grave 47, dated to the transition Este III C/Este D1 phases, around 525 B.C. (fig. 3).
- **PG-FM14, FM83 and FM89** (Tab. 1.6-15-18) are three brown/amber colored beads fragments from graves 14, 83 and 89, respectively. PG- FM14 is dated to Este III C phase (575-525 B.C.) whereas PG-FM83 and FM 89 belong to the Este III D1 (525-450 B.C.) phase. A white opalescent weathered layer characterizes sample PG-FM14 (fig. 4). In fig. 4 the image of fragment PG-FM147 is reported, as a representative example.
- **PG-FN** (Tab. 1.25) is a black fragment from grave 108 dated to the transition Este IIIC/Este D1 phases, around 525 B.C. (fig. 5).
- **PG-FA** (Tab. 1.23) is a blue fragment from grave 106 dated to the Este III D2 phase (450-350 B.C.), probably at the beginning of the phase (fig. 6).

Globular beads:

- **PG-GVA97** (Tab. 1.20) is a transparent green/blue globular bead from grave 97, dated to the Este IIID1 phase (525-450 B.C.), probably at the beginning of the 5th century. A particular porosity yellow weathering layer on the surface characterizes the ornament (fig. 7).
- **PG-GAT7** (Tab. 1.11) is a transparent pale blue globular bead belonging to grave 47, dated to the transition Este IIIC/Este IIID1 phases, around 525 B.C. It is assembled together with beads PG-AOBi and AN in the same pendant (fig. 1.6 and 8).
- **PG-GAT1** (Tab. 1.28) is a transparent blue globular bead from grave 121, dated to the Este IIIC phase, 575-525 B.C. (fig. 9).
- **PG-GOA-B-Bi** (Tab. 1.14) is a pale blue globular bead (GOA) with four double stratified eyes, blue (GOB) and white (GOBi), belonging to grave 83 and dated to the Este III D1 phase, 525-450 B.C. On two sides of the ornament, a residual bronze chain may be observed (fig. 10).
- **PG-GO3B-Bi** (Tab. 1.16) is a fragment of a blue globular bead (GO3B) with white eyes decoration (GO3Bi) from grave 83, dated to the Este IIID1 phase, 525-450 B.C. (fig. 11).

- **PG-GO6B-Bi** (Tab. 1.22) is a blue globular bead (GO6B) with white eyes – perhaps four – which are not preserved except for a small residue (GO6Bi). The bead is from grave 106, dated to Este phase IIID2 phase, 450-350 B.C., probably at the beginning of the phase (fig. 12).
- **PG-GOB8** (Tab. 1.26) is a blue globular bead with a three-eye decoration – not preserved – and a residual bronze chain on two sides of the object. The bead is particularly weathered on the surface and a corroded brown superficial layer is present. The bead belongs to grave 108 and dated to the transition Este IIIC/Este D1, around 525 B.C. (fig. 13).
- **PG-GO5-Bi-N** (Tab. 1.7) is a particularly large (about 2 cm) black globular bead (GO5N) with three white eyes decoration (GO5Bi) and a bronze chain on two sides of the object. The bead was found in grave 15 and dated to the Este III C phase, 575-525 B.C. (fig. 14).
- **PG-GONM-Bi** (Tab. 1.17) is a fragment of a brown globular bead (GONM) with a residual white eyes decoration (GONBi) from grave 86 dated to the Este IIID1 phase, 525-450 B.C. (fig. 15).

Annular beads:

- **PG-AVT** (Tab. 1.19) is a transparent green annular bead from grave 97, dated to the Este IIID1 phase (525-450 B.C.), probably at the beginning of the 5th century. A white weathering layer on the surface characterizes the ornament (fig. 16).
- **PG-AOBi and PG-AN** (Tab. 1.9-10) belong to grave 47, dated to the transition Este IIIC/Este D1 phase, around 525 B.C. The three beads are assembled in the same pendant as shown in fig. 1.6 and 8. PG-AOBi is a black annular bead with three white eyes decoration (two of which remained unaltered) and only the white glass was sampled. PG-AN is a black annular bead probably with a three eyes decoration, not preserved.
- **PG-AAB** (Tab. 1.33) is a blue annular bead fragment from grave 127 dated to the Este III D1 phase, 525-450 B.C. (fig. 17).
- **PG-AB9a-b-c-d, PG-ABOa-b and PG-AB8** (Tab. 1.31-32-34) are seven very small (about 0.4 cm large) blue annular beads from grave 127 dated to the Este IIID1 phase, 525-450 B.C. A representative example of these small beads is reported in fig. 18.

- **PG-AB and AB1/2 2** (Tab. 1.29-30) are two blue annular beads from grave 121 dated to the Este IIIC phase, 575-525 B.C. PG-AB is half-broken whereas AB1/2 is a half annular bead. The two beads are very similar and in fig. 19 the image of PG-AB is reported.

Particular shapes:

- **PG-CM** (Tab. 1.1) is a dark yellow biconical bead with ribbed edges from grave 1 bis, dated to the Este IIID1 phase (525-450 B.C). The bead has a particular porosity and an opaque brown weathering layer on its surface (fig. 20).
- **PG-SB** (Tab. 1.24) is a disc-shaped opaque blue bead with five horns, particularly porous and weathered on its surface, from grave 108, dated to the transition Este IIIC/Este D1 phase, 525 B.C. (fig. 21).
- **PG-FUA** (Tab. 1.5) is a blue bead with a residual bronze clip. The object is partially melted and it is not possible to establish its typology. It comes from grave 14, dated to the Este IIIC phase, 575-525 B.C. (fig. 22).

Table 3.2.4: Glass beads from the Piovego cemetery analysed in this work. (T = grave; Inv. = inventory number assigned by the University of Padova after the excavations; L = mean width; h = mean height; d. = mean hole diameter; int. = internal glass; est. = external surface).

Samples	Age	Prov.	Typology	Dim. (cm)	Color	NCS color	Wt. (g)
1. PG-CM	Este IIID1 525-450 B.C.	T. 1bis, Inv. 43	Biconical with ribbed edges	L = 1.50; h = 0.71; d. est. = 0.7; d.int. = 0.32	brown est.; yellow int.	Est: S8010-Y10R; Int.: S3030-Y30R	0.75
2. PG-FVA1	Este IIID1 525-450 B.C.	T. 1bis, Inv. 44	Fragment	L = 1; h = 0.37	Transparent green - blue	S0505-B80G	0.14
3. PG-FVA5	Transition Este III C/Este D1, around 525 B.C	T. 5, Inv. 8	Fragment	L = 0.92; h = 0.42	Transparent green - blue	S0505-B20G	0.25
4. PG-FVA7	Transition Este III C/Este D1, around 525 B.C	T. 7, Inv. 16 IG 149527	Fragment	L = 0.57; h = 0.40	Transparent green - blue	S0502-G	0.06
5. PG-FUA	Este III C 575-525 B.C.	T. 14, Inv. 19 IG 152903	Unknown	L =2.68; h = 1.15	Blue	S3060-B20G	5.77
6. PG-FM14	Este III C 575-525 B.C.	T. 14, Inv. 26 IG 152910	Fragment	L = 2.05; h = 1	Transparent brown/amber	Weathered: S0520-B30G; Int: S4550-Y60R	1.13
7. PG-GO5Bi-N	Este IIIC 575-525 B.C.	T. 15, Inv. 19 IG 152929	Globular with 4 eyes	L = 2.23; h = 1.65; d = 0.53	Black with white eyes	N = S7502-Y; Bi = S1002-Y	12.18
8. PG-FVA22	Transition Este III C/Este D1, around 525 B.C	T. 22, Inv. 35 IG 15024	Fragment	L = 1.39; h = 0.67	Transparent green - blue	S0510-B90G	0.64
9. PG-AOBi	Transition Este III C/Este D1, around 525 B.C	T. 47, Inv. α IG 34923	Annular with 3 eyes	L = 1.15; h = 0.77; d = 0.425	Black with white eyes	N = S8502-Y; Bi = S1002-Y	Pendant = 33.72
10. PG-AN			Annular	L = 0.92; h = 0.575; d = 0.25	Black	S8502-Y	
11. PG-GAT7			Globular	L = 1.6; h = 1.11; d = 0.65	Transparent blue	S0510-B30G	
12. PG-FGi	Transition Este III C/Este D1, around 525 B.C	T. 47, Inv. α IG 34923	Fragment	L = 0.97; h = 0.67; d = 0.47	Transparent yellow	S1070-Y10R	?

13. PG-FVA67	Este IIIC 575-525 B.C.	T. 67, Inv. 35 IG 149781	Fragment	L = 0.68; h = 0.5	Transparent green - blue	S0505-B20G	0.06
14. PG- GOA-B-Bi	Este III D1 525-450 B.C.	T. 83, Inv. 48	Globular with 4 eyes	L = 0.95; h = 0.97; d = 0.33	Pale blue with white and blue eyes	A = S3020-B10G; B = S4550-R70B; Bi = S1002-R50B	0.76
15. PG-FM83	Este III D1 525-450 B.C.	T. 83, Inv. 49	Fragment	L = 0.45; h = 0.3	Brown/amber	S8505-Y20R	0.03
16. PG-GO3-B-Bi	Este III D1 525-450 B.C.	T. 83, Inv. 59	Globular	L = 0.75; h = 0.52; d = 0.58	Blue with white eyes	Bi = S1002-Y50R; B = S6030-R80B	0.17
17. PG-GONM-Bi	Este IIID1 525-450 B.C.	T. 86, Inv. 27	Globular with residual eyes decoration	L = 1.9; h = 0.8	Black/brown	N = S8502-Y	1.86
18. PG-FM89	Este III D1 525-450 B.C.	T. 89, Inv. 62bis	Fragment	L = 1.38; h = 0.5	Brown/amber	S8502-Y20R	9.58
19. PG-AVT	Este IIID1 (525-450 B.C.), probably beginning 5th century	T. 97, Inv. 7	Annular	L= 2.18. h = 0.86; d = 1.03	Transparent green with a white weathered surface	Weathered = S0502-Y; Int. = S0520-G30Y	2.8
20. PG-GVA97	Este IIID1 (525-450 B.C.), probably beginning 5th century	T. 97, Inv. 17ter	Globular	L = 1.36; h = 0.91; d = 0.53	Transparent with a yellow weathered	S2020-Y20R	1.58
21. PG-FVA97	Este IIID1 (525-450 B.C.), probably beginning 5th century	T. 97, Inv. 69 and 69bis	Fragment	L = 1.2; h = 0.57	Transparent green - blue	S0505-B	0.2
22. PG-GO6B-Bi	Beginning Este IIID2 (450-350 B.C.)	T. 106, Inv. 52	Globular with probably 4 eyes	L = 1.40; h = 0.97; d = 0.4	Blue with white eyes	B = S5540-R90B; Bi = S1502-Y50R	1.72
23. PG-FA	Beginning Este IIID2 (450-350 B.C.)	T. 106, Inv. 108	Fragment	L = 0.64; h = 0.47	Blue	Weathered = S3050-R60B; Int = S5540-R70B	0.11

24. PG-SB	Transition Este III C/Este D1, around 525 B.C.	T. 108, Inv. 2	Disc - shaped with 5 horns	L = 2.95; h = 1.22; d = 0.51	Blue	S4020-B10G	5
25. PG-FN	Transition Este III C/Este D1, around 525 B.C.	T. 108, Inv. 40	Fragment	L = 0.73; h = 0.6	Black	S8005-Y80R	0.33
26. PG-GOB8	Transition Este III C/Este D1, around 525 B.C.	T. 108, Inv. 41	Globular with 3 eyes	L= 0.70; h= 0.53; d = 0.28	Dark blue	S7010-Y30R	0.22
27. PG-FGi8	Transition Este III C/Este D1, around 525 B.C.	T. 108, Inv. 48	Fragment	L = 0.98; h = 0.51	Transparent yellow	S2050-Y30R	0.21
28. PG-GAT1	Este IIIC 575-525 B.C.	T. 121, Inv. 4	Globular	L = 0.92; d = 0.29; h = 0.68	Transparent blue	S3060-B20G	0.63
29. PG-AB	Este IIIC 575-525 B.C.	T. 121, Inv. 4	Annular	L = 0.94; h = 0.61; d = 0.42	Blue	S6030-R80B	0.45
30. PG-AB½	Este IIIC 575-525 B.C.	T. 121, Inv. 4	Annular	L = 0.88; h = 0.6; d = 0.34	Blue	S6030-R80B	0.25
31. PG-AB9a-b-c-d	Este IIID1 525-450 B.C.	T. 127, Inv. 39	Annular	**a**: L = 0.34; d = 0.18; h = 0.3; **b**: L = 0.34; h = 0.23; d = 0.24; **c**: L = 0.33; d = 0.18; h= 0.27; **d**: L = 0.36; h= 0.28; d = 0.23	Blue	S6030-R70B	a = 0.02; b = 0.007; c = 0.02; d = 0.02
32. PG-ABOa-b	Este IIID1 525-450 B.C.	T. 127, Inv. O	Annular	**a**: L = 0.3; d = 0.15; h = 0.24; **b**: L = 0.3; h = 0.18; d = 0.2	Blue	S6030-R80B	a = 0.005; b = 0.006
33. PG-AAB	Este IIID1 525-450 B.C.	T. 127, Inv. O	Globular	L = 0.71; h= 0.66; d = 0.32	Blue	S4050-R80B	0.25
34. PG-AB8	Este IIID1 525-450 B.C.	T. 127, Inv. 38	Annular	L = 0.35; d = 0.19; h = 0.28	Blue	S6030-R80B	0.015

***Figures 2-22**: Optical microscope (OM) images of the glass beads from the Piovego cemetery analyzed in this work. For each figure, labels, provenance (T. = grave) and inventory number (Inv.) of the samples are reported. Images 7-10, 14, 16, 20-21 are courtesy of S. Castelli, Padova University. In the pink scale, 1 space corresponds to 1 mm.*

Fig. 2. PG-FVA67, T. 67, Inv. 35 IG 149781.

Fig. 3. PG-FGi, T. 47, Inv. α IG 34923.

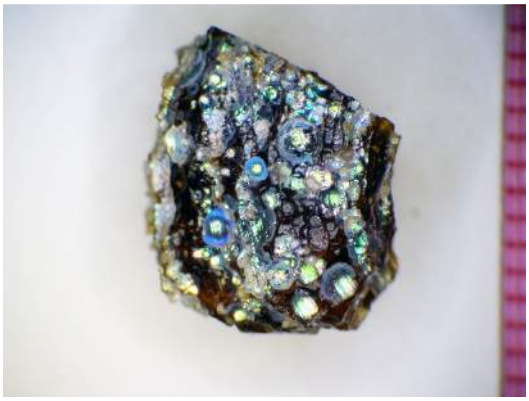

Fig. 4. PG-FM14, T. 14, Inv. 26 IG 152910.

Fig. 5. PG-FN, T. 108, Inv. 40.

Fig. 6. PG-FA, T. 106, Inv. 108.

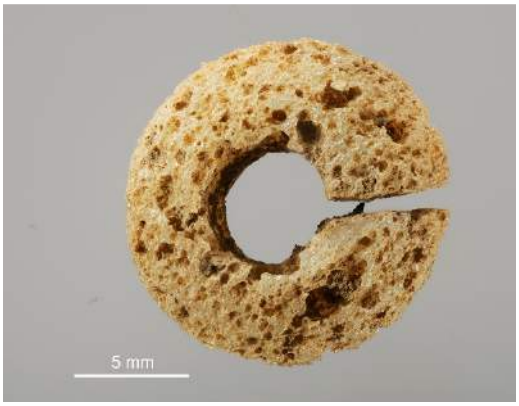

Fig. 7. PG-GVA97, T. 97, Inv. 17ter.

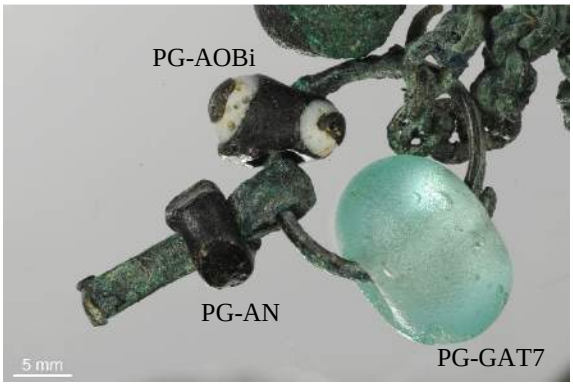

Fig. 8. PG-AOBi, AN, GAT7, T. 47, Inv. α IG 34923.

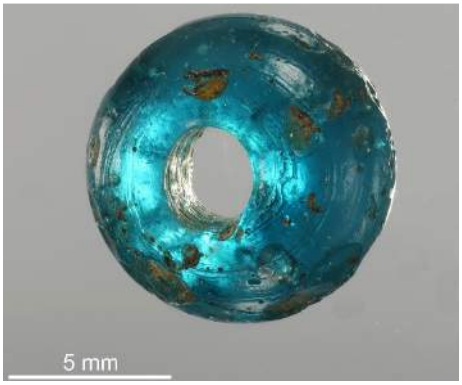

Fig. 9. PG-GAT1, T. 121, Inv. 4.

Fig. 10. PG-GOA-B-Bi, T. 83, Inv. 48.

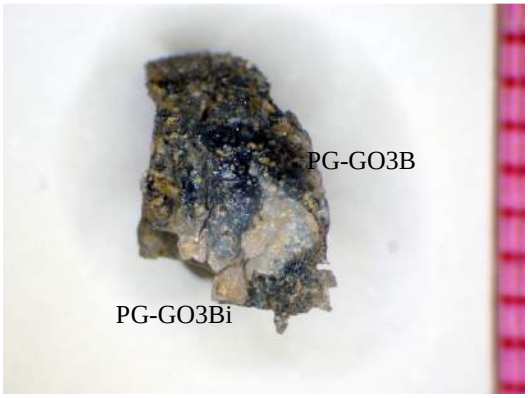

Fig. 11. PG-GO3B-Bi, T. 83, Inv. 59.

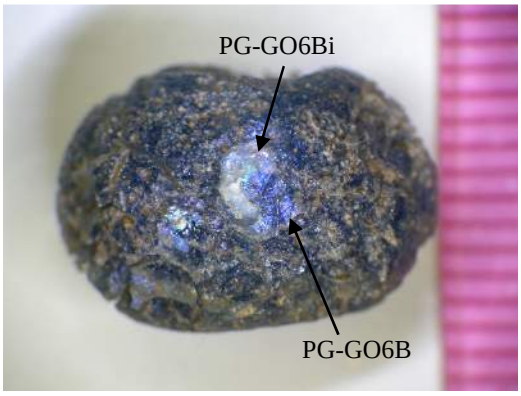

Fig. 12. PG-GO6B-Bi, T. 106, Inv. 52.

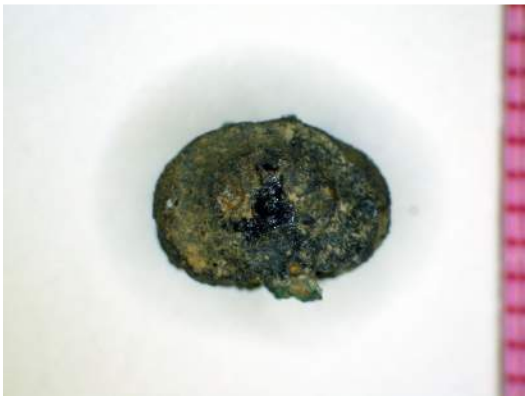

Fig. 13. PG-GOB8, T. 108, Inv. 41.

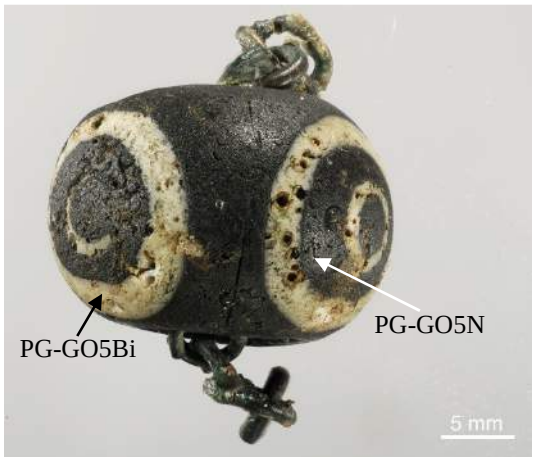

Fig. 14. PG-GO5Bi-N, T. 15, Inv. 19 IG 152929.

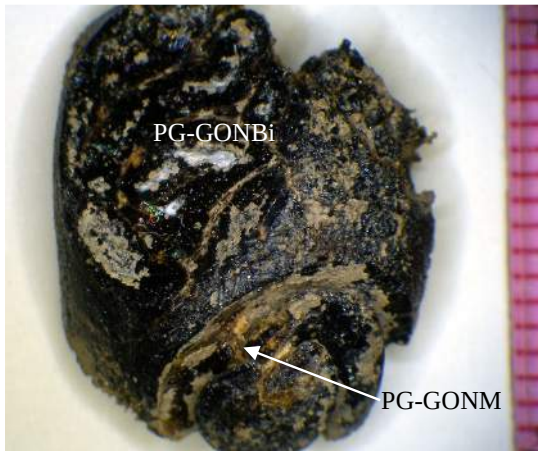

Fig. 15. PG-GONM-Bi, T. 86, Inv. 27.

Fig. 16. PG-AVT, T. 97, Inv. 7.

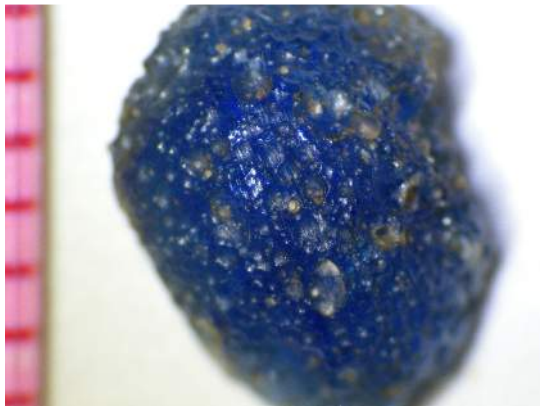

Fig. 17. PG-AAB, T. 127, Inv. O.

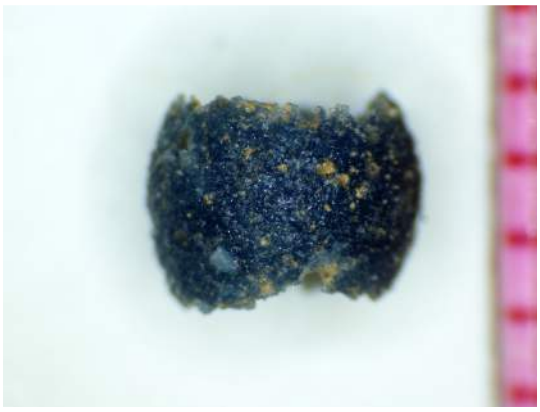

Fig. 18. PG-AB9-d, T. 127, Inv. 39.

Fig. 19. PG-AB, T. 121, Inv. 4.

Fig. 20. PG-CM, T. 1bis, Inv. 43.

Fig. 21. PG-SB, T. 108, Inv. 2.

Fig. 22. PG-FUA, T. 14, Inv. 19 IG 152903.

3.2.3 Villa di Villa

The vitreous materials found in the site are very different for typology and dating. They are composed by 2 annular beads, 1 globular bead with eyes decoration, 1 melon bead, 3 arm rings and 1 rod fragment with a semi-circular section. The ornaments were all unearthed from secondary deposition layers (stratigraphic units, SU), dated to widely different chronological ranges.

The complete details (dimension, weight, NCS color etc.) and images of the materials are collected in Table 2 and Figures 23-30, respectively.

Below is a summary of the samples' labels and the main characteristics of each find, together with typological comparisons from the literature:

- **VV-AB and VV-AB6** are two blue annular beads unearthed from SU 2 belonging to the protohistoric phase of the site (fig. 23 and 24). The annular shape is very common from the Bronze Age throughout the Iron Age and, therefore, no significant chronological information may be inferred from the typology.
- **VV-BRB2, VV-BRB5 and VV-BRB9** are three dark blue bracelet fragments coming from SU 2, SU 19 and SU 4, respectively (fig. 25-27). Samples VV-BR2 and VV-BR5 are characterized by a complex rib decoration similar to typology 8 (a and c) of Haevernick 1960. VV-BRB5 was found in the layers belonging to the phase 1 structure (2^{nd} – 1^{st} half of the 1^{st} century B.C.) and consequently dated to the 2^{nd} century B.C. due both to the lying position and the typology of the object. Fragment VV-BRB2 is dated to same period as it has the same typology of sample VV-BRB5. Typology Hevernick 8c is also attested in one bracelet from Aquileia (Mandruzzato 2008, cat. N. 43) dated to the 2^{nd}-1^{st} century B.C. This typology is considered of central European provenance and started spreading north of the Alps between the end of the 3^{rd} and the beginning of the 2^{nd} century B.C. (Tarpini 2007) with its maximum development in La Tène D period (Venclova 1989; Vellani 1997). In Italy, the typology is present in the Cisalpine area and in particular in the Emilia-Romagna region (Vellani 1996; Tarpini 2007). The BRB9 spaceman is a smaller undecorated fragment of a D section arm ring, belonging to typology 3a of Haevernick 1960, dated to the 3^{rd}-2^{nd} century B.C., based on the typology and context. This is the most common

typology and of longest duration, from the La Tène D, 600-500 B.C. (Haevernick 1960) to the Late Roman period (Roffia 1993). It is mostly diffused in the Danube and Rhine area (Karwowski 2004; Venclová et al. 2009; Březinová et al. 2013) whereas in Italy it is attested in the Lombardy-Piedmont area (Vellani 1996) and in Aquileia (Mandruzzato 2008, cat. 41-42).

- **VV-GGi** is an opaque yellow globular bead with four blue and white eyes (two of which double), a typology well attested during the Iron Age in the entire ancient world and also in the north Adriatic area, as Altino (Gambacurta 1987) and Aquileia (Mandruzzato 2008, cat. 85-86). The bead is a sporadic survey but it could be dated between the end of the 6th and the beginning of the 4th century B.C. according to/given its context. Unfortunately, to preserve the conservation of the bead, only a small fragment from the yellow body was sampled (fig. 28).
- **VV-FBT-Gi-Bi-B** is a transparent (T) rod fragment with a semi-circular section, decorated by pale blue (B), yellow (Gi) and white (Bi) glass spirals (fig. 29), probably used as a parietal decoration. This hypothesis is supported not only by the semicircular section with the undecorated flat side, but also by the marine shells (murex pecten) found in the SU together with the find, and similarly associated to glass rods applied in wall decorations of the 1st century A.D. as in Aquileia (Chiesa Sena et al. 1998). This use seems to have ancient origins and it was attested since the 1st century B.C. (Sear 1975; Barbet 1981) and not over the first half of the 1st century A.D. The rod here analysed comes from SU 11 and the provenance context allows dating the find between the end of the 1st century B.C. and the beginning of the 1st century A.D. All four different glass colours were sampled.
- **VV-MB** is a turquoise melon bead with marked ribs and a slender shape, unearthed from SU 4 (fig. 30). The typology is known in Northern Italy since late protohistory (Gambacurta 1986) but only in the 1st-2nd century A.D. it became largely used (Cavada 1986), until the 4th-5th century A.D. (Tori et al. 2006). Interestingly, a pale blue melon bead was also found in grave 16 of the S. Floriano di Polcenigo (PN) cemetery (Vitri et al. 2006), dated to the 4th-5th century A.D., 10 km away from the Villa di Villa site. Several turquoise melon beads are also attested in Aquileia and dated to the 1st-4th century A.D. (Mandruzzato 2008, cat. 71-74).

Even though the bead comes from a secondary deposition layer and its dating is not certain, the site excavations attested a lack of inhabitation between the end of the 1st century A.D. and the end of the 3rd century A.D. Moreover, the melon bead typology is not attested north of the Po before the late protohistory. According to these reasons, the sample here investigated could be doubtfully dated from the 1st century B.C. to the 1st century A.D. or to the 3rd – 4th century A.D.

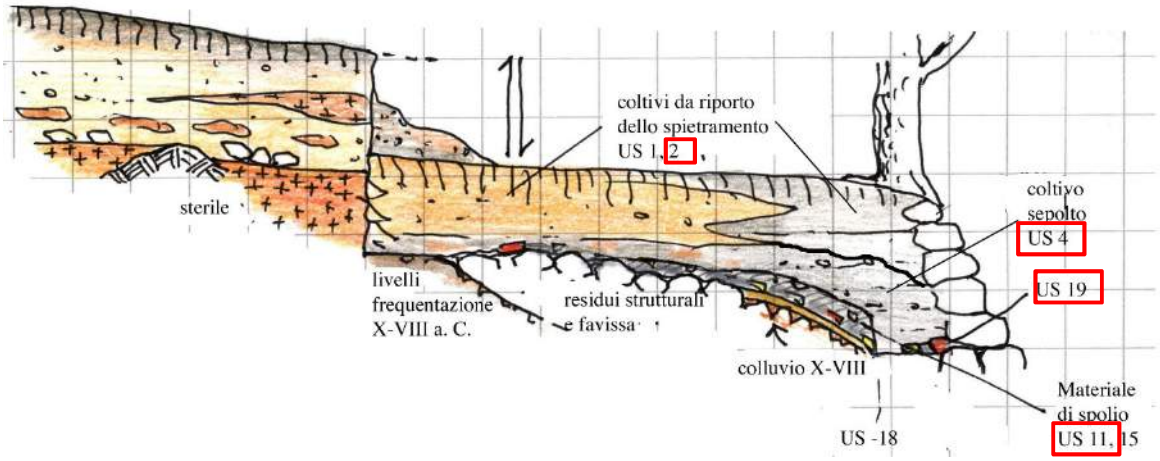

Fig. 3.2.. : Section of the examined area of the Villa di Villa site. In the red squares, the SU of provenance of the finds are reported (image courtesy of Stefano Boaro).

Table 3.2.5: Glass ornaments from the Villa di Villa site analysed in this work. (Inv. = inventory number assigned by the University of Padova after the excavations; US = stratigraphic unit; S = sporadic; L = mean width; h = mean height; d. = mean hole diameter; th. = thickness; int. = internal glass).

Samples	Ages	Prov.	Typology	Dim. (cm)	Color	NCS color	Wt. (g)
VV-BRB2	2nd B.C.	Inv. 3012 IG 311.209B, SU 2	Bracelet fragment	L= 1.44; h = 1.21; th. = 0.52	Blue	S4550-R70B	1.12
VV-BRB5	2nd B.C.	Inv. 1635 IG 311.256, SU 19	Bracelet fragment	L = 3.45; h = 1.89; th. = 0.68	Blue	S4550-R70B	5.37
VV-BRB9	3rd-2nd B.C.	Inv. 1539 IG 311.253, SU 4	Bracelet fragment	L = 2.25; h = 1.52; th. = 0.82	Blue	S4550-R70B	2.76
VV-GGi	Late 6th-Early 4th B.C.	Inv. S2 IG 311.235	Globular bead	L = 1.34; h = 0.89; d = 0.7	Yellow with blue and white eyes	Gi: S1050-Y10R; Bi: S1000-N; Blue: S2565-R80B	1.74
VV-MB	Early-Late Roman Age	Inv. 374 IG 311.181, SU 4	Melon bead fragment	L = 1.65; h = 1.29; d = 0.93	Pale blue	Weathered: S3030-B30G; Int.: S2020-Y20R	1.44
VV-AB	Final Bronze Age-Early Iron Age	Inv. 300 IG 311.239, SU 2	Annular bead fragment	L = 0.83; h= 0.5; d = 0.5	Blue	S2060-R80B	0.2
VV-AB6	Final Bronze Age - Early Iron Age	Inv. 2006 IG 311.254, SU 2	Annular bead fragment	L = 0.64; h = 0.38; d = 0.37	Blue	Weathered: S2050-Y40R; Int.: S7020-R80B	0.06
VV-FBT-Gi-Bi-B	1st B.C-1st A.D.	Inv. 311.402 IG 1577, SU 11	Rod fragment with semicircular section	L= 0.28; h = 2.33; th. = 0.67	Transparent with blue, yellow and white spirals	T: S0505-B20G; Bi: S1002-R50B; Gi: S0530-Y; B: S1040-B	2

***Figures 23-30**: Optical microscope (OM) images of the glass ornaments from the Villa di Villa site analyzed in this work. For each figure, labels, provenance (US) and inventory number of the samples are reported. Images 26, 28, 29-30 are courtesy of S. Castelli, Padova Univerity. In the scale, 1 space corresponds to 1 mm.*

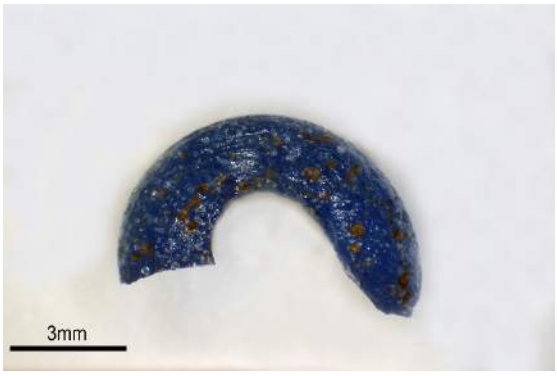

Fig. 23. VV-AB, Inv. 300 IG 311.239, SU 2.

Fig. 24. VV-AB6, Inv. 2006 IG 311.254, SU 2.

Fig. 25. VV-BRB2, Inv. 3012 IG 311.209B, SU 2.

Fig. 26. VV-BRB5, Inv. 1635 IG 311.256, SU 19.

Fig. 27. VV-BRB9, Inv. 1539 IG 311.253, SU 4.

Fig. 28. VV-GGi, Inv. S2 IG 311.235, sporadic survey.

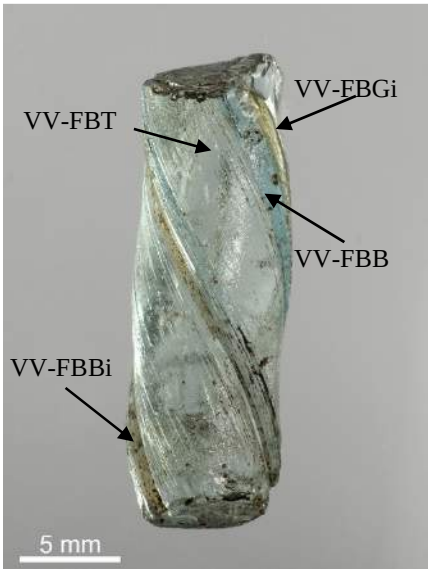

Fig. 29. VV-FBT-Gi-Bi-B, Inv. 311.402 IG 1577, SU 11.

Fig. 30. VV-MB, Inv. 374 IG 311.181, SU 4.

CHAPTER 4

ANALITHYCAL TECHNIQUES

The ornaments were first studied macroscopically to collect their external characteristics, such as dimension and color, by means of NCS (Natural Color System) tables. The whole objects were weighed and photographed. They were then analyzed under the optical microscope (OM) to observe the conservation status of the glass and choose the more representative sample from the examined object. The sampling of the bodies and the decoration of the ornaments was performed using a scalpel.

In order to obtain a flat surface for the chemical and textural analysis, 130 micro-samples (ca. 200-500 μm^2) were embedded in epoxy resin and manually lapped using 800, 1200, 2400 and 4000 grit SiC papers. Subsequently, samples were gently cleaned with ethanol and then smoothed by means of an automatized polisher (Planopol-V-Struers). The polishing was achieved using first 6 and then 1 micron size diamond suspension (Dp-suspension-Struers) on a silk cloth for 5 minutes at 300 RPM. The specimens, immersed in a colloidal silica suspension, were finally polished by means of an automatic vibratory polisher.

The samples prepared as indicated above were analyzed by SEM-EDS, EPMA-WDS and micro Raman spectroscopy, whereas non-invasive X-Ray Powder Diffraction was performed directly on the ornaments surfaces.

4.1 Optical microscopy (OM)

Stereoscopic optical microscopy (OM) was carried out on whole objects in order to study the weathering conditions, morphologic characteristics, traces of manufacturing and to collect detailed photographic images of the ornaments. The microscope used at the Geosciences Department of the Padova University is a Nikon SMZ 645 with a Photonic Optics led illumination, equipped with a digital camera for images collection (Nikon Coolpix 6.1).

4.2 Scanning Electron Microscopy (SEM-EDS)

Scanning Electron Microscopy (SEM) enabled the study of the morphological and textural characteristics of the glass matrix. In particular, backscattered electrons (BSE) images were used to detect the contrast between areas with different chemical compositions and to evaluate the weathering conditions of the samples. The chemical analyses on the crystalline inclusions dispersed in the amorphous phase were performed by x-ray energy dispersive spectrometer (EDS). SEM-EDS experiments were performed at the Department of Earth Science of the University of Milano using a Cambridge Stereoscan 360 scanning electron microscope connected to a Link ISIS X-ray energy dispersive spectrometer (EDS). It was run at 20 kV accelerating potential and with a beam current between 0.2 and 0.9 nA and a spot size of about 2 micron. The count time applied for the EDS analysis is 60 s. Internal standards (Jade, MgO, Al_2O_3, Orthoclasio, Wollastonite, pure elements) were used for the EDS measurements and data were automatically processed for ZAF correction.
Measurement precision with such instrumental conditions starts at about 0.2% for Na; the figure decreases for heavy elements, also according to the lateral resolution.
The analyses were performed on the polished sectioned samples, coated with a thin carbon layer.

4.3 Wavelength – dispersive electron probe microanalysis (EPMA-WDS)

Quantitative chemical analyses of the glass phase and mineral inclusions were performed at the CNR-IGG laboratory in Padova, using a CAMECA SX50 electron microprobe fitted with four vertical wavelength-dispersive spectrometers (WDS) and one energy dispersive spectrometer (EDS). The working conditions used were accelerating voltage of 20 kV, beam current intensity of 2nA for Na, K, Al, Si and of 20 nA for P, S, Cl, Ca, Ti, Mn, Fe, Co, Ni, Cu, Zn, As, Sn, Sb, Pb and counting times of 5-10-5 s on background-peak-background, respectively. The spot size of the beam was about 1-2 µm for the samples with a large number of inclusions, whereas to prevent the known migration phenomenon of alkalis under the electron beam, in the homogeneous samples a 10 µm defocused electron beam was used. Synthetic pure oxides were used as standards for Al, Fe, Ni and Sn, synthetic AsGa for As, a

synthetic MnTi oxide for Mn and Ti, diopside for Si, Ca and Mg, plagioclase for Na, vanadinite for Cl, galena for Pb, orthoclase for K, apatite for P, sphalerite for S and Zn, Sb_2S for Sb, and pure elements for Co and Cu. The analyzer crystals were: LIF (LiF) for Mn, Fe, Co, Ni, Cu and Zn; TAP ($C_8H_5O_4Tl$) for Na, Mg, Al, Si, P and As; PET ($C_5H_{12}O_4$) for S, Cl, K, Ca, Ti, Sn, Sb and Pb. The results were processed using the PAP (CAMECA) software for the ZAF corrections. Measurement precision was within 1% for major elements, about 3-4% for minor elements and about 8% for trace elements. The lowest detection limits of EMPA with these analytical conditions were approximately 0.1 wt% for the major and minor elements, and varied from 250 ppm for Co to 1400 ppm for Pb in trace elements. The results of the EPMA chemical analyses are expressed as weight percent (wt%) of element oxides, calculated as a mean of 5÷10 point analysis with the relative standard deviations (SD).
The analyses were performed on the polished sectioned samples coated with a thin carbon layer.

4.4 X-Ray Powder Diffraction (XRPD)

X-ray diffraction analyses were performed to identify the crystalline phases dispersed in the glass matrix. The measurements were acquired directly on the beads surfaces in a non-invasive mode, with a methodology developed in previous studies (Artioli et al. 2008). XRD data were obtained at the Geosciences Department of the Padova University using a computer-controlled Philips X'Pert PRO, with Bragg-Brentano θ- θ geometry, equipped with an X'Celerator detector. The normal focus Cu X-Ray tube (Cu $K\alpha_1$ λ = 0.154056 nm) operated at 40 kV and 40 mA. Data were recorded in the 3°-80° 2θ range, in step scan mode with step width increments of 0.017° 2θ and a step counting time of 100 s. Data were processed by X'Pert HighScore (PANalytical software).

4.5 Single-Crystal X-Ray Diffraction

Single-Crystal X-ray diffraction analyses were carried out to identify the crystalline phases dispersed in the glass matrix of samples which did not allow operating on the whole ornament (see par. 4.4). The measurements were acquired on glass fragments of about 1 mm. The

analyses were performed at the Geosciences Department of the Padova University using a single-crystal diffractometer Agilent Supernova equipped with a micro-X-ray source (using the Kalpha of Mo) working at 50 kV and 0.8 mA with a spot size of 0.11 mm. The instrument is also equipped with a Pilatus 200 K detector (Dectris) allowing very fast measurements accompanied by high sensitivity and dynamic range. Data were collected in micro-X-ray powder diffraction mode due to the presence of crystalline inclusions in the analyzed material.

4.6 Micro Raman Spectroscopy

Raman spectroscopy was performed on the polished sectioned samples in order to characterize unreacted raw materials and/or newly formed crystals dispersed in the amorphous phase. Indeed, the XRD analysis enabled the identification of the major mineral phases in the glass while the smaller and less abundant inclusions could not be detected.

The analyses were carried out using two different instruments. Some spectra were obtained at the Department of Scientific Research of the Metropolitan Museum of Art (New York City, NY) by means of a Bruker Senterra Raman microscope using 785 and 480 nm excitation lasers (spot size ~ 2 µm) with power ranging from 4 to 40 mW and by focusing with a 50 x objective (Olympus BX). The acquisition time for a single spectrum was 30 s, no spectra accumulation was used.

Other spectra where obtained at the Department of Chemistry Science of the Padova University using a DXR Thermo Scientific Raman microscope, equipped with a diode-pumped solid state 532 nm laser, operating at a power variable from 8 to 10mW, with a spectral resolution in the range of 2.7–4.2 cm^{-1} and a spatial resolution of 1.1 µm. The acquisition time adopted was 5 s for 32 or 64 scans accumulation. The point analyses were performed with a 50 x LWD (Low Working Distance) objective.

The attribution of the Raman signatures of crystalline phases was made by comparison with data in the literature as well as in the on-line RRUFF database (http://rruff.info).

CHAPTER 5

RESULTS

This chapter presents the results of the chemical, textural and mineralogical analysis of the samples. The data, grouped by archaeological site of provenance, will be discussed in Chapter 6.

5.1 Lipari and Salina

- *Sand and flux composition*

The results of the EPMA chemical analysis (Table 5.1) show that all samples are silica glasses with SiO_2 ranging from 57.10 to 77.17 wt%. The alkali content is extremely variable: Na_2O varying from 0.76 to 20 wt%, K_2O from 2.01 to 17.23 wt%, CaO from 1.30 to 12 wt% and MgO from 0.46 to 8.20 wt%. This clearly shows that different glass recipes were used; actually, considering the potassium, magnesium and sodium values (Fig. 1a-b), two compositional classes are present. The first one presents levels of K_2O ranging from 2 to 3.6 wt%, MgO from 4.9 to 8.2 wt% and Na_2O from 15.3 to 20 wt% as in the High Magnesium Glasses (HMG) obtained using soda-rich plant ashes as flux (Henderson 1989, 2000; Tite et al. 2003). Also the Ca and P contents fall within the compositional range typical for these glasses: CaO = 4.5÷9.5 wt% and P_2O_5 = 0.10÷0,30 wt%. Fifteen samples from Lipari and all those from Salina are HMG glasses. The second class is composed by fifty samples from Lipari, 48 of which containing 6.12÷12.38 wt% of K_2O, 0.47÷1.3 wt% of MgO and 7.37÷8.83 wt% of Na_2O, typical of the Low Magnesium High Potassium Glasses (LMHK) produced with mixed alkali plants ashes as flux (Angelini et al. 2004, 2010a; Brill 1992; Henderson 1988; Santopadre and Verità 2000; Towle et al. 2001). The calcium contents ranging from 1.30 to 2.90 wt% (CaO) is actually low for ash-based glasses but typical of the LMHK class, for which the use of leached plant ashes is hypothesized (Brill 1992; Tite et al. 2006). The highest levels of Ca (CaO = 8÷12 wt%) in the white glasses decorations are due to the presence of Ca silicates finely dispersed in the matrix (see below). The P content (P_2O_5 = 0.06÷0.34 wt%) is in the

range of the LMHK glasses. The Na_2O/K_2O ratio (Fig. 1b) ranging from 0.36 to 1.35, is typical for the use of mixed alkali plants ashes as flux.

Interestingly, the other two glasses from Lipari (L312AA2 and L18AA1) have a lower Na_2O/K_2O ratio (0.04÷0.14, fig. 1b, pink circles) due to a particularly high K content (K_2O = 17.23 and 16.05 wt%, respectively) and a lower Na amount (Na_2O = 0.76 in L312AA2 and 2.20 wt% in L18AA2). They are glasses produced using plant ashes rich in K as flux. Interestingly, the Ca and Mg contents are low (CaO = 2.06 and 2.18 wt%, MgO = 0.74 and 0.69 wt%), similarly to the other LMHK glasses. This glass type has been identified as a subgroup in the Frattesina productions (Angelini et al. 2010). For these reasons, the compositional class has been named here LMHK- K class.

Interestingly, the only MBA 1-2 sample is from Lipari and is an HMG glass; all the MBA3 samples are from Salina and are HMG glasses; the only RBA glass is from Lipari but, unfortunately, it is weathered and will not be considered in the discussion; all the FBA samples are from Lipari, 15 of them are HMG glasses while the other 50 are LMHK. This is evident in the MgO *vs* K_2O and Na_2O vs K_2O plots (fig. 5.1a-b) where provenance and ages of the finds are reported. For these reasons, considering that the only MBA 1-2 glass and all the FBA glasses are from Lipari and all the MBA 3 glasses are from Salina, in the other plots we have considered only compositional classes and ages, not provenances.

The use of sand as a source of silica in the majority of the samples is testified by the high quantity of Al and Fe as shown in fig. 5.2a and Tab. 5.1, even though in some blue-black glasses the high Fe contents could be linked to the coloring agents. However, a few samples (4 blue samples and 3 yellow/brown samples from Lipari) are characterized by particularly low Al and Fe contents ($Al_2O_3 < 1$ and $FeO < 0.5$) which could suggest the use of a pure sand or quartzite as a source of silica. They are all HMG glasses from Lipari, in detail 4 blue glasses dated to the FBA 1-2; one MBA 1-2 glass, brown colored; one FBA 1-2 brown glass and one FBA 1-2 yellow glass.

Four glasses from Salina show particularly high contents of Al and Fe in comparison with those from Lipari: two blue samples (SALCFR1 and SALFAS) and the white glass (SALCFR4-Bi) have 4.42, 4.47 and 3.10 wt% of Al_2O_3, respectively; the blue bead SALCFR3 has 3.25 wt% of FeO (fig. 5.1c).

Considering the MnO *vs* Sb_2O_3 contents they are mostly under the detection limits or present in low amounts (fig. 5.1 bis). Antimony, when present, is related to the coloring/opacifying agents. Manganese is present in significant amounts only in two blue samples from Salina, SALFAS and SALCFR1, and in one yellow/brown sample from Lipari, L311GM1, presenting 0.17, 0.16 and 0.83 wt% of MnO, respectively. Titanium levels are low in all glasses, ranging from 0.03 to 0.14 wt%.

The amounts of all other oxides are mainly linked to the color and the opacity of the samples.

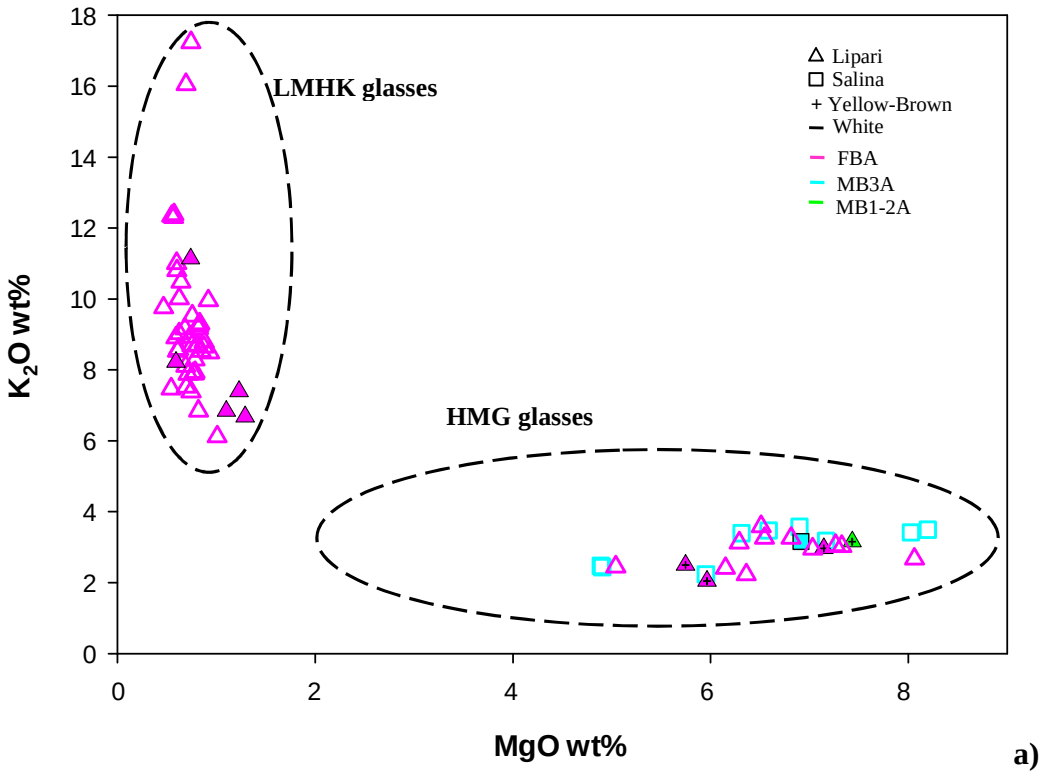

Fig. 5.1. ***a)*** *and* ***b)*** *MgO* vs K_2O *and* Na_2O vs K_2O *contents of the glass phase in the analyzed samples, respectively. Dotted lines are the conventional areas of the compositional classes (geometric shapes = provenances; colors = ages; empty symbols = blue beads; crossed full symbols = yellow-brown beads; black- bordered full symbols = white beads).* ***c)*** *FeO* vs Al_2O_3 *contents of the glass phase in the analyzed samples. (geometric shapes = compositional classes; colors = ages; empty symbols = blue beads; crossed full symbols = yellow-brown beads; black- bordered full symbols = white beads).*

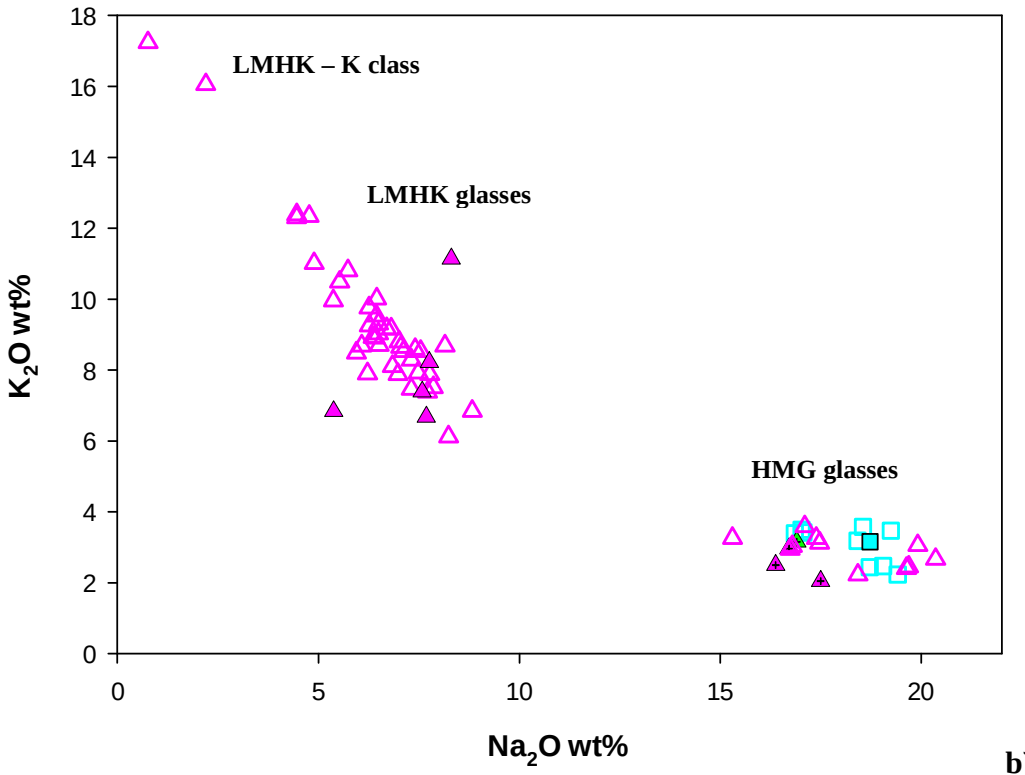
LMHK – K class
LMHK glasses
HMG glasses
K2O wt%
Na2O wt%
0
2
4
6
8
10
12
14
16
18
0
5
10
15
20

b)

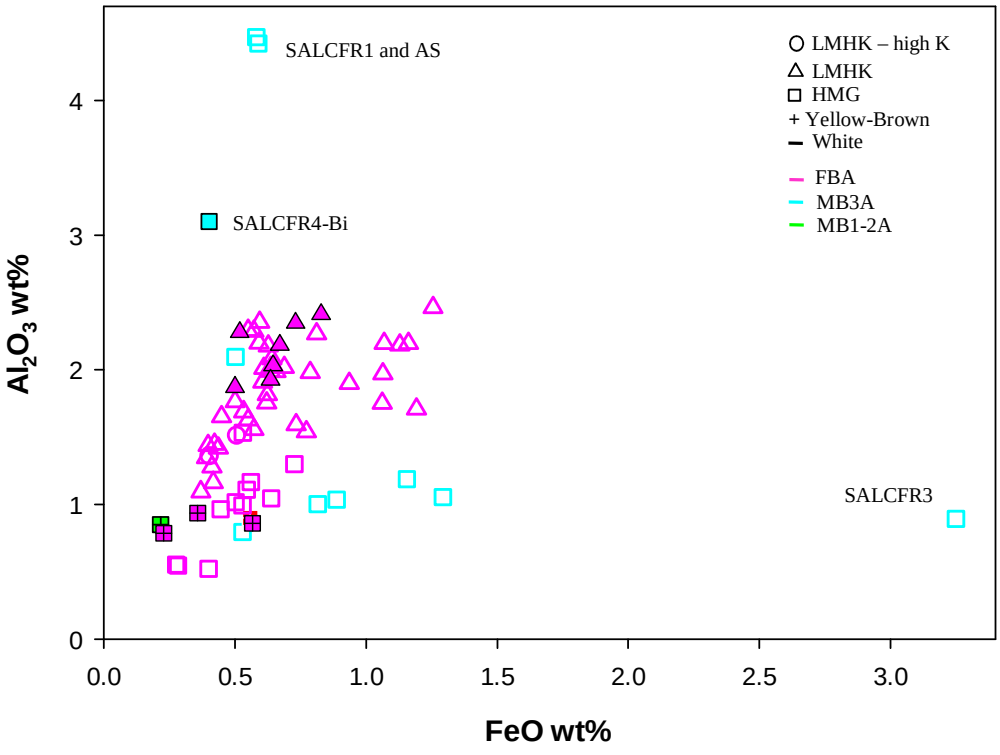
SALCFR1 and AS
SALCFR4-Bi
SALCFR3
LMHK – high K
LMHK
HMG
+ Yellow-Brown
White
FBA
MB3A
MB1-2A
Al2O3 wt%
FeO wt%
0
1
2
3
4
0.0
0.5
1.0
1.5
2.0
2.5
3.0

c)

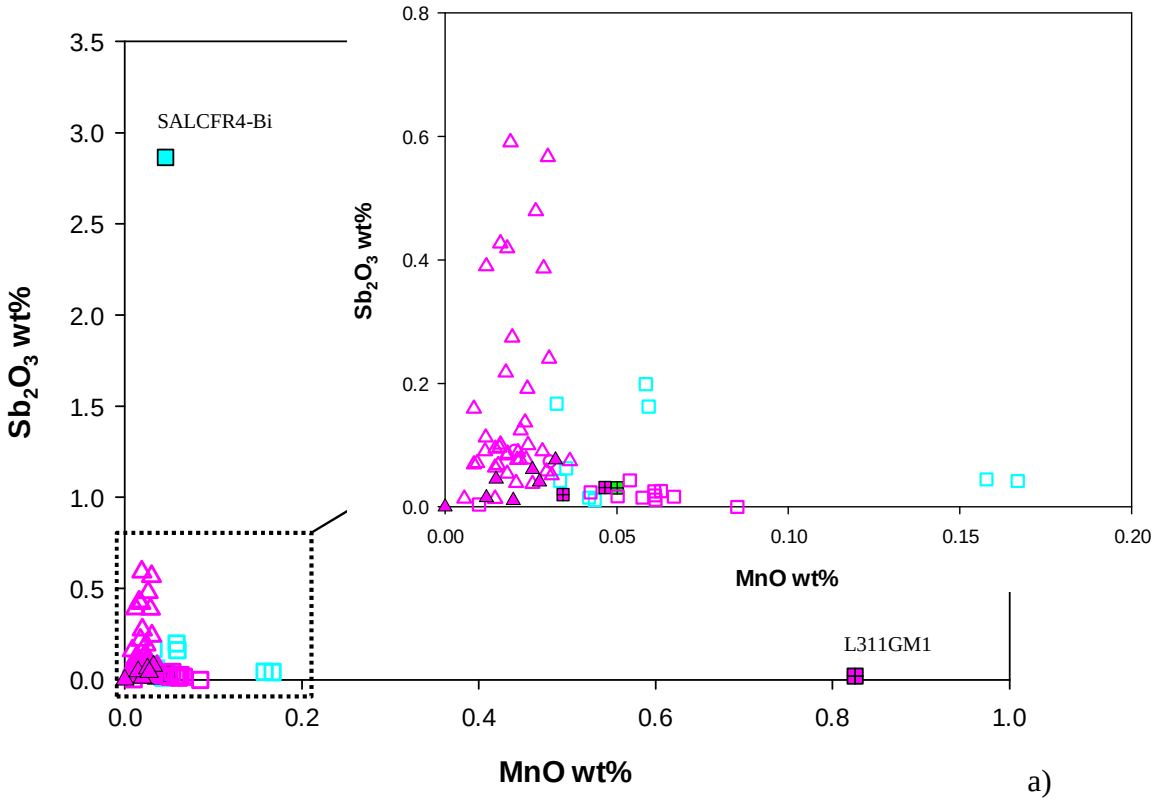

Fig. 5.1 bis: *MnO* vs *Sb_2O_3 contents of the glass phase in the analyzed samples. A detail of the dotted square is reported (geometric shapes = compositional classes; colors = ages; empty symbols = blue beads; crossed full symbols = yellow-brown beads; black- bordered full symbols = white beads).*

- *Colorants and opacifiers*

Blue glasses

Most of the beads are blue colored with different shades, due to Co and/or Cu. Observing the CoO *vs* CuO contents of the blue beads in fig. 5.2, three compositional groups are clearly identified. The first group (1) is characterized by high levels of Cu (CuO = 2.8 ÷5 wt%) and Co under the detection limit (CoO < 0.03 wt%). This group is represented by 26 LMHK glasses (including the 2 LMHK- K class) from Lipari. The second group (2) is composed by Co-colored glasses (CoO = 0.05÷0.25 wt%) and with Cu contents ranging from 0.1 to 2 wt%. They are 13 LMHK glasses from Lipari and 6 HMG glasses from Salina. The third samples' set (3) is formed of glasses colored by low contents of Cu (CuO = 0.5 ÷0.87 wt%) and Co under the detection limit (CoO < 0.03 wt%). They are 10 HMG glasses from Lipari. Two blue glasses from Salina, SALFFR and FR3 (black narrows in fig. 5.2), have very low contents of Co (CoO <0.03 and 0.03 wt%, respectively) and Cu (CuO = 0.18 and 0.06 wt%, respectively). However, the color may also be due to Fe, possibly in a reduced oxidation state, present in particularly high contents in SALCFR3 (FeO = 3.25 wt%) and in traces in SALFFR (FeO = 0.53 wt%). One blue sample from Salina, SALCFR4 B, has no Co or Cu and the only chromophore element is Fe (FeO = 0.50 wt%), probably in a reduced oxidation state.

Interestingly, the Cu contents in the LMHK and HMG glasses vary largely. In LMHK glasses, copper is very high in the copper colored glasses (group 1, CuO = 2.8 ÷5 wt%) and has significant levels in the Co-Cu colored ones, too (group 2), in which copper ranges from 0.1 to 2 wt% (CuO). Conversely, in HMG glasses, copper is definitely lower both in the copper colored glasses (group 3, CuO = 0.5 ÷0.87 wt%) and in the Co-Cu colored ones (CuO < 0.35 wt%, dotted line in fig. 5.2).

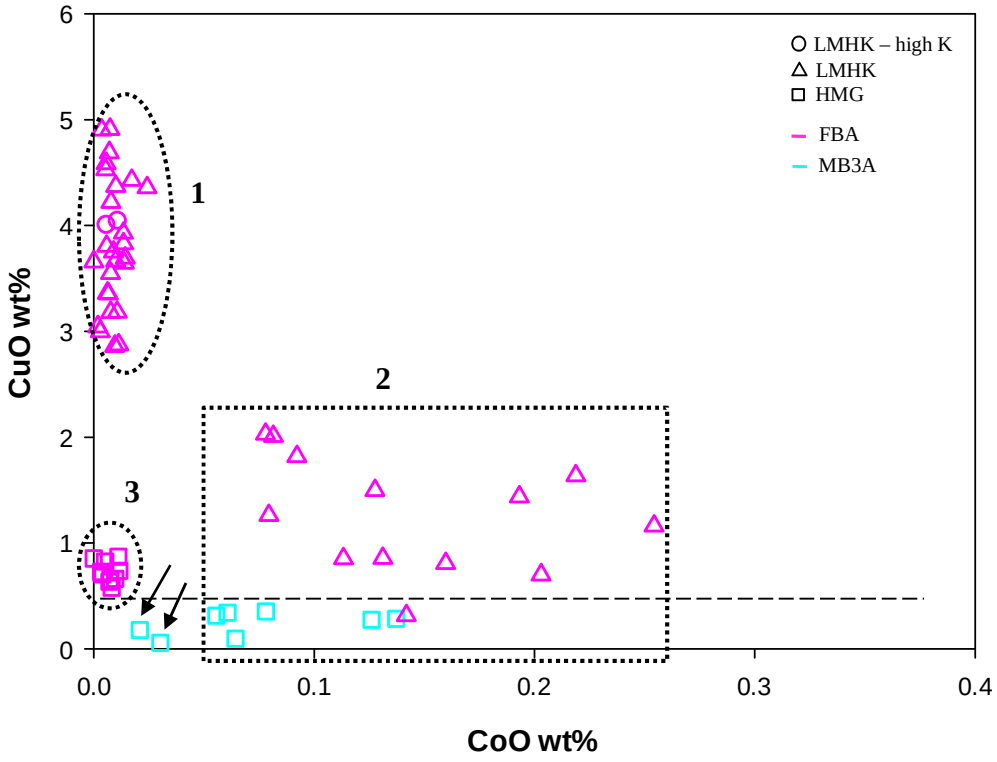

Fig. 5.2. CoO vs *CuO contents of the glass phase in the analyzed samples. Dotted lines highlight the three different compositional groups (geometric shapes = compositional classes; colors = ages; empty symbols = blue beads; crossed full symbols = yellow-brown beads; black- bordered full symbols = white beads).*

As regards the trace elements in the Co and/or Cu colored glasses, they vary depending on the different colorant sources. Cu-colored HMG glasses from Lipari have no trace elements correlated to the colorant. Cu-colored LMHK glasses from the same site have traces of Sb (Sb_2O_3 = 0.04÷0.14 wt%) and about one half of them of Sn, too (Sn_2O = 0.04÷0.35 wt%). Instead, the Co-colored glasses have various trace elements in the two compositional groups, LMHK and HMG, showing that different cobalt sources were used. In three HMG glasses from Salina, SALFA1-A2 and A4, Co is associated to Sb (Sb_2O_3 = 0.16÷0.20 wt%) and in SALFA1 and A4 to Pb, too (PbO = 0.12 wt%). SALCFR4 has no traces of Sb and Zn (values with the same magnitude of the detection limits). The other two HMG glasses from Salina, SALFAS and SALCFR1, present Ni (NiO = 0.12 and 0.11 wt%) and Zn (ZnO = 0.16 and 0.13 wt%) together with Mn (MnO = 0.17÷0.16 wt%, respectively) and high contents of Al (Al_2O_3 = 4.47 and 4.42 wt%, respectively). Conversely, Co-colored LMHK glasses have Cu contents ranging from 0.1 to 2 wt% and traces of Ni (NiO = 0.23÷0.64 wt%), As (As_2O_3 = 0.10÷0.47 wt%) and

Sb (Sb_2O_3 = 0.10÷0.6 wt%). Samples L314AN1-AN2-CO1 and XA also have significant Zn traces (ZnO = 0.06÷0.12 wt%). Sample L18DA has no As and presents traces of Pb (PbO = 0.12 wt%).

The Ni *vs* Sb_2O_3 contents of the Co-colored glasses (fig. 5.3), clearly distinguish HMG glasses from LMHK glasses which present higher contents of Ni and Sb.

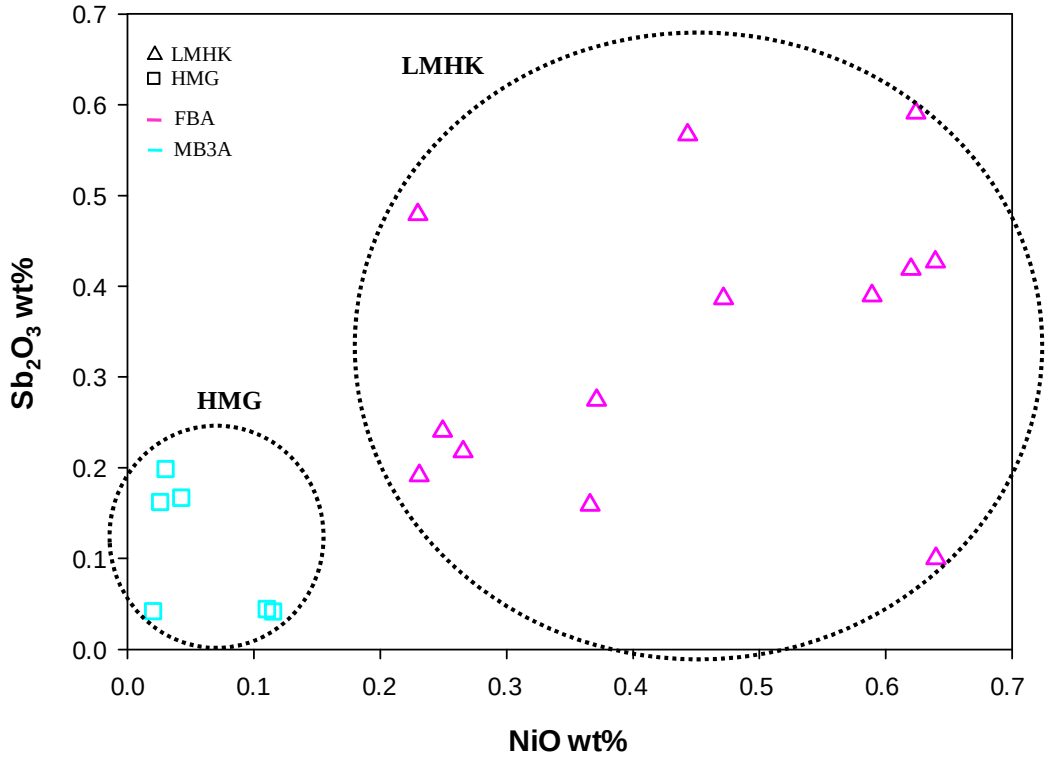

Fig. 5.3. NiO vs *Sb_2O_3 contents of the glass phase in Co-colored glasses from Lipari and Salina (geometric shapes = compositional classes; colors = ages).*

In the blue glasses both homogeneous and heterogeneous texture are present. HMG glasses are generally more homogeneous, while LMHK glasses are characterized by numerous SiO_2 inclusions dispersed in the glass phase, with elongated or rectangular morphologies. HMG glasses present in some cases newly formed crystals of Ca-Mg and Na-Ca silicates. The characteristics of the inclusions will be discussed in detail below (*texture*).

Yellow/Brown glasses

There are four yellow/brown glasses: two from the Lipari Acropolis, Lβ5AG and LC21M, and two from grave 31 of Piazza Monfalcone cemetery, L31CCR and L311GM1. They are all HMG glasses (Fig. 1a-b, full-crossed symbols) with no trace elements but only characterized by low contents of Fe (FeO = 0.22÷0.57 wt%) and S (SO_3 = 0.11÷0.36 wt%). The darker brown sample, L311GM1, has higher contents of Fe and S with respect to the other three glasses and presents also manganese (MnO = 0.83 wt%). Interestingly, the finds dated to different ages: LC21M to the MBA 1-2, L31CCR and L311GM1 to FBA 1-2 and Lβ5AG to FBA 2-3.

Black glass

The only black bead, L311AN1, is from Lipari and presents high levels of both Fe (FeO = 0.73 wt%) and S (SO_3 = 0.60 wt%) with no other trace elements. It has a homogeneous texture with no inclusions or bubbles.

White glasses

No white beads are present in the finds from the Aeolian islands and white glass is used only for the bead decorations.

Nine white glasses were sampled from the beads decorations. The first, SALCFR4Bi, is the only white glass from Salina and is part of the blue HMG fragment SALCFR4B, Fe-colored (see above). The other eight, L311FR1Bi, L311O2B-O3B-O4B, L31CGB, L31CB2B, L31COB and L31CB1B, are LMHK glasses from the Lipari cemetery (grave 31), all applied on Cu-colored beads with different typologies. SALCF4Bi is a HMG glass colored and opacified by Ca antimonates crystals dispersed in the matrix (see below *texture* and *crystalline phases*) and presents high levels of Sb in the glass phase (Sb_2O_3 = 2.86 wt%, fig. 4). The white glasses from Lipari are obtained with two different technologies. Samples L311FRBi, L311O2B-O3B-O4B and L31COB contain a large number of SiO_2 inclusions (see below) and low levels of Ca (CaO = 1.63÷ 1.92 wt%). Instead, samples L31CGB, L31CB2B and L31CB1B have a large number of Ca silicates inclusions dispersed in the glass matrix (see

below) and present higher contents of Ca (CaO = 8÷12 wt%) with respect to the type with SiO_2 inclusions.

Considering the CaO and MgO contents of all glasses (fig. 5.4), the difference between LMHK and HMG types, in particularly for the white ones, is clear. Indeed, LMHK glasses have generally low Mg and Ca contents except for sample L12BOTA that has a value of Ca slightly higher than the other (CaO = 5.40 wt%). The white glasses opacified by Ca silicates have the highest Ca amounts (CaO = 8.7÷12 wt%) and slightly higher Mg contents (MgO = 1.10÷1.30 wt%), while the white glasses opacified by SiO_2 inclusions have the same Ca and Mg contents of the other LMHK glasses. Conversely, all HMG glasses have high Mg and high Ca contents. Interestingly, the white HMG glass obtained with Ca antimonates has a lower Ca content (CaO = 6.91 wt%) with respect to the white LMHK glasses obtained with Ca silicates (CaO = 8÷12 wt%).

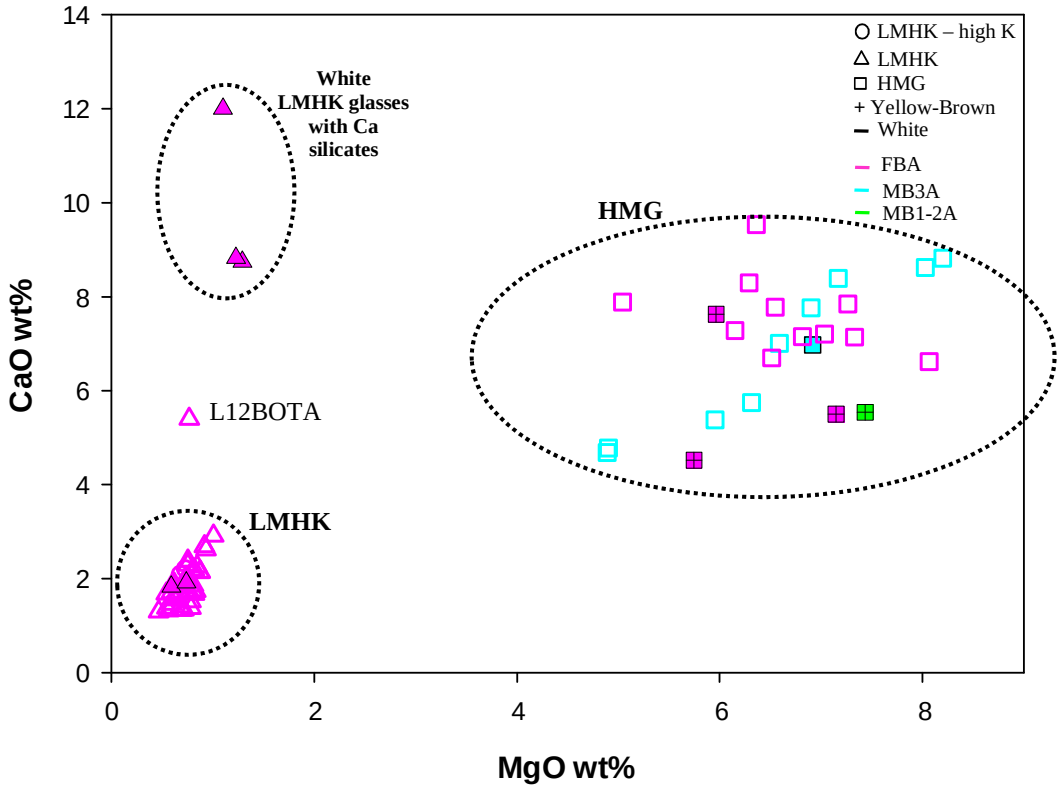

Fig. 5.4. MgO vs *CaO contents of the glass phase in the analyzed glasses from Lipari and Salina (geometric shapes = compositional classes; colors = ages).*

- *Texture*

SEM analyses show that both homogenous and heterogeneous textures are present in Lipari and Salina samples. However, LMHK glasses are more heterogeneous due to the presence of numerous SiO_2 inclusions dispersed in the glass phase (Fig. 6-7). HMG glasses are generally more homogeneous (fig. 5) and are only characterized in some cases by the nucleation of Ca-Mg and Na-Mg silicates or residual metal inclusions (Fig. 9-10).

Except for 4 homogeneous beads (example in fig. 5a), all Cu-colored LMHK glasses from Lipari have a large number of SiO_2 inclusions; they are single elongated crystals or more rectangular when grouped in big aggregates. L31CB2A, L31COA and L311O2A SEM-BSE images are reported as representative examples (Fig. 6a-e). The single elongated crystals have a size of about 10 µm while the aggregates are up to 100÷200 µm large. The largest grains are systematically surrounded by large fractures due to changes in volume during glass cooling (Artioli et al. 2008) (details in fig. 6c-e, 7b-c, and 8b). Beside the SiO_2 inclusions, one Cu-colored sample (L311AA2) has a residual inclusion rich in Sn with a rounded morphology (fig. 6f).

Similarly, only three Co-colored LMHK glasses from Lipari are homogeneous. The sample in fig. 7a, L18DA, shows a texture without inclusions characterized only by a few bubbles of about 50 µm. All the others have numerous elongated inclusions of SiO_2 dispersed in the glass matrix, grouped in aggregates with dimensions ranging from 50 to 100 µm (Fig. 7b-c). Interestingly, sample L12AN1 presents a recrystallization of lamellar inclusions on the edges of the largest grains (fig. 7c).

Several Cu- and Co-colored LMHK glasses have bands with a different chemical composition due to a variation in the Cu content (Fig. 8a-b). EPMA analysis show that lighter gray bands observed at the SEM correspond to higher contents of Cu (CuO up to 4.63 wt%) with respect to the dark grey ones (CuO up to 3.07 wt%). In the Co-Cu colored glasses the variation of Cu corresponds to the variation of Co (CoO up to 0.18 wt% in the dark gray band and up to 0.24 wt% in the light grey one).

Cu- colored HMG glasses from Lipari dated to the FBA are mostly homogeneous, except for samples L31CSB and L311SPA, which are characterized by numerous crystals of Ca-Mg silicates and Na-Ca silicates (fig. 9a-d) and rare small rounded Cu drops (Cu = 97.7 wt%, EDS

data, Fig. 9e). The silicate inclusions have rectangular or polygonal shapes, sometimes dendritic (fig. 9d), and a size ranging from 10 to 20 µm. Sample L311SPA presents, as previously seen for other samples, bands with a different chemical composition due to the variation in their Cu content (CuO up to 0.78 wt% in the dark gray band and up to 0.89 wt% in the light gray one, fig. 9a).

All MBA 3 HMG blue glasses from Salina are mostly homogeneous, except for occasional inclusions of Ca-Mg silicates and Na-Ca silicates with angular shapes and dimensions of about 10÷20 µm (fig. 10a). Sample SALFA1 has different chemical composition bands caused by a Cu content variation (CuO up to 0.12 wt% in the dark gray band and up to 0.57 wt% in the light gray one – Fig. 10b). Interestingly, it presents lamellar-shaped Ca antimonates inclusions (fig. 10c) of about 20 µm in length and very thin (~ 5µm) rounded metal inclusions made of Cu-Sb-Ni-As (fig. 10d). At the same time, SALFFR shows a heterogeneous chemical distribution with zones particularly rich of Cu (CuO up to 0.34 wt%) with respect to the mean value in the glass matrix (CuO < d.l.). Moreover, it rarely presents rounded inclusions of Cu-Pb-Sb-S and occasionally crystals of Ca-Na silicates.

Sample SALCFR3 has a dark blue color and shows different chemical composition areas due to the Fe content variation. In particular, dark gray zones have Fe mean contents up to 3.34 wt% while the light grey one is up to 6.51 wt% (fig. 11a). According to the high level of Fe in the glass phase, SALCFR3 have numerous inclusions of Fe-rich Ca-Mg silicates (FeO up to 14.38 wt%) with different chemical composition zones depending on the Fe contents; specifically, dark gray zones have lower Fe amounts than the light gray ones (fig. 11b and c). The inclusions have angular or dendritic shapes and dimensions ranging from 20 to 100 µm.

Moreover, SALCFR3 presents rounded metal inclusions of Cu-Fe-S alloy with segregations of Pb, Ni and Sb, with dimensions about of about 8 µm, and are distributed mainly in the Fe-rich bands of the glass (e.g. fig. 11d).

The only HMG white glass SALCFR4 Bi comes from Salina, is dated to the MBA 3 and has a heterogeneous texture due to the presence of numerous Ca antimonates finely dispersed in the glass phase (fig. 12a-c). As shown in fig. 12a, both the blue body and the white decoration are partially weathered; however, some portions are well preserved and useful for the analysis. The Ca antimonates have irregular morphologies with dimensions ranging from a few microns

to 20 µm. The passage between the blue body and the white decorations is clear and no blending between the two colors occurs (fig. 12a).

The white LMHK decoration glasses from Lipari dated to the FBA can be distinguished in two groups. In the first one, constituted by five samples (L311FRBi, L311O2B-O3B-O4B and L31COB), the glass matrix contains numerous SiO_2 inclusions with rounded and/or elongated shapes of dimensions ranging from 20 to 100 µm (fig. 13a). This glasses are strongly weathered, characterized by fractures and pores large up to 50 µm (fig. 13a) and is associated to beads with eyes decorations. The contact between the blue body and the white decoration is clearly visible and the colors do not seem to be mixed (fig. 13aa).

The white glasses belonging to the second group, composed by 3 samples (L31CB2B, L31CGB and L31CB1B), are characterized by anhedral Ca silicates crystals finely dispersed in the glass phase and bubbles with a size ranging from 10 to 50µm. In sample L31CB2B, Ca silicates have a composition including Na, K and Mg in a variable stoichiometry; a few SiO_2 crystals are also present in the glass phase. The Ca silicates inclusions have irregular and not defined shapes with particularly small dimensions, ranging from a few microns to 20 µm (fig. 13b).

Samples L31CGB and L31CB1B are characterized only by small and euhedral crystals of Ca silicates (13c and d). The dimensions of the aggregates range from a few microns to 20 µm and the stoichiometry is very close to wollastonite ($CaSiO_3$). Both types of glass with Ca silicates are associated to globular or barrel beads with spiral decoration. The passage between the blue body and the white decorations is not marked and the two colors are partially mixed. In sample L31CB1B some bubbles appear concentrated in the boundary line of the two colors (fig. 13c).

Yellow/brown glasses have a homogeneous texture while the only black glass (L311-AN1, Lipari) presents a few metal inclusions of Cu-Fe-S with traces of Ni, particularly small (1-2µm).

- *Crystalline phases*

The crystalline phases of the inclusions studied at the SEM-EDS were characterized by µ-Raman spectroscopy.

All SiO_2 inclusions in LMHK glasses are mainly tridymite with occasional traces of quartz. The analyses were carried out both on the single elongated crystals and on the large aggregates considering the core and the edges of the grains. The spectra highlights in the different morphologies the same peaks at 435, 353, 306, 211 and 143 cm^{-1} typical of tridymite (fig. 15a); in several cases a low intense peak at 463 cm^{-1} appear, typical of quartz (fig. 15a). The presence of tridymite as the only phase is confirmed by the Single Crystal X-ray diffraction. The X-ray pattern diffraction has d spacing of 2θ at 4.34Å, 4.12 Å, 3.84 Å, 2.58 Å and 2.51 Å typical of tridymite (fig. 15b).

Ca-Mg silicates in HMG glasses from Lipari and Salina are composed by diopside ($CaMgSi_2O_6$), with main peaks at 1012, 856, 668, 391, 366, 325, 230 and 140 cm^{-1} (fig. 16a). Fe-rich Ca-Mg silicates in sample SALCFR3 are characterized by diopside in the grey zone observed at the SEM-EDS and by a phase more similar to augite in the light gray one (richer in Fe), that does not have a peak at 366 cm^{-1} (fig. 16b). The phases identified at the Raman spectroscopy are consistent with what observed at the SEM-EDS.

Ca-Na silicates are probably due to devrification phases in the glass (e.g., combeite, devitrite) even though so far no match between the collected spectra and those in the literature has been identified.

Lamellar Ca antimonates in sample SALFA1 are present in the hexagonal habit, $CaSb_2O_6$, as shown by its characteristic peak at 670 cm^{-1} in fig. 17a.

The only white glass from Salina has numerous Ca antimonates finely dispersed in the glass phase in the orthorhombic structure, $Ca_2Sb_2O_7$, which has two characteristic peaks at 635 and 482 cm^{-1} (fig. 17b).

In the Lipari LMHK white glasses, Ca silicate crystals are made of wollastonite ($CaSiO_3$) with main peaks at 969, 636 and 410 cm^{-1} (fig. 18a-b); however, in the inclusions with anhedral morphologies (L31CB2B) the spectrum presents peaks at 1096 and 550 cm^{-1} related to the amorphous phase (fig. 18a), while the well-crystallized aggregates (L31CGB and L31CB1B) present a pure wollastonite spectrum (fig. 18b). SiO_2 crystals in sample L31CB2B are mostly

of tridymite and rare quartz with the characteristic peak at 465 cm^{-1} (fig. 19a and b, respectively).

The white glasses opacified by SiO_2 inclusions dispersed in the glass matrix were analyzed by Single Crystal X-ray Diffraction. The analyses were carried out on a glass fragment of about 1mm analyzing the entire volume. The analyses show that the only phase present is tridymite, which has characteristic d spacing of 2θ at 4.31 Å, 4.09 Å, 3.8 Å, 2.97 Å and 2.49 Å (fig. 20).

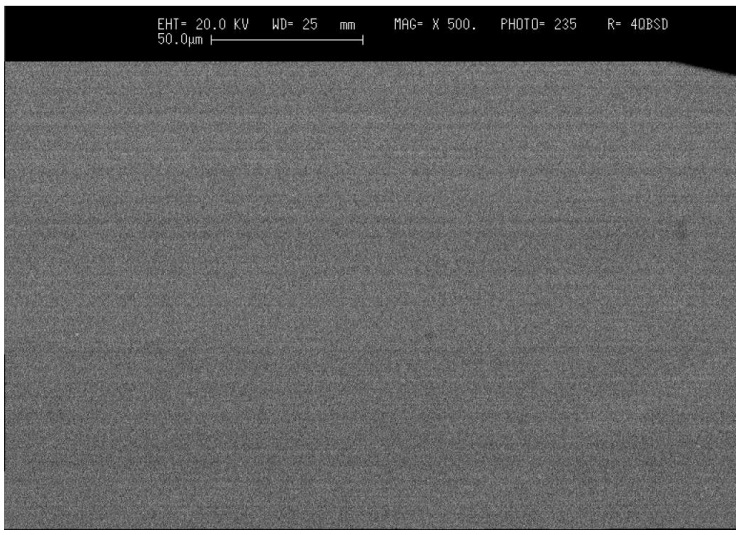

Fig. 5. SEM-BSE image of HMG sample L12SM characterized by a homogeneous texture.

Fig. 6. SEM-BSE images of Cu colored LMHK samples: a) L31CB2A, b) L31COA, c) detail of the white square in fig. 6b, d) L311O2A, e) detail of the SiO_2 inclusions of the sample L311O2A and f) detail of an inclusion rich in Sn in sample L311AA2, with EDS data reported.

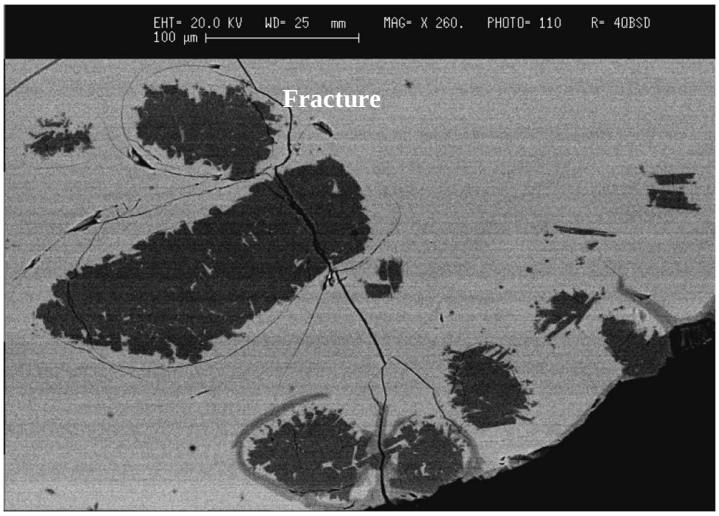

a)

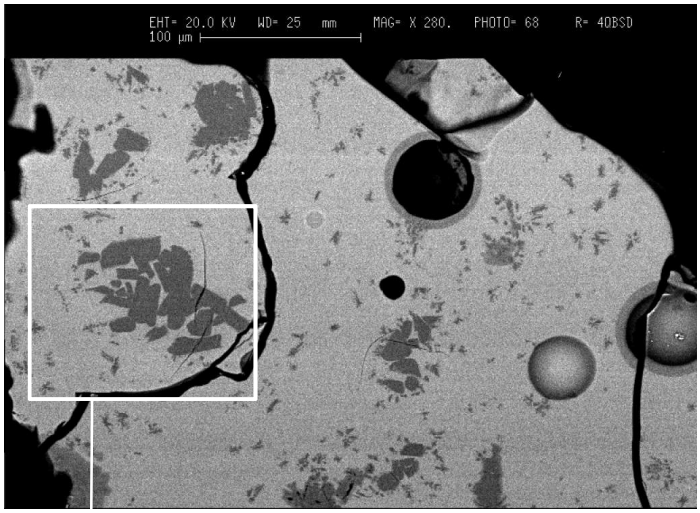

b)

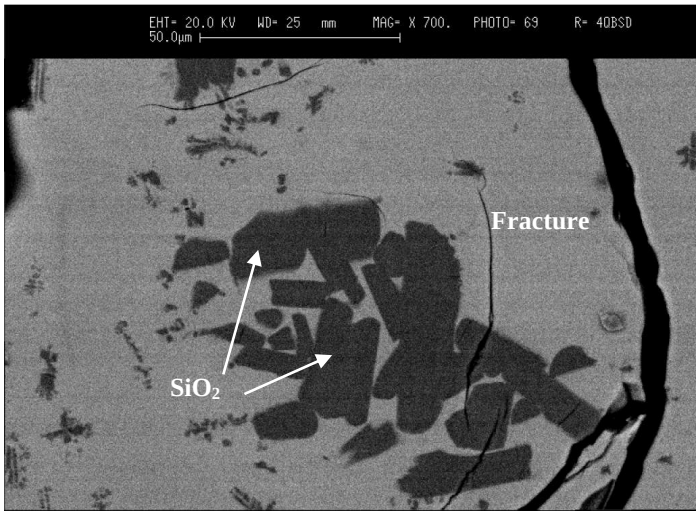
EHT= 20.0 KV WD= 25 mm MAG= X 700. PHOTO= 69 R= 4QBSD
50.0µm
Fracture
SiO2
c)

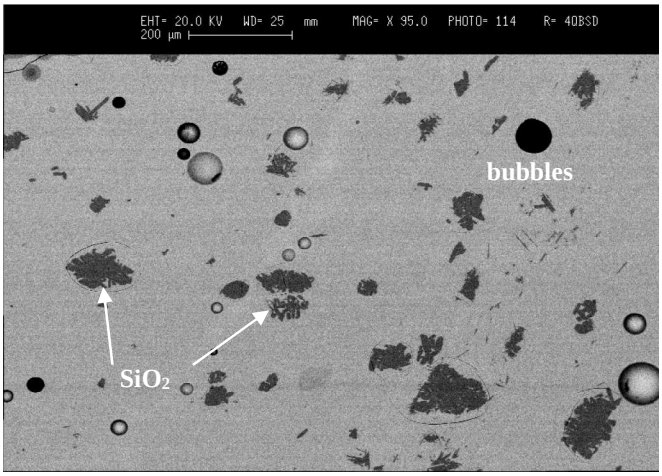
EHT= 20.0 KV WD= 25 mm MAG= X 95.0 PHOTO= 114 R= 4QBSD
200 µm
bubbles
SiO2
d)

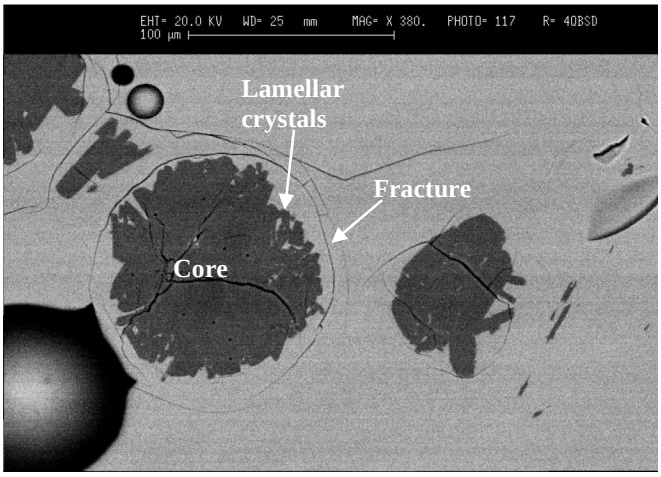
EHT= 20.0 KV WD= 25 mm MAG= X 380. PHOTO= 117 R= 4QBSD
100 µm
Lamellar crystals
Fracture
Core
e)

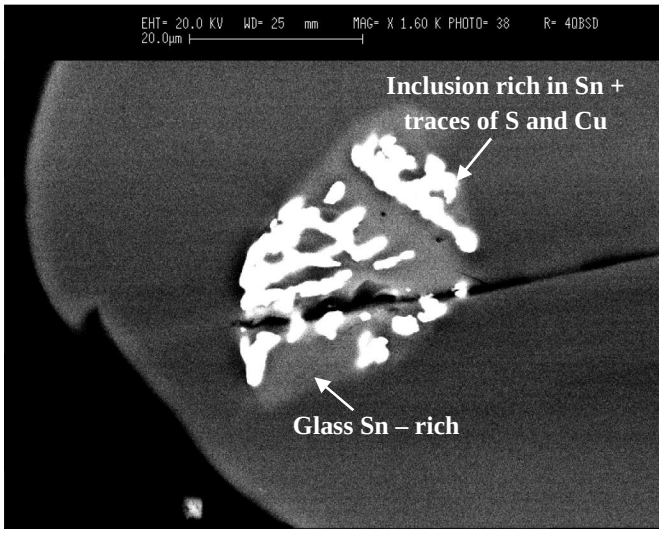

f)

Fig. 7. SEM-BSE images of Co-colored LMHK samples: a) L18DA, b) L12BOTA and c) L12AN1

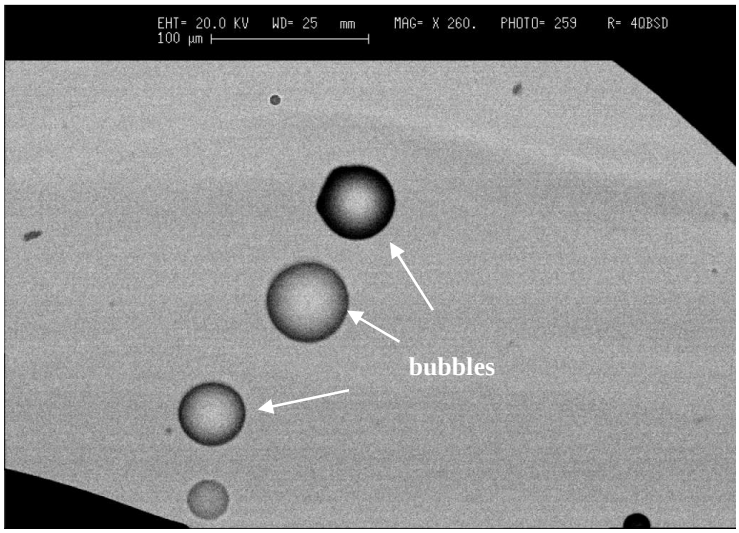

a)

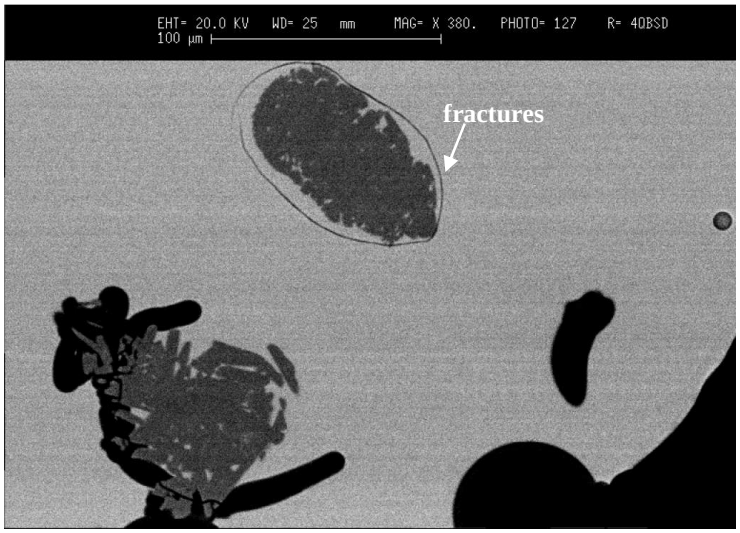
EHT= 20.0 KV WD= 25 mm MAG= X 380. PHOTO= 127 R= 40BSD
100 µm
fractures

b)

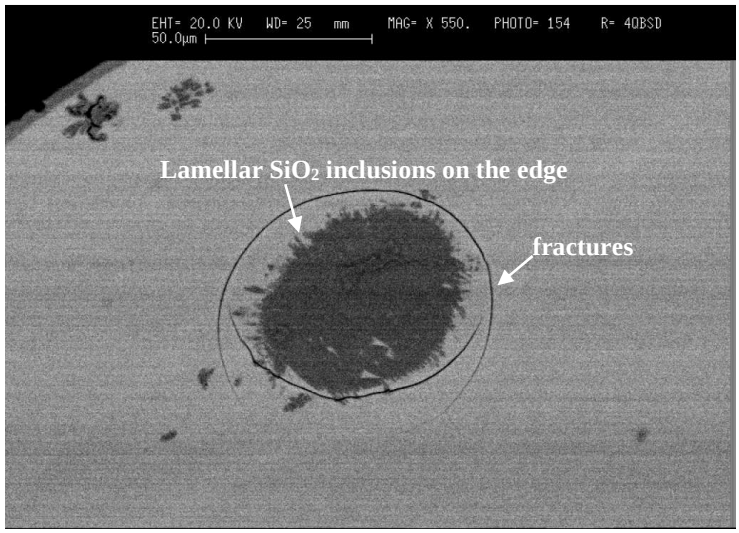
EHT= 20.0 KV WD= 25 mm MAG= X 550. PHOTO= 154 R= 40BSD
50.0µm
Lamellar SiO_2 inclusions on the edge
fractures

c)

.

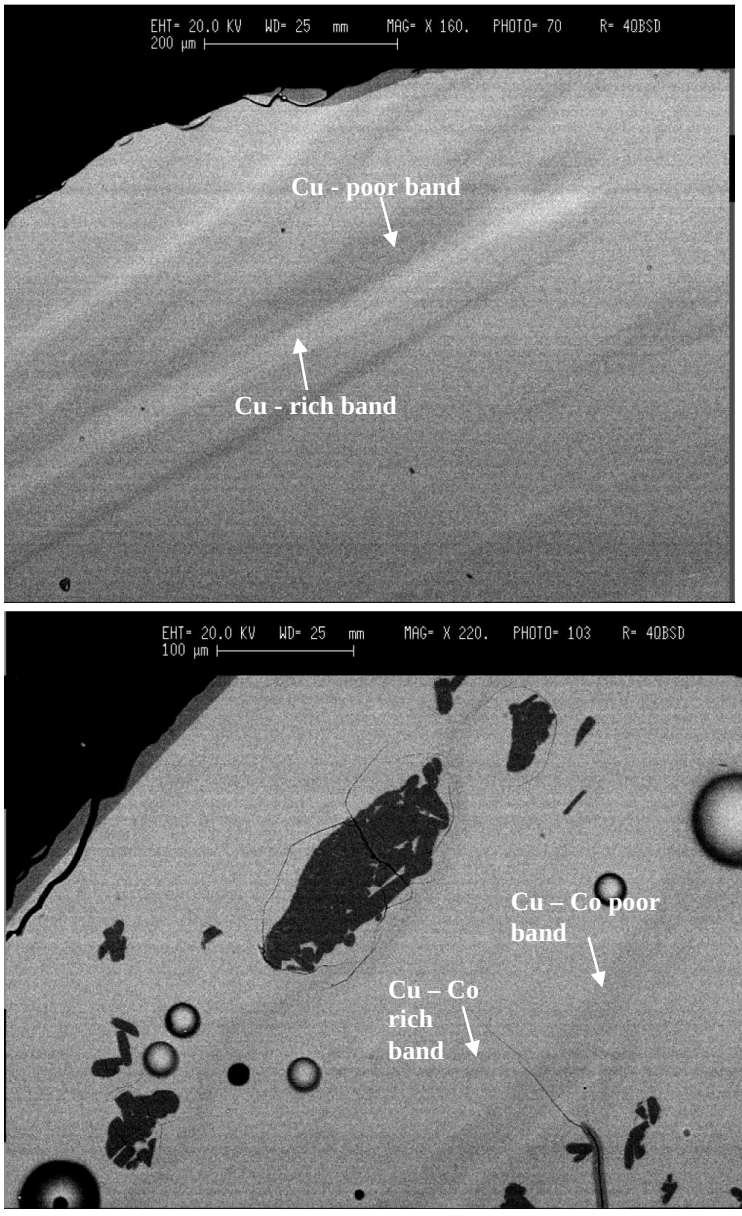

Fig. 8. SEM-BSE images of the different chemical compositional bands in a) Cu-colored LMHK sample L314AZ1 and b) Co-colored LMHK sample L314CO1.

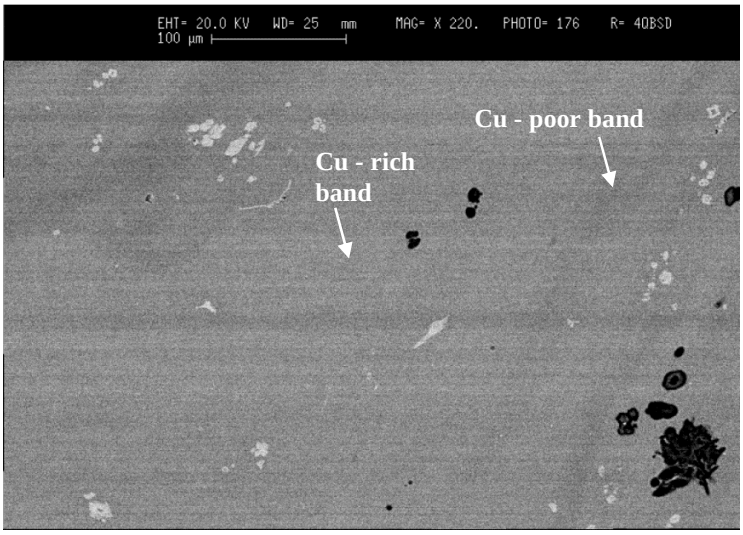

a)

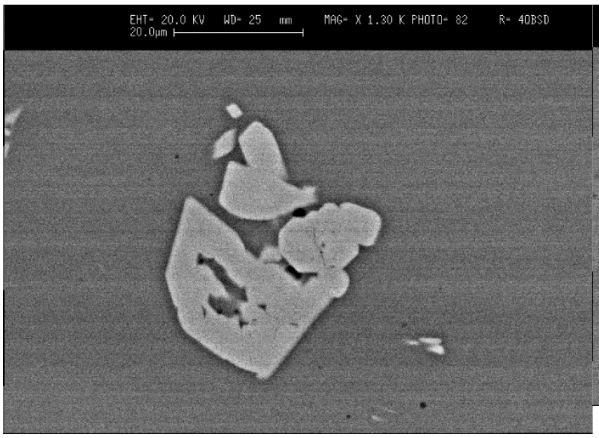

b)

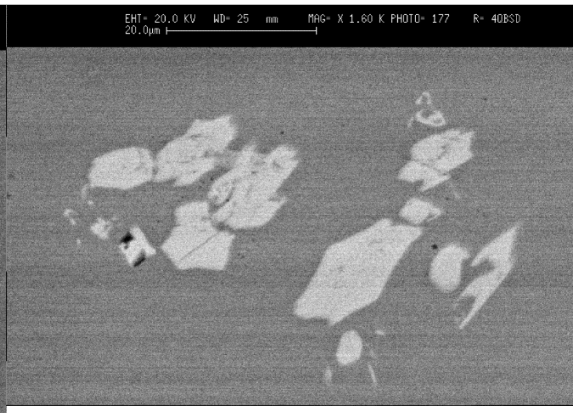

c)

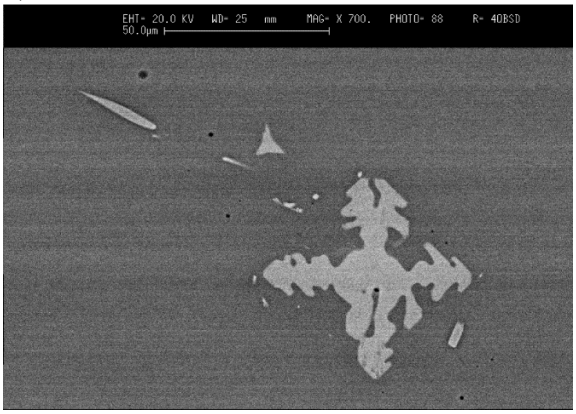

d)

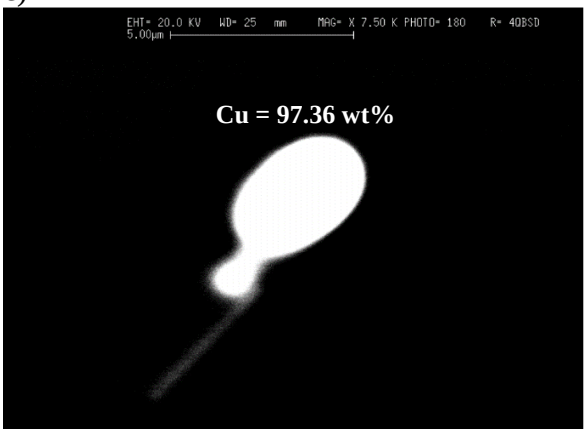

e)

Fig. 9. a) SEM-BSE image of Cu-colored HMG sample L311SPA from Lipari, b) detail of Ca-Mg silicate from blue sample L31CSB, c) and d) details of Ca-Na silicate from blue samples L311SPA and L31CSB, respectively, e) detail of a Cu drop from sample L311SPA with EDS data reported.

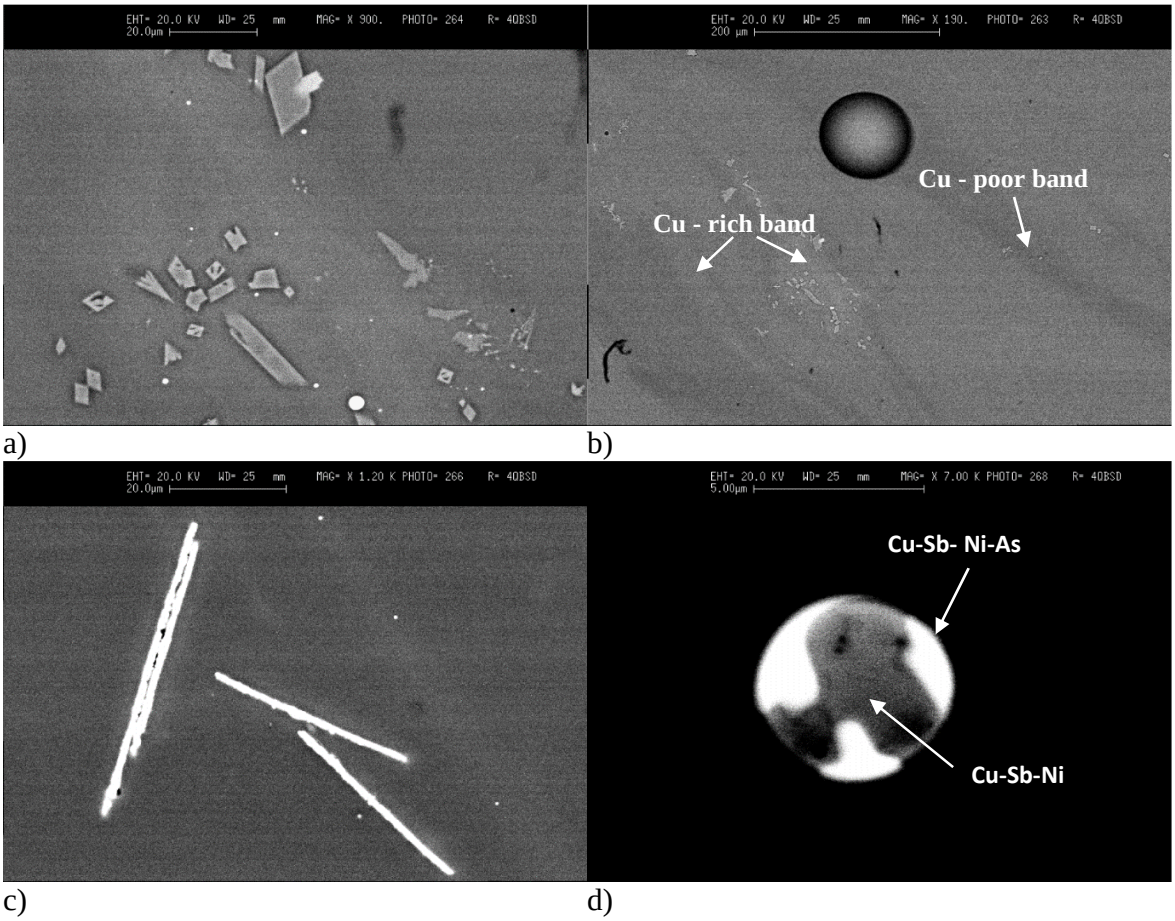

Fig. 10. SEM-BSE image of Co-colored HMG sample SALFA1 from Salina, a) detail of Ca-Mg silicates with stoichiometry close to diopside, b) different chemical compositional bands, c) detail of elongated Ca antimonates and d) detail of an inclusion rich in metals.

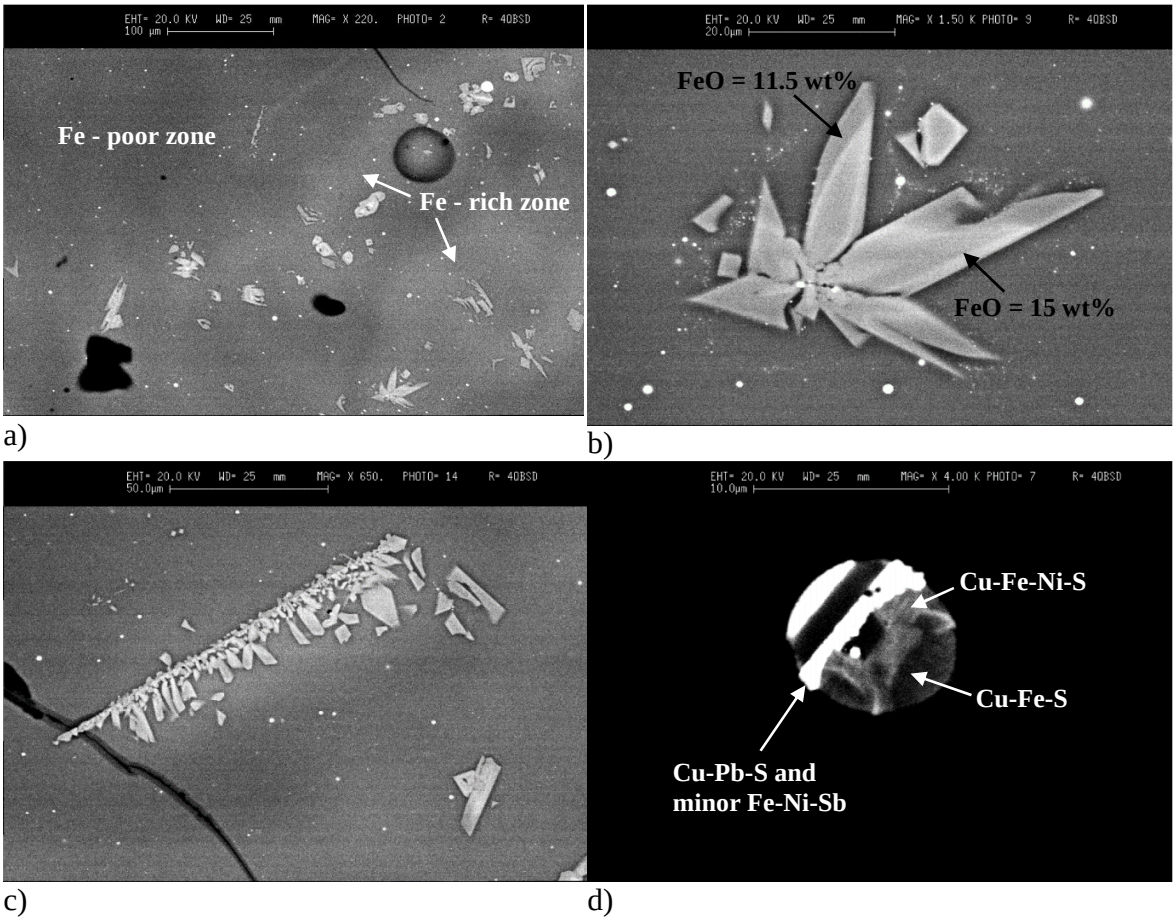

Fig. 11. a) SEM-BSE image of Co colored HMG sample SALCFR3 from Salina with different chemical composition zones, b) and c) details of Fe-rich Ca-Mg silicates with different chemical composition zones and variable EDS data, d) detail of an inclusion of Cu-Fe-S alloy with segregations of Pb, Ni and Sb.

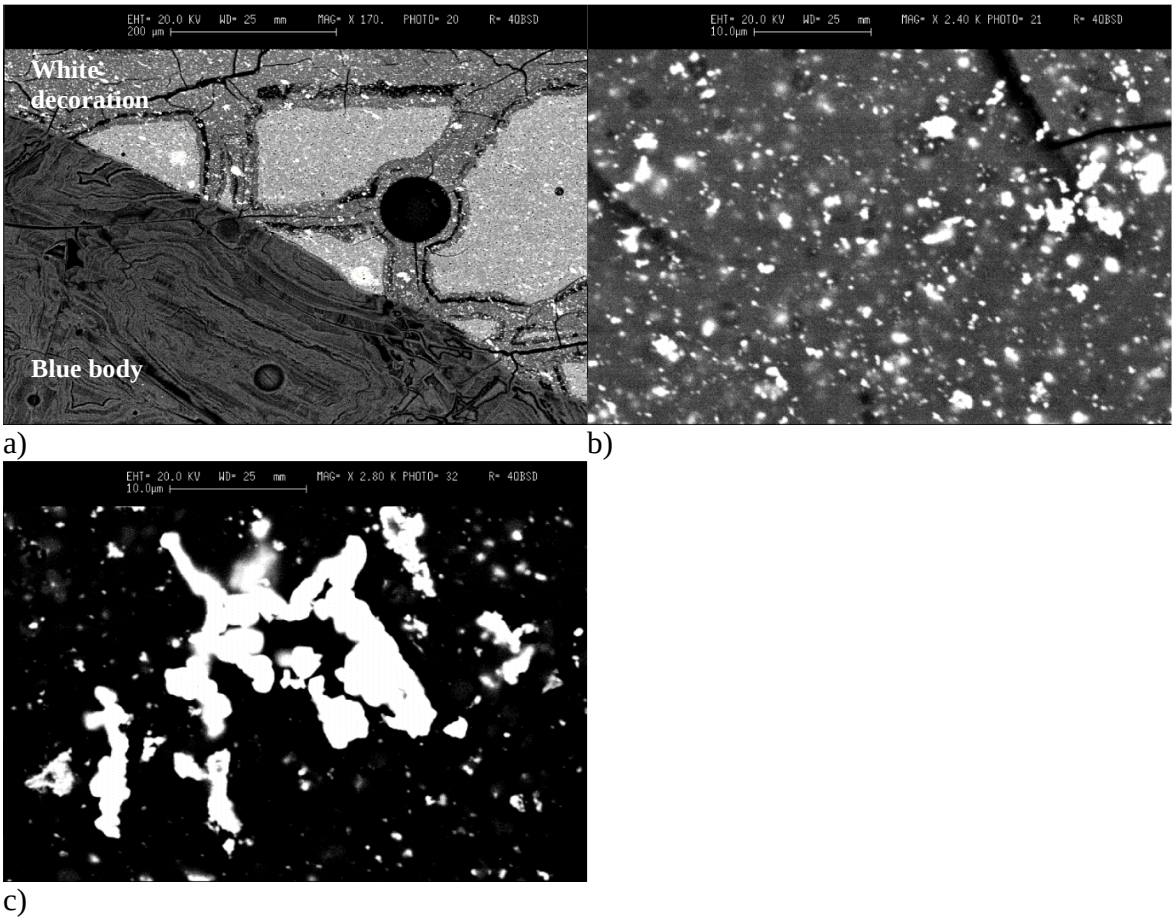

Fig. 12. a) SEM-BSE image of blue body and white decoration (with aggregates) of sample SALCFR4BBi from Salina, b) detail of Ca antimonates finely dispersed in the glass phase, c) detail of a Ca antimonate crystal with crystals grouped in aggregates with irregular morphologies.

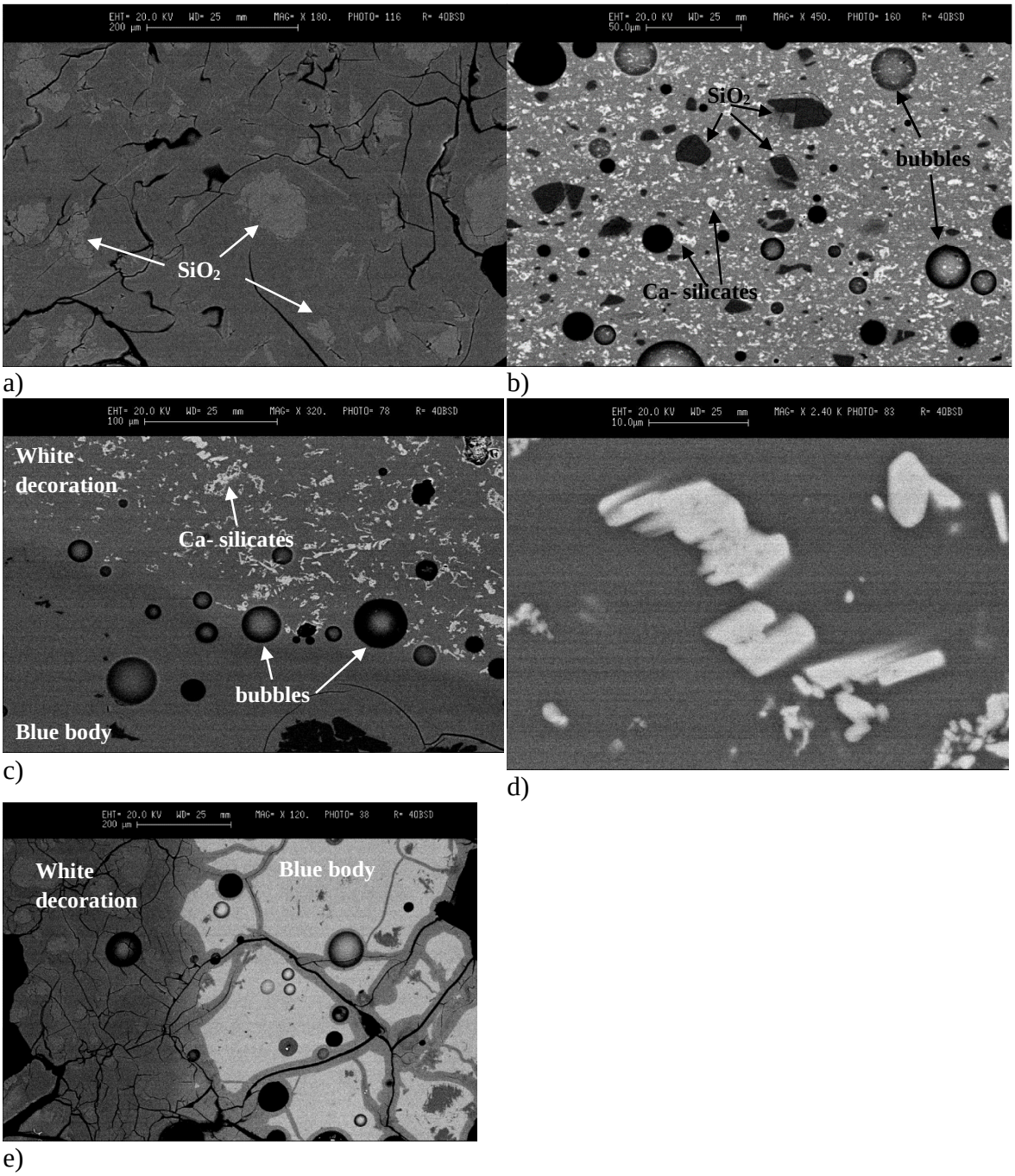

Fig. 13. SEM-BSE images of LMHK white decorations from : a) L31COB with SiO_2 inclusions, aa) detail of the contact zone between the body and the decoration, b) L31CB2B with Ca silicates and SiO_2 inclusions, c) L31CB1B, with Ca silicates and d) detail of an euhedral aggregate.

a) b)

Fig. 14. a) SEM-BSE images of the black HMG glass L311AN1, b) detail of the metal inclusions in the white square of fig. 14a.

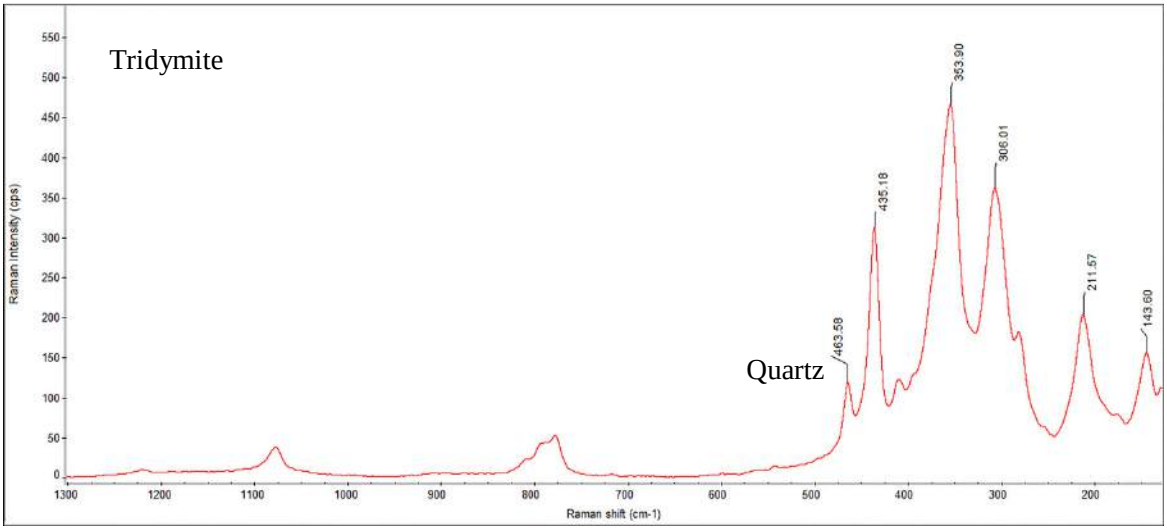

a)

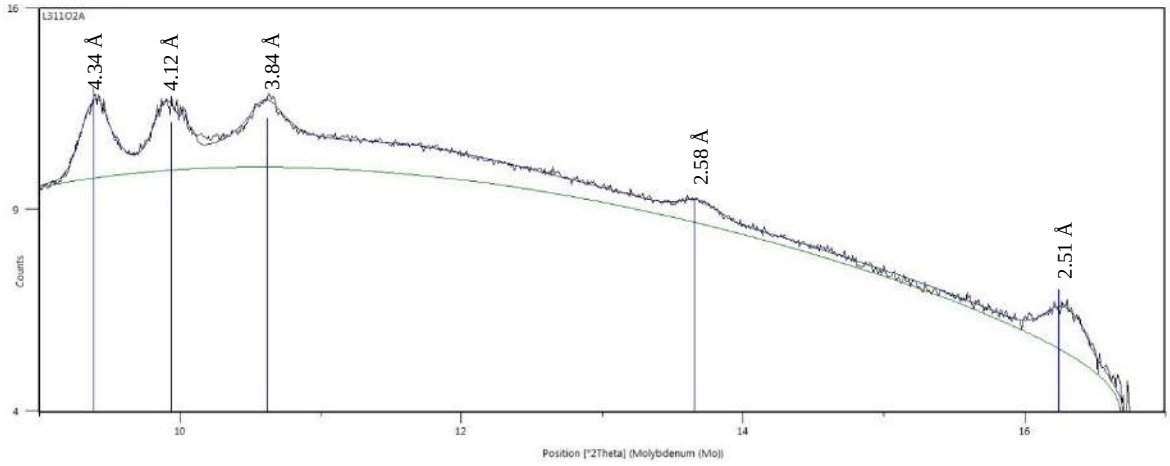

b)

Fig. 15. a) Raman Spectra of a SiO_2 inclusion in the LMHK sample L311O2A that is comparable to those obtained in all the analyzed LMHK blue samples, b) X-ray pattern diffraction of the LMHK sample L311O2A that is comparable to those obtained in all the analyzed LMHK blue samples.

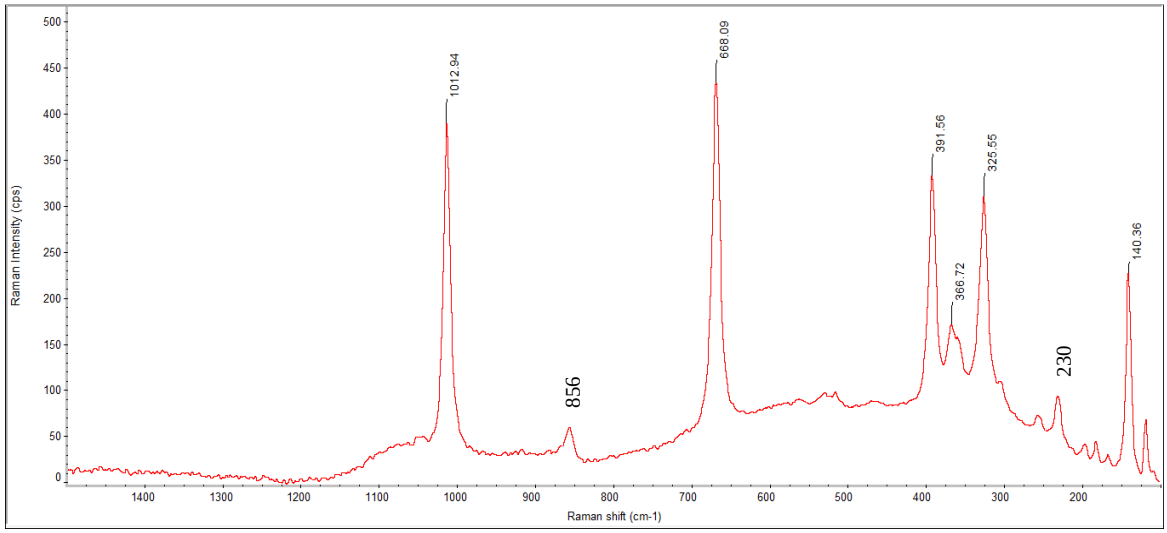

a)

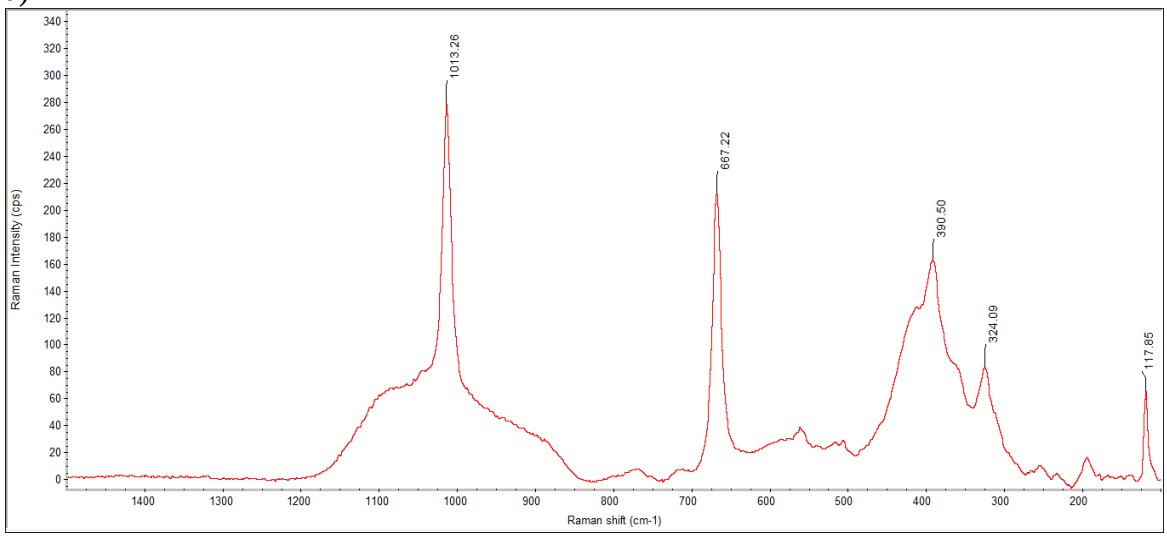

b)

Fig. 16. Raman Spectra of a) diopside crystal in HMG glasses from Lipari and Salina, b) augite in sample SALCFR3 from Salina.

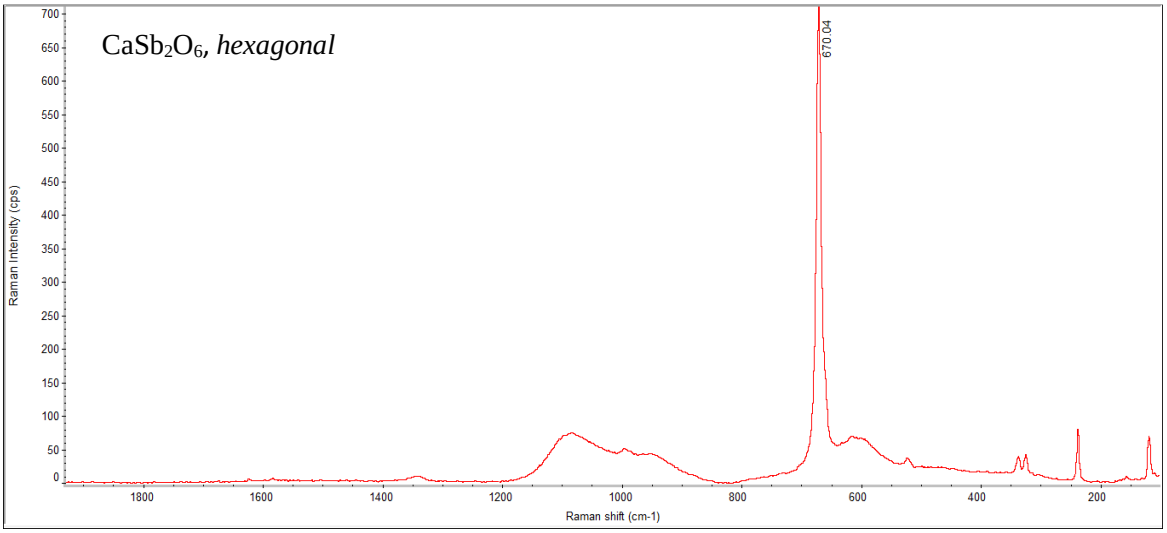

a)

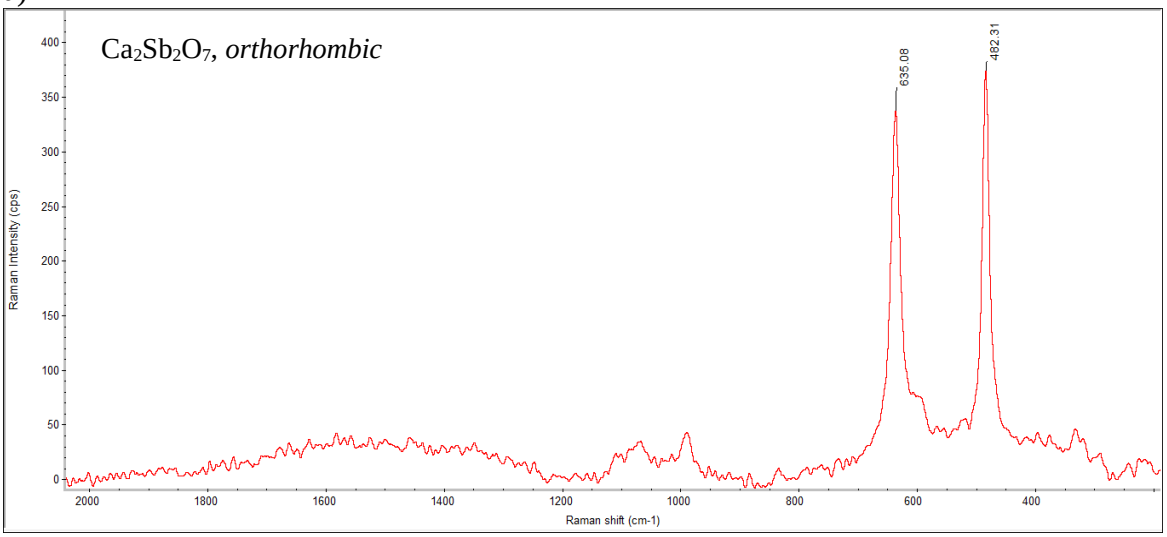

b)

Fig. 17. Raman Spectra of Ca antimonates a) $CaSb_2O_6$ hexagonal habit, sample SALFA1 (fig. 10c), b) $Ca_2Sb_2O_7$, orthorhombic structure, sample SALCFR4Bi (fig. 12a-c).

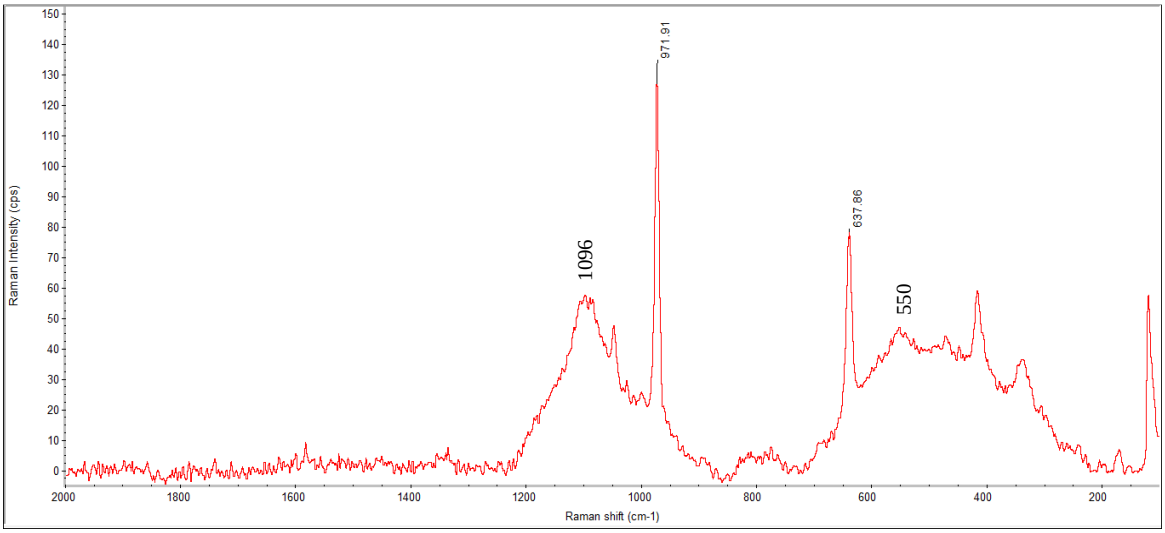

a)

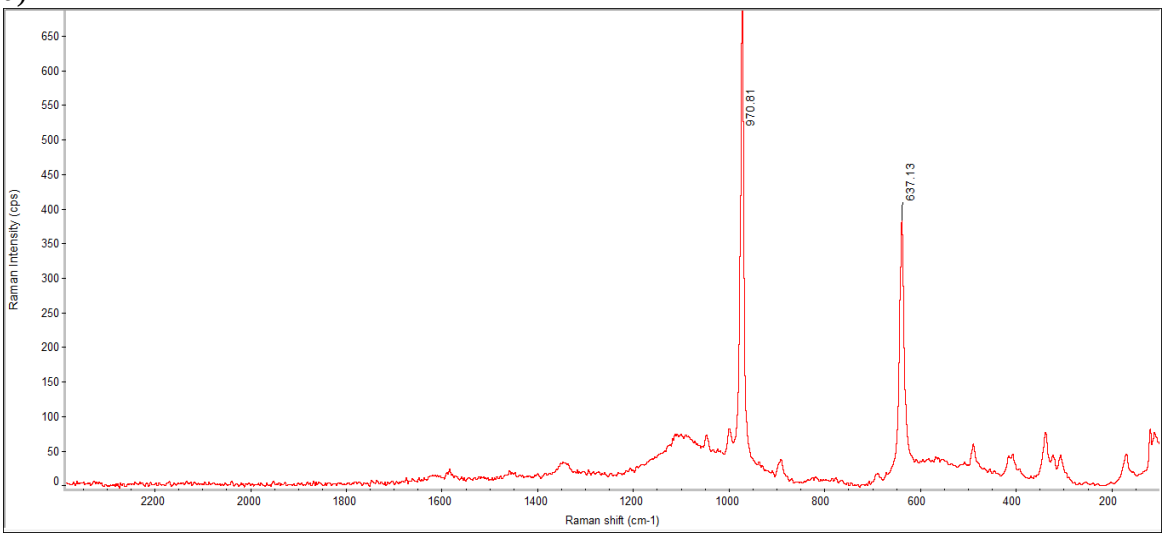

b)

Fig. 18. Raman Spectra of Ca silicates a) wollastonite, $CaSiO_3$, with amorphous phase in sample L31CB2B, b) wollastonite, $CaSiO_3$, in samples L31CGB and L31CB1B.

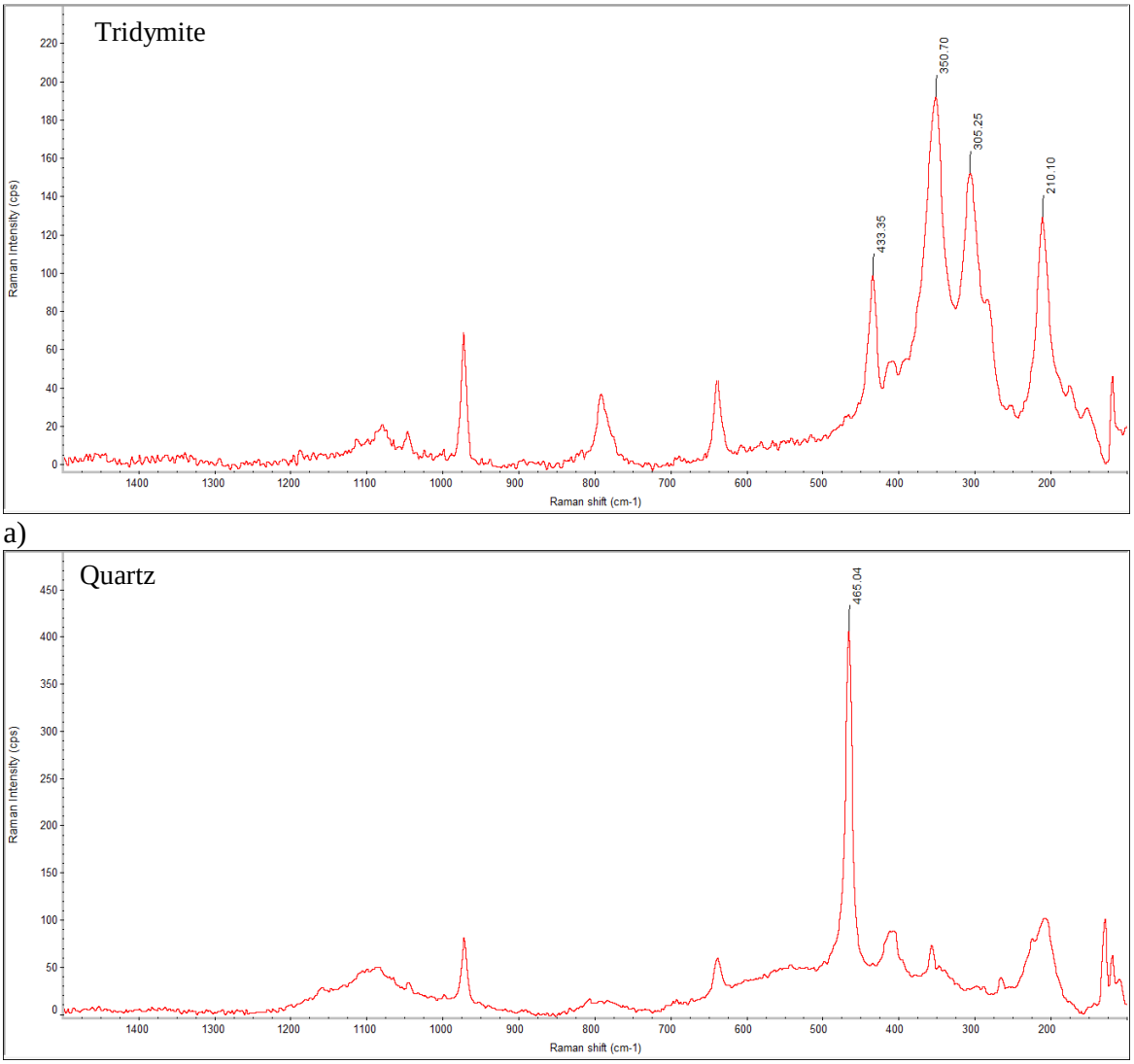

Fig. 19. Raman Spectra of SiO_2 inclusions in sample L31CB2B. a) tridymite spectrum obtained in a rectangular crystal , b) quartz obtained on a rounded crystal.

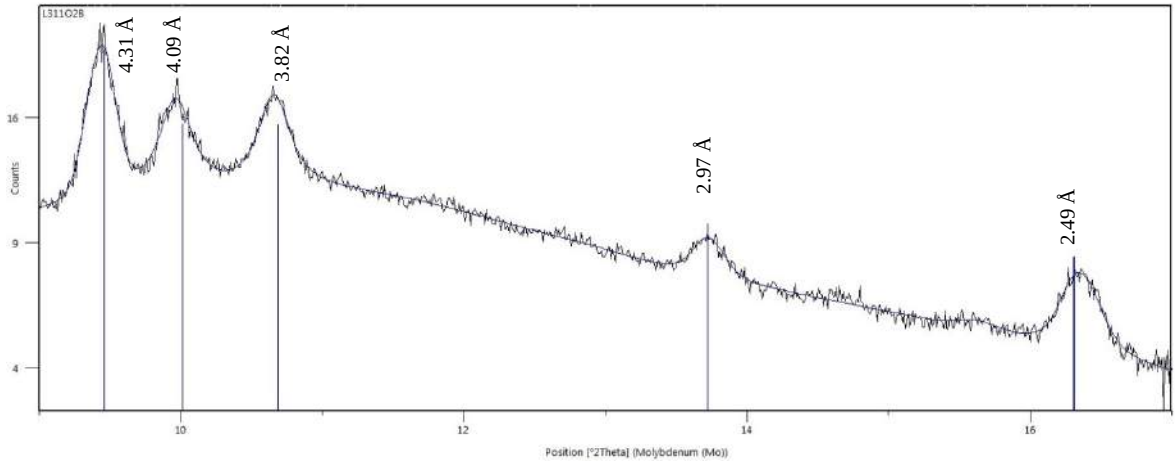

Fig. 20: X-ray pattern diffraction of LMHK sample L311O2B.

Sample	Na_2O	MgO	Al_2O_3	SiO_2	P_2O_5	SO_3	Cl	K_2O	CaO	TiO_2	MnO	FeO	CoO	NiO	CuO	ZnO	As_2O_3	SnO_2	Sb_2O_3	PbO	Tot.
d.l. (%)	0.13	0.05	0.07	0.1	0.05	0.03	0.02	0.08	0.03	0.03	0.05	0.05	0.03	0.04	0.03	0.04	0.1	0.04	0.04	0.1	
LC2IM	16.90	7.43	0.85	65.86	0.10	0.29	1.08	3.15	5.54	0.03	0.05	0.22	<d.l.	<d.l.	<d.l.	<d.l.	<d.l.	<d.l.	<d.l.	<d.l.	**101.61**
SD	0.27	0.09	0.07	0.34	0.03	0.03	0.05	0.19	0.07	0.02	0.01	0.03		0.01							
SALFA1																					
Cu-rich*	17.7	5.1	2.2	56.8	<d.l.	0.2	0.2	5.1	8.5	<d.l.	<d.l.	2.8	<d.l.	<d.l.	0.6	<d.l.	<d.l.	<d.l.	<d.l.	<d.l.	99.3
Cu-poor*	15.7	5.8	1.1	59.1	<d.l.	0.3	0.3	5.3	8.3	<d.l.	<d.l.	1.3	<d.l.	<d.l.	0.1	<d.l.	<d.l.	<d.l.	<d.l.	<d.l.	97.4
mean	17.02	8.20	1.19	60.07	0.20	0.31	0.61	3.49	8.82	0.10	0.06	1.16	0.06	<d.l.	0.34	<d.l.	<d.l.	<d.l.	0.16	0.12	**101.96**
SD	0.29	0.10	0.11	0.65	0.05	0.05	0.08	0.16	0.30	0.02	0.01	0.22	0.04	0.02	0.05				0.09	0.06	
SALFA 2	17.07	8.03	1.05	59.70	0.17	0.32	0.58	3.42	8.62	0.08	0.06	1.29	0.06	<d.l.	0.31	<d.l.	<d.l.	<d.l.	0.20	<d.l.	**101.12**
SD	0.43	0.09	0.27	0.84	0.07	0.02	0.09	0.17	0.51	0.03	0.02	0.24	0.02	0.02	0.04				0.07		
SALFA3	19.24	6.59	1.04	61.67	0.20	0.45	0.97	3.47	7.01	0.07	<d.l.	0.89	0.06	<d.l.	0.10	<d.l.	<d.l.	<d.l.	0.04	<d.l.	**101.97**
SD	0.11	0.11	0.06	0.29	0.05	0.03	0.02	0.12	0.18	0.01		0.04	0.02	0.02	0.05				0.03		
SALFA4	18.55	6.90	1.00	60.27	0.25	0.46	0.71	3.58	7.76	0.09	<d.l.	0.82	0.08	0.04	0.35	<d.l.	<d.l.	<d.l.	0.17	0.12	**101.21**
SD	0.25	0.04	0.10	0.33	0.06	0.03	0.04	0.14	0.06	0.02		0.04	0.02	0.03	0.06				0.05	0.07	
SALFAS	18.71	4.91	4.47	62.27	0.16	0.43	0.81	2.44	4.78	0.12	0.17	0.58	0.14	0.12	0.28	0.16	<d.l.	<d.l.	0.04	<d.l.	**100.66**
SD	0.32	0.04	0.16	0.28	0.04	0.03	0.04	0.11	0.07	0.03	0.04	0.04	0.02	0.03	0.04	0.06			0.04		
SALCFR1	19.05	4.89	4.42	62.09	0.23	0.48	0.82	2.47	4.68	0.12	0.16	0.59	0.13	0.11	0.28	0.13	<d.l.	<d.l.	0.04	<d.l.	**100.76**
SD	0.27	0.07	0.23	0.28	0.05	0.06	0.03	0.22	0.04	0.02	0.03	0.03	0.03	0.04	0.02	0.04			0.03		
SALFFR																					
Cu-poor	18.33	7.29	0.90	62.29	0.21	0.46	0.90	3.21	8.47	0.06	0.05	0.35	<d.l	<d.l.	<d.l.	<d.l.	<d.l.	<d.l.	<d.l.	<d.l.	102.62
SD	0.49	0.19	0.23	0.66	0.05	0.04	0.11	0.18	0.20	0.02	0.01	0.10									
Cu-rich	18.50	7.05	0.69	62.40	0.17	0.54	0.78	3.15	8.32	0.03	<d.l	0.71	0.03	<d.l.	0.34	<d.l.	<d.l.	<d.l.	<d.l.	<d.l.	102.80
SD	0.33	0.23	0.02	0.47	0.04	0.05	0.01	0.16	0.22	0.01		0.50	0.01		0.42						
mean	18.42	7.17	0.79	62.35	0.19	0.50	0.84	3.18	8.39	0.05	<d.l.	0.53	<d.l.	<d.l.	0.18	<d.l.	<d.l.	<d.l.	<d.l.	<d.l.	**102.71**
SD	0.42	0.22	0.21	0.55	0.05	0.05	0.11	0.16	0.20	0.02		0.30			0.25						
SALCFR3																					
Fe-rich*	17.0	4.5	1.2	58.8		0.2	0.8	5.0	5.7		<d.l	6.5	<d.l	<d.l	<d.l	<d.l	<d.l	<d.l	<d.l	<d.l	99.7
mean	16.86	6.31	0.89	63.15	0.15	0.49	0.91	3.39	5.75	0.06	<d.l.	3.25	0.03	<d.l.	0.06	<d.l.	<d.l.	<d.l.	0.06	<d.l.	**101.48**
SD	0.40	0.15	0.15	1.15	0.02	0.06	0.03	0.22	0.22	0.02		0.62	0.02		0.03				0.04		
SALCFR4 Bi	18.73	6.92	3.10	57.10	0.19	0.38	0.83	3.16	6.98	0.06	0.05	0.40	<d.l.	<d.l.	<d.l.	<d.l.	<d.l.	<d.l.	2.86	<d.l.	**100.84**
SD	0.78	0.31	0.16	1.03	0.01	0.04	0.05	0.22	0.72	0.01	0.02	0.05							0.52		
SALCFR4 B	19.41	5.95	2.10	63.93	0.14	0.55	1.00	2.23	5.37	0.14	<d.l.	0.50	<d.l.	<d.l.	<d.l.	<d.l.	<d.l.	<d.l.	<d.l.	<d.l.	**101.50**
SD	0.33	0.11	0.13	0.43	0.02	0.05	0.06	0.20	0.14	0.02		0.02									

Sample	Na_2O	MgO	Al_2O_3	SiO_2	P_2O_5	SO_3	Cl	K_2O	CaO	TiO_2	MnO	FeO	CoO	NiO	CuO	ZnO	As_2O_3	SnO_2	Sb_2O_3	PbO	Tot.
LO-IIIG**	0.07	1.59	0.90	85.39	0.14	0.04	<d.l.	0.19	0.90	0.03	<d.l.	0.56	<d.l.	<d.l.	0.03	<d.l.	<d.l.	<d.l.	0.11	1.16	**91.20**
SD	0.04	0.70	0.06	1.52	0.27	0.03		0.06	0.51	0.02		0.10			0.02				0.02	0.37	
Lβ5AG	16.38	5.75	0.93	70.50	0.11	0.11	1.23	2.50	4.52	0.07	0.05	0.36	<d.l.	<d.l.	<d.l.	<d.l.	<d.l.	<d.l.	<d.l.	<d.l.	**102.60**
SD	0.26	0.10	0.06	0.41	0.03	0.04	0.05	0.04	0.06	0.03	0.03	0.02									
L31CCR	16.71	7.15	0.78	66.42	0.15	0.30	1.05	2.96	5.50	0.03	<d.l.	0.23	<d.l.	<d.l.	<d.l.	<d.l.	<d.l.	<d.l.	<d.l.	<d.l.	**101.39**
SD	0.28	0.04	0.04	0.79	0.03	0.05	0.02	0.17	0.06	0.02		0.03									
L311GM1	17.49	5.97	0.86	65.06	0.30	0.36	1.21	2.04	7.63	0.11	0.83	0.57	<d.l.	<d.l.	0.04	<d.l.	<d.l.	<d.l.	<d.l.	<d.l.	**102.55**
SD	0.32	0.20	0.09	0.44	0.05	0.03	0.03	0.05	0.16	0.02	0.03	0.03			0.03						
L311AN1	17.10	6.51	1.30	63.63	0.23	0.60	1.19	3.59	6.70	0.08	0.06	0.73	<d.l.	<d.l.	<d.l.	<d.l.	<d.l.	<d.l.	<d.l.	<d.l.	**101.80**
SD	0.66	0.48	0.49	1.79	0.10	0.10	0.19	0.13	0.32	0.04	0.04	0.06							<d.l.	<d.l.	
L311SPA																					
Cu-rich*	17.7	4.2	0.6	62.3	<d.l.	0.4	1.0	3.3	8.2	<d.l.	<d.l.	0.4	<d.l.	<d.l.	0.9	<d.l.	<d.l.	<d.l.	<d.l.	<d.l.	99.0
Cu-poor*	16.4	3.9	0.5	63.9	<d.l.	0.4	1.1	3.4	5.8	<d.l.	<d.l.	0.3	<d.l.	<d.l.	0.8	<d.l.	<d.l.	<d.l.	<d.l.	<d.l.	96.5
mean	18.42	6.36	0.52	61.48	0.21	0.36	1.40	2.22	9.54	0.06	0.09	0.40	<d.l.	<d.l.	0.85	<d.l.	<d.l.	<d.l.	<d.l.	<d.l.	**101.96**
SD	0.11	0.09	0.06	0.81	0.07	0.05	0.04	0.03	0.19	0.02	0.01	0.11			0.03				<d.l.		
L311FR2	19.68	5.04	0.55	63.22	0.19	0.34	1.41	2.45	7.89	0.05	<d.l.	0.28	<d.l.	<d.l.	0.83	<d.l.	<d.l.	<d.l.	<d.l.	<d.l.	**101.98**
SD	0.22	0.08	0.09	0.40	0.02	0.03	0.06	0.22	0.17	0.02		0.04			0.02				<d.l.		
L311AB1	20.36	8.06	1.02	61.27	0.16	0.43	0.99	2.66	6.62	0.06	0.06	0.50	<d.l.	<d.l.	0.66	<d.l.	<d.l.	<d.l.	<d.l.	<d.l.	**102.98**
SD	0.39	0.17	0.07	0.19	0.03	0.04	0.04	0.02	0.03	0.01	0.00	0.02			0.06				<d.l.		
L311AB2	19.63	6.15	0.55	63.35	0.16	0.39	1.43	2.41	7.28	0.06	0.05	0.28	<d.l.	<d.l.	0.87	<d.l.	<d.l.	<d.l.	<d.l.	<d.l.	**102.71**
SD	0.25	0.05	0.10	0.29	0.03	0.04	0.06	0.16	0.07	0.02	0.01	0.01			0.02				<d.l.		
L31CAA1	15.30	6.82	1.17	65.24	0.16	0.35	0.78	3.25	7.15	0.09	0.06	0.56	<d.l.	<d.l.	0.64	<d.l.	<d.l.	<d.l.	<d.l.	<d.l.	**101.68**
SD	0.39	0.43	0.07	0.73	0.04	0.03	0.06	0.17	0.08	0.02	0.02	0.03			0.13				<d.l.		
L31CAA2	17.48	6.29	0.99	61.91	0.21	0.45	0.69	3.12	8.30	0.07	0.07	0.53	<d.l.	<d.l.	0.66	<d.l.	<d.l.	<d.l.	<d.l.	<d.l.	**100.90**
SD	0.31	0.04	0.10	0.45	0.02	0.05	0.02	0.08	0.10	0.02	0.03	0.04			0.03				<d.l.		
L31CAA3	17.39	6.55	0.96	62.99	0.18	0.45	0.69	3.26	7.78	0.07	<d.l.	0.45	<d.l.	<d.l.	0.74	<d.l.	<d.l.	<d.l.	<d.l.	<d.l.	**101.66**
SD	0.46	0.09	0.07	0.23	0.04	0.07	0.03	0.14	0.09	0.00		0.04			0.02				<d.l.		
Lα7AA	16.79	7.33	1.05	63.90	0.16	0.44	0.73	3.02	7.14	0.07	0.06	0.64	<d.l.	<d.l.	0.58	<d.l.	<d.l.	<d.l.	<d.l.	<d.l.	**101.97**
SD	0.22	0.19	0.07	0.43	0.03	0.05	0.05	0.16	0.21	0.01	0.02	0.04			0.07				<d.l.		
L31CTA	16.74	7.04	1.53	63.41	0.14	0.50	0.64	2.95	7.21	0.09	0.06	0.53	<d.l.	<d.l.	0.70	<d.l.	<d.l.	<d.l.	<d.l.	<d.l.	**101.63**
SD	0.40	0.05	0.16	0.56	0.02	0.05	0.05	0.08	0.11	0.01	0.03	0.02			0.09						
L31CSB	19.91	7.27	1.11	59.03	0.15	0.51	0.53	3.05	7.85	0.07	0.05	0.54	<d.l.	<d.l.	0.73	<d.l.	<d.l.	<d.l.	0.04	<d.l.	**100.92**
SD	0.51	0.57	0.07	0.74	0.04	0.01	0.02	0.12	0.36	0.02	0.01	0.05			0.02				0.04		

Sample	Na_2O	MgO	Al_2O_3	SiO_2	P_2O_5	SO_3	Cl	K_2O	CaO	TiO_2	MnO	FeO	CoO	NiO	CuO	ZnO	As_2O_3	SnO_2	Sb_2O_3	PbO	Tot.
L312AA2	0.76	0.74	1.36	72.91	0.26	0.04	<d.l.	17.23	2.18	0.05	<d.l.	0.40	<d.l.	<d.l.	4.00	<d.l.	<d.l.	<d.l.	0.07	<d.l.	**100.18**
SD	0.06	0.02	0.11	0.82	0.04	0.04		0.27	0.08	0.02		0.02			0.05				0.02		
L18AA1	2.20	0.69	1.51	72.06	0.24	0.03	<d.l.	16.05	2.06	0.07	<d.l.	0.51	<d.l.	<d.l.	4.04	<d.l.	<d.l.	0.16	0.09	<d.l.	**99.82**
SD	0.10	0.09	0.21	0.34	0.04	0.02		0.36	0.14	0.02		0.10			0.40			0.10	0.03		
L311FR1-A	7.54	0.61	1.99	74.62	0.16	0.05	0.12	8.53	1.88	0.09	<d.l.	0.63	<d.l.	<d.l.	3.65	<d.l.	<d.l.	<d.l.	0.09	<d.l.	**100.08**
SD	0.33	0.04	0.08	0.62	0.04	0.04	0.02	0.31	0.09	0.01		0.05			0.10				0.03		
L311FR1-Bi	7.76	0.59	2.03	75.67	0.12	0.04	0.11	8.22	1.83	0.08	<d.l.	0.64	<d.l.	<d.l.	3.02	<d.l.	<d.l.	<d.l.	0.08	<d.l.	**100.29**
SD	0.16	0.03	0.11	0.51	0.05	0.03	0.01	0.18	0.03	0.01		0.05			0.07				0.04		
L311AA1	6.26	0.47	1.28	75.70	0.12	0.03	0.04	9.76	1.30	0.05	<d.l.	0.41	<d.l.	<d.l.	4.90	<d.l.	<d.l.	<d.l.	0.10	<d.l.	**100.53**
SD	0.31	0.03	0.08	0.24	0.04	0.02	0.01	0.32	0.04	0.01		0.05			0.08				0.04		
L311AA2**	0.05	0.70	1.42	79.94	0.28	<d.l.	<d.l.	1.55	2.07	0.04	<d.l.	0.44	<d.l.	<d.l.	2.86	<d.l.	<d.l.	0.16	<d.l.	<d.l.	**89.62**
SD	0.05	0.02	0.04	0.97	0.03			0.41	0.02	0.02		0.03			0.09			0.04			
L312AA1																					
Cu-poor	4.84	0.63	2.57	75.46	0.09	0.05	0.04	11.06	1.51	0.10	<d.l.	0.65	<d.l.	<d.l.	2.91	<d.l.	<d.l.	<d.l.	0.11		100.11
SD	0.27	0.01	0.13	1.15	0.04	0.01	0.01	0.16	0.03	0.04		0.06			0.29				0.02		
Cu-rich	4.93	0.58	2.21	75.79	0.11	0.05	0.04	10.97	1.42	0.08	<d.l.	0.56	<d.l.	<d.l.	3.37	<d.l.	<d.l.	<d.l.	0.08		100.29
SD	0.19	0.06	0.27	0.87	0.03	0.03	0.02	0.12	0.06	0.01		0.10			0.13				0.02		
mean	4.89	0.60	2.35	75.66	0.10	0.05	0.04	11.01	1.46	0.08	<d.l.	0.59	<d.l.	<d.l.	3.18	<d.l.	<d.l.	<d.l.	0.10	<d.l.	**100.22**
SD	0.22	0.05	0.28	0.94	0.03	0.02	0.01	0.14	0.07	0.03		0.09			0.31				0.02		
L312AA3																					
Cu-poor	4.71	0.56	1.47	75.10	0.15	0.05	0.05	12.53	1.40	0.05	<d.l.	0.40	<d.l.	<d.l.	3.07	<d.l.	<d.l.	0.28	0.11	<d.l.	99.97
SD	0.24	0.03	0.06	0.32	0.01	0.03	0.01	0.21	0.06	0.02		0.03			0.37			0.13	0.02		
Cu-rich	4.80	0.54	1.43	74.87	0.14	0.04	0.06	12.21	1.36	0.06	<d.l.	0.42	<d.l.	<d.l.	3.36	<d.l.	<d.l.	0.31	0.12	<d.l.	99.80
SD	0.24	0.02	0.12	0.51	0.02	0.02	0.00	0.23	0.04	0.01		0.05			0.34			0.04	0.01		
mean	4.77	0.55	1.45	74.96	0.14	0.05	0.05	12.34	1.38	0.06	<d.l.	0.42	<d.l.	<d.l.	3.36	<d.l.	<d.l.	0.30	0.11	<d.l.	**99.99**
SD	0.23	0.02	0.10	0.44	0.01	0.02	0.01	0.27	0.05	0.02		0.04			0.36			0.08	0.02		
L314AZ1																					
Cu-poor	6.15	0.95	2.37	75.48	0.21	0.02	0.07	9.20	2.28	0.09	<d.l.	0.83	<d.l.	<d.l.	2.56	<d.l.	<d.l.	0.05	0.10	<d.l.	100.46
SD	0.42	0.09	0.30	0.37	0.03	0.02	0.01	0.22	0.07	0.03		0.08			0.29			0.06	0.03		
Cu-rich	7.03	0.73	1.80	73.48	0.16	0.04	0.08	9.16	2.13	0.09	<d.l.	0.60	<d.l.	<d.l.	4.63	<d.l.	<d.l.	0.16	0.14	<d.l.	100.35
SD	0.85	0.04	0.17	1.69	0.05	0.03	0.03	0.33	0.21	0.01		0.02			0.61			0.03	0.04		
mean	6.69	0.82	2.02	74.24	0.18	0.03	0.08	9.17	2.19	0.09	<d.l.	0.69	<d.l.	<d.l.	3.83	<d.l.	<d.l.	0.12	0.12	<d.l.	**100.40**
SD	0.82	0.13	0.36	1.65	0.05	0.03	0.03	0.29	0.18	0.02		0.13			1.16			0.07	0.04		

Sample	Na_2O	MgO	Al_2O_3	SiO_2	P_2O_5	SO_3	Cl	K_2O	CaO	TiO_2	MnO	FeO	CoO	NiO	CuO	ZnO	As_2O_3	SnO_2	Sb_2O_3	PbO	Tot.
L314AZ2	6.36	0.73	2.01	74.69	0.14	0.04	0.10	8.93	2.01	0.07	<d.l.	0.61	<d.l.	<d.l.	4.22	<d.l.	<d.l.	0.15	0.14	<d.l.	**100.34**
SD	0.26	0.04	0.16	0.52	0.03	0.02	0.02	0.33	0.17	0.02		0.04			0.18			0.04	0.04		
L314AA1	7.86	0.69	2.02	75.80	0.06	0.04	0.14	7.51	1.33	0.10	<d.l.	0.65	<d.l.	<d.l.	3.55	<d.l.	<d.l.	0.23	0.07	<d.l.	**100.16**
SD	0.19	0.06	0.10	0.60	0.03	0.02	0.02	0.20	0.04	0.01		0.03			0.11			0.04	0.05		
L314AA2	7.77	0.72	2.08	75.39	0.06	<d.l.	0.11	7.88	1.34	0.08	<d.l.	0.64	<d.l.	<d.l.	3.36	<d.l.	<d.l.	0.14	0.07	<d.l.	**99.75**
SD	0.28	0.02	0.11	0.64	0.04		0.01	0.16	0.04	0.01		0.02			0.09			0.04	0.04		
L12AA1	4.46	0.57	1.44	74.59	0.15	0.05	0.05	12.30	1.32	0.06	<d.l.	0.40	<d.l.	<d.l.	3.69	<d.l.	<d.l.	0.27	0.06	<d.l.	**99.48**
SD	0.24	0.01	0.14	0.50	0.03	0.03	0.01	0.26	0.04	0.01		0.03			0.16			0.03	0.04		
L12AA2	4.46	0.57	1.35	74.23	0.15	0.06	0.04	12.39	1.32	0.06	<d.l.	0.39	<d.l.	<d.l.	3.81	<d.l.	<d.l.	0.29	0.07	<d.l.	**99.25**
SD	0.14	0.02	0.08	0.65	0.03	0.02	0.01	0.26	0.03	0.01		0.03			0.09			0.03	0.04		
L12SM	7.31	0.78	1.81	74.84	0.13	<d.l.	0.10	8.29	1.37	0.09	<d.l.	0.62	<d.l.	<d.l.	4.53	<d.l.	<d.l.	0.06	0.07	<d.l.	**100.09**
SD	0.19	0.01	0.06	0.56	0.05		0.01	0.19	0.02	0.02		0.04			0.08			0.02	0.04		
L12V1	6.84	0.69	1.91	74.65	0.20	0.03	0.08	8.11	1.81	0.07	<d.l.	0.61	<d.l.	<d.l.	4.91	<d.l.	<d.l.	<d.l.	0.08	<d.l.	**100.11**
SD	0.18	0.05	0.10	0.56	0.02	0.03	0.01	0.25	0.04	0.02		0.06			0.15				0.04		
L12V2	6.98	0.77	1.56	75.09	0.17	0.03	0.09	7.88	1.69	0.06	<d.l.	0.57	<d.l.	<d.l.	4.59	<d.l.	<d.l.	0.30	0.04	<d.l.	**99.90**
SD	0.16	0.02	0.09	0.42	0.03	0.02	0.02	0.16	0.03	0.02		0.03			0.06			0.02	0.03		
L12VA**	0.07	0.64	1.16	77.52	0.34	0.03	<d.l.	1.77	1.91	0.05	<d.l.	0.42	<d.l.	<d.l.	4.37	<d.l.	<d.l.	0.25	<d.l.	<d.l.	**88.63**
SD	0.08	0.03	0.07	0.48	0.03	0.02		0.22	0.05	0.01		0.02			0.12			0.06			
L18AA2	6.81	0.68	2.29	74.91	0.11	0.04	0.15	9.16	1.41	0.08	<d.l.	0.57	<d.l.	<d.l.	3.93	<d.l.	<d.l.	<d.l.	0.08	<d.l.	**100.31**
SD	0.25	0.05	0.11	0.50	0.05	0.02	0.01	0.21	0.09	0.02		0.04			0.17				0.03		
L12GA	5.53	0.64	1.09	75.46	0.09	0.03	<d.l.	10.48	1.60	0.05	<d.l.	0.37	<d.l.	<d.l.	4.43	<d.l.	<d.l.	0.05	0.06	<d.l.	**100.05**
SD	0.21	0.02	0.16	0.48	0.05	0.02		0.19	0.05	0.03		0.04			0.17			0.02	0.03		
L314GA	5.73	0.60	1.65	73.43	0.15	0.05	0.11	10.80	1.83	0.06	<d.l.	0.45	<d.l.	<d.l.	4.69	<d.l.	<d.l.	0.17	0.05	<d.l.	**99.84**
SD	0.31	0.03	0.08	0.57	0.03	0.03	0.01	0.26	0.04	0.02		0.03			0.11			0.03	0.03		
L311O1A	6.49	0.62	2.29	76.15	0.12	0.04	0.10	9.03	1.63	0.08	<d.l.	0.55	<d.l.	<d.l.	3.00	<d.l.	<d.l.	0.04	0.09	<d.l.	**100.30**
SD	0.15	0.03	0.18	0.56	0.01	0.02	0.01	0.17	0.05	0.01		0.03		0.01	0.07		0.00	0.02	0.02		
L312AN1	6.50	0.83	1.54	77.16	0.18	<d.l.	0.04	9.30	1.73	0.07	<d.l.	0.77	0.13	0.25	0.86	<d.l.	0.16	<d.l.	0.24	<d.l.	**99.88**
SD	0.30	0.03	0.08	0.23	0.04		0.01	0.27	0.05	0.02		0.05	0.03	0.01	0.03		0.04		0.04		
L312AN2	6.45	0.62	1.99	75.53	0.10	0.05	0.12	10.01	1.56	0.06	<d.l.	0.66	0.08	0.59	1.26	<d.l.	0.47	<d.l.	0.39	<d.l.	**100.03**
SD	0.15	0.06	0.12	0.40	0.03	0.03	0.03	0.30	0.15	0.02		0.04	0.01	0.03	0.05		0.03		0.03		
L314AN1	7.12	0.84	2.20	74.36	0.14	0.05	0.15	8.53	2.25	0.11	<d.l.	1.07	0.09	0.47	1.82	0.11	0.25	<d.l.	0.39	0.10	**100.09**
SD	0.16	0.03	0.10	0.30	0.03	0.02	0.03	0.21	0.07	0.01		0.05	0.01	0.01	0.05	0.02	0.02		0.04	0.04	
L314AN2	7.05	0.87	2.20	74.27	0.18	0.05	0.16	8.64	2.13	0.09	<d.l.	1.16	0.08	0.64	2.03	0.10	0.34	<d.l.	0.43	<d.l.	**100.52**
SD	0.28	0.03	0.09	0.48	0.04	0.03	0.02	0.33	0.03	0.02		0.04	0.02	0.05	0.05	0.03	0.07		0.05		

Sample	Na_2O	MgO	Al_2O_3	SiO_2	P_2O_5	SO_3	Cl	K_2O	CaO	TiO_2	MnO	FeO	CoO	NiO	CuO	ZnO	As_2O_3	SnO_2	Sb_2O_3	PbO	Tot.
L314CO1																					
Cu-poor	6.64	0.58	1.74	76.21	0.10	<d.l.	0.05	8.84	1.67	0.08	<d.l.	1.06	0.18	0.33	1.33	0.05	0.24	<d.l.	0.43	<d.l.	99.64
SD	0.09	0.01	0.09	0.50	0.01		0.01	0.10	0.06	0.01		0.05	0.03	0.07	0.07	0.01	0.03		0.03		
Cu-rich	6.31	0.59	1.70	76.13	0.10	<d.l.	0.05	8.94	1.73	0.08	<d.l.	1.25	0.24	0.49	1.77	0.06	0.33	<d.l.	0.62	<d.l.	100.47
SD	0.35	0.02	0.09	0.65	0.04		0.02	0.28	0.05	0.02		0.05	0.03	0.03	0.08	0.03	0.05		0.02		
mean	6.41	0.59	1.71	76.15	0.10	<d.l.	0.05	8.91	1.71	0.08	<d.l.	1.19	0.22	0.44	1.64	0.06	0.30	<d.l.	0.57	<d.l.	**100.22**
SD	0.33	0.02	0.09	0.58	0.03		0.02	0.24	0.05	0.02		0.10	0.04	0.09	0.23	0.02	0.06		0.10		
L314CO2	6.08	0.80	2.46	75.93	0.11	0.04	0.07	8.69	2.16	0.10	<d.l.	1.26	0.20	0.37	0.70	<d.l.	0.18	<d.l.	0.27	<d.l.	**99.53**
SD	0.26	0.03	0.16	0.41	0.04	0.02	0.03	0.26	0.05	0.04		0.05	0.08	0.14	0.25		0.08		0.10		
L314XA	7.01	0.87	2.19	73.73	0.17	0.05	0.17	8.80	2.14	0.09	<d.l.	1.13	0.08	0.62	2.01	0.12	0.30	<d.l.	0.42	0.10	**100.02**
SD	0.32	0.04	0.12	0.62	0.06	0.02	0.02	0.28	0.07	0.01		0.03	0.02	0.04	0.10	0.03	0.05		0.05	0.07	
L12AN1	5.94	0.93	2.27	77.15	0.17	<d.l.	0.05	8.49	2.62	0.10	<d.l.	0.81	0.14	0.23	0.32	<d.l.	0.10	<d.l.	0.19	<d.l.	**99.63**
SD	0.22	0.04	0.16	0.46	0.04		0.01	0.19	0.08	0.02		0.02	0.02	0.04	0.03		0.03		0.05		
L12AN2	6.51	0.81	1.75	75.56	0.19	0.04	0.03	8.70	1.86	0.06	<d.l.	1.06	0.25	0.62	1.16	<d.l.	0.38	<d.l.	0.59	<d.l.	**99.66**
SD	0.25	0.03	0.10	0.27	0.04	0.03	0.01	0.32	0.04	0.02		0.05	0.04	0.05	0.04		0.03		0.05		
L12CO	6.44	0.75	1.90	74.84	0.18	0.05	0.06	9.53	2.38	0.08	<d.l.	0.94	0.13	0.23	1.50	<d.l.	0.18	0.04	0.48	<d.l.	**99.75**
SD	0.34	0.07	0.14	0.81	0.04	0.04	0.01	0.28	0.18	0.01		0.07	0.03	0.03	0.09		0.06	0.02	0.09		
L18CO	6.27	0.82	1.59	77.17	0.17	<d.l.	0.04	9.25	1.74	0.07	<d.l.	0.73	0.11	0.27	0.85	<d.l.	0.19	<d.l.	0.22	<d.l.	**99.60**
SD	0.27	0.02	0.07	0.47	0.04		0.01	0.23	0.04	0.01		0.04	0.02	0.02	0.05		0.04		0.03		
L18DA	5.37	0.92	1.97	75.26	0.21	0.05	<d.l.	9.95	2.69	0.08	<d.l.	1.06	0.19	0.37	1.44	<d.l.	<d.l.	<d.l.	0.16	0.12	**99.98**
SD	0.41	0.07	0.23	0.49	0.03	0.02		0.12	0.21	0.02		0.11	0.03	0.05	0.09				0.03	0.02	
L311O2B	7.48	0.95	2.72	76.59	0.14	0.04	0.11	8.20	1.91	0.12	<d.l.	0.92	<d.l.	<d.l.	0.03	<d.l.	<d.l.	<d.l.	0.10	<d.l.	**99.38**
SD	0.82	0.13	0.27	0.27	0.03	0.02	0.01	0.61	0.12	0.02		0.15			0.03				0.04		
L311O2A	7.41	0.62	2.02	74.88	0.17	0.04	0.12	8.59	1.89	0.08	<d.l.	0.64	<d.l.	<d.l.	3.66	<d.l.	<d.l.	<d.l.	0.09	<d.l.	**100.26**
SD	0.33	0.01	0.11	0.93	0.03	0.04	0.02	0.10	0.14	0.02		0.05			0.17				0.02		
L311O3A	7.87	0.58	1.89	74.74	0.14	0.04	0.09	8.04	1.80	0.06	<d.l.	0.54	<d.l.	<d.l.	4.01	<d.l.	<d.l.	<d.l.	0.09	<d.l.	**100.00**
SD	0.49	0.07	0.13	1.09	0.03	0.03	0.02	0.53	0.12	0.02		0.05			0.24				0.04		
L311O3B**	0.06	0.50	1.87	85.68	0.14	0.03	0.09	0.35	1.84	0.07	<d.l.	0.50	<d.l.	<d.l.	0.36	<d.l.	<d.l.	<d.l.	<d.l.	<d.l.	**91.59**
SD	0.06	0.10	0.27	2.58	0.05	0.03	0.03	0.58	0.34	0.02		0.10			0.94						
L311O4B**	0.16	0.83	2.28	81.10	0.13	0.09	0.08	0.37	1.63	0.07	<d.l.	0.52	<d.l.	<d.l.	0.65	<d.l.	<d.l.	<d.l.	<d.l.	<d.l.	**88.00**
SD	0.17	0.56	0.30	5.99	0.06	0.12	0.03	0.23	0.62	0.02		0.09			1.06						
L311O4A	8.15	0.75	2.20	73.48	0.26	0.06	0.12	8.68	2.29	0.07	<d.l.	0.59	<d.l.	<d.l.	2.88	<d.l.	<d.l.	0.06	0.09	<d.l.	**99.81**
SD	0.44	0.17	0.57	1.45	0.09	0.03	0.01	0.30	0.37	0.03		0.14			0.48			0.05	0.03		

Sample	Na_2O	MgO	Al_2O_3	SiO_2	P_2O_5	SO_3	Cl	K_2O	CaO	TiO_2	MnO	FeO	CoO	NiO	CuO	ZnO	As_2O_3	SnO_2	Sb_2O_3	PbO	Tot.
L31CGA	8.24	1.01	2.18	74.49	0.22	0.04	0.24	6.12	2.91	0.10	<d.l.	0.63	<d.l.	<d.l.	3.67	<d.l.	<d.l.	0.35	0.04	<d.l.	**100.32**
SD	0.46	0.12	0.11	1.26	0.05	0.02	0.02	0.27	2.42	0.03		0.04			1.18			0.16	0.03		
L31CGB	7.68	1.29	2.18	71.55	0.26	0.09	0.24	6.68	8.75	0.10	<d.l.	0.67	<d.l.	<d.l.	0.27	<d.l.	<d.l.	<d.l.	0.04	<d.l.	**99.86**
SD	0.49	0.04	0.07	0.40	0.04	0.01	0.02	0.33	0.28	0.01		0.04			0.15				0.03		
L31CB2B	5.38	1.10	1.93	71.32	0.24	<d.l.	0.07	6.83	12.00	0.09	<d.l.	0.64	<d.l.	<d.l.	0.15	<d.l.	<d.l.	<d.l.	0.06	<d.l.	**99.94**
SD	0.44	0.07	0.17	2.11	0.06		0.02	0.48	2.79	0.02		0.07			0.03				0.04		
L31CB2A	7.71	0.74	1.63	75.38	0.06	<d.l.	0.17	7.38	1.73	0.07	<d.l.	0.55	<d.l.	<d.l.	4.36	<d.l.	<d.l.	0.23	0.05	<d.l.	**100.21**
SD	0.21	0.05	0.14	0.95	0.01		0.02	0.39	0.65	0.02		0.03			0.35			0.04	0.03		
L31COA	8.83	0.82	1.69	76.55	0.17	<d.l.	0.23	6.84	1.67	0.07	<d.l.	0.53	<d.l.	<d.l.	3.05	<d.l.	<d.l.	0.14	0.08	<d.l.	**100.76**
SD	0.27	0.09	0.11	1.02	0.05		0.04	0.26	0.19	0.01		0.06			0.39			0.03	0.04		
L31COB**	0.06	0.61	2.30	85.75	0.08	<d.l.	0.19	0.38	1.63	0.08	<d.l.	0.68	<d.l.	<d.l.	0.05	<d.l.	<d.l.	<d.l.	<d.l.	<d.l.	**91.94**
SD	0.08	0.24	0.20	0.81	0.02		0.08	0.13	0.21	0.02		0.05			0.03						
L31CB1B	7.58	1.23	2.35	69.72	0.21	0.07	0.12	7.39	8.83	0.09	<d.l.	0.73	<d.l.	<d.l.	0.86	<d.l.	<d.l.	0.04	0.04	<d.l.	**99.34**
SD	0.17	0.02	0.05	0.58	0.03	0.04	0.01	0.15	0.09	0.02		0.04			0.16			0.05	0.04		
L31CB1A	7.48	0.78	1.75	76.53	0.09	0.03	0.14	7.93	1.52	0.07	<d.l.	0.62	<d.l.	<d.l.	3.18	<d.l.	<d.l.	0.19	0.09	<d.l.	**100.51**
SD	0.17	0.02	0.05	0.58	0.03	0.04	0.01	0.15	0.09	0.02		0.04			0.16			0.05	0.04		
L12BOTA	6.22	0.77	1.98	74.12	0.26	0.04	0.11	7.90	5.40	0.07	<d.l.	0.79	0.16	0.64	0.81	<d.l.	0.30	<d.l.	0.10	<d.l.	**99.74**
SD	0.25	0.03	0.08	0.59	0.04	0.02	0.02	0.31	0.12	0.02		0.03	0.03	0.04	0.04		0.05		0.04		
L12BOTB	6.03	0.79	2.07	74.02	0.28	0.06	0.10	8.07	5.48	0.08	<d.l.	0.82	0.15	0.64	0.80	<d.l.	0.30	<d.l.	0.10	<d.l.	**99.84**
SD	0.23	0.04	0.04	0.55	0.04	0.02	0.02	0.18	0.06	0.01		0.06	0.02	0.02	0.03		0.01		0.06	0.02	

Tab. 5.1. EPMA chemical analyses (oxides wt%) of the glass phase in the Lipari and Salina analyzed beads. The labels are the same reported in Tables 1-3 (par. 3.2.1). Data are calculated as a mean of 5÷10 point analysis (d.l.= detection limit; SD = EPMA standard deviation; * = EDS data; ** weathered glasses: they will be considered only partially in the discussion).

5.2 Piovego cemetery

- *Silica source and flux composition*

The chemical composition of the glass phases performed by means of EPMA (Tab. 5.2.1), highlights that the samples are soda-lime-silica glasses composed of SiO_2 ranging from 50 to 70 wt%, Na_2O from 7 to 20 wt% and CaO from 5 and 11 wt%. Figures 5.2.1 and 5.2.2 report the MgO *vs* K_2O and Na_2O *vs* K_2O contents of the glass phases, commonly used to define the compositional classes of protohistoric vitreous materials. Plots are based on objects' typologies and colors. In fact, even though they may be subdivided into chronological sub-phases (see Tab. 1 par. 3.2.2); compositional variations do not seem to be related to the objects' age. For example, in the MgO *vs* K_2O plot in which samples are grouped by colors and chronological phases (Fig. 5.2.1 bis) it is clear that glasses belonging to the same phase (e.g. Este IIIC phase) have different Mg and K contents.

The Mg and K amounts (Fig. 5.2.1) are particularly low for all but two of the samples (K_2O = 0.08÷0.66 wt% and MgO = 0.34÷0.78 wt%) as it is typical in the Low Magnesium Glasses (LMG) obtained using *natron* as flux. Similarly, the S and Cl contents (SO_3 = 0.08÷0.55 wt%, Cl_2O = 0.65÷2.11 wt%) are in the range of the *natron*-based glasses (Shortland et al 2009). Interestingly, only the bead PG-FUA presents 2.82 wt% of K_2O and 3.13 wt% of MgO as in the High Magnesium Glasses (HMG) produced with soda-rich plant ashes as flux (Fig. 5.2.1). Sample PG-GON5 presents an intermediate composition between these two compositional classes, with slightly higher contents of Mg (MgO = 1.76 wt%) and K (K_2O = 0.74 wt%) (Fig. 5.2.1). Except for sample PG-FUA, the Na_2O *vs* K_2O contents (fig. 5.2.2) are in the range of the *natron*-based glasses, even though the Na_2O/K_2O ratio is variable. In fact, colorless and transparent glasses (pale blue, pale green and yellow/brown) have a high Na_2O/K_2O ratio (114÷426) due to very low K contents (up to 0.16 wt%, see tab. 5.2.1). In the other samples, the ratio ranges from 23 to 80 depending on the K contents varying from 0.20 to 0.67 wt% (tab. 5.2.1). Potash can also be introduced by the sand and consequently the variation of K content may be related to a variation in the raw material used as source of silica (Tite et al. 2008c). Among the LMG glasses, samples PG-CM and PG-GOB8 have the lowest Na_2O/K_2O ratio (10.5 and 16.8, respectively) due to both higher K contents (K_2O = 0.66 and 0.57 wt%,

respectively) and lower Na amounts (Na_2O = 6.98 and 9.54 wt%, respectively) (Fig. 5.2.2). Similarly, sample PG-GO5Bi presents a low Na level (Na_2O = 11.96 wt%, Tab. 5.2.1) even though the Na_2O/K_2O ratio (about 22) is comparable to other analyzed glasses. Besides the low contents of Na, samples PG-GO5Bi, PG-CM and PG-GOB8 are characterized by high concentrations of Pb (PbO = 16÷25 wt%), which helps the glass matrix fluidity (Fig. 5.2.3 bis) with a good negative correlation between the two oxides. Moreover, samples PG-CM and PG-GOB8 have high levels of Al (Al_2O_3 = 2.0 and 1.63 wt% respectively), Fe (FeO = 4.83 and 6.92 wt%) (fig. 5.2.3) and Mn (MnO = 0.87 and 0.57 wt%). Other opaque blue beads (Pg-FA, PG-AB and PG-AB1_2) show significant Pb amounts (PbO = 6.70, 2.57 and 2.81 wt%, respectively) even though Na contents are comparable with the other samples (Fig. 5.2.3 bis). Generally, Al and Fe contents are low in the colorless, transparent pale blue and yellow/amber glasses (Al_2O_3 = 0.30÷0.55 wt% and FeO = 0.20÷0.38 wt%) and pure sand or quartzite may be used for the production of these glasses. Instead, in the other samples alumina and iron concentrations are variable but mainly high (Al_2O_3 = 0.40÷2.60 wt% and FeO = 0.30÷6.4 wt%) suggesting the use of sand as source of silica (Freestone et al. 2002). The highest percentages of Fe (2.78÷6.90 wt%) are attested in the dark blue and brown/black opaque beads (fig. 5.2.3) and are related also to the color.
The other minor and trace elements are variable depending on the color and opacity/transparency of the glasses.

- *Colorants and opacifiers*

Blue glasses

The blue beads are mostly colored by Co (CoO = 0.04÷0.47 wt%), contain also minor amounts of Cu (CuO = 0.08÷1.07 wt%) and present a particular texture (see below). They are seven small annular beads (PG-AB8, PG-AB9a/b/c/d and PG-ABOa/b), three annular beads (PG-AB, PG-AB1_2, and AAB), two eyes globular beads (pale blue body PG-GOA and blue eye PG-GOB-Bi, and PG-GOB8), a 5 horned bead (PG-SB) and one bead fragment with undefined shape (PG-FA). Only three glasses are Cu-colored (CuO = 0.09÷1.00 wt%) with Co under the

detection limit and they are: one simple globular bead (PG-GAT1), one eyes globular bead (GO6B-Bi) and the HMG blue bead with unknown typology (PG-FUA).

The Co colored glasses have similar monovalent (Na_2O, K_2O) and bivalent (MgO, CaO) alkali contents (Tab. 5.2.1), even though three samples (PG-GOB8, PG-GO3B-Bi and PG-FA) have higher CaO amounts (7÷8.75 wt%) than the other (CaO = 4÷6 wt%). The Al content is mostly < 1 wt% (Tab. 5.2.1) except for samples PG-GOB8, GO3B-Bi, PG-GOA and GOB-Bi in which it ranges from 1.63 to 3.00 wt%. Iron is generally > 1 wt% and particularly high (FeO = 6.97 wt%) in sample PG-GOB8 that presents also manganese (MnO = 0.54 wt%).
The Co and Cu contents in the Co-colored glasses are variable (Fig. 5.2.4). In the samples the Cu content is higher than Co and the CuO/CoO ratio generally ranges from 1.20 to 4.31 except for sample PG-AAB in which it is particularly high (13.41) due to a higher Cu content (CuO = 1.07 wt%) than Co (Co = 0.08 wt%). Only sample PG-GOB-Bi presents a higher content of Co (Co = 0.24 wt%) with respect to Cu (CuO = 0.08 wt%) and a CuO/CoO ratio of 0.34 (Fig. 5.2.4). Mostly of the small annular beads have the highest Co contents (CoO = 0.39÷1.07 wt%) associated to significant Cu amounts (CuO = 0.66÷1.07 wt%) (Fig. 5.2.4 dotted line).
In addition to copper, the other elements associated to cobalt are extremely variable. Samples PG-AB8, ABOa/b and AB9a/b/c/d have Ni (NiO = 0.42÷0.69 wt%), As (As_2O_3 = 0.17÷0.68 wt%) and Sb (Sb_2O_3 = 0.21÷0.34 wt%); moreover, samples PG-ABOa/b and PG-AB9c also have Pb (PbO = 0.30÷0.47 wt%). Interestingly, they are all small annular beads belong to grave 127 and dated to the Este IIID phase, 525-450 B.C. (tab. 1.31-32-34, par. 3.2.2).
Considering the Ni *vs* As_2O_3 contents (fig. 5.2.5) these samples can be distinguished in two groups: the first constituted by samples PG-ABOa/b and PG-AB9c (inside the continuous line) and the second characterized by samples PG-AB8 and AB9a/b/d (inside the dotted line). Moreover, the second group seems to show a linear correlation between Ni and As that does not occur in the first one. Interestingly, the group of samples ABOa/b and PG-AB9c is different from samples PG-AB8 and AB9a/b/d also for the presence of Pb, as previously said.
Samples PG-AB1_2 and AB present only Sb (Sb_2O_3 about 0.35 wt%) and Pb (PbO = 2.57÷2.81 wt%) as other minor elements (fig. 5.2.5bis). The ornaments are: one annular bead (PG-AB) and half annular bead (PG-AB1_2) belonging to grave 121 dated to the Este IIIC phase, 525-450 B.C. (tab. 1.29-30, par. 3.2.2). Similarly, samples PG-GO3B-Bi and PG-FA have

significant levels of Sb and Pb but with different amounts (fig. 5.2.5bis). Sample PG-GO3B have a Sb content in the range of the other cobalt blue beads (Sb_2O_3 = 0.33 wt%) but the Pb amount is lower than in samples PG-AB1_2 and AB (PbO = 0.17 wt%). PG-FA has the highest Sb level (Sb_2O_3 = 2.77 wt%) and a high Pb content (PbO = 6.70 wt%) together with traces of Zn (ZnO = 0.04 wt%). Sample PG-GOB8 has the highest Pb content (PbO = 18.50 wt%) together with lower contents of Ni (NiO = 0.07 wt%), As (As_2O_3 = 1.68 wt%), Sb (Sb_2O_3 = 0.64 wt%) and traces of Zn (ZnO = 0.05 wt%). Sample PG-GOB-Bi (blue eye decoration) has a significant amount of Sb (Sb_2O_3 = 1.95 wt%) and traces of Zn (ZnO = 0.04 wt%) while sample PG-SB only has Ni traces (NiO = 0.36 wt%). Sample PG-GOA (pale blue body) has Sb (Sb_2O_3 = 1.92 wt%) and Pb (PbO = 0.17 wt%); the presence of Sb in the pale blue body PG-GOA is consistent also with the Ca antimonate crystals dispersed in the glass matrix (see below) as opacifier. Interestingly, sample PG-AAB has no other element associated to cobalt beyond copper.

Summarizing the results it is possible to note that the chemical composition of the elements related to the coloring agent is extremely variable in type and amounts, and this testifies the use of different cobalt sources.

The copper-colored sample PG-FUA has an HMG composition that is comparable with both HMG glasses dated to the MBA3-BR (Angelini et al. 2009, 2010b) and those rarely found in the Early Iron Age (Angelini et al. 2011, Arletti et al. 2010, Polla et al. 2011). The other two copper colored LMG glasses (samples PG-GAT1 and PG-GO6B-Bi) have similar monovalent and bivalent alkali contents (Tab. 5.2.1). Interestingly, sample PG-GAT1 has a lower Ca content (Ca= 4.73 wt%) than the other (CaO = 8÷10 wt%) and presents manganese (MnO = 0.92 wt%).

The Al_2O_3 amount ranges from 1 to 2.50 wt% except for samples PG-GAT1 and PG-FUA in which it is 0.85 and 0.68 wt% respectively. Iron concentration is 0.86 wt% only in sample PG-GO6B-Bi while in the others is < 0.50 wt%.

In samples PG-FUA and PG-GAT1, copper ranges from 0.90 to 1 wt% while the globular bead PG-GO6B-Bi has a particularly low Cu content (CuO = 0.09 wt%). The HMG glass PG-FUA

has no trace elements associated to the coloring agent. Sample PG-GO6B-Bi only has traces of Sb (Sb_2O_3 = 0.52 wt%).

Yellow glasses

PG-FGi and PG-FG8 are two transparent yellow glasses from two different graves and dated to different phases (tab. 1.12-27, par. 3.2.2). They have a very similar chemical composition. They were both obtained with a pure sand or quartzite since the Al content is very low (Al_2O_3 = 0.30 wt%) as well as Fe (FeO = 0.16÷0.17 wt%). Consequently, in the absence of any other coloring elements, the color is due to Fe associated to S (SO_3 = 0.10÷0.15 wt%).

Brown glasses

The five brown glasses analyzed are different for typologies and chemical characteristics. The transparent fragment PG-FM14 was produced with a particularly pure sand as source of silica, since it has very low contents of Al (Al_2O_3 = 0.33 wt%) and Fe (FeO = 0.20 wt%). A similar composition characterized the amber glasses (PG-FGi and PG-FGi8). The color is due to an iron sulfide complex formed in a reducing atmosphere (Jackson et al. 2006; Nenna et al. 1997). The opaque fragment PG-FM89 and the opaque globular bead fragment PG-GONM have similar monovalent e bivalent alkali contents (Tab. 5.2.1), very low Al amounts (Al_2O_3 = 0.37 wt%) and low Ti (TiO_2 = 0.11 wt%). By contrast, the Fe content is high in PG-FM89 (FeO = 2.57 wt%) and very high in sample PG-GONM (FeO = 4.09 wt%). Moreover they both have traces of Sb (Sb_2O_3 = 0.04 wt% and 0.19 wt%, respectively). The opaque fragment PG-FM83 and the biconical bead with ribbed edges PG-CM are both characterized by higher levels of Al (Al_2O_3 = 2.41 and 2 wt%, respectively) and K (K_2O = 0.63 and 0.66 wt% respectively) than the other brown glasses (Al_2O_3 about 0.30 wt% and K_2O = 0.07÷0.14 wt%). In both samples, the color is due to Fe probably present in its highest oxidized state (FeO = 2.78 wt% in PG-FM83 and 4.83 wt% in PG-CM). However, PG-CM is completely different from the other brown glasses both for texture (see below) and chemical composition of the glass phase. In fact, it has lower contents of SiO_2 (49.86 wt%), CaO (4.19 wt%) and Na (6.98 wt%) than the other *natro*n-based glasses (Tab. 5.2.1). Interestingly, it has a very high Pb amount (PbO = 25.23 wt%) found for Iron Age ornaments only in some glasses and *glassy faïence* from

Lombardy (Angelini et al. 2011). Moreover, it presents high Fe contents (FeO = 4.83 wt%), significant Mn amounts (MnO = 0.87 wt%) and traces of Co (CoO = 0.03 wt%), Cu (CuO = 0.12 wt%), Zn (ZnO = 0.29 wt%), As (As_2O_3 = 1.91 wt%) and Sb (Sb_2O_3 = 0.11 wt%).

Black glasses

Two opaque black glasses are present in the Piovego cemetery, they have different typologies and chronological phases (tab. 1.7-10, par. 3.2.2): PG-GO5N is a large globular bead with a three white eyes decoration, while PG-AN is an annular bead probably with a three eyes decoration not preserved.

PG-AN is colored by high contents of Fe (FeO = 6.40 wt%) since there are no other coloring elements. The Al content is low (Al_2O_3 = 0.52 wt%) and it has a presence of Ti (TiO_2 = 0.19 wt%) and Sb (Sb_2O_3 = 0.09 wt%).

As mentioned above, PG-GO5N has a particularly intermediate composition due to higher Mg and K contents than the other *natron*-based glasses (Fig. 5.2.1 and tab. 5.2.1). It also presents lower Ca (CaO = 6.65 wt%) and higher Al (Al_2O_3 = 1.74 wt%) contents than PG-AN (tab. 5.2.1). The coloring of PG-GO5N is due to poorer Fe amounts (FeO = 0.80 wt%). And to traces of Mn (MnO = 0.50 wt%); moreover, Sb (Sb_2O_3 = 0.40 wt%) and Pb (PbO = 0.66 wt%) are present in the glass phase. Interestingly, it presents numerous small copper sulfides inclusions finely dispersed in the glass matrix (see below).

White glasses

Six white glasses (PG-GO3Bi, GO5Bi, GONBi, GO6Bi, GOBi and AOBi) were selected for this study and they are all eyes decoration of opaque black, brown and blue globular or annular beads (Tab. 1.7-9-14-16-17-22, Par. 3.2.2). They are opacified by the presence of Ca antimonates dispersed in the matrix (see below) with a Sb content in the glass phase ranging from 2.76 to 8.52 wt% (Sb_2O_3). All but one white glass have similar monovalent and bivalent

alkali contents (Tab. 5.2.1 and Fig. 5.2.1-2). The Al content is variable and ranging from 0.36 to 2.24 wt% while Fe is < 1 wt%. Sample PG-GO5Bi has lower Na (Na_2O = 11.60 wt%) and Ca (CaO = 4.50 wt%) contents than the other (CaO = 8÷10 wt%) and presents high Pb amounts in the glass phase (PbO = 15.92 wt%) (fig. 5.2.3bis). Interestingly the glass of the associated black body (sample PG-GO5N) does not show the presence of high Pb contents (PbO = 0.66 wt%). Low Pb amounts are also present in sample PG-GO3Bi and GO6Bi (PbO = 0.93 and 0.50 wt%, respectively), in the latter together with a low manganese content (MnO = 0.10 wt%).

Transparent and colorless glasses

Among the analyzed glasses there are nine transparent and colorless glasses with shades from very pale green to very pale blue. They are six beads fragments with undefined typologies (PG-FVA1, FVA5, FVA7, FVA22, FVA67 and FVA97), two globular beads (PG-GVA97 and PG-GAT7) and one annular bead (PG-AVT). They have comparable monovalent and bivalent alkali contents (Tab. 5.2.1) together with low alumina (Al_2O_3 = 0.30÷0.50 wt%) and Fe amounts (FeO = 0.20÷0.36 wt%) testifying the use of quartzite and/or a pure sand as source of silica. Sample PG-FVA67 is different from the other for the lower content of Ca (CaO = 5.84 wt%) and the presence of manganese (MnO = 0.42 wt%). However, that amount of manganese is too low to decolorize since at least 1 wt% of MnO is required to ensure the glass is decolorized (Brems et al. 2012) and, in any case, a $MnO/(Fe_2O_3)_{TOT}$ ratio > 2 is required (Silvestri et al. 2008). Considering the Sb_2O_3 *vs* MnO contents of the transparent samples (Fig. 5.2.6) it is clear that, except for PG-FVA67, manganese is under the detection limit while antimony ranges from 0.17 to 1.64 wt% for colorless glasses and is 3.57 wt% in the transparent green one. This testifies an intentional addition of antimony to decolorize the glass since small quantities (0.2 wt%) are required to render the glass colorless (Sayre 1963), although two or possibly three samples are borderline (dotted line, fig. 5.2.6). The semi-transparent green glass (PG-GVA97) has the highest content of Sb (Sb_2O_3 = 3.57 wt%) and presents Ca antimonate crystals dispersed in the glass matrix (see below). However, Ca antimonite crystals are numerically scarce and do not opacify the glass.

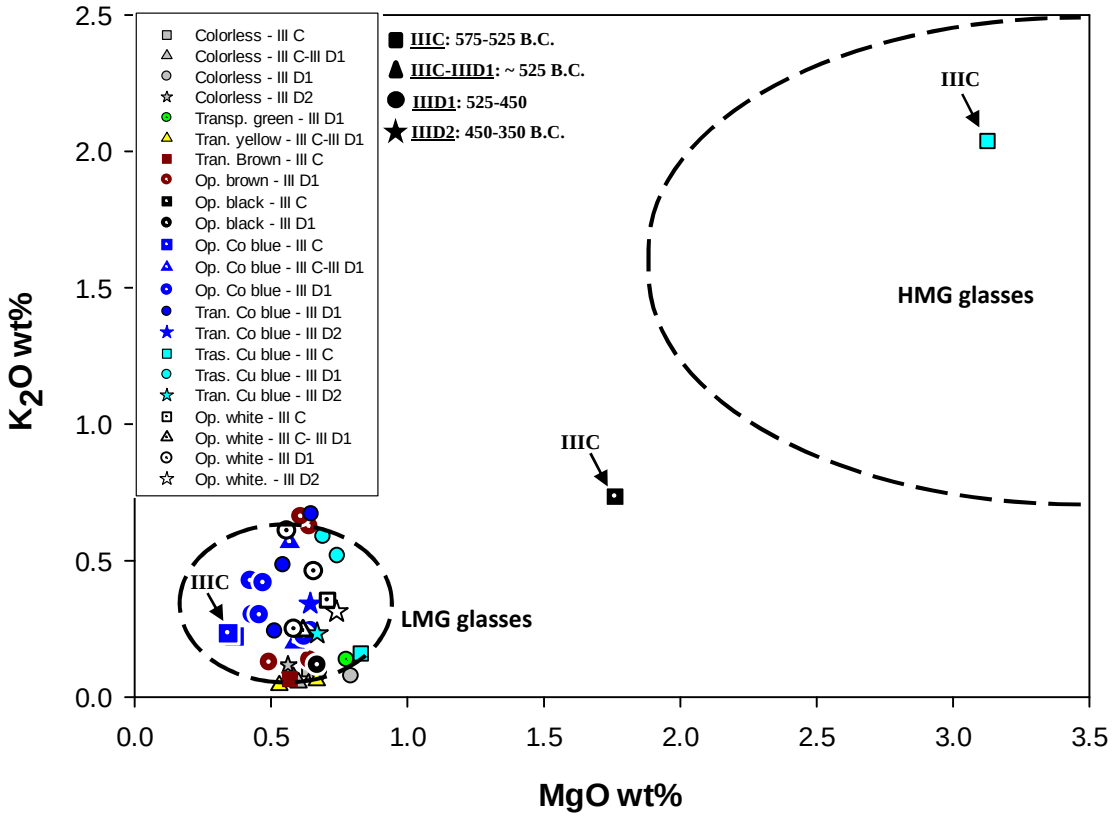

Fig. 5.2.1bis: MgO *vs* K_2O contents of the glass phase in the analyzed samples from the Piovego cemetery (symbols = Este phases; colors = color of the vitreous material).

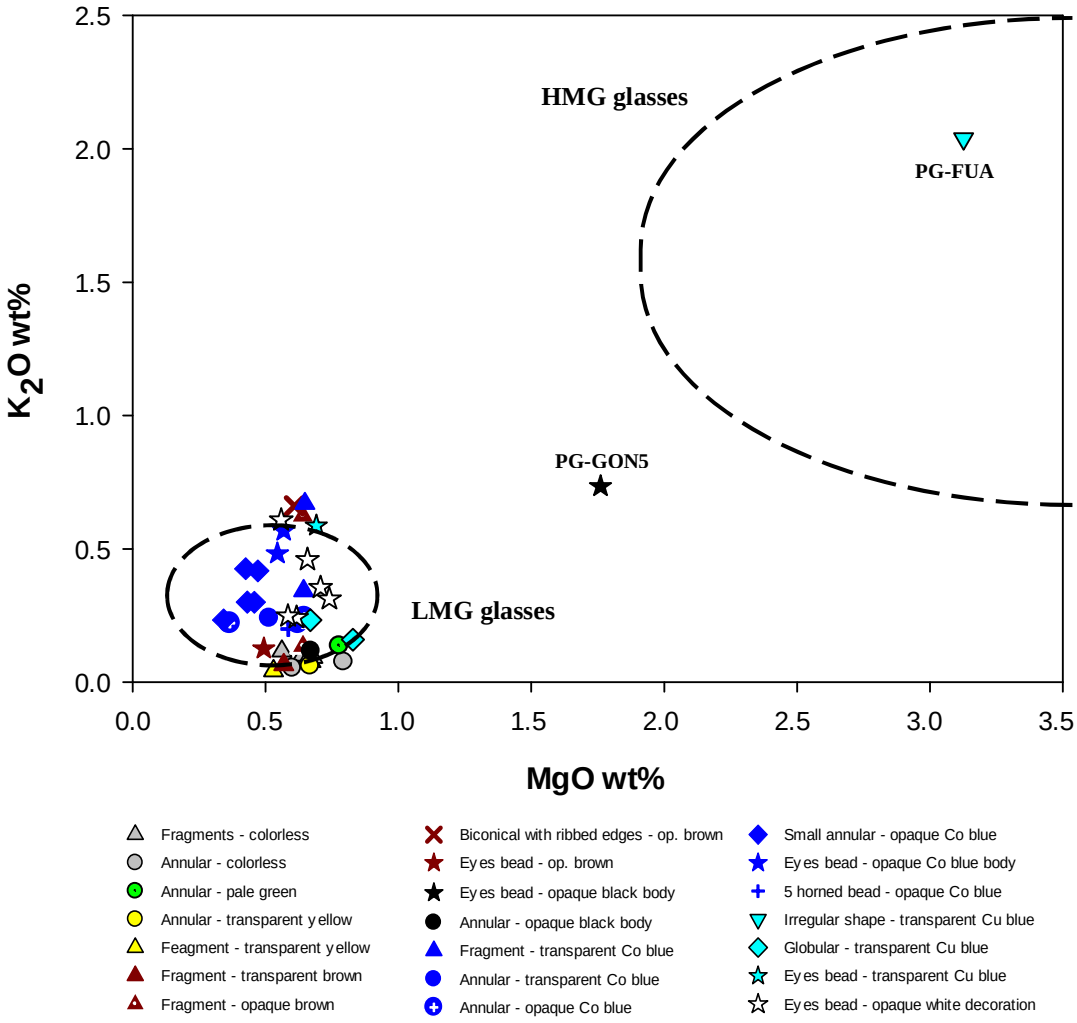

Fig. 5.2.1: MgO *vs* K_2O contents of the glass phase in the analyzed samples from the Piovego cemetery (symbols = typologies; colors = color of the vitreous material).

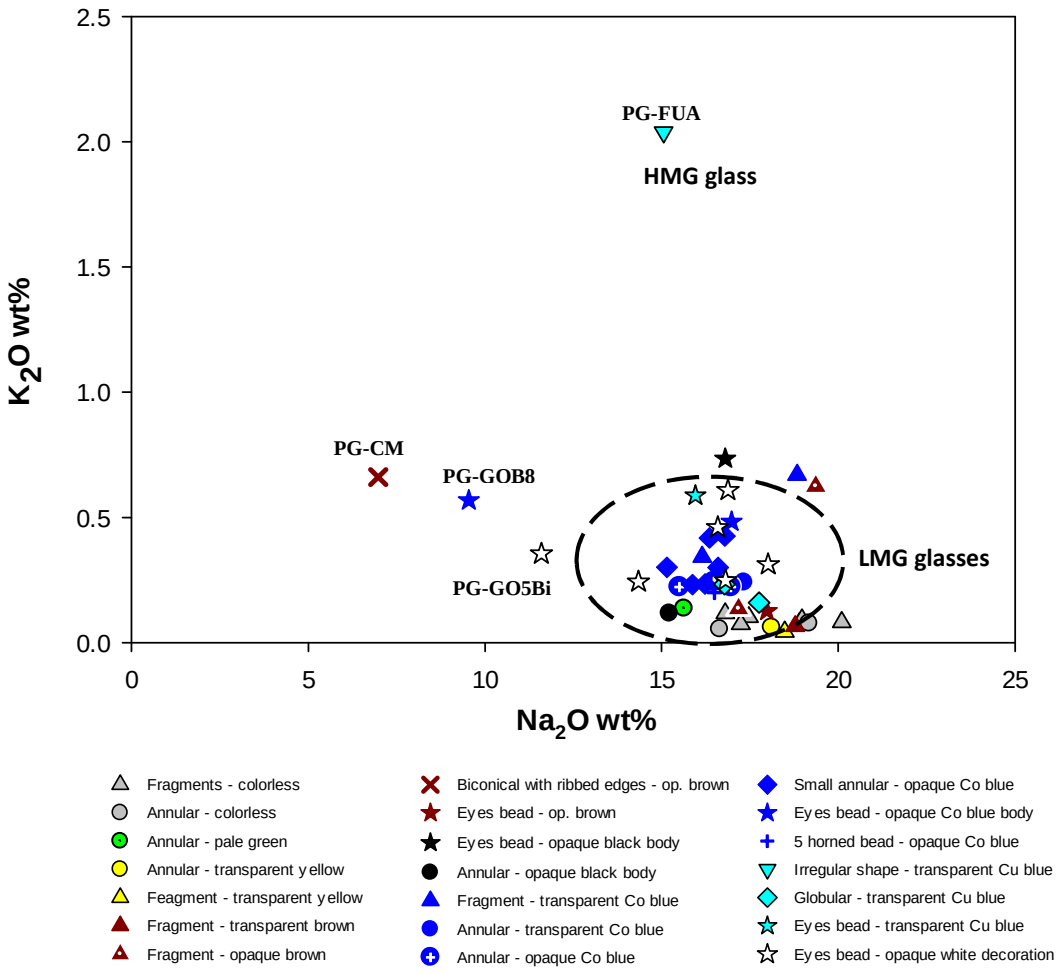

Fig. 5.2.2: Na_2O *vs* K_2O contents of the glass phase in the analyzed samples from the Piovego cemetery (symbols = typologies; colors = color of the vitreous material).

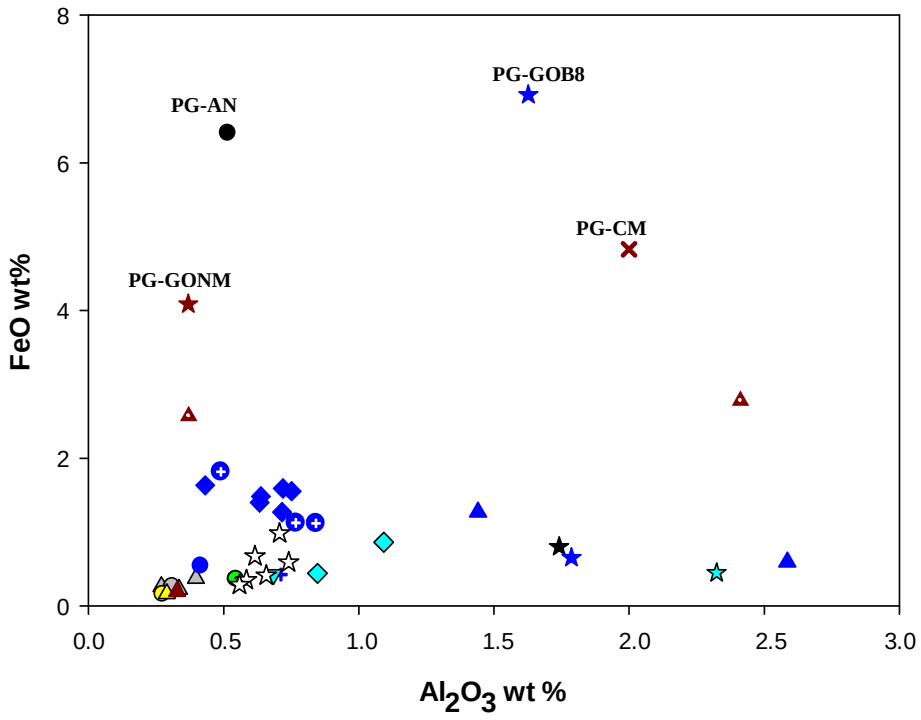

Fig. 5.2.3: Al_2O_3 *vs* FeO contents of the glass phase in the analyzed samples from the Piovego cemetery (symbols = typologies; colors = color of the vitreous material).

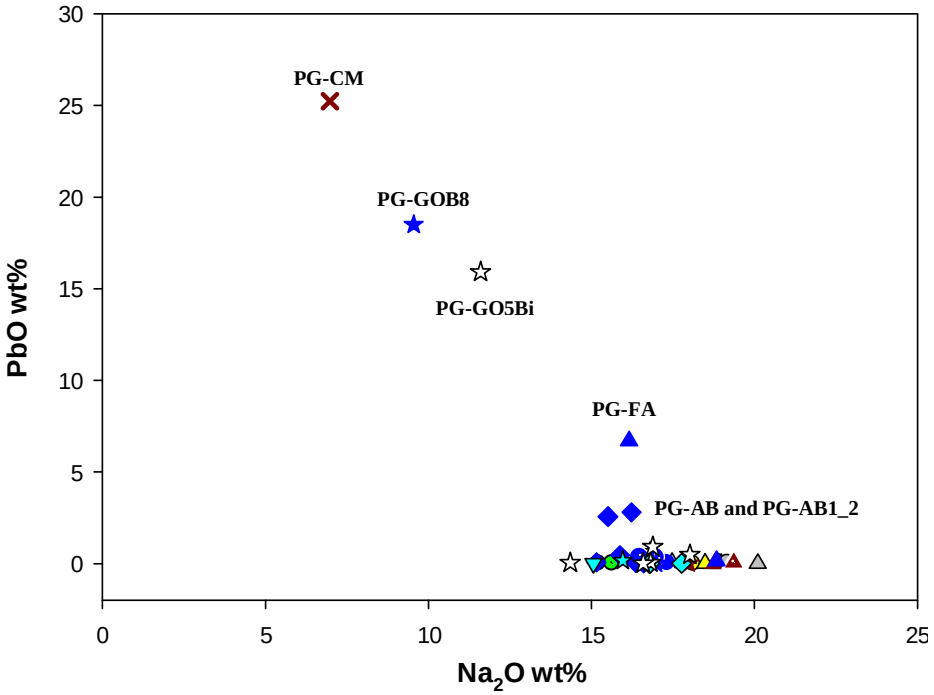

Fig. 5.2.3 bis: Na_2O *vs* PbO contents of the glass phase in the analyzed samples from the Piovego cemetery (symbols = typologies; colors = color of the vitreous material).

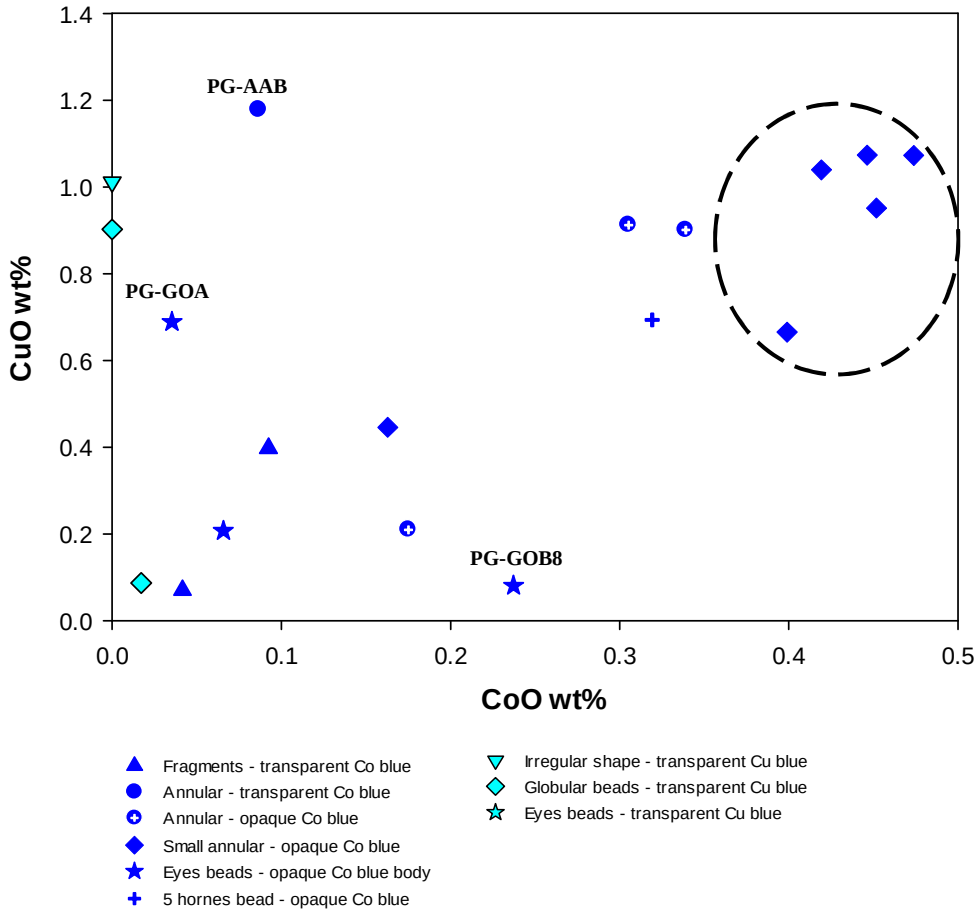

Fig. 5.2.4: CoO *vs* CuO contents of the glass phase in the analyzed blue colored samples from the Piovego cemetery (symbols = typologies; colors = color of the vitreous material).

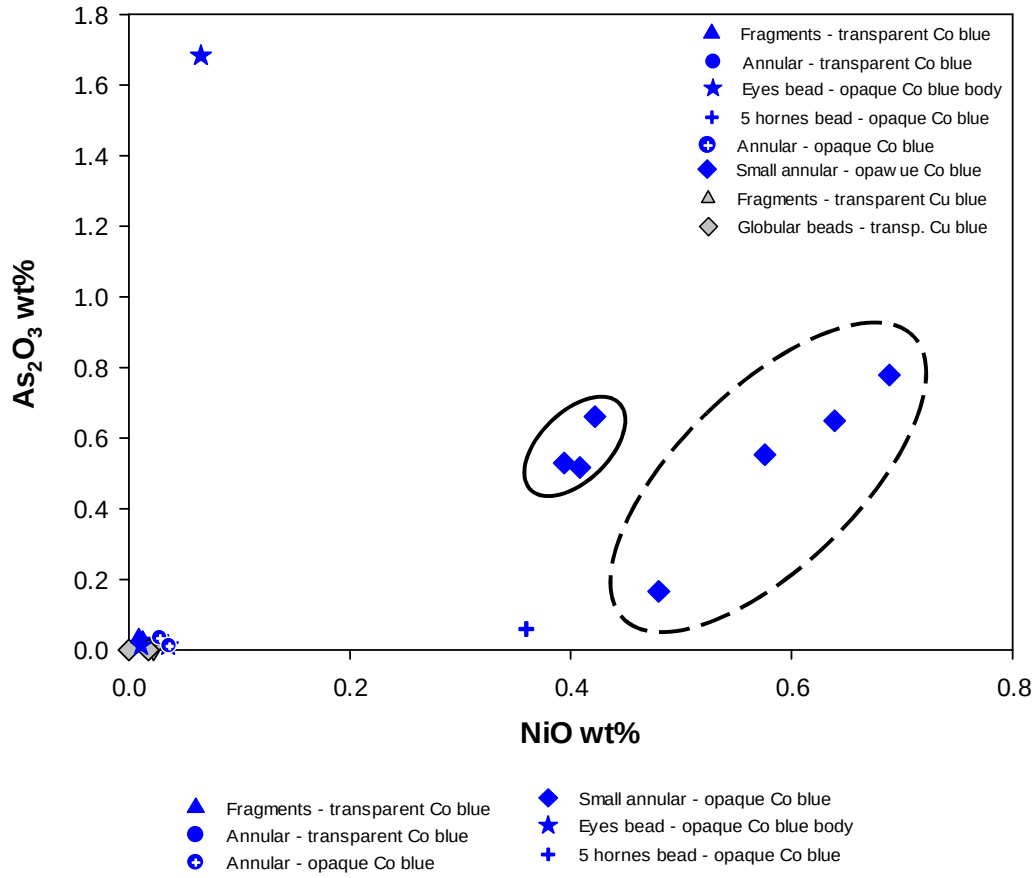

Fig. 5.2.5: NiO *vs* As_2O_3 contents of the glass phase in the analyzed blue colored samples (symbols = typologies; colors: blue = cobalt colored glasses; gray = copper colored glasses).

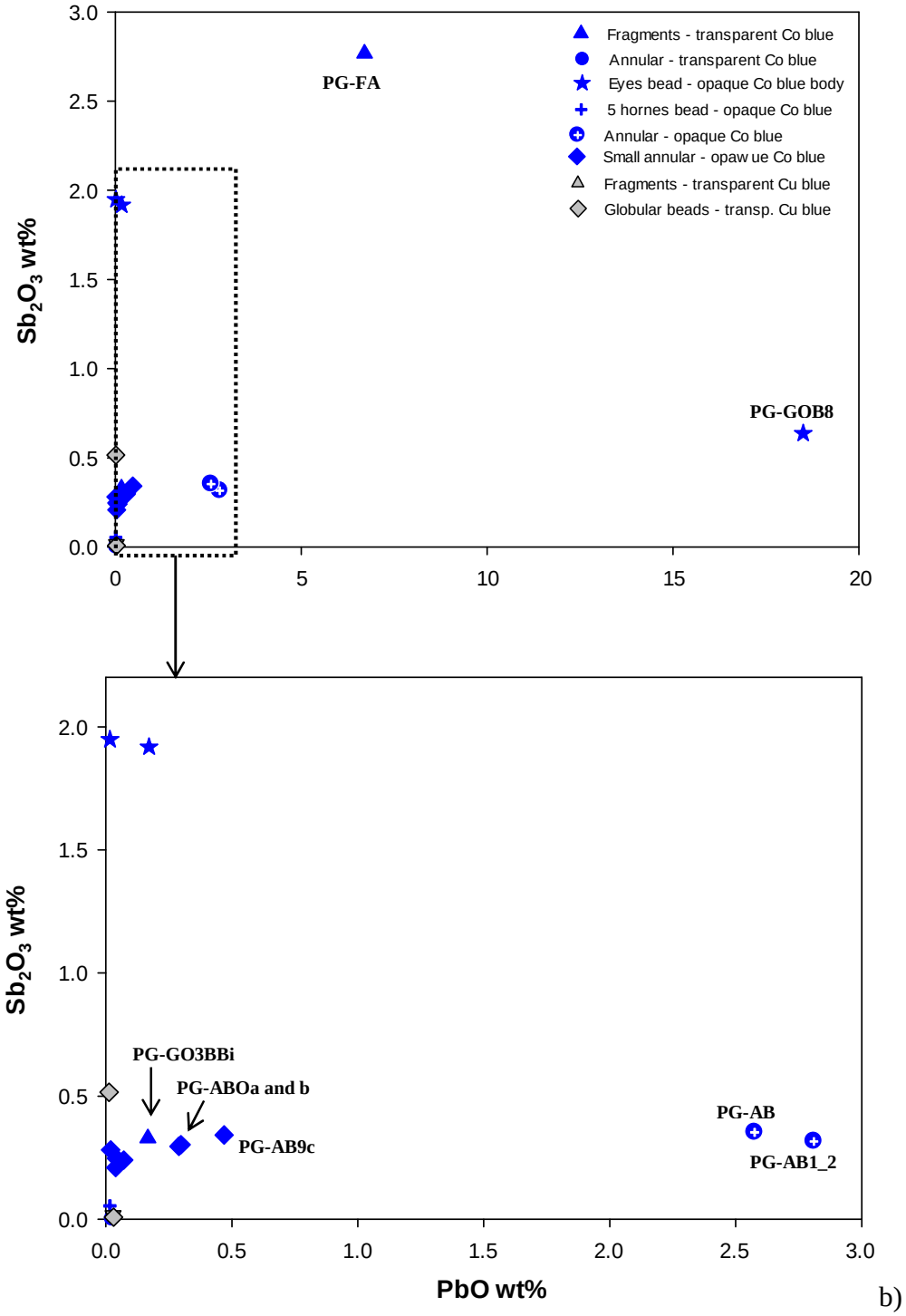

Fig. 5.2.5 bis: a) PbO *vs* Sb_2O_3 content of the glass phase in the analyzed blue colored samples and b) a detail of the plot (symbols = typologies; colors: blue = cobalt colored glasses; gray = copper colored glasses).

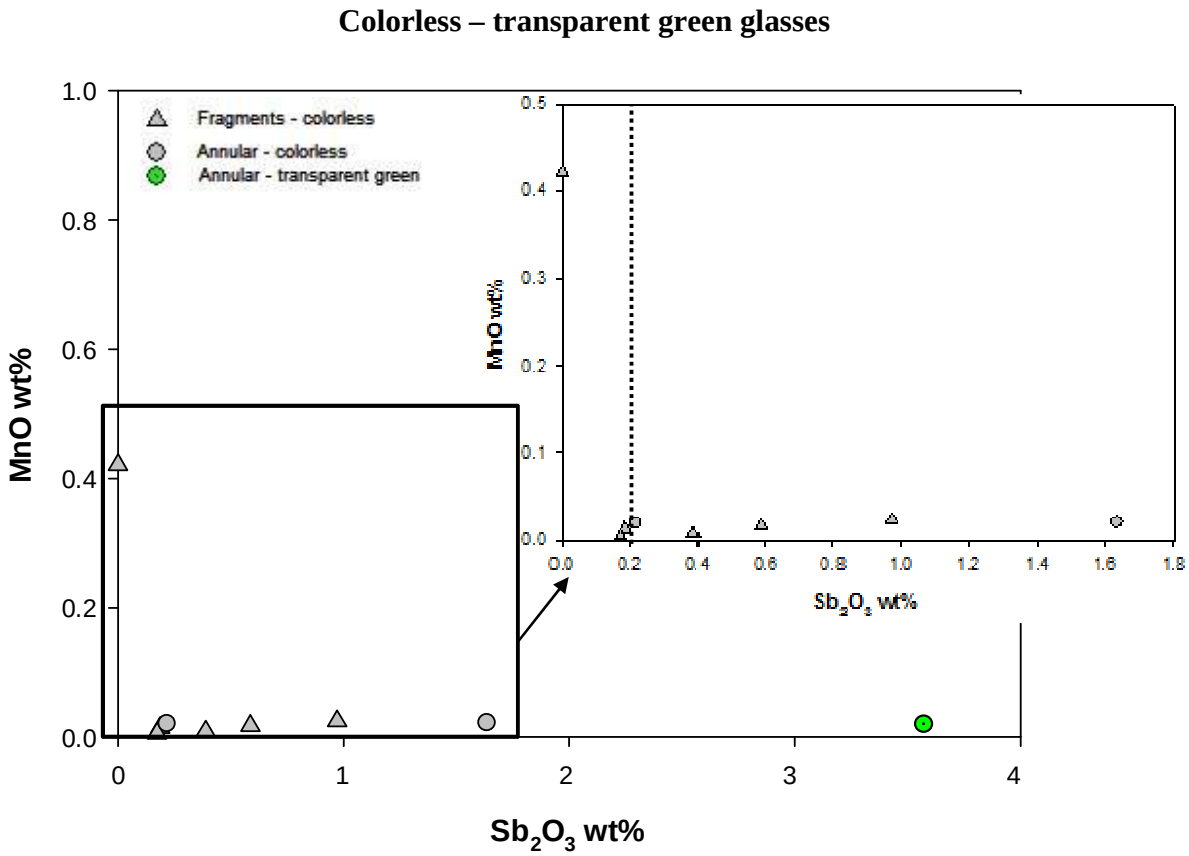

Fig. 5.2.6: Sb_2O_3 *vs* MnO contents of the glass phase in the colorless/transparent green glasses from the Piovego cemetery and an enlarged detail of the diagram (symbols = typologies; colors = color of the vitreous material).

- *Texture*

Both homogeneous and heterogeneous textures characterized the Piovego cemetery glasses. The heterogeneous texture is due to the presence of opacifiers, as in the white or turquoise glasses, or to metal inclusions, unreacted raw materials and/or newly formed crystals, like in some dark blue and brown glasses. In some samples the crystalline inclusions are particularly numerous and the texture is similar to a *glassy faïence*, in which the quantity of crystalline inclusions (i.e., quartz, feldspar and metals) is comparable with the quantity of amorphous phases (Angelini et al. 2002).

Colorless, transparent pale blue and transparent yellow/amber glasses mostly have a homogeneous texture without bubbles as well as the black glass PG-AN. The colorless sample PG-GVA97 is the only transparent glass that presents numerous inclusions of Ca antimonates, finely dispersed in the glass matrix and concentrated into preferential bands. The bands in which they are concentered have a higher amount of Sb (light gray band, mean value of Sb_2O_3 = 4.5 wt%, Fig. 5.2.7a and Tab. 5.2.1) with respect to the mean value in the glass matrix (dark gray band, Sb_2O_3 = 3.1 wt%, Fig. 5.2.7a and Tab. 5.2.1). The inclusions have irregular morphologies – in some cases elongated and in others rounded – and dimensions ranging from a few microns to 50 µm (Fig. 5.2.7b). The Raman analyses (see below) show that the inclusions are composed by $CaSb_2O_6$.

Transparent brown samples have generally a homogeneous texture; rarely, they present devitrification inclusions such as Ca silicates (close to $CaSiO_3$) or Na-Ca silicates. They present dendritic or elongated morphologies and dimensions ranging from a few microns to 50 µm (Fig. 5.2.8a-b); interestingly, sample PG-FM83 presents an inclusion of $CaSiO_3$ with iron oxides (FeO) finely dispersed and newly formed crystals of Na-Fe silicates (stoichiometry close to $NaFeSi_2O_6$) with elongated morphology and about 10 µm large (Fig. 5.2.9a-b).

The only opaque brown glass, PG-CM, presents numerous inclusions of different nature dispersed in the glass matrix (Fig. 5.2.10a). In particular there are numerous residual Ca-Mg silicates and SiO_2 relics, followed by minor Ca-silicates, Na-Ca silicates, Ca phosphates and CuS inclusions. Ca-Mg silicates have a variable composition ranging from an estimated stoichiometry of $CaMgSi_2O_6$ similar to diopside (fig. 5.2.10d) to a stoichiometry of (Na,

Ca)(Fe, Mg, Al) Si_2O_7 similar to aegirine-augite (fig. 5.2.10c). They have irregular morphologies and dimensions of 15÷30 µm. Besides these, some devetrification phases are present such as Ca silicates (about $CaSi_2O_3$) and Na-Ca silicates with irregular morphologies and dimensions of about 10 µm (detail in fig. 5.2.10b and d). Interestingly, numerous small (about 5 µm) Ca phosphates are finely dispersed in the glass matrix with elongated or sometimes polygonal shapes (fig. 5.2.10e). Several metal inclusions are also observed; they are particularly small (~5µm) rounded and made of copper sulfides (about Cu_2S) with segregation rich in Pb and traces of Ag (fig. 5.2.10f).

A similar texture characterized the Co-colored blue bead PG-GOB8. Similarly to sample PG-CM it presents numerous Ca silicates (about $CaSiO_3$, fig. 5.2.11a) and SiO_2 relics (fig. 5.2.11b). Moreover it has numerous iron oxides (about FeO, fig. 5.2.11b) and small rounded particles of copper sulfide (about CuS). Interestingly, it presents elongated crystals with a complex and variable stoichiometry based on Pb (22.6÷43.1 wt%), As (3.4÷14.5 wt%), Ca (11.8÷15.9 wt%), Fe (2.0÷5.5 wt%), S (1.2÷1.7 wt%), P (5.7÷8.1 wt%) and O (32.1÷35.9 wt%) (fig. 5.2.11c).

A large number of SiO_2 relicts characterize the annular and small annular Co-colored beads. The morphologies of the inclusions vary from elongated to sub-angular and the dimensions range from a few microns to 100 µm testifying an inaccurate grinding of the raw material (fig. 5.2.12a). Sometimes the SiO_2 inclusions are surrounded by fractures occurred during the glass cooling. Some samples present other unreacted or partially reacted raw crystals derived from raw materials such as: Na-Al silicates ($NaAlSi_3O_8$), K-feldspars ($KAlSi_3O_8$) and zircon ($ZrSiO_4$). In particular, silicates crystals present rounded edges partially reacted and the dimensions are of about 10÷20 µm (fig. 5.2.12b). All these inclusions are possibly related to the sand used. The other inclusions are related to the coloring agent, specifically several copper sulfides are observed in the glass matrix: they are rounded and particularly small (up to 10 µm) and with a stoichiometry close to Cu_2S. Frequently, the sulfides present segregations rich in Ni, As and Ag (Fig. 5.2.12c-d) and in some case with traces of Sb. Interestingly most of them have very small and irregular inclusions of Ca-Na phosphates ($NaCaPO_4$) (Fig. 5.2.12e-f).

The five horns sample PG-SB has a very similar texture to that of the annular blue beads and presents copper sulfides inclusions (Cu_2S) enriched in Ni, As and Ag.

Cu-colored glasses are perfectly homogeneous as well as the Co-colored blue bodies of samples PG-GOBBi and GO3BBi, and the annular fragment PG-AAB. The Co-colored

turquoise body PG-GOA has numerous Ca antimonates finely dispersed in the glass matrix with some aggregates with dimensions of up to 5 µm (fig. 5.2.14a-b). The Co-colored blue fragment PG-FA presents a poor quantity of Ca antimonates dispersed in the glass matrix and most of them are particularly small (1-2 µm) except for a few crystals aggregates large about 10 µm (fig. 5.2.13).

The six white glasses belonging to eyes decorations are opacified and colored by a large number of Ca antimonates finely dispersed in the glass matrix. Morphologies are euhedral and they generally present particularly small dimensions of about 1-2 µm and sometimes they group in larger aggregates up to 20÷30 µm (fig. 5.2.15a-c). In three samples (PG-GOBBi, GO3BBi and GO6BBi) we have sampled together the blue body and the white decoration. The passage from the body to the decoration is well defined and the two colors are not mixed (fig. 5.2.15d-e). Interestingly, the bubbles are concentrated in the boundary line from the two types of glass (fig. 5.2.15d-e).

The large globular black colored bead, PG-GO5N, is characterized by numerous small (a few microns) rounded inclusions of Cu_2S. Some of them also present traces of Pb, Ni and Sb (fig. 5.2.16a-b).

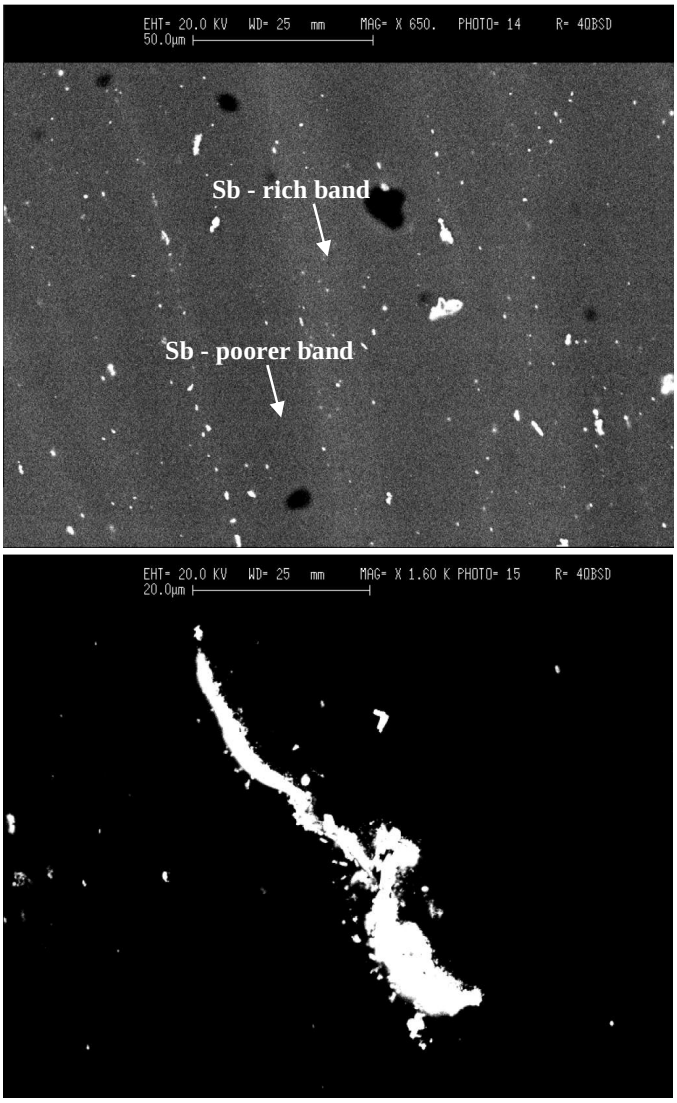

Fig. 5.2.7: SEM-BSE images of sample PG-GVA97. a) detail of the Ca antimonates dispersed in the glass matrix and of the bands with different Sb amounts. b) detail of an aggregate of Ca antimonate crystals.

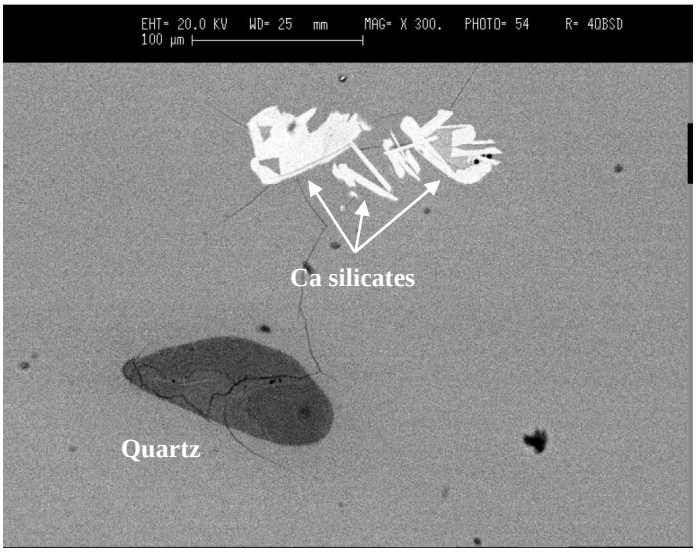

a)

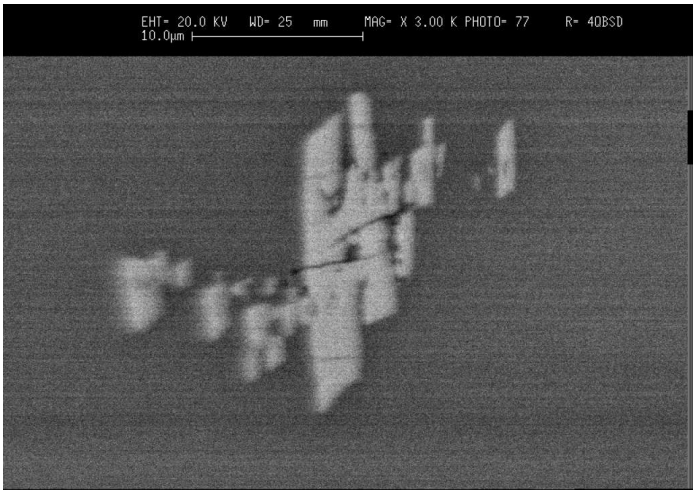

b)

Fig. 5.2.8: SEM-BSE images of a) sample PG-FM83 with a detail of the Ca silicate ($CaSiO_3$) and a residual quartz. b) sample PG-FM89 detail of a Na-Ca silicate ($NaCaSi_3O_7$).

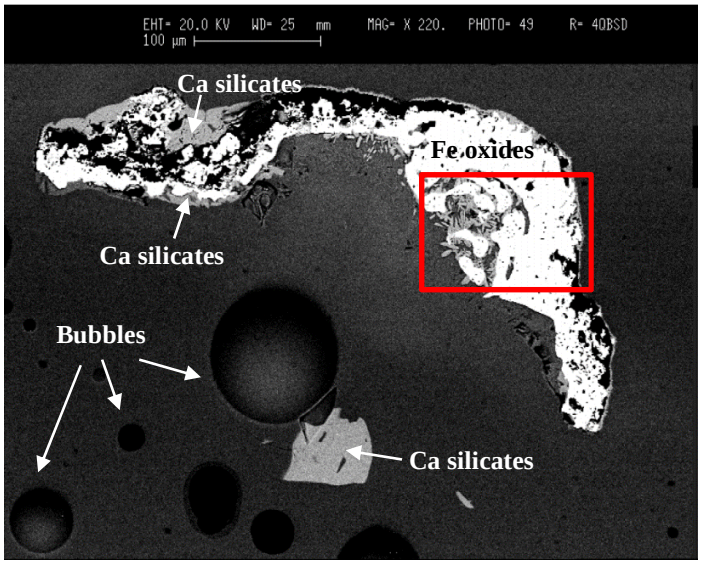

a)

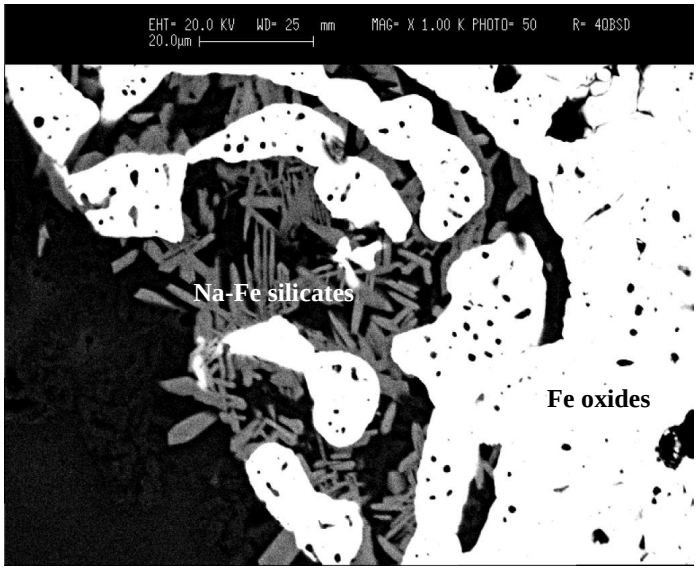

b)

Fig. 5.2.9: SEM-BSE images of sample PG-FM83. a) Ca silicate ($CaSiO_3$) and Ca silicate enriched of iron oxides with different morphologies. b) detail in the red square in fig. a) of elongated Na-Fe silicates ($NaFeSi_2O_6$).

Fig. 5.2.10: a) SEM-BSE image of sample PG-CM. b) and c) SE images of details n.1 and 2 in fig. a. d) SE image of a detail of Ca-Mg and Na-Ca silicates. e) BSE image of a detail of Ca phosphates. f) BSE image of copper sulfide inclusions.

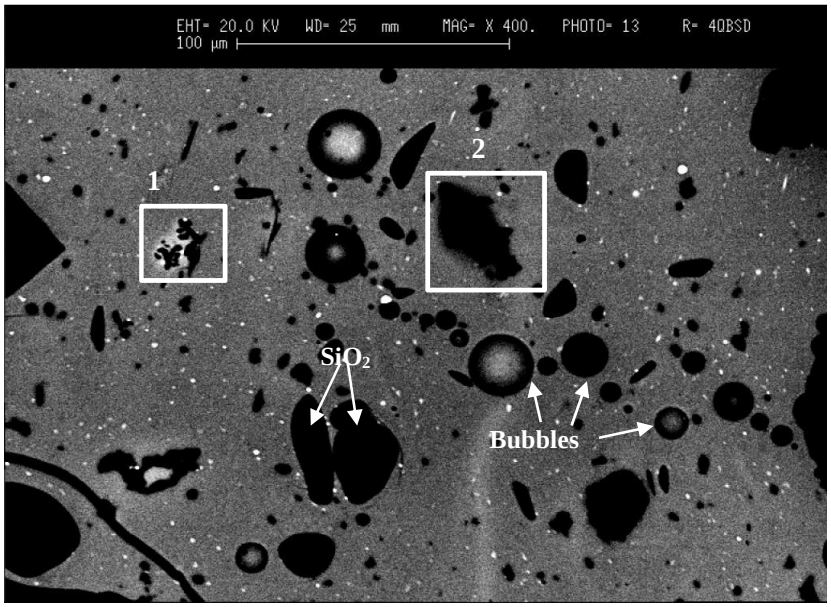

a)

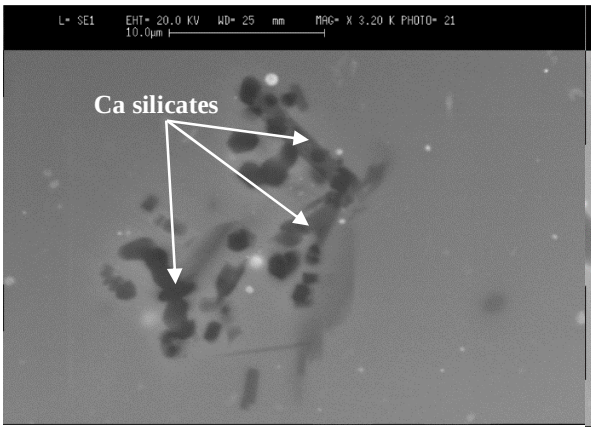

b)

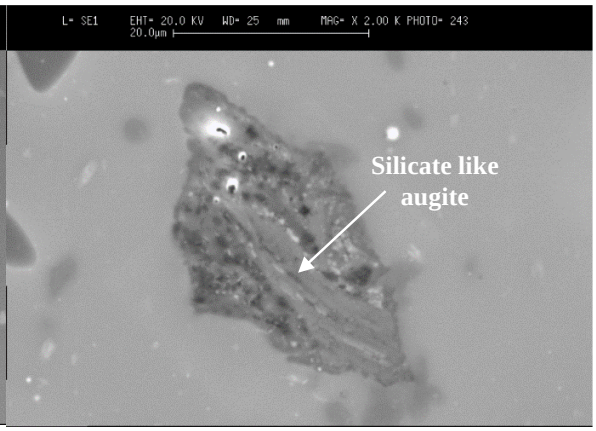

c)

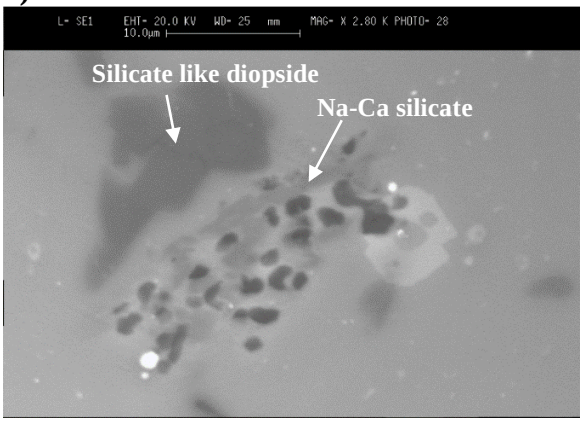

d)

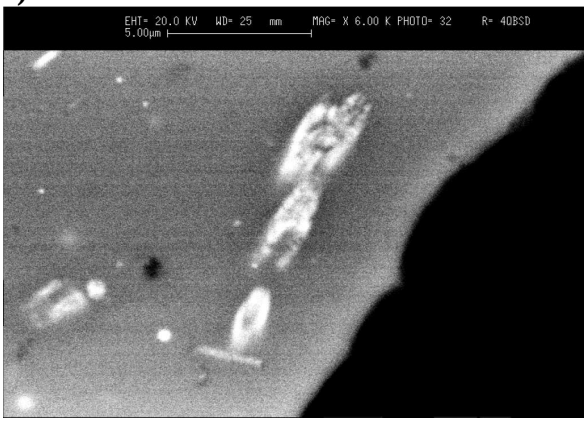

e)

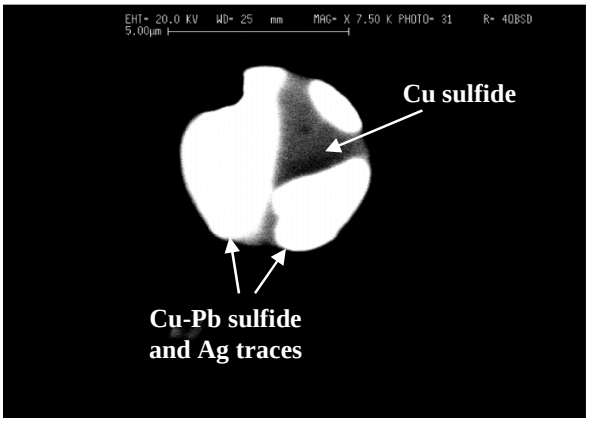

f)

Fig. 5.2.11: BSE images of sample PG-GOB8. a) detail of the Ca silicates dispersed in the glass matrix. b) detail with marked SiO_2 relicts, iron oxides and bubbles. c) detail of inclusions with a complex chemical composition (black harrows).

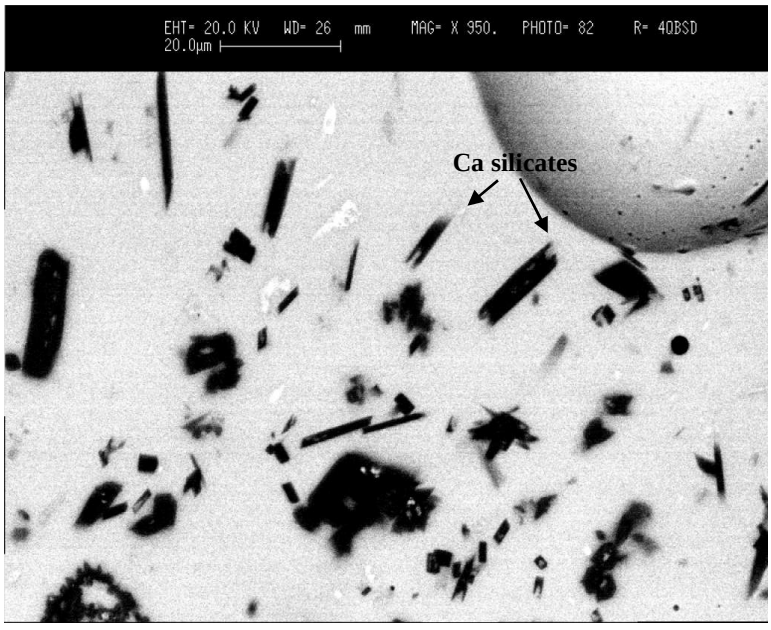

a)

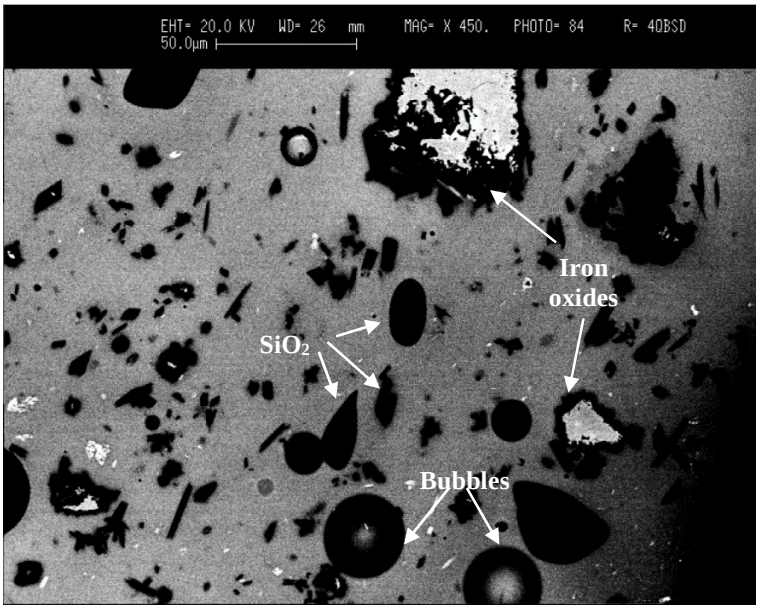
EHT= 20.0 KV WD= 26 mm MAG= X 450. PHOTO= 84 R= 4QBSD
50.0µm
Iron oxides
SiO2
Bubbles

b)

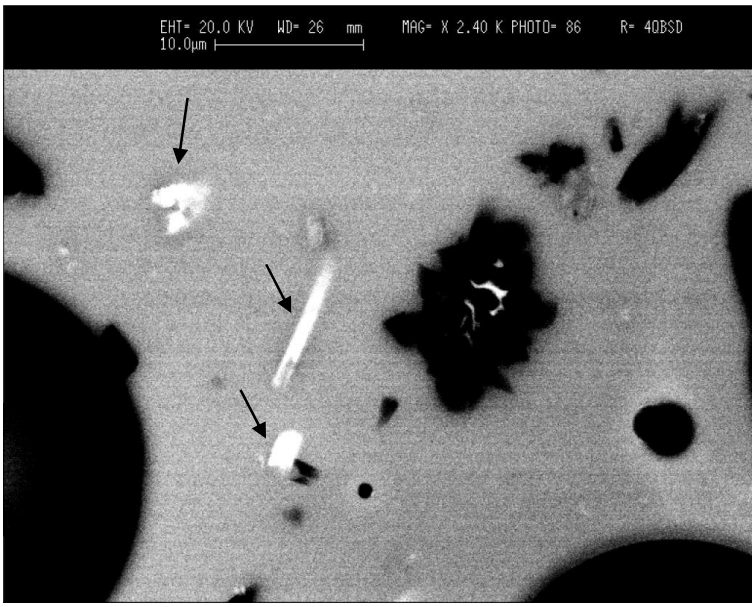
EHT= 20.0 KV WD= 26 mm MAG= X 2.40 K PHOTO= 86 R= 4QBSD
10.0µm

c)

Fig. 5.2.12: a) BSE image of sample PG-AB8. b) detail of a K-feldspar in the white square in fig. a. c) and d) details of a copper sulfides with segregations rich in Ni, As and Ag in samples PG-AB8 and AB9c, respectively. e) and f) details of Ca-Na phosphates in samples PG-AB9c.

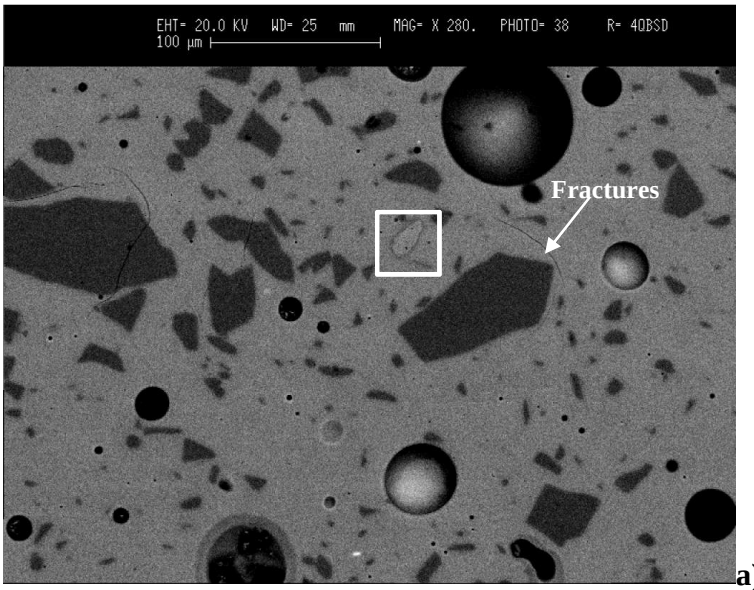

a)

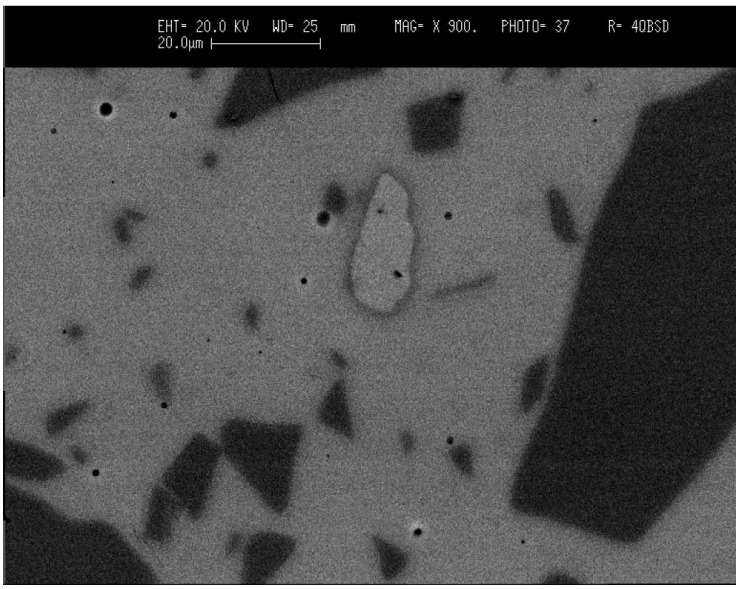

b)

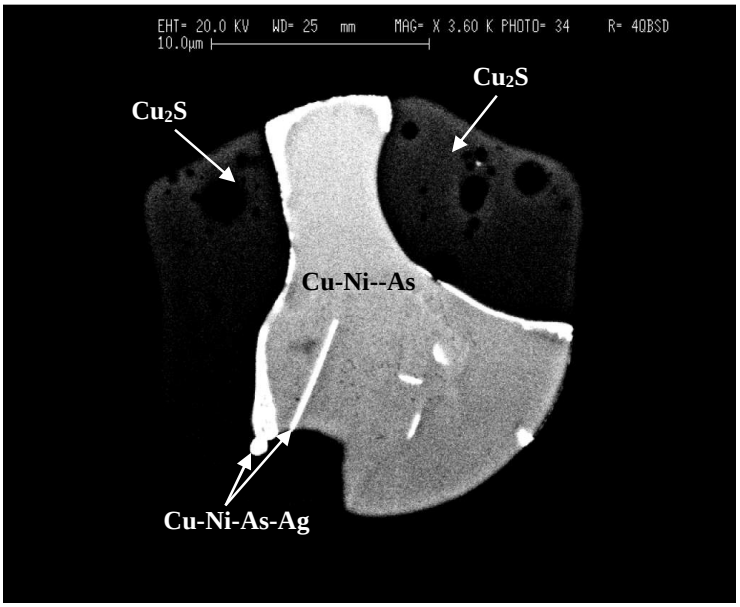
EHT= 20.0 KV WD= 25 mm MAG= X 3.60 K PHOTO= 34 R= 4OBSD
10.0µm
Cu2S
Cu2S
Cu-Ni--As
Cu-Ni-As-Ag

c)

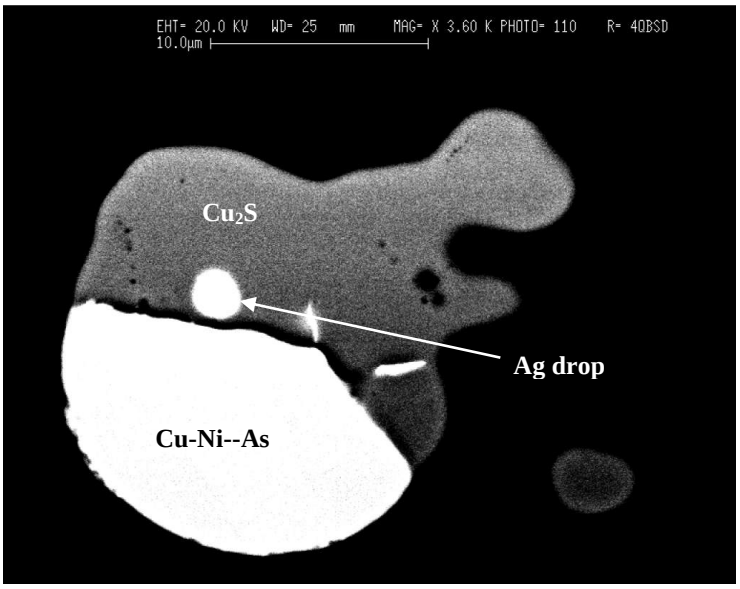
EHT= 20.0 KV WD= 25 mm MAG= X 3.60 K PHOTO= 110 R= 4OBSD
10.0µm
Cu2S
Ag drop
Cu-Ni--As

d)

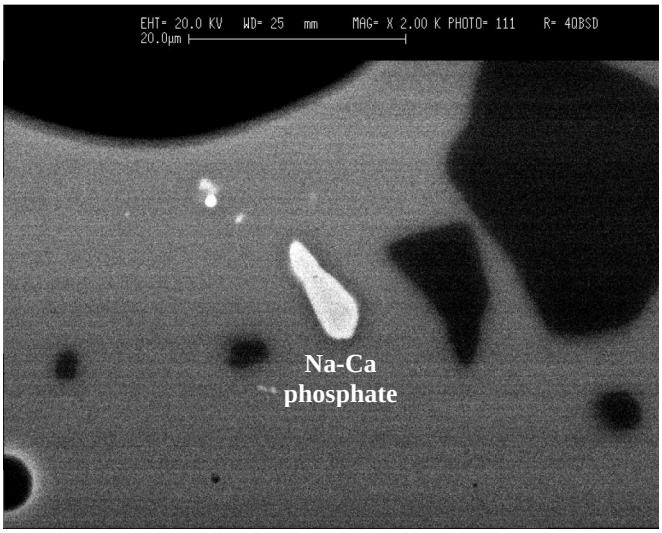
EHT= 20.0 KV WD= 25 mm MAG= X 2.00 K PHOTO= 111 R= 4QBSD
20.0µm
Na-Ca
phosphate

e)

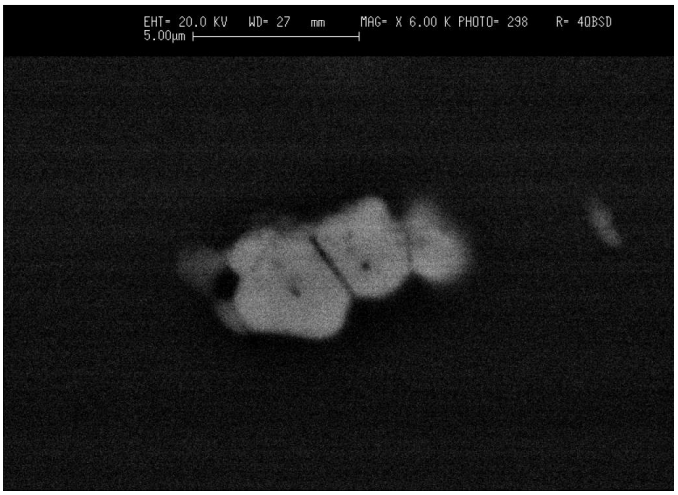
EHT= 20.0 KV WD= 27 mm MAG= X 6.00 K PHOTO= 298 R= 4QBSD
5.00µm

f)

Fig. 5.2.14: BSE image of sample PG-FA characterized by very small Ca antimonates (white) dispersed in the glass matrix and several larger ones.

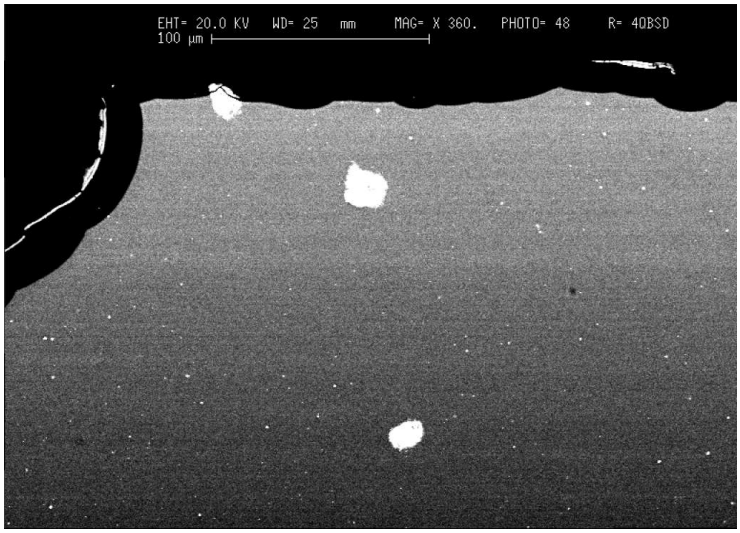

Fig. 5.2.13: a) BSE images of sample PG-GOA characterized by Ca antimonates (white) finely dispersed in the glass matrix and b) detail of Ca antimonate crystals.

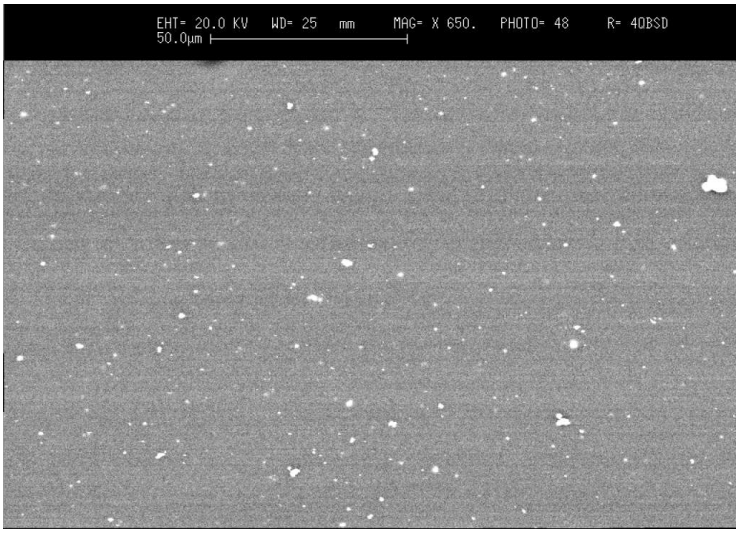

a)

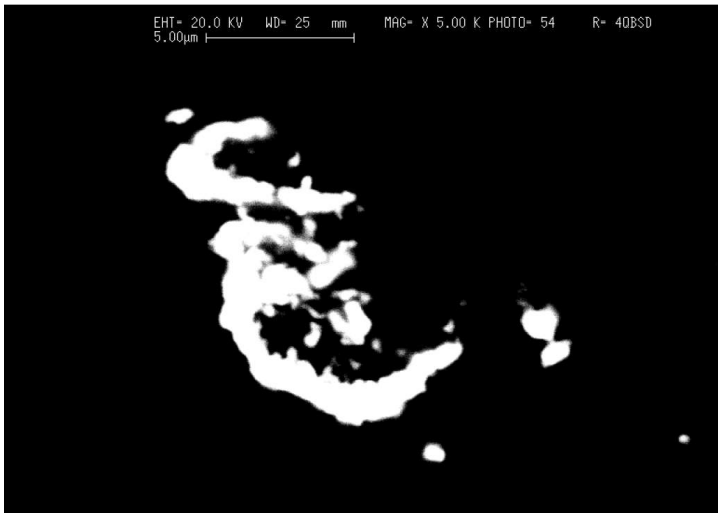

b)

Fig. 5.2.15: BSE images of white glasses. a) sample PG-GO6BBi characterized by numerous Ca antimonates finely dispersed in the glass matrix sometimes aggregates in particular morphologies. b) and c) details of some euhedral Ca antimonates crystals in samples PG-GO3Bi and PG-GO5Bi, respectively. d) sample PG-GO3BBi, detail of the blue body and the white decoration. e) sample PG-GOBBi, detail of the blue body and of the double white eyes decorations.

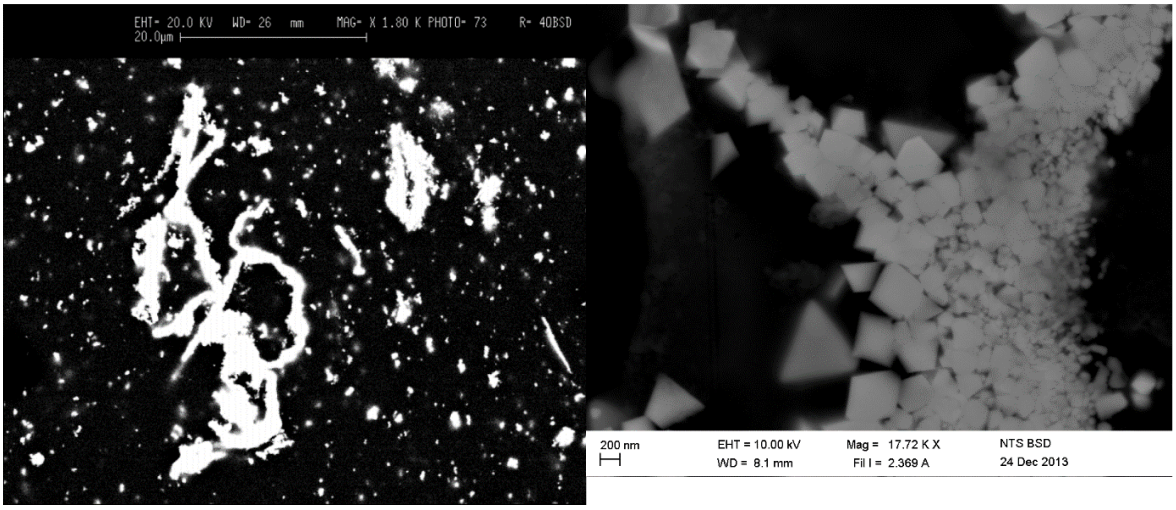

a) **b)**

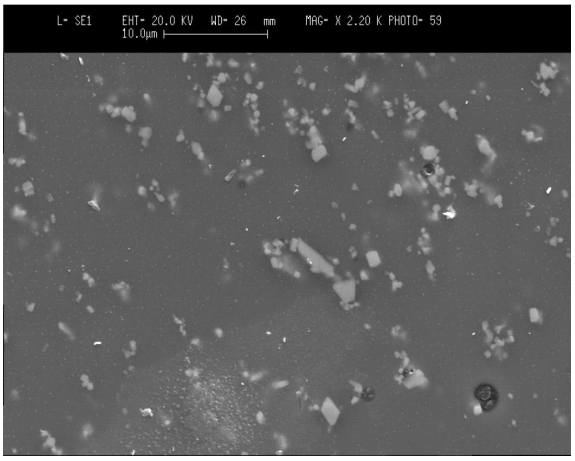
L- SE1 EHT= 20.0 KV WD= 26 mm MAG= X 2.20 K PHOTO= 59
10.0µm

c)

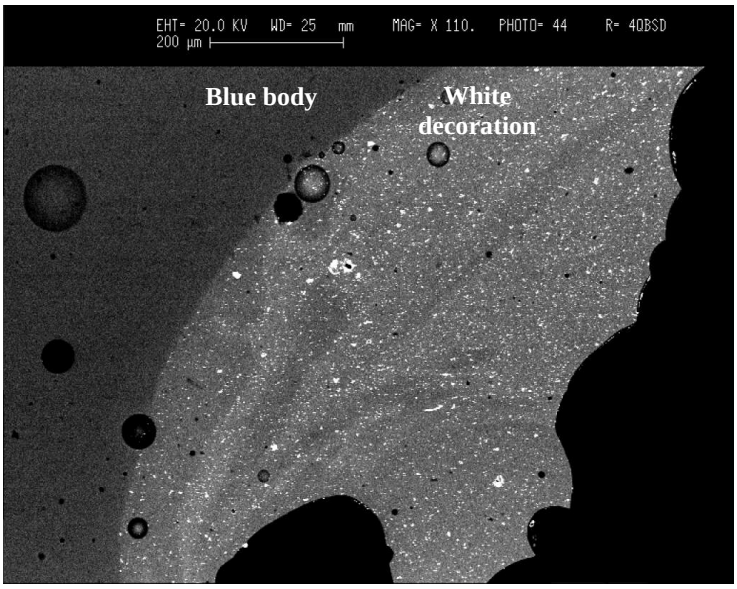
EHT= 20.0 KV WD= 25 mm MAG= X 110. PHOTO= 44 R= 40BSD
200 µm
Blue body
White decoration

d)

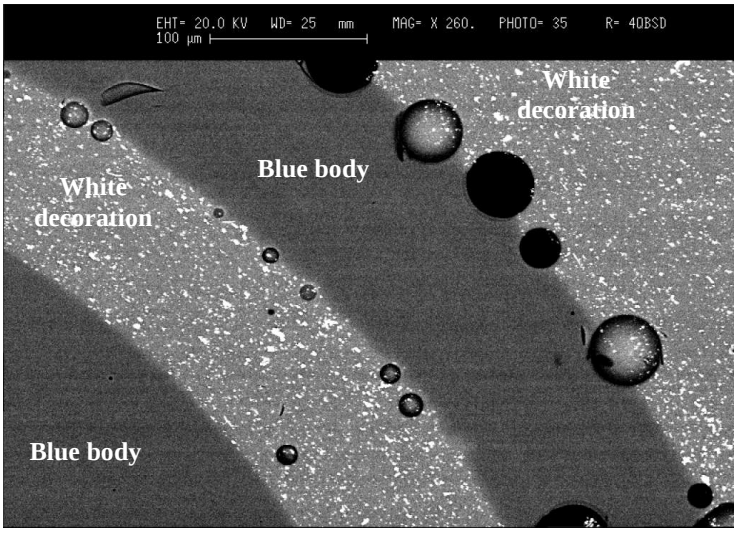
EHT= 20.0 KV WD= 25 mm MAG= X 260. PHOTO= 35 R= 40BSD
100 µm
White decoration
Blue body
White decoration
Blue body

e)

Fig. 5.2.16: BSE images of sample PG-GO5N. a) Glass phase with copper sulfides inclusions dispersed in the glass phase. b) detail of a copper sulfide inclusion with metals segregations.

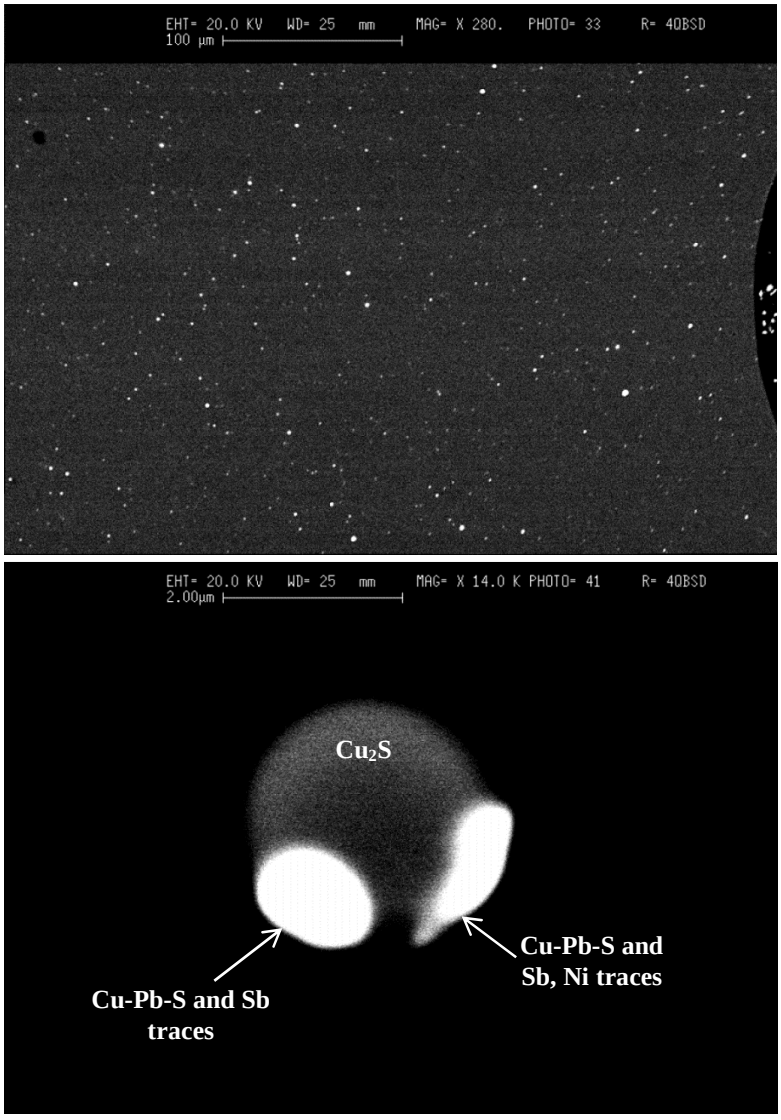

- *Crystalline phases*

The crystalline inclusions of some beads were analyzed by XRPD and/or by micro Raman spectroscopy.

The XRPD analyses performed on the whole blue annular beads show that the SiO_2 inclusions are composed by quartz, while no trydimite or cristobalite are present (example in fig. 5.2.16). This is confirmed by the Raman spectra obtained on the SiO_2 inclusions that generally may be identified as quartz (example in fig. 5.2.17).

However, the analyses performed on some SiO_2 inclusions with a lamellar shape, highlight the presence of both quartz and cristobalite. In particular, the spectrum obtained in the core of the inclusion in fig. 5.2.18a, presents an intense peak at 463 cm^{-1} corresponding to the main peak of quartz, while the cristobalite signal at 415 and 228 cm^{-1} is lower (red spectrum, fig. 5.2.18b). Conversely, the spectra obtained on the lamellar crystals in fig. 5.2.18a, shows a more intense signal of cristobalite with respect to quartz (green spectra, fig. 5.2.18b).

The unreacted Na-Al silicates in the blue annular beads analyzed by micro Raman result very similar to anorthoclase, (NaK) $AlSi_3O_8$ (example fig. 5.2.19). The Na-Ca phosphates have a stoichiometry very similar to buchwaldite ($NaCaPO_4$) but, to date, non-standard spectra are available for this mineral on the online databases or in the literature. However, comparing the experimental spectrum of this inclusion with the spectra of the RRUFF database, it results very close to apatite (example fig. 5.2.20).

The XRPD analysis of the biconical bead with ribbed edges PB-CM highlights that quartz is the most abundant phase present (fig. 5.2.21), even though the interpretation of the spectrum is not easy because of the irregular morphology of the bead, which is not optimal for the non-invasive XRPD analyses. The micro Raman analyses allow defining accurately the main inclusions dispersed in the glass matrix. The Ca-Mg silicates are composed of diopside/augite while the Ca silicates are wollastonite crystals (fig. 5.2.22a-c). The Raman spectra of Na-Ca silicates (about $NaCaSi_3O_8$) and Ca phosphates (about $Ca_2SiP_2O_{10}$) have no correspondence in the RRUFF database and in the literature at present.

Similarly, sample PG-GOB8 presents diopside and wollastonite crystals but in addition to iron oxides very close to magnetite (fig. 5.2.23).

The characterization of the Ca-antimonates inclusions in the white and blue/turquoise samples highlights the presence of both *hexagonal* phase $CaSb_2O_6$ and the *orthorhombic* one, $Ca_2Sb_2O_7$. XRPD analyses carried out on the whole objects do not allow obtaining clear Ca antimonates X-Ray diffraction patterns, because most of the beads are globular with eyes decoration, and Ca antimonates are present only in the white decoration, that sometimes remains only in small areas. However, in some cases the determination of the Ca antimonate phase was obtained, as in sample PG-GO5Bi that presents the hexagonal phase $CaSb_2O_6$ (fig. 5.2.24). In the other samples the characterization of the Ca antimonates phases was performed accurately on the single crystal by means of micro Raman spectroscopy.

The Co-colored blue fragment PG-FA and the Cu-colored turquoise body PG-GOA present the orthorhombic phase, $Ca_2Sb_2O_7$, which has two characteristic peaks at 635 and 482 cm^{-1} (fig. 5.2.25, green and red spectrum, respectively).

The white glass PG-GO5Bi seems to have only the hexagonal phase, $CaSb_2O_6$, according to what observed at the XRPD (fig. 5.2.24), which has its characteristics peak at 670 cm^{-1} (fig. 5.2.26). The other white glasses present both phases of antimonate. However, in samples PG-GO3Bi, GO6Bi and AOBi, the orthorhombic phase is predominant while in sample PG-GONBi the hexagonal antimonate is the major phase identified. Sample PG-GOBi seems to present an equal distribution of the two phases. Interestingly in some cases, as sample PG-GO6Bi, inclusions with both phases in the same aggregate are present (fig. 5.2.27).

The only colorless glass that has Ca antimonates, PG-GVA97, presents as predominant phase the hexagonal one, $CaSb_2O_6$ (fig. 5.2.28).

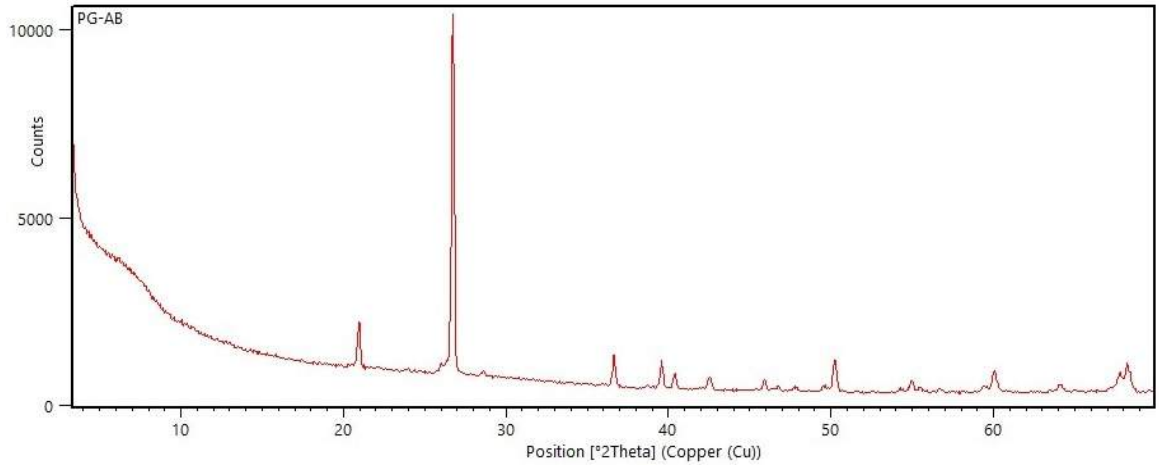

Fig. 5.2.16: X-Ray Powder Diffraction pattern of sample PG-AB that presents quartz as main phase.

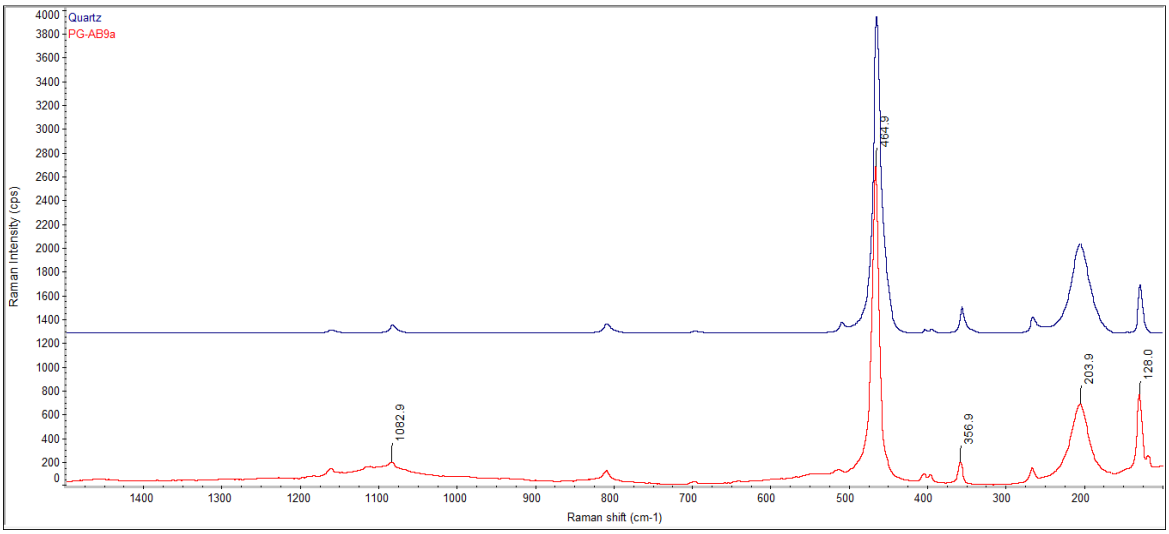

Fig. 5.2.17: Raman spectrum of sample PG-AB9a (red one) performed on one Si_2O rounded inclusion. A standard spectrum of quartz from RRUFF library (blue one) is also reported.

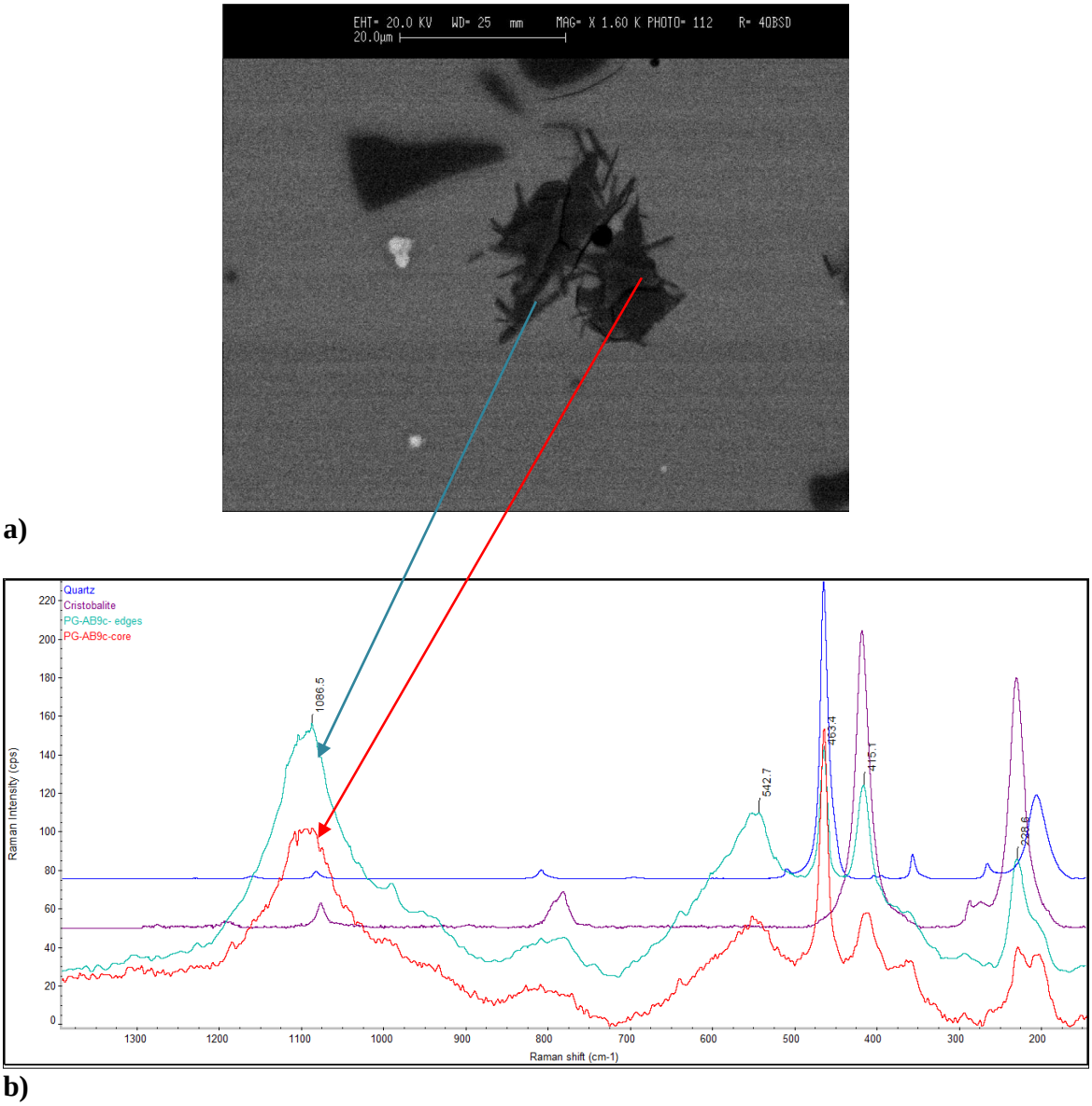

Fig. 5.2.18: a) BSE image of a SiO_2 inclusion in sample PG-AB9c. b) Raman spectra of sample PG-AB9c performed on the core (red one) and on the edges (green one) of the SiO_2 inclusions in fig. a. Standard spectra of quartz and cristobalite from RRUFF library (blue and violet ones) are also reported.

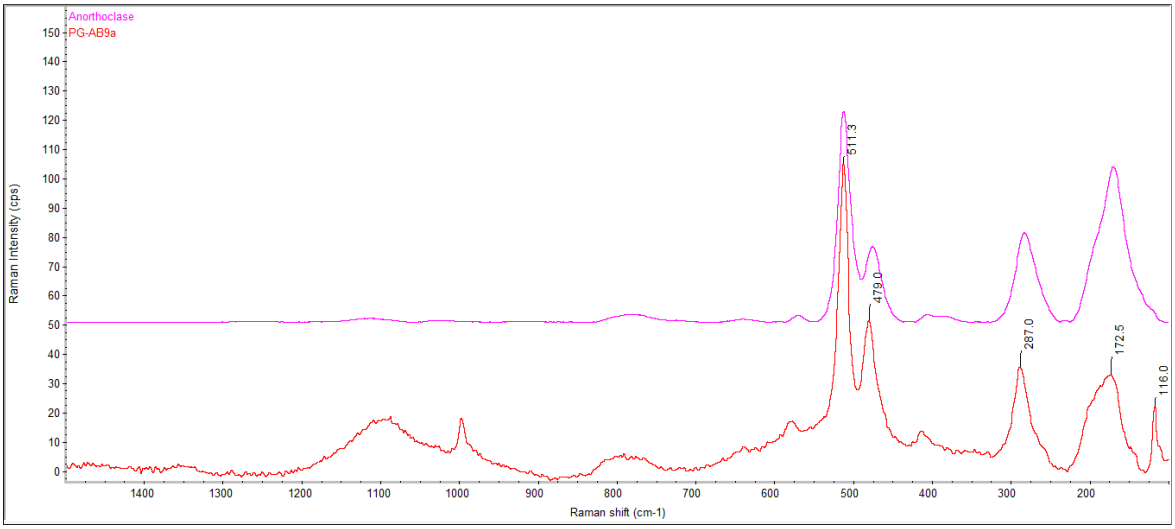

Fig. 5.2.19: Raman spectrum of sample PG-AB9a (red one) performed on one Na-Al silicate. A standard spectrum of anorthoclase from RRUFF library (blue one) is also reported.

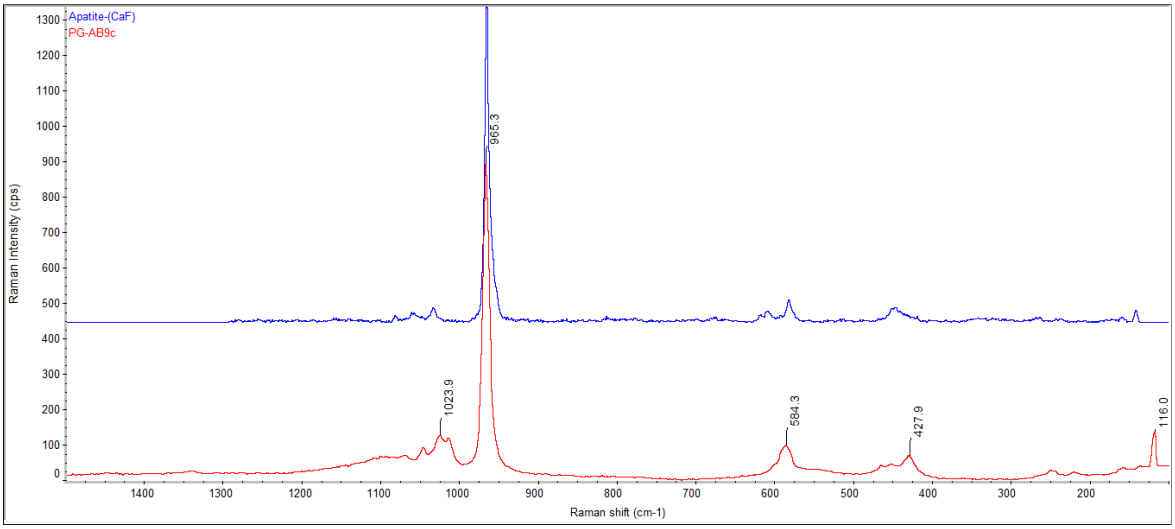

Fig. 5.2.20: Raman spectrum of sample PG-AB9c performed on a Na-Ca phosphate inclusion (red one). A standard spectrum of apatite (blue one) is also reported.

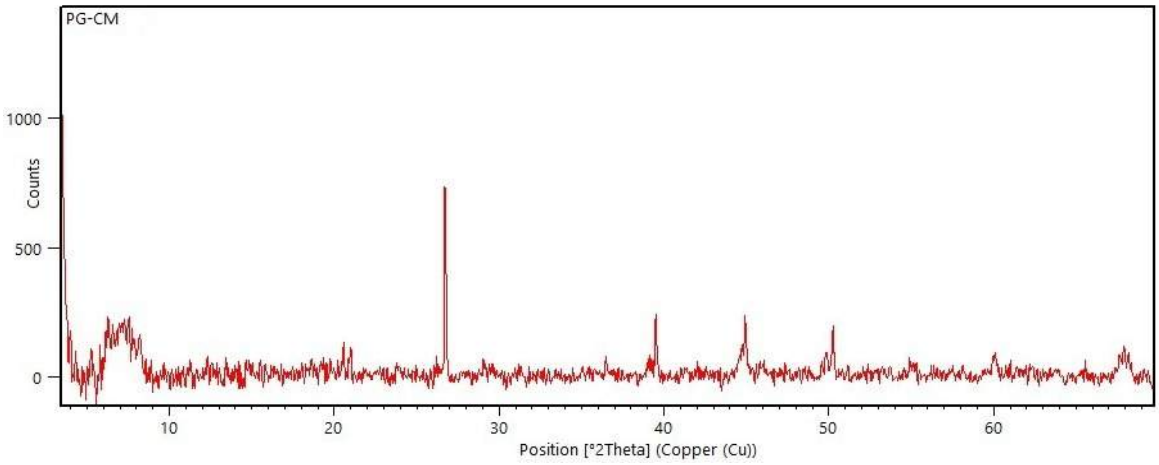

Fig. 5.2.21: X-Ray powder diffraction pattern of sample PG-CM, presenting quartz as main phase.

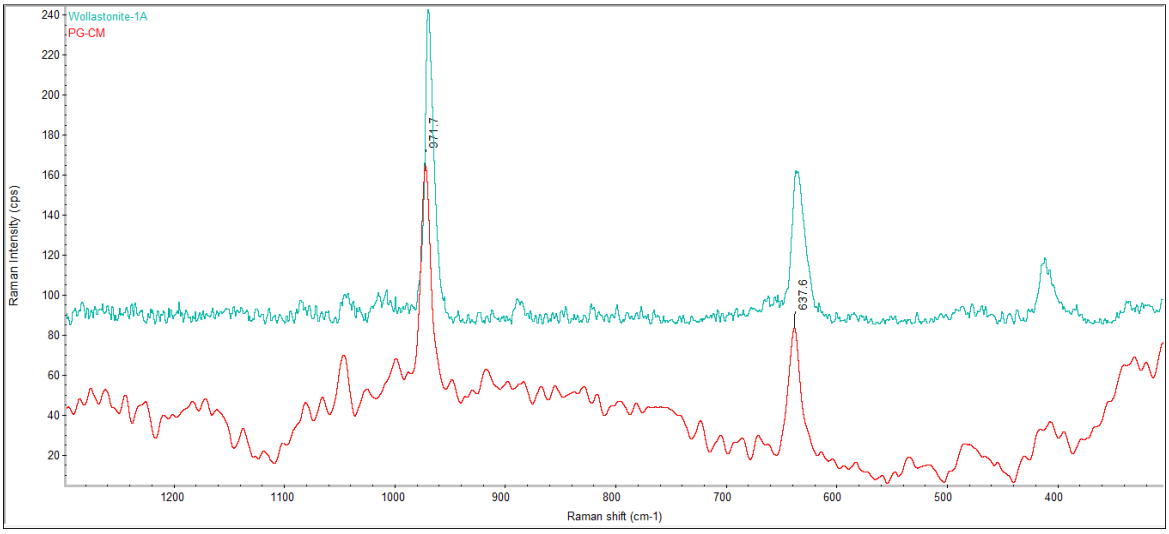

a)

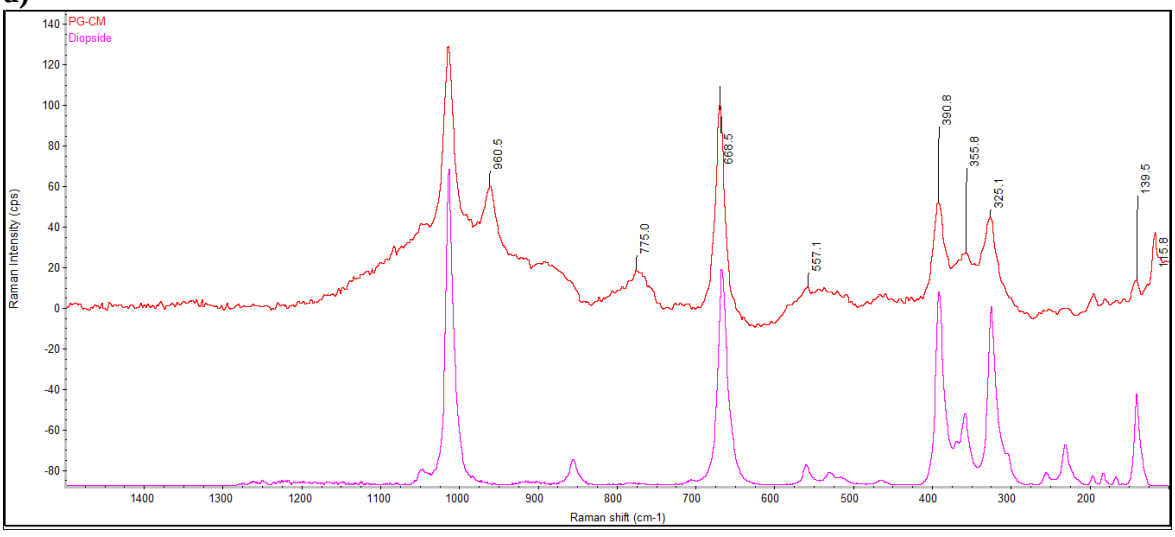

b)

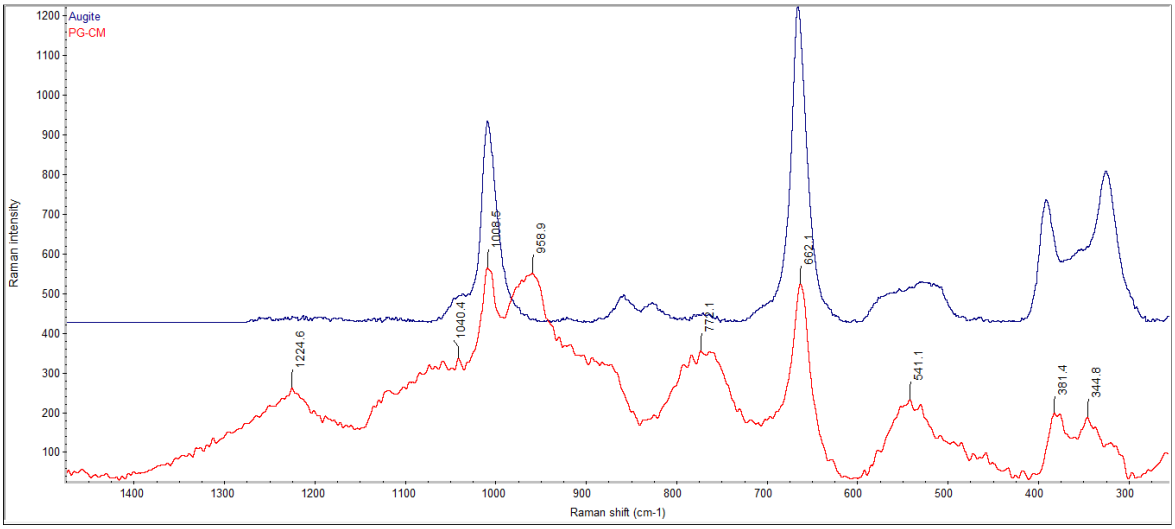

c)

Fig. 5.2.22: Raman spectra of sample PG-CM performed on a) Ca silicate (red one), b) and c) Ca-Mg silicate (red one). Standard spectra of wollastonite (green one), diopside (pink one) and augite (blue one) are also reported.

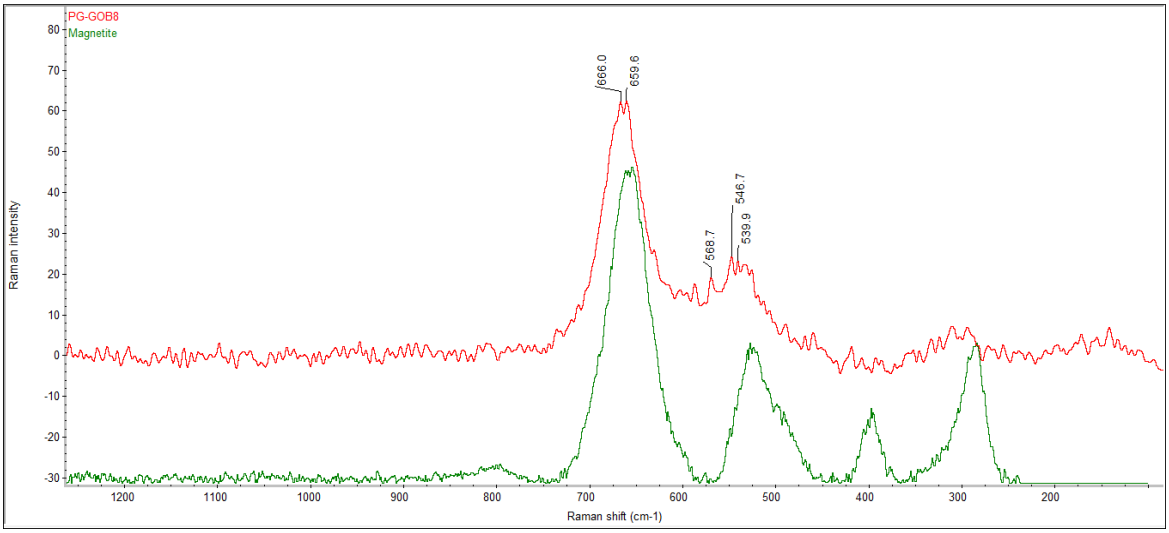

Fig. 5.2.23: Raman spectra of sample PG-GOB8 performed on an iron oxide (red one). Standard spectra of magnetite (green one) are also reported.

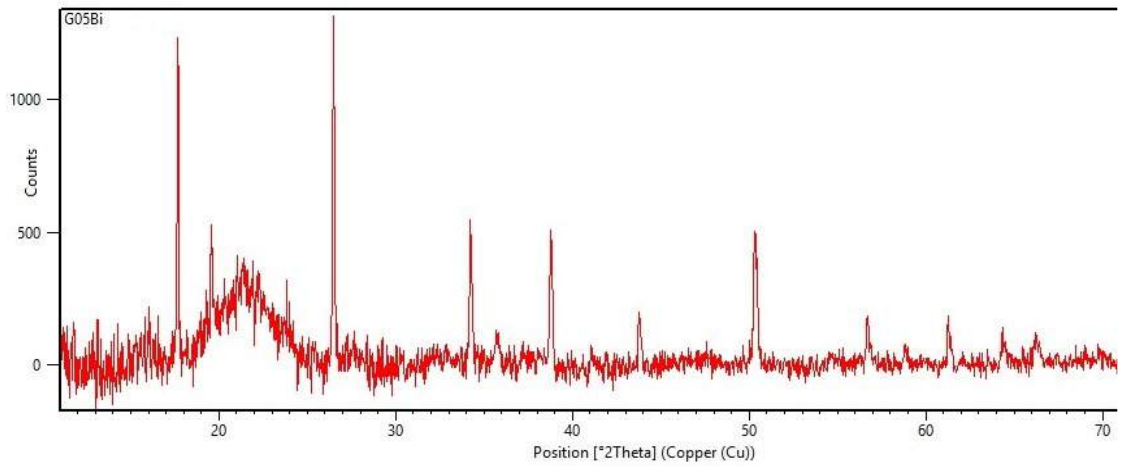

Fig. 5.2.24: X-Ray powder diffraction pattern of sample PG-GO5Bi that shows the presence of the hexagonal phase $CaSb_2O_6$.

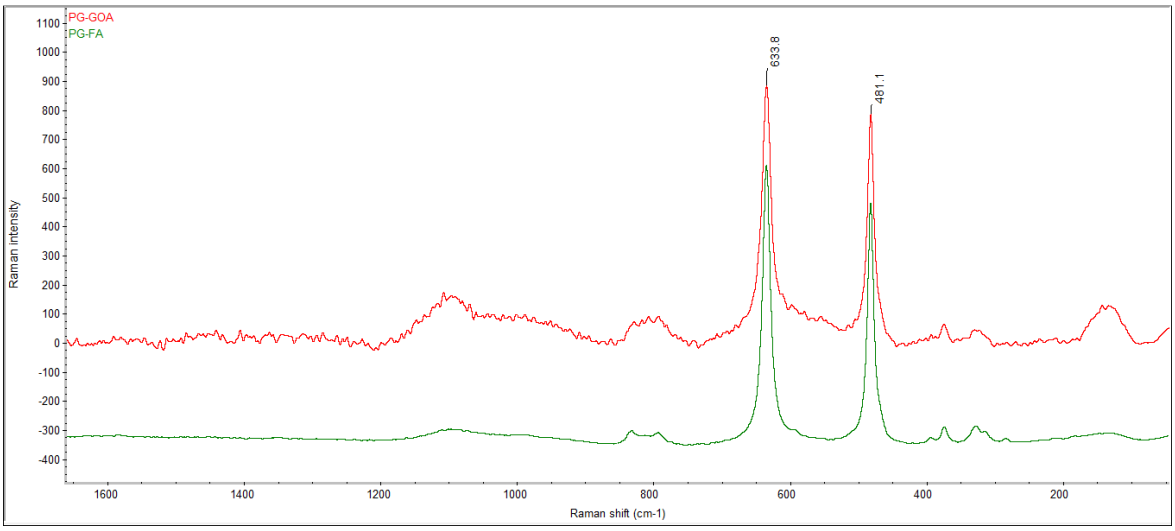

Fig. 5.2.25: Raman spectra of samples PG-GOA (red one) and PG-FA (green one) performed on a Ca antimonate that presents its orthorhombic phase, $Ca_2Sb_2O_7$.

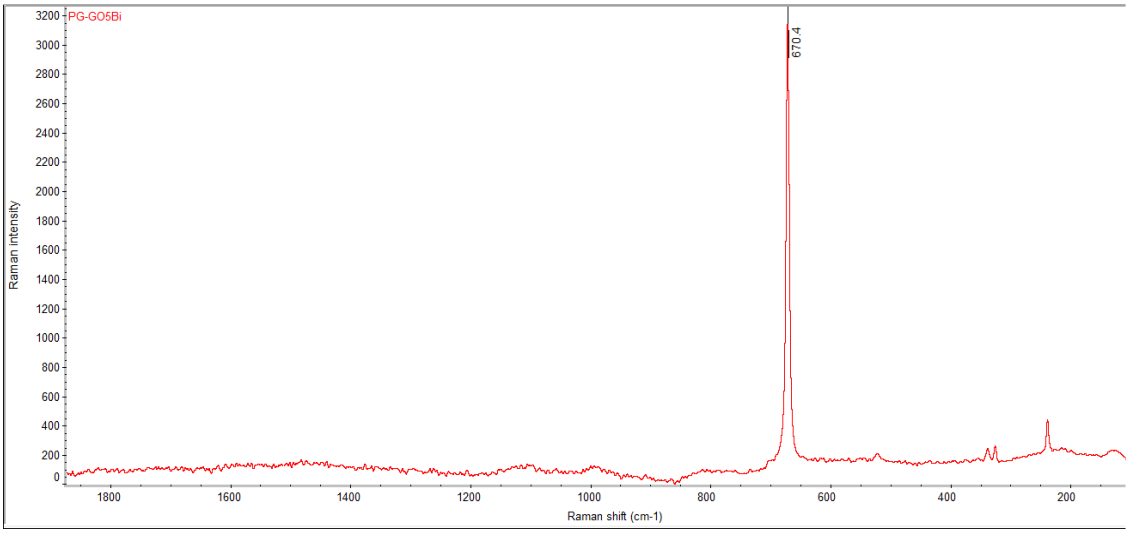

Fig. 5.2.26: Raman spectrum of sample PG-GO5Bi performed on a Ca antimonate that presents a hexagonal phase, $CaSb_2O_6$.

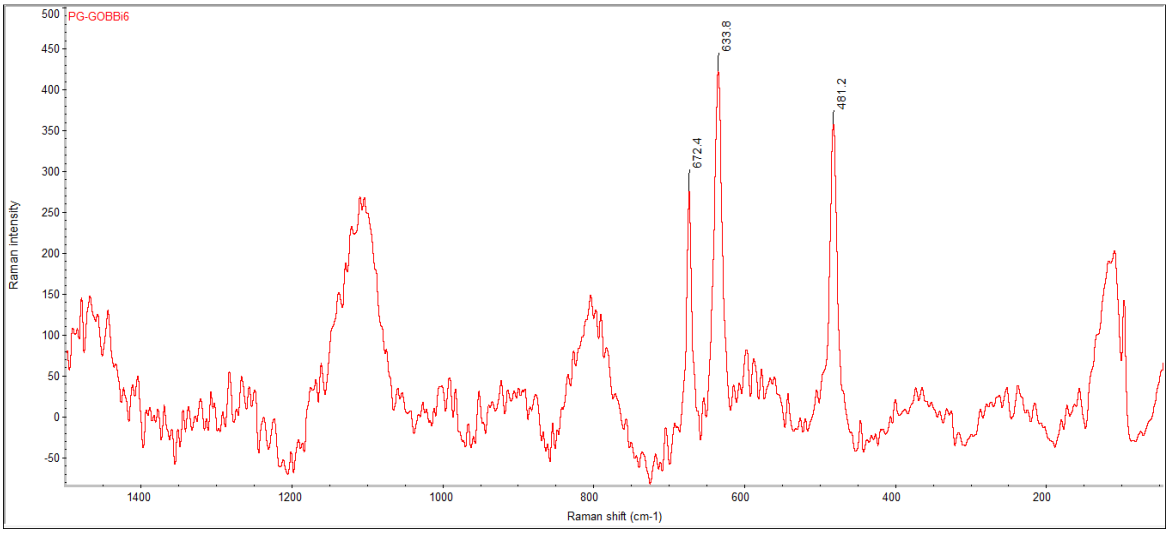

Fig. 5.2.27: Raman spectrum of sample PG-GO6Bi performed on a Ca antimonate that presents both hexagonal, $CaSb_2O_6$, and orthorhombic phase, $Ca_2Sb_2O_7$.

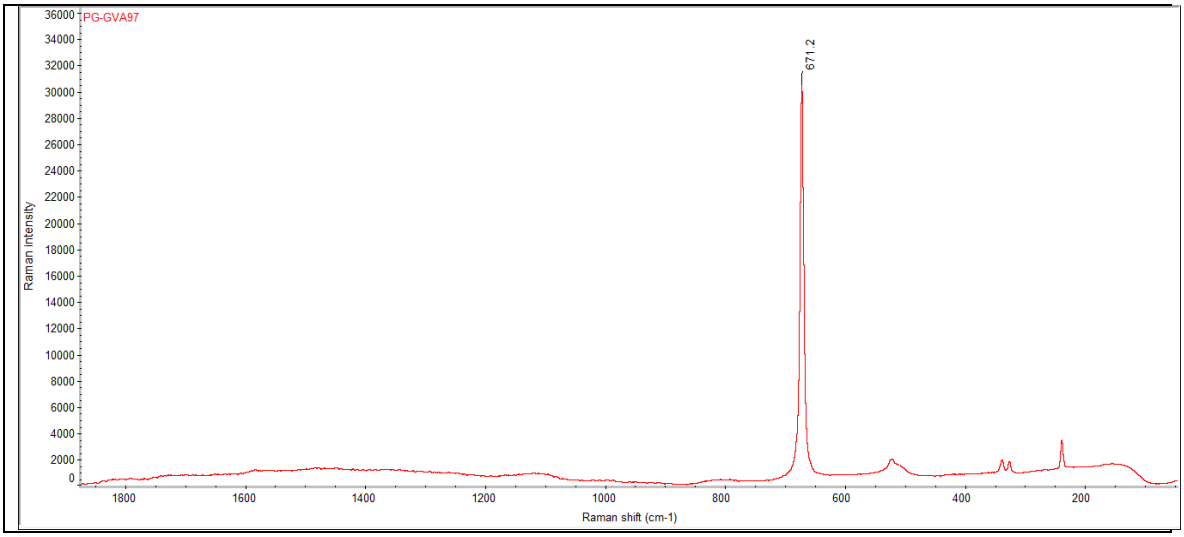

Fig. 5.2.28: Raman spectrum of sample PG-GVA97 performed on a Ca antimonate that presents hexagonal phase, $CaSb_2O_6$.

Sample	Na_2O	MgO	Al_2O_3	SiO_2	P_2O_5	SO_3	Cl_2O	K_2O	CaO	TiO_2	MnO	FeO	CoO	NiO	CuO	ZnO	As_2O_3	SnO_2	Sb_2O_3	PbO	Tot.
d.l. (%)	0.13	0.05	0.07	0.10	0.05	0.03	0.02	0.08	0.03	0.03	0.05	0.05	0.03	0.04	0.03	0.04	0.10	0.04	0.04	0.10	
PG-FVA1	18.90	0.67	0.29	68.44	< d.l.	0.19	1.83	0.08	9.44	0.12	< d.l.	0.22	< d.l.	< d.l.	< d.l.	< d.l.	< d.l.	< d.l.	0.59	< d.l.	**100.84**
SD	0.14	0.02	0.04	0.37		0.04	0.04	0.02	0.07	0.01		0.01							0.06		
PG-FVA5	20.10	0.66	0.31	66.75	< d.l.	0.29	1.83	0.08	9.12	0.07	< d.l.	0.21	< d.l.	< d.l.	< d.l.	< d.l.	< d.l.	< d.l.	0.97	< d.l.	**100.51**
SD	0.28	0.02	0.05	0.28		0.02	0.03	0.04	0.13	0.01		0.01							0.06		
PG-FVA7	17.24	0.58	0.33	70.95	< d.l.	0.08	1.56	< d.l.	9.32	0.06	< d.l.	0.23	< d.l.	< d.l.	< d.l.	< d.l.	< d.l.	< d.l.	0.19	< d.l.	**100.72**
SD	0.35	0.02	0.05	0.39		0.03	0.04		0.11	0.02		0.03							0.03		
PG-FVA22	16.80	0.56	0.27	71.37	< d.l.	0.16	1.52	0.12	9.03	0.12	< d.l.	0.26	< d.l.	< d.l.	< d.l.	< d.l.	< d.l.	< d.l.	0.17	< d.l.	**100.47**
SD	0.46	0.04	0.05	0.48		0.03	0.06	0.04	0.18	0.01		0.06							0.04		
PG-FVA67	17.47	0.64	0.40	72.82	< d.l.	0.51	0.71	0.10	5.84	0.16	0.42	0.38	< d.l.	< d.l.	< d.l.	< d.l.	< d.l.	< d.l.	< d.l.	< d.l.	**99.54**
SD	0.32	0.02	0.06	0.28		0.07	0.05	0.03	0.08	0.01	0.05	0.03									
PG-GVA97																					
Sb-rich*	9.8	0.5	0.6	61.7			1.2	0.1	7.9			0.3							4.5		86.5
Sb-poorer*	10.7	0.5	0.6	62.8			1.2	0.2	8.3			0.5							3.1		87.8
mean	15.64	0.78	0.55	67.66	0.10	0.13	1.68	0.14	8.89	0.10	< d.l.	0.36	< d.l.	< d.l.	< d.l.	< d.l.	< d.l.	< d.l.	3.57	< d.l.	**99.68**
SD	0.43	0.03	0.05	0.59	0.01	0.03	0.06	0.04	0.10	0.02		0.11							0.41		
PG-FV97	18.97	0.68	0.31	67.21	< d.l.	0.19	1.69	0.09	9.61	0.07	< d.l.	0.20	< d.l.	< d.l.	< d.l.	< d.l.	< d.l.	< d.l.	0.39	< d.l.	**99.51**
SD	0.25	0.02	0.06	0.34		0.04	0.04	0.03	0.09	0.02		0.02							0.05		
PG-AVT	19.17	0.79	0.32	64.36	< d.l.	0.20	2.11	0.08	11.36	0.05	< d.l.	0.21	< d.l.	< d.l.	< d.l.	< d.l.	< d.l.	< d.l.	1.64	< d.l.	**100.43**
SD	0.24	0.02	0.03	0.45		0.03	0.05	0.02	0.08	0.03		0.03							0.05		
PG-GAT7	16.65	0.60	0.31	71.25	< d.l.	0.13	1.58	< d.l.	9.24	0.14	< d.l.	0.26	< d.l.	< d.l.	< d.l.	< d.l.	< d.l.	< d.l.	0.22	< d.l.	**100.53**
SD	0.70	0.02	0.07	0.42		0.03	0.04		0.15	0.02		0.05							0.03		
PG-FGi	18.12	0.67	0.27	69.79	< d.l.	0.15	1.96	< d.l.	10.00	0.04	< d.l.	0.16	< d.l.	< d.l.	< d.l.	< d.l.	< d.l.	< d.l.	< d.l.	< d.l.	**101.32**
SD	0.43	0.08	0.05	0.32		0.03	0.12		0.17	0.02		0.02									
PG-FGi8	18.48	0.53	0.29	70.46	0.08	0.10	1.92	< d.l.	8.53	0.06	< d.l.	0.17	< d.l.	< d.l.	< d.l.	< d.l.	< d.l.	< d.l.	< d.l.	< d.l.	**100.75**
SD	0.36	0.04	0.08	0.55	0.02	0.03	0.05		0.11	0.00		0.03									
PG-FM14	18.79	0.57	0.33	69.10	0.11	0.14	1.94	< d.l.	9.22	0.05	< d.l.	0.20	< d.l.	< d.l.	< d.l.	< d.l.	< d.l.	< d.l.	< d.l.	< d.l.	**100.60**
SD	0.35	0.03	0.02	0.24	0.02	0.03	0.07		0.07	0.01		0.02									
PG-GONM	17.98	0.49	0.37	65.95	0.10	0.27	1.64	0.13	8.51	0.11	< d.l.	4.09	< d.l.	< d.l.	< d.l.	< d.l.	< d.l.	< d.l.	0.19	< d.l.	**99.90**
SD	0.54	0.05	0.02	0.80	0.03	0.03	0.05	0.03	0.13	0.02		0.15							0.05		
PG-FM83	19.36	0.64	2.41	64.44	0.11	0.24	1.37	0.63	8.06	0.06	< d.l.	2.78	< d.l.	< d.l.	< d.l.	< d.l.	< d.l.	< d.l.	< d.l.	< d.l.	**100.28**
SD	0.42	0.04	0.18	0.50	0.02	0.03	0.05	0.06	0.34	0.02		0.33									
PG-CM	6.98	0.61	2.00	49.86	0.94	0.11	0.65	0.66	4.19	0.12	0.87	4.83	0.03	< d.l.	0.12	0.29	1.91	< d.l.	0.11	25.23	**99.51**
SD	0.24	0.06	0.09	0.30	0.34	0.07	0.08	0.13	0.31	0.01	0.05	0.26	0.03		0.11	0.01	0.13		0.03	0.71	
PG-FM89	17.18	0.64	0.37	68.19	< d.l.	0.29	1.74	0.14	9.55	0.11	< d.l.	2.57	< d.l.	< d.l.	< d.l.	< d.l.	< d.l.	< d.l.	0.04	< d.l.	**100.97**
SD	0.20	0.03	0.10	0.26		0.05	0.10	0.03	0.08	0.02		0.13							0.03		

Sample	Na_2O	MgO	Al_2O_3	SiO_2	P_2O_5	SO_3	Cl_2O	K_2O	CaO	TiO_2	MnO	FeO	CoO	NiO	CuO	ZnO	As_2O_3	SnO_2	Sb_2O_3	PbO	Tot.
PG-GO5N	16.80	1.76	1.74	68.95	0.05	0.16	0.87	0.74	6.65	0.12	0.55	0.80	< d.l.	< d.l.	0.10	< d.l.	< d.l.	< d.l.	0.40	0.66	**100.44**
SD	0.43	0.03	0.19	0.36	0.05	0.07	0.03	0.09	0.15	0.02	0.02	0.02			0.08				0.17	0.09	
PG-AN	15.22	0.67	0.52	65.28	0.10	0.24	1.66	0.12	9.54	0.19	< d.l.	6.40	< d.l.	< d.l.	< d.l.	< d.l.	< d.l.	< d.l.	0.09	< d.l.	**100.10**
SD	0.28	0.02	0.06	0.44	0.04	0.07	0.05	0.03	0.08	0.02		0.08							0.08		
PG-FN	1.32	4.83	10.80	48.61	3.67	0.05	0.00	2.81	19.59	0.70	0.40	7.18	< d.l.	< d.l.	< d.l.	< d.l.	< d.l.	< d.l.	< d.l.	< d.l.	**100.04**
SD	0.38	0.35	0.80	1.84	0.66	0.03	0.00	0.52	1.55	0.04	0.04	1.00									
PG-AB8	16.79	0.42	0.75	70.94	0.06	0.19	1.60	0.43	4.83	0.14	0.08	1.55	0.45	0.48	0.95	< d.l.	0.17	< d.l.	0.28	< d.l.	**100.14**
SD	0.08	0.03	0.06	0.71	0.02	0.03	0.06	0.10	0.12	0.02	0.01	0.03	0.03	0.03	0.06		0.03		0.04		
PG-AB1_2	16.23	0.34	0.43	70.95	0.05	0.21	1.16	0.23	5.32	0.04	< d.l.	1.63	0.16	< d.l.	0.45	< d.l.	< d.l.	< d.l.	0.32	2.81	**100.43**
SD	0.36	0.05	0.04	0.94	0.05	0.10	0.08	0.07	0.08	0.02		0.02	0.03		0.12				0.07	0.30	
PG-AB9a	15.15	0.43	0.64	72.34	< d.l.	0.26	1.48	0.30	4.54	0.14	0.06	1.48	0.45	0.64	1.07	< d.l.	0.65	< d.l.	0.24	< d.l.	**100.02**
SD	3.44	0.06	0.16	5.73		0.06	0.16	0.08	0.41	0.02	0.01	0.13	0.05	0.07	0.10		0.11		0.03		
PG-AB9b	16.36	0.47	0.72	70.31	0.05	0.29	1.55	0.42	4.80	0.15	0.08	1.59	0.47	0.69	1.07	< d.l.	0.78	< d.l.	0.25	< d.l.	**100.12**
SD	0.47	0.06	0.08	0.47	0.04	0.04	0.05	0.07	0.07	0.02	0.04	0.07	0.02	0.04	0.01		0.04		0.02		
PG-AB9c	15.87	0.62	0.72	69.64	0.43	0.22	1.51	0.23	5.97	0.12	< d.l.	1.27	0.40	0.42	0.67	< d.l.	0.66	< d.l.	0.34	0.47	**99.62**
SD	0.35	0.03	0.08	0.62	0.15	0.05	0.05	0.05	0.14	0.02		0.06	0.03	0.04	0.04		0.04		0.04	0.06	
PG-AB9d	16.60	0.46	0.63	71.67	< d.l.	0.27	1.47	0.30	4.40	0.13	0.06	1.40	0.42	0.58	1.04	< d.l.	0.55	< d.l.	0.21	< d.l.	**100.30**
SD	1.68	0.08	0.09	3.39		0.05	0.30	0.06	0.80	0.04	0.03	0.26	0.08	0.13	0.17		0.14		0.04		
PG-ABOa	16.49	0.65	0.77	69.65	0.76	0.25	1.56	0.24	5.89	0.10	0.08	1.13	0.34	0.41	0.90	< d.l.	0.52	< d.l.	0.30	0.29	**100.33**
SD	0.22	0.02	0.08	0.60	0.05	0.04	0.04	0.02	0.09	0.02	0.01	0.03	0.04	0.04	0.05		0.06		0.03	0.03	
PG-ABOb	16.97	0.62	0.84	69.85	0.81	0.26	1.59	0.22	5.91	0.11	0.07	1.12	0.31	0.39	0.91	< d.l.	0.53	< d.l.	0.30	0.30	**101.16**
SD	0.34	0.03	0.22	0.49	0.10	0.07	0.04	0.04	0.09	0.01	0.02	0.08	0.02	0.02	0.06		0.03		0.03	0.06	
PG-AB	15.51	0.37	0.49	69.73	0.06	0.18	1.37	0.22	5.62	0.06	< d.l.	1.82	0.18	0.04	0.21	< d.l.	< d.l.	< d.l.	0.35	2.57	**98.84**
SD	0.23	0.02	0.07	0.64	0.02	0.01	0.04	0.08	0.13	0.02		0.11	0.02	0.01	0.03				0.03	0.09	
PG-SB	16.50	0.59	0.71	70.85	0.19	0.15	1.71	0.20	7.10	0.07	< d.l.	0.43	0.32	0.36	0.69	< d.l.	< d.l.	< d.l.	0.05	< d.l.	**100.03**
SD	0.27	0.01	0.08	0.35	0.01	0.03	0.04	0.05	0.05	0.01		0.03	0.01	0.03	0.03				0.03		
PG-GOB8	9.54	0.57	1.63	51.82	0.31	0.22	0.81	0.57	4.11	0.09	0.57	6.92	0.07	0.07	0.21	0.05	1.68	< d.l.	0.64	18.50	**98.38**
SD	0.57	0.05	0.11	0.50	0.05	0.02	0.04	0.05	0.12	0.01	0.04	0.13	0.01	0.02	0.09	0.01	0.03		0.06	0.33	
PG-GO3B	18.83	0.65	2.59	66.70	0.13	0.21	1.16	0.67	7.64	0.07	< d.l.	0.59	0.04	< d.l.	0.07	< d.l.	< d.l.	< d.l.	0.33	0.17	**99.96**
SD	0.26	0.02	0.20	0.31	0.02	0.01	0.05	0.07	0.10	0.03		0.03	0.01		0.01				0.03	0.04	
PG-FA	16.15	0.64	1.44	59.37	< d.l.	0.38	1.09	0.34	8.75	0.10	0.06	1.27	0.09	< d.l.	0.40	0.04	< d.l.	< d.l.	2.77	6.70	**99.68**
SD	0.20	0.03	0.11	0.28		0.03	0.04	0.06	0.10	0.02	0.03	0.05	0.03		0.04	0.03		0.01	0.13	0.38	
PG-GOB	16.98	0.54	1.79	69.54	< d.l.	0.27	1.58	0.48	5.36	0.06	< d.l.	0.66	0.24	< d.l.	0.08	0.04	< d.l.	< d.l.	1.95	< d.l.	**99.63**
SD	0.67	0.03	0.10	0.32		0.02	0.10	0.07	0.27	0.01		0.02	0.04		0.03	0.02			0.10		
PG-AAB	17.33	0.51	0.41	70.16	< d.l.	0.26	1.36	0.24	7.48	0.08	< d.l.	0.54	0.09	< d.l.	1.18	< d.l.	< d.l.	< d.l.	< d.l.	< d.l.	**99.78**
SD	0.43	0.02	0.10	0.60		0.03	0.03	0.06	0.07	0.01		0.04	0.03		0.06						

Sample	Na_2O	MgO	Al_2O_3	SiO_2	P_2O_5	SO_3	Cl_2O	K_2O	CaO	TiO_2	MnO	FeO	CoO	NiO	CuO	ZnO	As_2O_3	SnO_2	Sb_2O_3	PbO	Tot.
PG-FUA	15.06	3.13	0.68	68.66	0.15	0.25	0.94	2.04	8.00	0.06	< d.l.	0.43	< d.l.	< d.l.	1.01	< d.l.	< d.l.	< d.l.	< d.l.	< d.l.	**100.53**
SD	0.34	0.05	0.06	0.43	0.03	0.04	0.04	0.13	0.07	0.02		0.02			0.03						
PG-GAT1	17.76	0.83	0.85	71.88	< d.l.	0.29	1.18	0.16	4.73	0.13	0.92	0.44	< d.l.	< d.l.	0.90	< d.l.	< d.l.	< d.l.	< d.l.	< d.l.	**100.20**
SD	0.20	0.03	0.07	0.58		0.05	0.03	0.03	0.15	0.02	0.03	0.03			0.06						
PG-GO6B	16.78	0.67	1.09	67.59	0.14	0.20	1.37	0.23	10.77	0.10	< d.l.	0.86	< d.l.	< d.l.	0.09	< d.l.	< d.l.	< d.l.	0.52	< d.l.	**100.50**
SD	0.32	0.02	0.08	0.19	0.03	0.02	0.09	0.07	0.20	0.01		0.04			0.01				0.02		
PG-GOA	15.96	0.69	2.32	67.02	< d.l.	0.17	1.72	0.59	8.59	0.05	< d.l.	0.45	0.04	< d.l.	0.69	< d.l.	< d.l.	< d.l.	1.92	0.17	**100.47**
SD	0.26	0.03	0.09	0.76		0.03	0.03	0.11	0.08	0.02		0.02	0.01		0.11				0.07	0.07	
PG-GO3Bi	16.88	0.56	2.24	66.51	0.06	0.30	1.42	0.61	8.18	0.05	< d.l.	0.29	< d.l.	< d.l.	< d.l.	< d.l.	< d.l.	< d.l.	2.76	0.93	**100.85**
SD	0.40	0.02	0.05	1.12	0.03	0.04	0.11	0.09	0.34	0.02		0.03							0.64	0.11	
PG-GO5Bi	11.60	0.71	0.52	57.71	< d.l.	0.48	0.65	0.36	4.49	0.06	< d.l.	0.98	< d.l.	< d.l.	0.05	< d.l.	< d.l.	< d.l.	5.20	15.92	**98.98**
SD	0.43	0.03	0.05	1.19		0.22	0.03	0.09	0.26	0.00		0.03			0.02				1.89	0.77	
PG-GONBi	16.81	0.58	0.36	64.32	0.11	0.12	1.55	0.25	8.93	0.04	< d.l.	0.35	< d.l.	< d.l.	< d.l.	< d.l.	< d.l.	0.04	6.07	< d.l.	**99.70**
SD	0.49	0.04	0.08	0.41	0.02	0.01	0.28	0.04	0.11	0.01		0.03						0.03	0.33		
PG-GO6Bi	18.02	0.74	1.63	61.88	0.13	0.55	1.22	0.31	10.23	0.07	0.10	0.59	< d.l.	< d.l.	0.03	< d.l.	< d.l.	< d.l.	4.65	0.50	**100.71**
SD	0.63	0.03	0.13	0.88	0.01	0.06	0.06	0.05	0.37	0.02	0.02	0.06			0.01				0.37	0.05	
PG-AOBi	14.35	0.62	0.42	63.16	< d.l.	0.18	1.46	0.24	9.67	0.05	< d.l.	0.67	< d.l.	< d.l.	< d.l.	< d.l.	< d.l.	< d.l.	8.52	< d.l.	**99.59**
SD	1.06	0.02	0.06	0.81		0.01	0.06	0.07	0.28	0.01		0.04							0.65		
PG-GOBi	16.59	0.66	2.17	63.49	< d.l.	0.36	1.57	0.46	8.36	0.04	< d.l.	0.41	< d.l.	< d.l.	0.08	< d.l.	< d.l.	< d.l.	5.18	< d.l.	**99.48**
SD	0.49	0.03	0.12	0.76		0.05	0.07	0.06	0.20	0.02		0.03			0.03				0.60		

Tab. 5.2.1: EPMA chemical analyses (oxides wt%) of the glass phase of Piovego cemetery beads. The labels are the same as reported in Table 1 of par. 3.2.2, and are calculated as a mean of 5÷10 point analysis. Data are reported as obtained by the analyses and detection limits are also described (SD = standard deviation of the measures; * = EDS data).

5.3 Villa di Villa site

The results of the chemical analysis (Tab. 5.3.1) show that all the samples are silica soda lime glasses with values of SiO_2 ranging from 61.70 to 76.95 wt%, Na_2O from 7.45 to 18.60 wt% and CaO from 2 to 8.45 wt%.

The levels of MgO, K_2O and Na_2O in Fig. 5.3.1 a and b show that the analyzed glasses contain different compositional groups. In seven samples (represented by empty symbols) MgO and K_2O never exceed 0.7 wt% and Na_2O levels range between 12.15 and 18.60 wt%. These data indicate that the glasses were produced using *natron* as flux (LMG, Low Magnesium Glass), which is also consistent with the contents of SO_3 (0.07÷0.43 wt%) and Cl_2O (0.77÷1.73 wt%). VV-AB6 is the only sample with low MgO content (0.5 wt%), lower Na_2O concentration (7.45 wt%) and high K_2O (8.37 wt%), typical of Low Magnesium High Potassium glasses (LMHK) produced with mixed alkali ashes as flux (Fig. 5.3.1 a and b, black circle). The turquoise melon bead (VV-MB) and the two decorated bracelet fragments (VV-BRB5 and VV-BRB9) have particular intermediate compositions with MgO contents ranging between 0.92 and 1 wt% and K_2O between 1.80 and 2.45 wt% (Fig. 5.3.1a black star and diamonds).

The use of sand as a source of silica, instead of pure quartz or quartzite, is proved by the significant presence of alumina and iron in all the samples and ranging between 1.82 and 3.29 wt% (Al_2O_3) and from 0.26 to 1.01 wt% (FeO) (fig. 5.3.2).

The other minor and trace elements in the samples are variable and depend on the color and opacity/transparency of the glasses.

Below are the main compositional features of the finds according to their specific typologies.

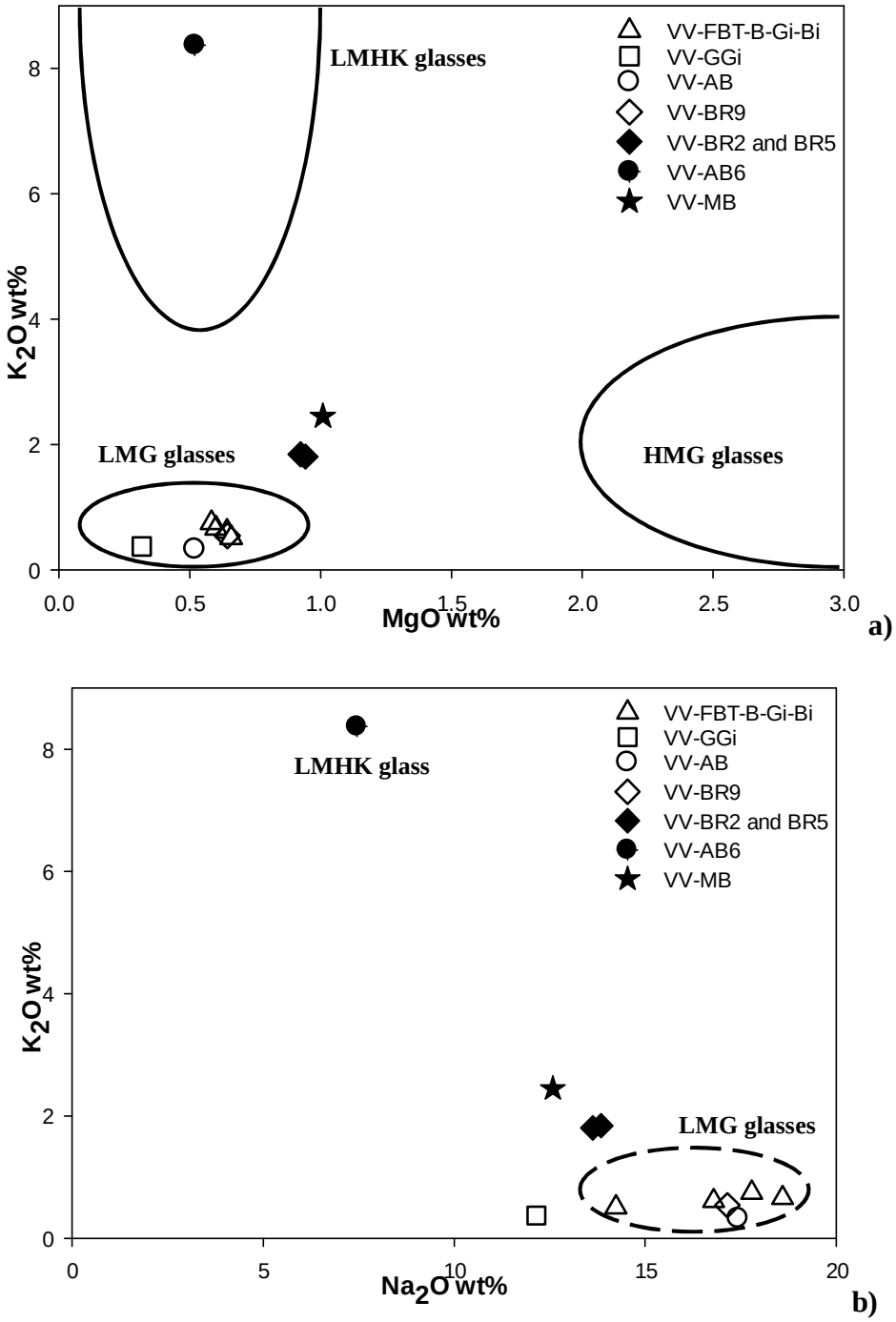

Fig. 5.3.1: a) and b) MgO *vs* K_2O and Na_2O *vs* K_2O contents of the glass phase in the analyzed samples from the Villa di Villa site (symbols = sample; colors: empty = *natron* – based glasses; full = other composition).

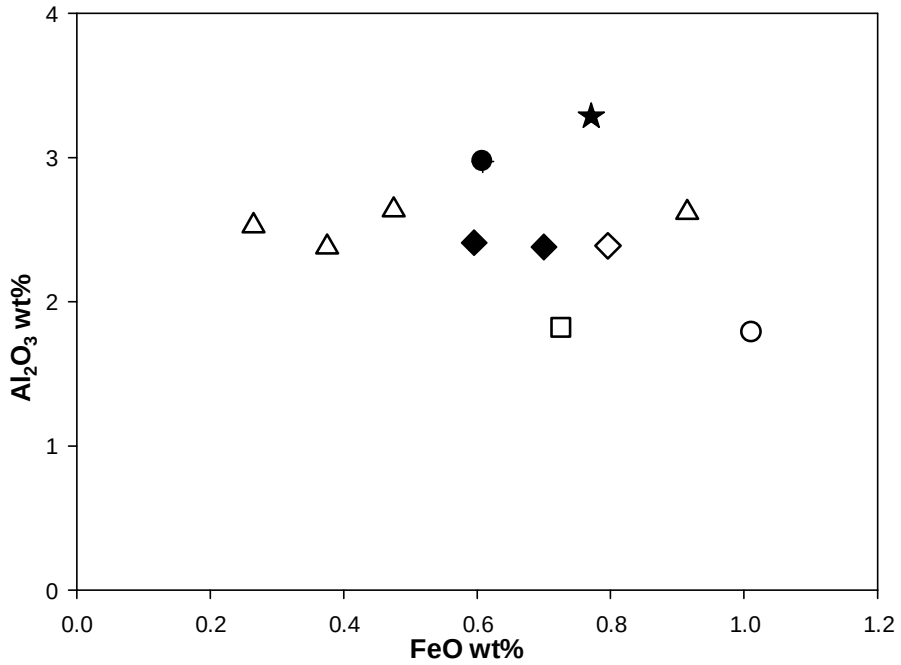

Fig. 5.3.2: Feo *vs* Al_2O_3 contents of the glass phase in the analyzed samples from the Villa di Villa site (symbols = sample; colors: empty = *natron* – based glasses; full = other composition).

Annular beads

The two annular blue beads were produced using two different fluxing agents. Sample VV-AB6 is a LMHK glass as shown by the MgO *vs* K_2O and Na_2O *vs* K_2O plots (Fig. 5.2.1a and b): it has 7.45 wt% of Na_2O, 0.52 wt% of MgO and 8.37 wt% of K_2O. The CaO (1.57 wt%) and P_2O_5 (0.22 wt%) contents also are in the range of the LMHK glasses (Angelini et al. 2004, 2010a; Brill 1992; Henderson 1988; Towle et al. 2001; Santopadre and Verità 2000)

By contrast, sample VV-AB is a typical LMG glass obtained with *natro*n as flux, and presents 17.43 wt% of Na_2O, 0.52 wt% of MgO and 0.33 wt% of K_2O (Fig. 5.3.1a and b). The contents of SO_3 and Cl_2O – 0.19 and 1.73 wt%, respectively – are consistent with the use of *natron* as flux.

Sample VV-AB presents a significant Al content (Al_2O_3=1.78 wt%) suggesting use of impure sand made of feldspar minerals and small amounts of heavy metals, in accordance with the Fe content (FeO = 1.01 wt%). The same may be said of sample VV-AB6, which has greater Al content (Al_2O_3 = 2.97 wt%) but lower Fe (FeO = 0.6 wt%) (Fig. 5.3.2).

The blue color of VV-AB and VV-AB6 is due to Co (CoO 0.04 and 0.15 wt%, respectively) associated to low contents of Cu (CuO 0.12 and 0.15 wt%, respectively). In addition, cobalt in the LMHK bead is associated with Sb (Sb_2O_3 = 0.12 wt%). Instead, cobalt is not associated with any other element in VV-AB.

SEM-EDS analysis shows that in contrast with sample VV-AB, whose homogeneous texture has rare bubbles of about 10 µm, sample VV-AB6 has large numbers of SiO_2 inclusions (Fig. 5.3.3a). The crystals have lamellar or rectangular morphologies, with size ranging from a few microns to 10 µm, and are frequently grouped in large rounded or sub rounded aggregates with dimensions up to 100 µm. The biggest grains are often surrounded by large fractures due to changes in volume during glass cooling, especially when phase transitions from quartz to tridymite and/or cristobalite occur (Angelini et al. 2004; Artioli et al. 2008) (Fig. 5.3.3b-c).

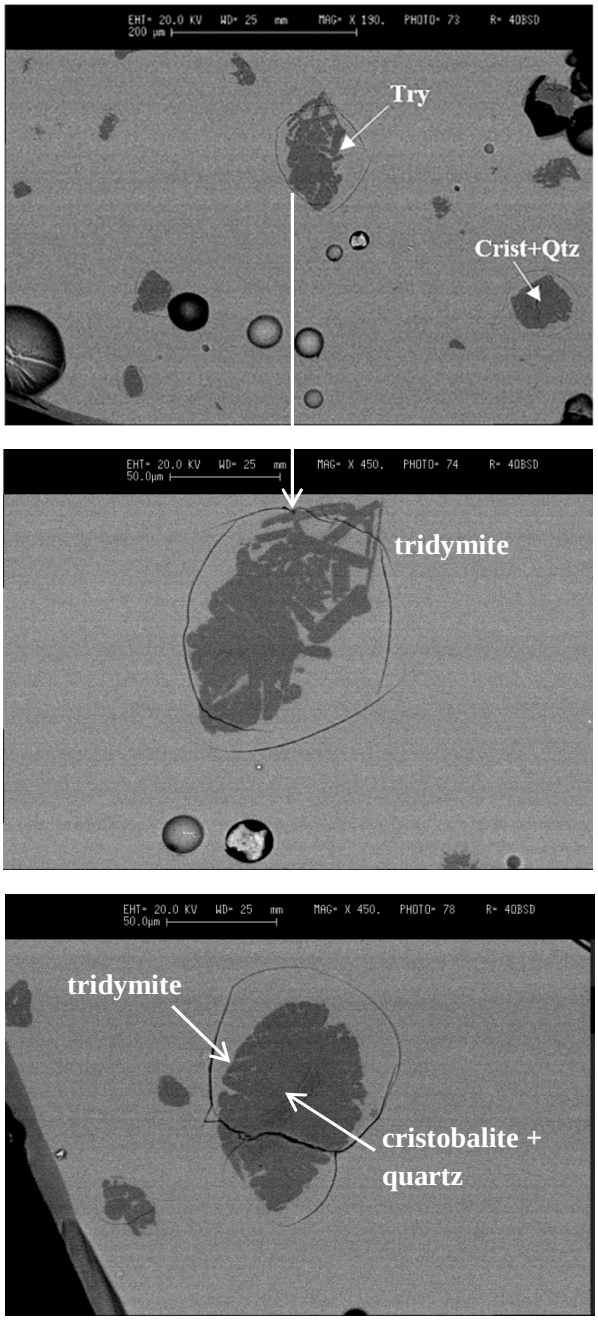

Fig. 5.3.3: a) SEM-BSE image of the LMHK sample VV-AB6 characterized by numerous SiO_2 inclusions in the glass matrix. b) and c) SEM-BSE images of SiO_2 inclusions of tridymite (a) and of a grain with cristobalite and quartz in the core and tridymite in the edges (b) (Try = tridymite; Crist = cristobalite; Qtz = quartz).

The lamellar crystals- analyzed through µ-Raman spectroscopy – are of tridymite (Fig. 5.3.3b and 5.3.4a) while the more rectangular are of cristobalite (Fig. 5.3.4b). The rectangular crystals

grouped in large rounded aggregates are characterized by cristobalite and quartz in the core and by trydimite in the edges (Fig. 5.3.3c and 5.3.4c-d).

The presence of cristobalite is indicative, since it is one of the high-temperature polymorphs of silica (see details in the discussion, par. 6.3).

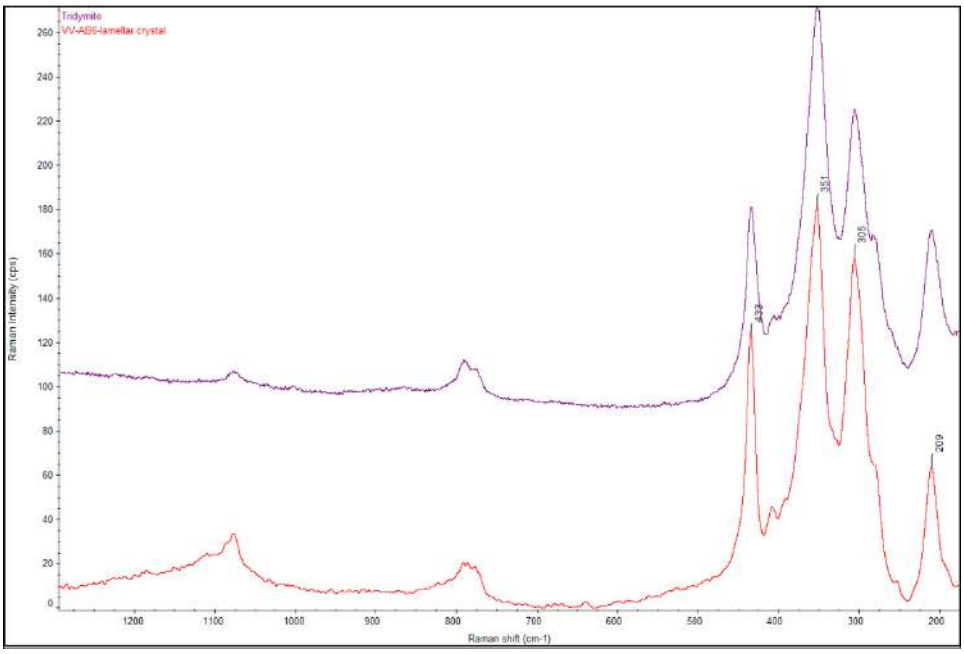

a)

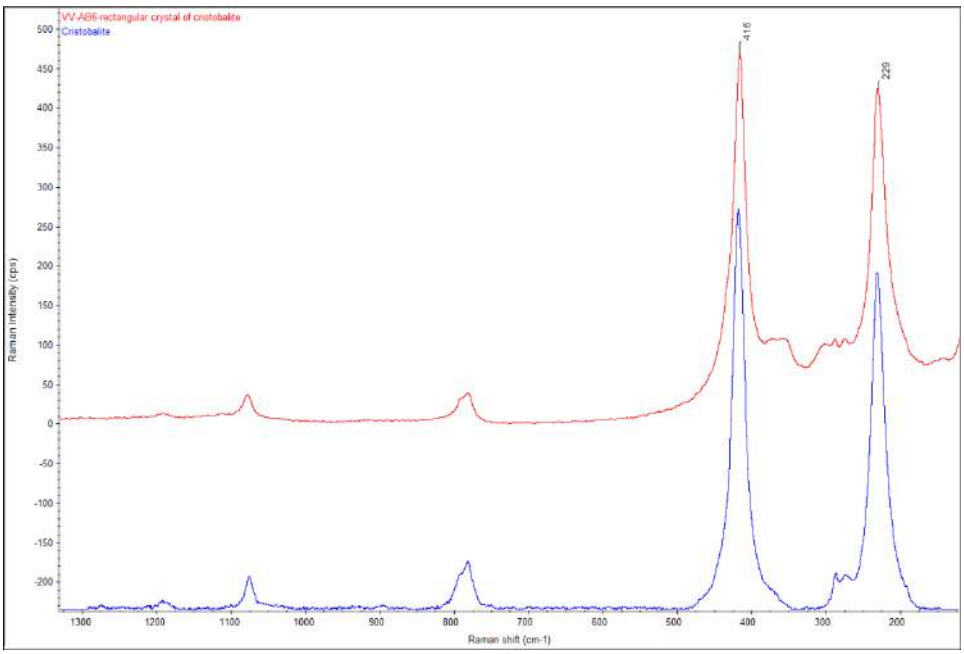

b)

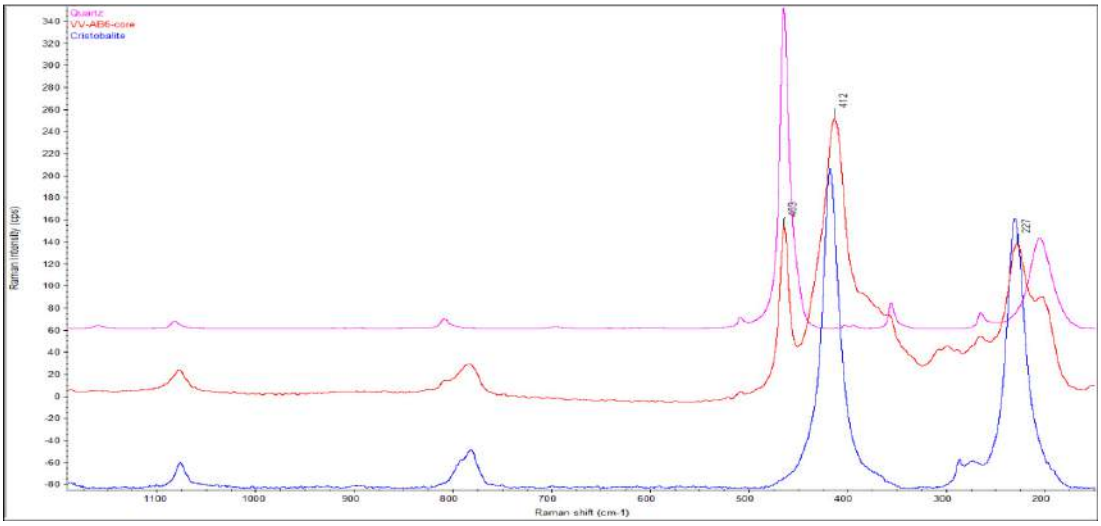

c)

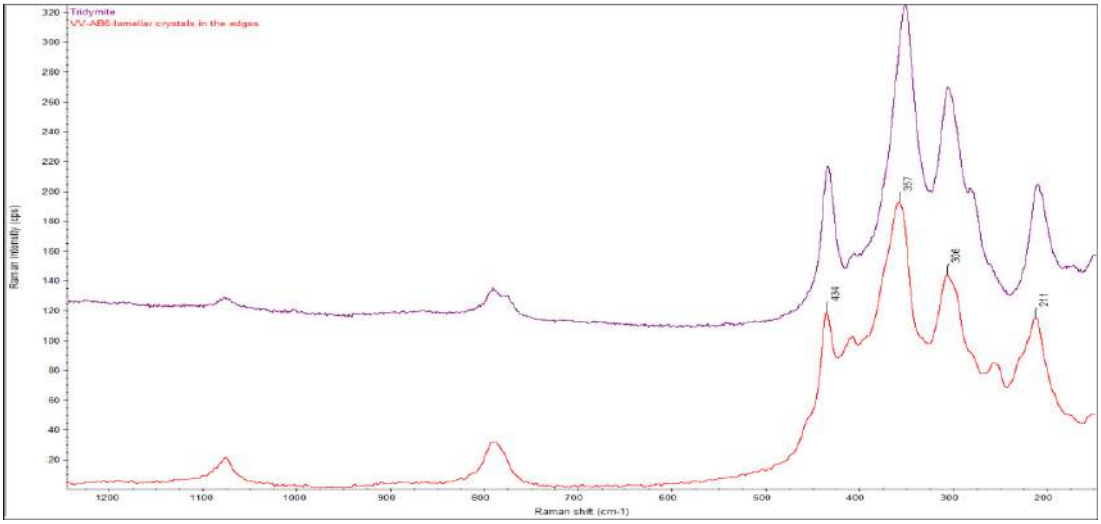

d)

Fig. 5.3.4: Raman Spectra of some SiO_2 inclusions of sample VV-AB6. a) lamellar crystal of tridymite; b) rectangular crystal of cristobalite; c) and d) analyses on a rounded inclusion performed on the core (c) and on crystals in the edges (d). In the images, the spectra on the sample inclusions (in red) and standard spectra from the RRUFF database are reported.

Bracelet fragments

The three blue bracelet fragments belong to different typologies: VV-BRB9 is plain with a D-shaped section and corresponds to group 3a of Haevernick 1960, while VV-BRB5 and VV-BRB2 are decorated by ribbing similar to group 8a and c of Haevernick 1960. The different typologies are associated with different glass classes. VV-BRB9 is a typical LMG *natron*-based glass, with 0.64 wt% MgO and 0.54 wt% K_2O (Fig. 5.3.1a empty diamond), in accordance with the contents of Cl_2O (1.15 wt%) and SO_3 (0.24 wt%). VV-BRB5 and VV-BRB2 have higher levels of MgO (0.94 and 0.92 wt%, respectively) and especially K_2O (1.80 and 1.84 wt%) (Fig. 5.3.1a black diamonds) which usually never exceed 1.5 wt% in typical *natron*–based glasses. However, the flux is probably *natron* due to the Na_2O/K_2O ratio (about 7.5 in both arm rings) and the high K content is associated with sand type (see below). On the other hand, it is worth noting that the low S amount (SO_3 about 0.05 wt%) and P content (P_2O_5 about 0.19 wt%) are compatible with the use of plant ash.

The levels of Al_2O_3 and FeO are similar in all three samples and range between 2.38 and 2.41 wt%, and between 0.60 to 0.80 wt%, respectively.

The three glasses are colored by Co (CoO = 0.11÷0.16 wt%) associated to Cu (CuO = 0.20÷0.24 wt%). Moreover, they contain Mn in similar concentrations (MnO = 0.41÷0.79 wt%). These quantities are not sufficient to obtain decoloration, and were therefore probably introduced as impurities from the raw materials used (possibly the coloring agent).

The three arm rings have a homogenous texture only characterized by a few bubbles with size up to 100 µm (Fig. 5.3.5).

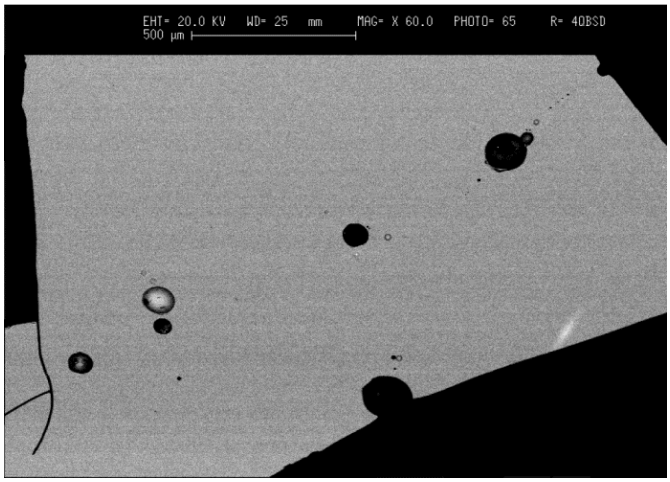

Fig. 5.3.5: SEM-BSE image of sample VV-BRB9. The texture is homogeneous except for a few bubbles.

Globular bead with eyes decoration

The globular yellow bead VV-GGi was produced using *natron* as flux, as suggested by its levels of MgO and K_2O <1 wt% (Fig. 5.3.1), Cl_2O (1.23 wt%) and SO_3 (0.07 wt%). The glass phase of the bead body shows PbO and Sb_2O_3 of 10.71 and 1.05 wt%, respectively, with Na_2O (12.15 wt%) lower than the other *natron*-based glasses from Villa di Villa (Fig. 5.3.2, empty square).

This is consistent with numerous crystals rich in Pb and Sb in the glass matrix, as observed by SEM-EDS (Fig. 5.3.6). The Pb antimonates are variable in size from a few microns to 25-30 µm, and these inclusions are generally grouped in aggregates with irregular shapes (Fig. 5.3.6a and c, white aggregates). Crystals of SiO_2 are also present, with lamellar or rectangular morphologies 20 to 50 µm in size (Fig. 5.3.6 a and b) and sometimes grouped in large rounded aggregates with lamellar inclusions on the edges (Fig. 5.3.6a, dark gray grains). XRD characterization of the mineral phases on the whole object identified quartz, tridymite, cristobalite and bindheimite (Fig. 5.3.7a). Raman spectroscopy identified Pb antimonates as bindheimite phases ($Pb_2Sb_2O_7$), with characteristic peaks at 140, 335, 458 and 513 cm^{-1} (Fig. 5.3.7b). As regards the distribution of silica phases, the µ-Raman data show that the bigger aggregates are characterized in the center by cristobalite (Fig. 5.3.7c) and in the edges by lamellar crystals of tridymite (main peaks: 446, 375, 289 cm^{-1}) plus cristobalite (main peaks:

423 and 221 cm^{-1}) (Fig. 5.3.7d). As for sample VV-AB6, the presence of both cristobalite and tridymite is indicative of the temperature reached during the melting process. The quartz identified by X-ray diffraction is not confirmed by Raman spectroscopy in the yellow glass, and is probably associated with the blue and white eyes.

Fig. 5.3.6: SEM-BSE images of the LMG yellow eye bead VV-GGi. a) detail of the heterogeneous texture due to Pb antimonates aggregates (white ones), lamellar crystals of tridymite and cristobalite and large aggregates of cristobalite in the core and of cristobalite and tridymite in the edges. b) detail of lamellar crystals of tridymite plus cristobalite. c) detail of Pb antimonates aggregates. (Try = tridymite; Crist = cristobalite).

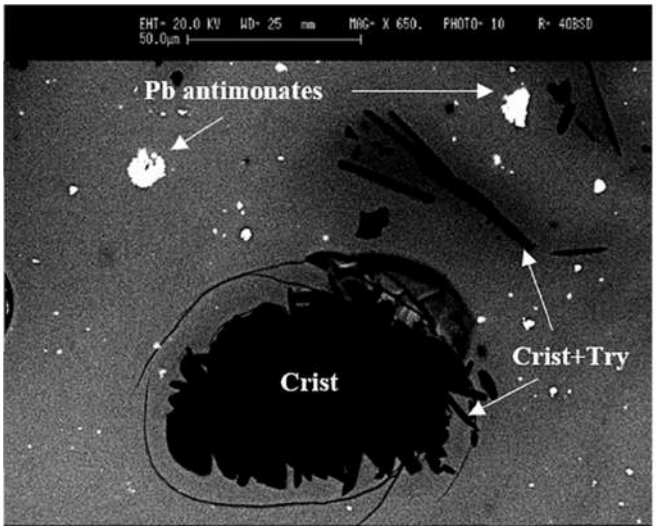

a)

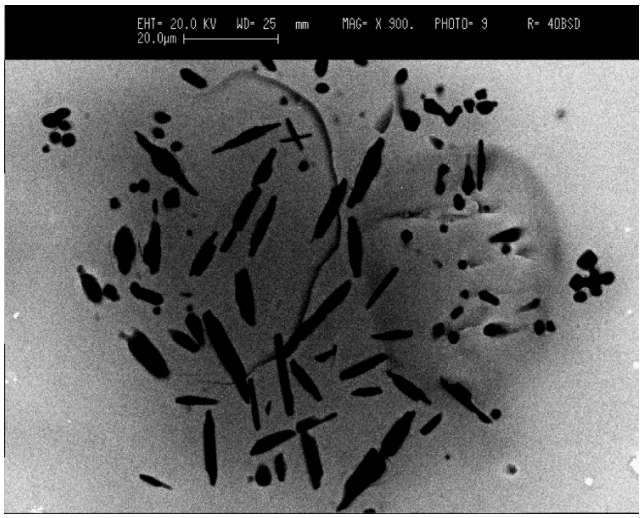

b)

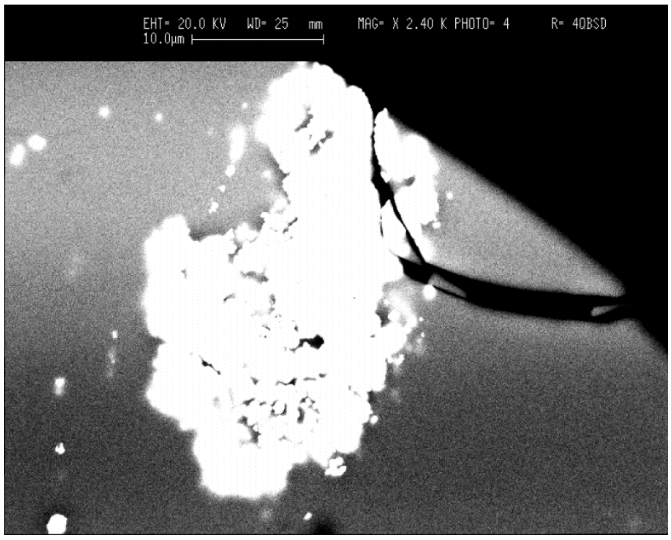

c)

Fig. 5.3.7: a) X-Ray pattern diffraction obtained from surface analysis of eye bead VV-GGi. b)-d) Raman Spectra of some inclusions in sample VV-GGi obtained on Pb antimonates (b) and on SiO_2 particles (c and d).

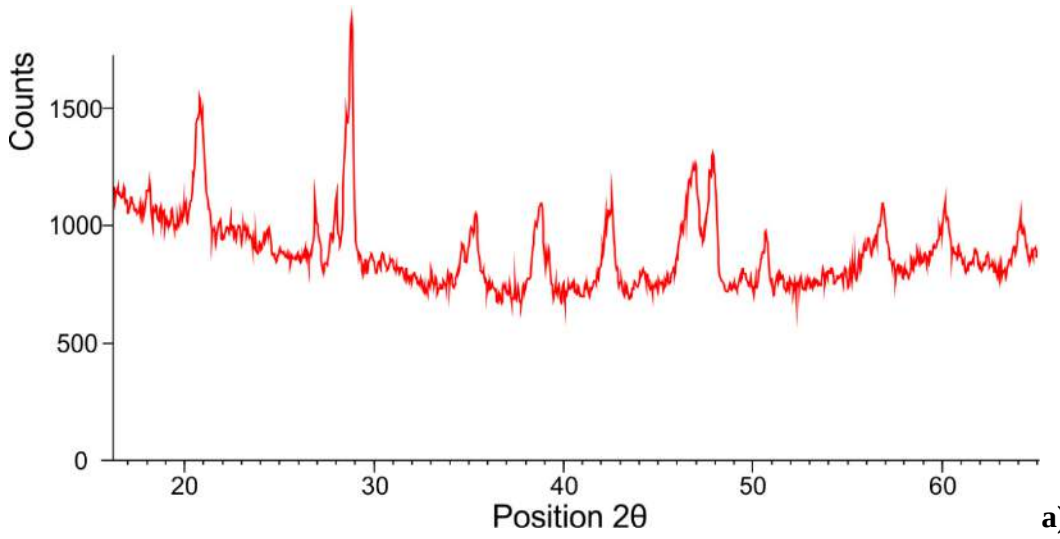

a)

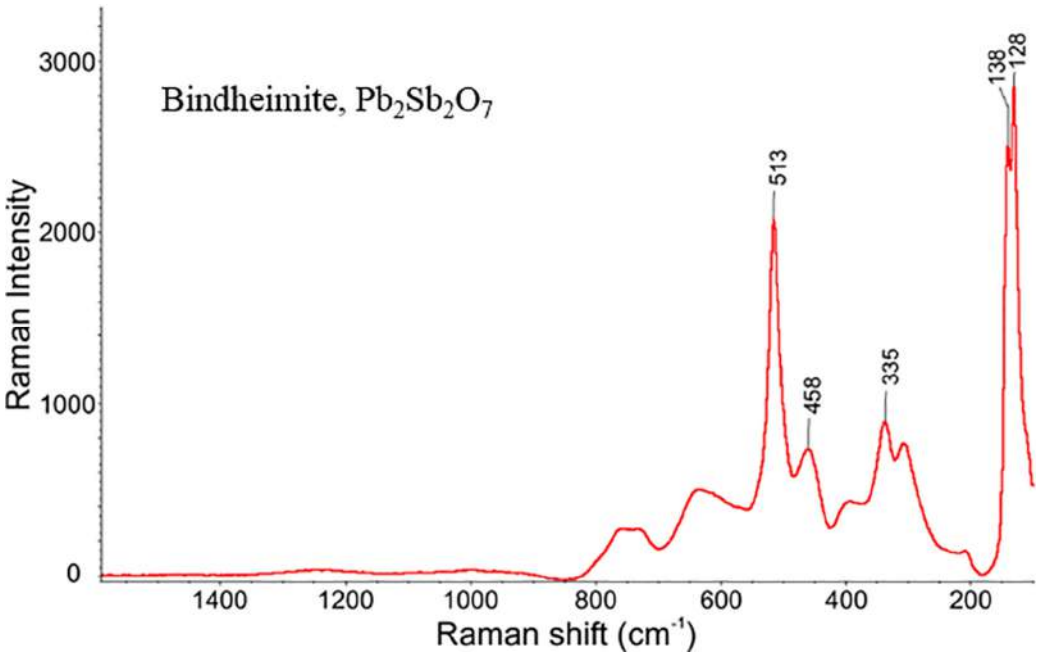
Bindheimite, $Pb_2Sb_2O_7$
Raman Intensity
Raman shift (cm^{-1})
513
458
335
138
128

b)

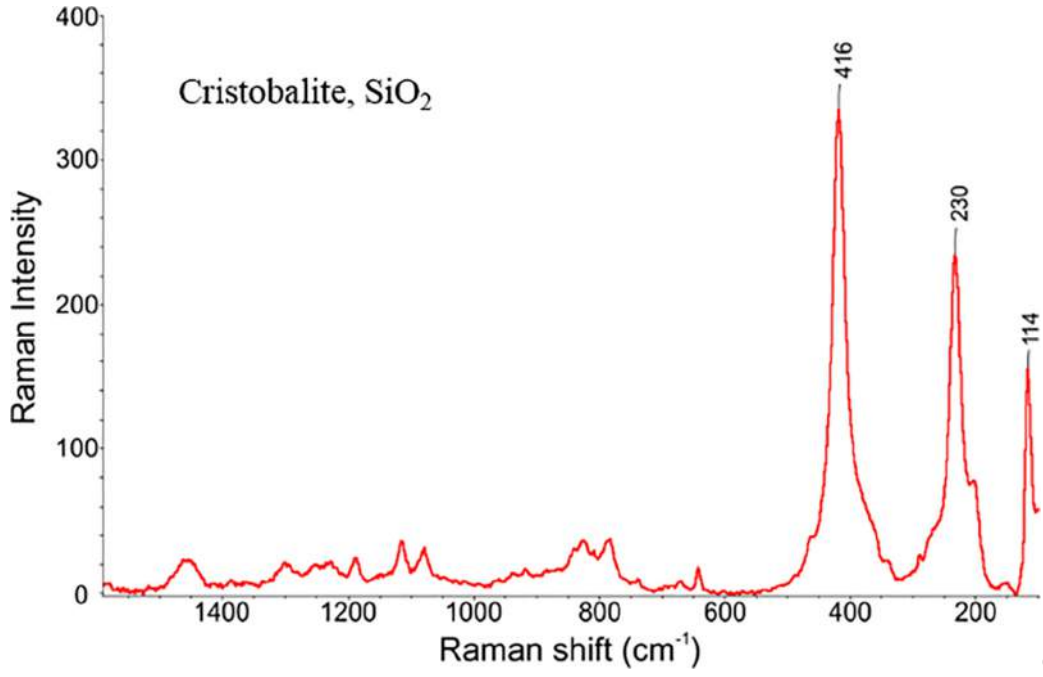
Cristobalite, SiO_2
Raman Intensity
Raman shift (cm^{-1})
416
230
114

c)

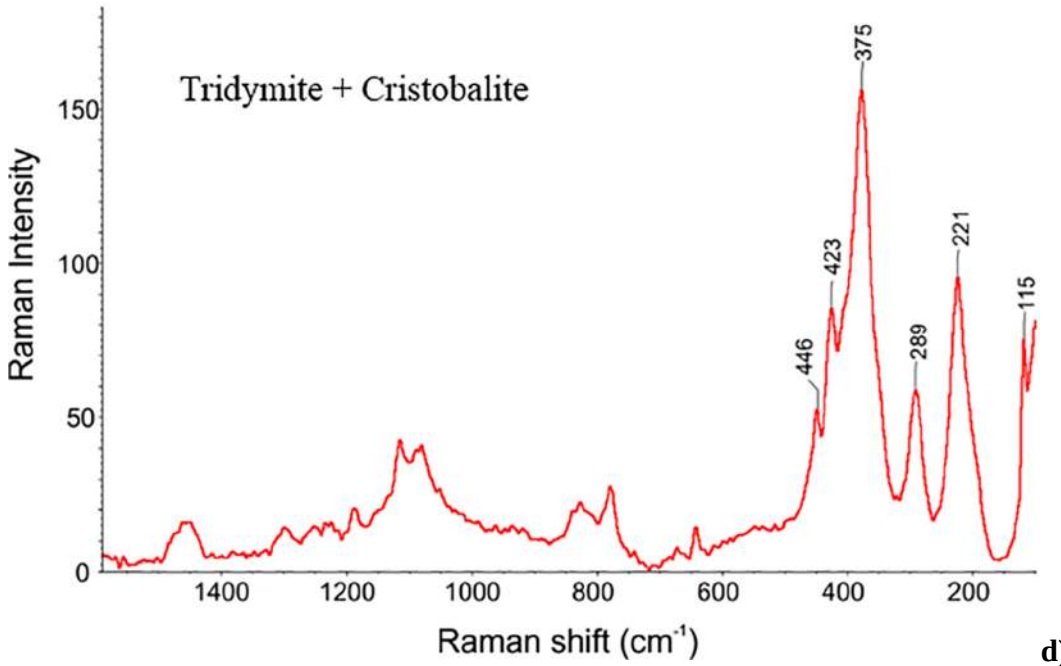

d)

Rod fragment

The rod fragment with semicircular section has a transparent body (VV-FBT) decorated with yellow (VV-FBGi), blue (VV-FBB) and white (VV-FBBi) spirals. The four glasses are all *natron* based, with levels of MgO and K_2O < 1 wt% (Fig. 5.3.1, empty triangles) and in line with Cl_2O (0.77÷1.46 wt%) and SO_3 (0.14÷0.43 wt%) contents.

MnO and FeO contents in samples VV-FBT, B and Bi range between 0.32 to 0.58 wt% and between 0.37 and 0.91 wt%, respectively.

The transparent yellow spiral, VV-FBGi, has a lower content of FeO (0.26 wt%) than the other 3 analyzed glasses, suggesting use of a purer sand or quartzite as source of silica. As there are no other coloring elements, the color may have been produced by an iron sulphide complex producing this shade in a reducing atmosphere (Jackson et al. 2006; Nenna et al. 1997; Schreurs and Brill 1984).

The blue spiral is colored by Fe (FeO = 0,91 wt%) probably in a bivalent oxidation state and presents also traces of Cu (CuO = 0,09 wt%).

The white glass is colored and opacified by finely dispersed Ca antimonates in the glass matrix (Sb_2O_3 in the glass phase = 8,86 wt%). The Ca-antimonate crystals (Fig. 5.3.8a, white

aggregates) have particularly small (1- 30 µm) irregular morphologies (Fig. 5.3.8b), apparently elongated and oriented like the bubbles. Micro Raman analysis on the Ca antimonates shows they are all composed by the orthorhombic phase, $Ca_2Sb_2O_7$.

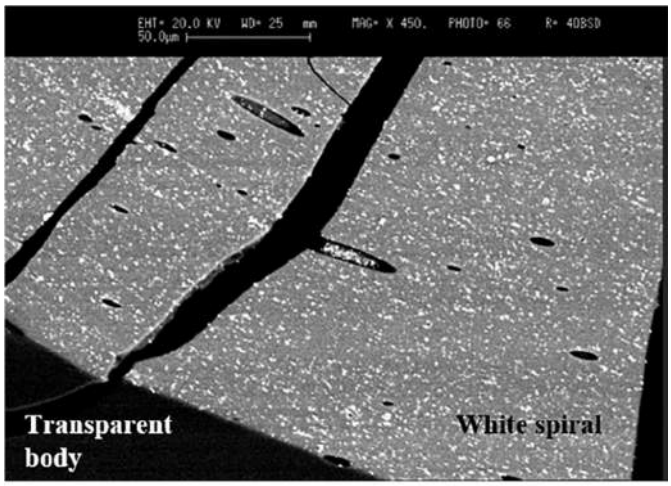

a)

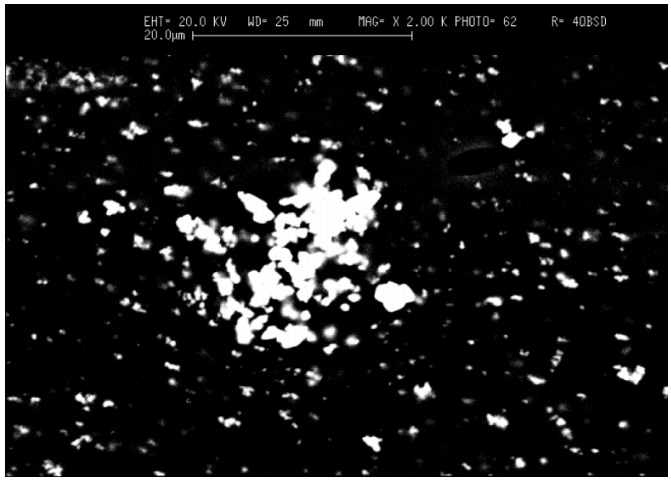

b)

Fig. 5.3.8: SEM-BSE images of rod sample VV-FBT-Gi-B-Bi. a) detail of white spiral VV-FBBi (with Ca antimonates, white aggregates) and transparent body VV-FBT. b) detail of a Ca antimonate aggregate.

Melon bead

The glass phase of the blue melon bead VV-MB is made up of K_2O = 2.45 wt%, MgO = 1.01 wt% and CaO = 3.56 wt%. The Na content is associated with *natron* as flux (Na_2O = 13 wt%), although levels of K and Mg are slightly high (Fig. 5.3.1a and b). However, as the last 2

elements partially derive from the particular type of sand used (see below), we can assume that the glass phase is a LMG type.

The high content of both alumina (Al_2O_3 = 3.29 wt%) and K suggest the sand used was rich in feldspar minerals with traces of heavy metals, as shown by FeO (0.77 wt%) and TiO_2 (0.16 wt%) (Freestone et al. 2002). The blue color is due to high concentrations of Cu (CuO = 3.78 wt%) associated to Sn (SnO_2 in the glass matrix = 0.11 wt%, Tab. 2), and dispersed cassiterite inclusions suggest that Cu could derive from bronze.

The heterogeneous texture is typical of a *faïence*, in which there are greater concentrations of crystalline inclusions (i.e., quartz, feldspar and metals) than glass matrix (Angelini et al. 2002). The melon bead of Villa di Villa does not preserve the glaze phase, except for a small weathered relict 120 µm thick (Fig. 5.3.9a). The glass phase in the core is well preserved and the texture is scarcely porous with bubbles up to 50 µm in diameter. The mineral grain sizes range between 30 and 150 µm, showing both round and rectangular shapes, so no accurate grinding and dimensional selection of the sand was carried out when producing the bead. SEM-EDS data show that the inclusions are mostly of SiO_2, possibly due to unreacted quartz crystals (Fig. 5.3.9b dark grey grains). Occasionally, also K-feldspars relicts (detail in Fig. 5.3.9b) are present.

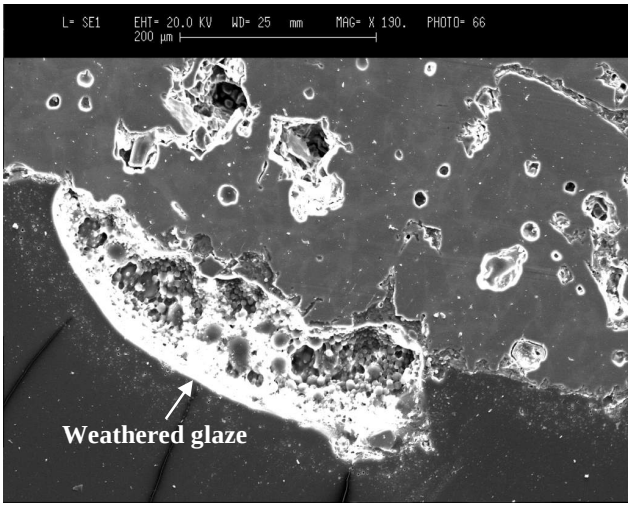

a)

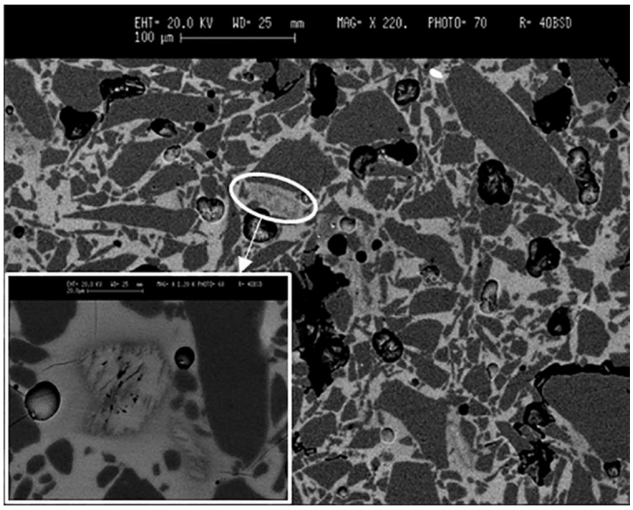

b)

Fig. 5.3.9: a) SEM-SE image of the melon bead that highlights the weathered glaze. b) SEM-BSE image of the melon bead with quartz inclusions (dark gray) and detail of a K-feldspar relict (dark gray in the white-bordered picture).

The micro Raman analyses on the K-feldspar crystals show a high compatibility with microcline (fig. 5.3.10).

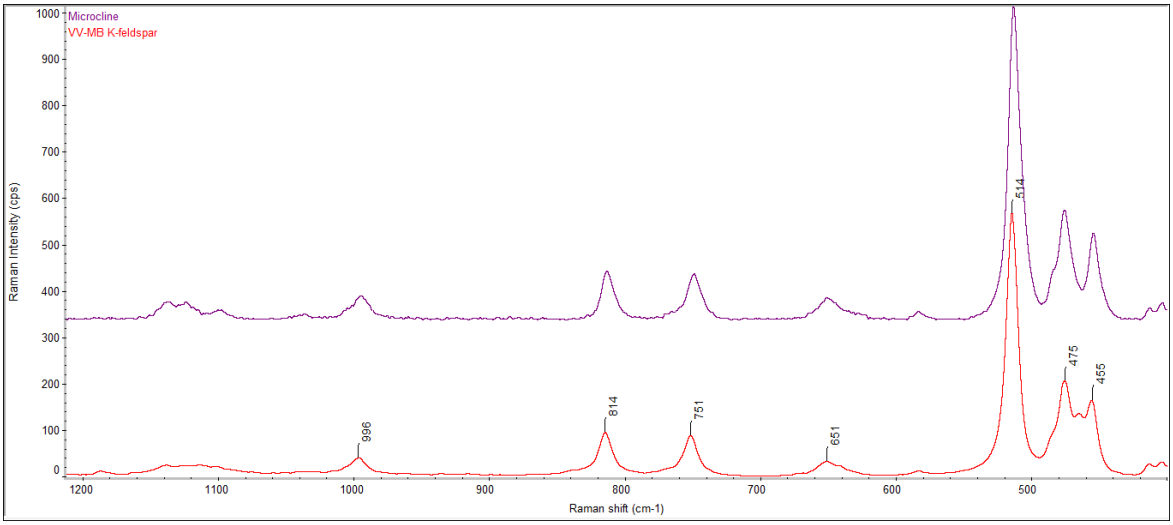

Fig. 5.3.10: Raman spectra of a K-feldspar inclusion in the sample VV-MB (red one) and of a standard microcline (violet one) from the RRUFF database.

Sample	Na_2O	MgO	Al_2O_3	SiO_2	P_2O_5	SO_3	Cl_2O	K_2O	CaO	TiO_2	MnO	FeO	CoO	NiO	CuO	ZnO	As_2O_3	SnO_2	Sb_2O_3	PbO	Total
VV-FBT	16.79	0.64	2.64	68.60	0.09	0.23	1.46	0.61	8.12	0.08	0.48	0.47	<d.l.	<d.l.	<d.l.	<d.l.	<d.l.	<d.l.	<d.l.	<d.l.	**100.29**
SD	0.45	0.04	0.15	0.42	0.05	0.04	0.05	0.07	0.08	0.01	0.03	0.03									
VV-GGi	12.15	0.32	1.82	65.48	<d.l.	0.07	1.23	0.37	5.74	0.07	<d.l.	0.73	<d.l.	<d.l.	<d.l.	<d.l.	<d.l.	<d.l.	1.05	10.71	**99.87**
SD	0.24	0.02	0.20	0.57		0.02	0.04	0.06	0.12	0.01		0.04							0.14	0.39	
VV-FBGi	17.79	0.58	2.53	68.37	0.07	0.14	1.35	0.75	8.45	0.06	<d.l.	0.26	<d.l.	<d.l.	<d.l.	<d.l.	<d.l.	<d.l.	<d.l.	<d.l.	**100.45**
SD	0.98	0.04	0.12	0.55	0.02	0.01	0.07	0.05	0.27	0.02		0.02									
VV-BRB2	13.85	0.92	2.41	70.44	0.19	0.05	0.92	1.84	7.92	0.08	0.49	0.60	0.11	<d.l.	0.24	<d.l.	<d.l.	<d.l.	<d.l.	<d.l.	**100.14**
SD	0.26	0.04	0.11	0.64	0.03	0.03	0.03	0.11	0.11	0.01	0.09	0.03	0.04		0.03						
VV-BRB5	13.63	0.94	2.38	70.66	0.19	0.05	0.93	1.80	7.85	0.07	0.79	0.70	0.10	<d.l.	0.20	<d.l.	<d.l.	<d.l.	0.06.	<d.l.	**100.44**
SD	0.25	0.04	0.08	0.41	0.04	0.02	0.01	0.12	0.09	0.01	0.11	0.06	0.03		0.04				0.03		
VV-BRB9	17.15	0.64	2.39	69.64	<d.l	0.24	1.15	0.54	6.60	0.06	0.41	0.80	0.16	<d.l.	0.20	<d.l.	<d.l.	<d.l.	<d.l.	<d.l.	**100.11**
SD	0.35	0.02	0.13	0.28		0.03	0.05	0.06	0.09	0.03	0.03	0.03	0.02		0.03						
VV-AB	17.43	0.52	1.78	69.67	<d.l.	0.19	1.73	0.33	7.04	0.07	<d.l.	1.01	0.04	<d.l.	0.12	<d.l.	<d.l.	<d.l.	<d.l.	<d.l.	**100.06**
SD	0.35	0.02	0.07	0.33		0.03	0.04	0.06	0.07	0.01		0.04	0.02		0.03						
VV-AB6	7.45	0.52	2.97	76.95	0.22	<d.l.	0.10	8.37	1.57	0.07	<d.l.	0.61	0.15	0.06	0.15	<d.l.	<d.l.	<d.l.	0.12	<d.l.	**99.43**
SD	0.29	0.04	0.13	0.44	0.06		0.02	0.25	0.04	0.02		0.05	0.03	0.02	0.04				0.03		
VV-FBB	18.60	0.60	2.62	66.01	0.11	0.22	1.38	0.66	8.19	0.06	0.58	0.91	<d.l.	<d.l.	0.09	<d.l.	<d.l.	<d.l.	<d.l.	<d.l.	**100.19**
SD	0.42	0.05	0.23	0.48	0.03	0.02	0.04	0.08	0.18	0.01	0.06	0.03			0.03						
VV-MB	12.59	1.01	3.29	70.91	0.07	0.06	0.99	2.45	3.56	0.16	<d.l.	0.77	<d.l.	<d.l.	3.78	<d.l.	<d.l.	0.11	<d.l.	<d.l.	**99.82**
SD	0.58	0.21	0.55	1.45	0.02	0.02	0.09	0.16	0.62	0.04		0.13			0.34			0.03			
VV-FBBi	14.23	0.66	2.38	61.70	0.10	0.43	0.77	0.51	8.41	<d.l.	0.32	0.37	<d.l.	<d.l.	<d.l.	<d.l.	0.11	<d.l.	8.86	<d.l.7	**99.08**
SD	0.76	0.02	0.05	0.96	0.01	0.06	0.04	0.03	0.24	0.02	0.02	0.03	0.01	0.02	0.00	0.03	0.09	0.02	0.32	0.06	

Table 5.3.1: EPMA chemical analyses (oxides wt%) of the glass phase in the finds of Villa di Villa site. The labels are the same as reported in Table 3.2.5, and are calculated as a mean of 5÷10 point analysis (d.l.= detection limit; SD = standard deviation).

CHAPTER 6

DISCUSSION

6.1 Lipari and Salina

In the discussion of the analytical data the different provenances, ages and typologies of the beads were considered; however, except for the type of flux used, the major chemical differences are related to the nature of the glass: color and opacity/transparency. Moreover, most of the beads have a simple typology (Tabb. 1-3 par. 3.1) and specific typological comparisons are not always possible. Therefore, after some general compositional consideration, the results will be presented and discussed for material colors.

The chemical composition of the analyzed glasses (par. 5.1, tab. 1) allows their classification as silica glasses produced with two main different fluxes: soda – rich ashes and mixed – alkali ashes plus a subclass of glass (two samples) produced with K plant ashes (composition close to LMHK glass except for the Na-K contents). Samples LC21M (Middle Bronze Age 1-2) and LOIIIG (Recent Bronze Age) from Lipari Acropolis, all samples from Salina – Villaggio di Portella (Middle Bronze Age 3) and fourteen samples from Lipari Acropolis and grave 31 of Piazza Monfalcone cemetery (Final Bronze Age 1-2 and 2-3) are HMG glasses produced using soda-rich plant ashes as flux. Most of them are blue and only four are yellow/brown colored. They have mostly simple typologies (annular, globular or fragments), two are cylindrical beads with spiral decorations and one is globular with a spiral decoration. The first HMG glasses appeared in the 19th century B.C. in the Near East (at Deir 'Ain 'Abata, Jordan, and Tel Dan, Israel) and since the 16th-14th centuries B.C. also in Egypt and in the Eastern Mediterranean (Henderson 1989, 2000; Tite et al. 2003). The soda-rich source used in these glasses comes from halophytic ashes (Henderson 2000; Towle et al. 2001; Gratuze and Billaud 2003) obtained from burning plants, mainly of the *Salicornia* and *Salsola* species, growing in salty lacustrine environments and desert areas (Henderson 1985, 2000). Today, these species occur in Iraq, Iran, Syria and Egypt (Henderson 1985, 2000, 2006) but also in Western Europe and Greece (Tite et al. 2006). The presence of HMG glasses in Italy is attested since the Middle

Bronze Age 1-2 in Central and Southern Italy (Angelini et al. 2003, 2005; Bellintani et al. 2006), generally colored by copper. In the same period in Northern Italy there were only *glassy faïence* with a special local typology (conical buttons) and LMHK glass phase composition. Some *glassy faïence* conical buttons were also found in Central Italy (Angelini et al. 2005) but with a different Na/K ratio than in the Northern Italy ones. The particular typology, not found in Southern Italy, and the LMHK composition, suggest a local production for the *glassy faïence* conical buttons. The HMG glasses, present in this phase only in Central and South Italy, were probably traded from the Near East or Egypt, as well as the only HMG samples from Lipari dated to the MBA 1-2, even if presents a transparent yellow/brown color not detected in the coeval Southern Italian objects. During the MBA 3 – RBA the local production of LMHK *glassy faïence* stopped and only HMG vitreous materials, widespread in the entire Italian peninsula and in Sardinia, were present (Angelini et al. 2002, 2005, 2012; Bellintani et al. 2006). The objects were both glasses and mostly glassy faience beads of Eastern provenances (Mycenaean area), included the first Italian Co-colored glassy faience (Angelini et al. 2005; Santopadre and Verità 2000) similar to the blue colored Aegean beads (Tite et al. 2005; Angelini et al. 2005). In this line, the HMG glasses of MBA3 from Salina were considered of Near Eastern/Egypt or Aegean origin. HMG glasses have not been attested in the Italian peninsula during the Final Bronze Age and the HMG glasses from Lipari dated to that period may be the first evidence, together with a few samples from Sardinia (Angelini et al. 2012). Both at Lipari and Salina HMBG glasses are not attested, i.e. HMG brown glasses having a unique composition and texture and considered a Northern Italy local production (Angelini et al. 2005; Artioli et al. 2008).

Thirteen samples from graves 31 and 18 of Lipari - Piazza Monfalcone cemetery (Final Bronze Age 1-2 and 2-3) are LMHK glasses obtained using mixed-alkali plant ashes. They are all blue colored with different shades; the typologies are mostly simple annular (large or small size) together with several fragments and other typologies (globular, barrel, cylindrical, horned eyes, trunk-conic) sometimes with white eyes or spirals decorations. This composition is exclusively typical of the central European productions of the Final Bronze Age (Brill 1992; Henderson 1988, 1993; Gratuze et al. 1998; Santopadre et al. 2000; Towle et al. 2001; Bellintani et al. 2006; Angelini et al. 2002, 2004, 2005, 2010; Angelini 2009, 2011; Artioli e Angelini 2013).

Interestingly, the only known working/production centers of the period were all in the Veneto region and, among these, Frattesina (Rovigo) is surely the most important and best known one (Angelini et al. 2004, 2010a; Brill 1992; Henderson 1988; Santopadre and Verità 2000; Towle et al. 2001). Other working/production centers are located in Mariconda di Melara (Rovigo), Montagnana (Padova), Caorle (Venezia) and Fondo Paviani (Verona) (Angelini et al. 2010a and b). LMHK glasses, largely diffused in Northern Italy, start to be massively produced and they have been found also in several Italian sites located in Emilia Romagna, Trentino Alto Adige, Lombardy, Piedmont and central Italy (Angelini et al. 2002, 2004, 2010b, 2006, 2007, 2009; Tecchiati et al. 2006). LMHK glasses were occasionally found in several Early Iron Age beads dated to the 9th c. B.C. from Lombardy (Angelini et al. 2011) and in Villanovian beads of the 8th century B.C. from Bologna (Arletti et al. 2010). The source of alkali used for their production has long been discussed (Henderson 1988; Biavati and Verità 1989; Brill 1992; Santopadre et al. 2000); at present, on the basis of the analysis of different plants ashes species, the most widespread hypothesis is the use of leached mixed-alkali plants ashes (Brill 1992; Tite et al. 2006; Santopadre and Verità 2000).
Interestingly, the other two glasses from Lipari – Piazza Monfalcone cemetery dated to the FBA 1-2, are similar to the LMHK glasses but have different Na and K contents and are produced using plant ashes rich in K. This glass type has been identified also as a subgroup in the Frattesina productions (Angelini et al. 2010) and has been named here LMHK- K class.
The presence of the LMHK glasses in the Lipari samples, is particularly interesting because it testifies a circulation of the vitreous productions from north to south Italy.

Blue glasses

The blue beads are colored by Cu or Co and Cu, except for samples SALFFR3 and SALCFR4B whose color is probably due to Fe^{2+} ions. The glasses dated to the Middle Bronze Age are all HMG glasses, while those dated to the Final Bronze Age have both LMHK and HMG composition.

HMG glasses colored by Co are all dated to the Middle Bronze Age 3 and come from Salina. The main recipes of these glasses are in line with the coeval Italian production, even though

Italian HMG blue glasses are colored by copper while cobalt has been attested only in the Sardinia samples (Angelini et al. 2012). The coloring is due to cobalt and copper ranging from 0.05 to 0.3 wt% (CoO) and from 0.09 to 0.35 wt% (CuO), respectively. The chemical composition is variable, but the alkali content is characteristic of the soda-rich glasses (Na = 17÷19.41 wt%, K = 2.23÷3.58 wt%, Mg = 8.20 ÷4.89 wt%, Ca = 4.68÷8.82 wt%) and comparable with both the coeval Italian and Near East/Egyptian productions (Angelini et. al 2002, 2005, 2012; Brill 1999; Nikita et al. 2006; Shortland and Eremin 2006; Tite et al. 2008a; Walton et al. 2009). However, samples SALFAS and SALCFR1 show significantly lower Ca (CaO = 4.78 and 4.68 wt%, respectively) and Mg (MgO = 4.91 and 4.89 wt%, respectively) contents, probably related to minor concentrations of this two elements in the plant ashes used as flux and/or in the sand. These two samples have a particularly high content of Al and Fe, the last element also related to the coloring agent (see below). All the other samples have low Al and Fe contents that testify the use of sand as source of silica. The minor and trace elements are related to the coloring agent and are variable depending on the different cobalt source. Four samples (SALFA1, A2, A3 and A4) have traces of Sb (Sb_2O_3 = 0.04÷0.20) and two of them also of Pb (PbO = 0.12 ca.). The occurrence of antimony in the glass matrix is consistent with the presence in the glass phase of Cu-Sb inclusions enriched of Ni and As traces (fig. 10d, Ch. 5). Similar elements associated to Co are present in *faïence* from central Italy dated to the MBA 3-RBA (Santopadre et al. 2000; Angelini et al. 2005) and in a few Mycenaean *faïence / glassy faïence* from Crete and Psara dated to the 1400 B.C. ca. (Tite et al. 2008a). However, in the mentioned vitreous materials the amounts of Co, Cu, Sb and Pb are significantly higher (CoO = 0.83÷1.60 wt%; CuO = 1.60÷2.70 wt%; Sb_2O_3 = 0.75÷1.20 wt%; PbO = 2.15÷2.82 wt%) than in Salina glasses. Therefore, the elements association seems to suggest the same type of cobalt source even though the elements ratios are not the same and may be due to different concentration of the elements in the same cobalt source or to the use of different cobalt sources. The SEM study highlights in some samples the presence of numerous diopside ($CaMgSi_2O_6$) inclusions with angular and/or dendritic morphology (fig. 9b-c, Ch. 5) dispersed in the glass matrix. From the crystal morphology shown in the figures, there is no doubt that a crystallization process took place during the cooling of the material from the melt, in presence of high Ca and Mg amounts that is typical in the HMG glasses (Artioli et al. 2008). Moreover, other newly formed crystals occur in presence of high levels of Ca, such as elongated crystals

of Ca antimonates (hexagonal habit, $CaSb_2O_6$) in sample SALFA1, according to the Sb observed in the glass phase.
It also presents compositional bands with a higher content of Cu (CuO up to 0.57 wt%) with respect to the Cu mean value in the glassy matrix (CuO up to 0.12 wt%). This suggests that the colorless glass bead was produced first and secondarily the coloring agent was added, which did not blend perfectly into the glass mixture creating the different compositional bands.

Two samples (SALFAS and SALCFR1) show different trace elements associated to Co. In particular, they present Ni, Zn together with Fe and high contents of Al and Mn that are typical of the cobaltiferous alum salts, sulphates of Al-Mg-Mn containing Ni and Zn, found in the Kharga and Dakhla Oasis in the Western Desert in Egypt (Tite et al. 2008b). This is considered the main coloring agent in the cobalt blue glasses during the 18th Egyptian Dynasty (Shortland 2000; Shortland et al. 2000; Reheren 2001; Tite et al. 2008b). The same colorant was found in several ingots from Uluburun (Brill 1999; Jackson et al. 2010) and in some vitreous material from the Eastern Mediterranean (Nikita et al. 2006; Bouquillon et al. 2007; Tite et al. 2008a).

Three HMG samples from Salina, similarly dated to the MBA 3, have a different coloring technology. Samples SALFFR and SALCFR3 have very low Cu (CuO = 0.18 and 0.06 wt%, respectively) and especially low Co contents (Co ≤ d.l.), while SALCFR4B have both elements under the detection limits. In sample SALCFR4B the color is probably due to Fe possibly present in its reduced oxidation state; Fe amount is low (FeO ~ 0.60 wt%) and therefore involuntarily added through the sand used as a raw material, according to the high level of Al (Al_2O_3 = 2.10 wt%).
Instead, sample SALFFR has the same mean level of Fe, but has a low level of Al (Al_2O_3 = 0.8 wt%) and shows a heterogeneous texture due to zones with higher levels of copper (up to 0.34 wt%) and zones with copper under the detection limits. As in sample SALFA1, it seems that the coloring agent was added in a later stage to the colorless glass bead. Moreover, in the glass phase there are rare inclusions of Cu-Pb-Sb-S, related to the use of metal sulphides as source of colorant. Occasionally it presents devrification phases (e.g., combeite, devitrite) that normally occur in silica-soda-lime glasses at temperatures between 750 to 1200°C (Morey 1930; Simmons et al. 1981) and observed in early Egyptian glasses, too (Lahlil et al. 2010a).

SALCFR3 has the same Al level of sample SALFFR but a higher Fe amount intentionally added to the glass (FeO = 3.25 wt%) that caused the blue coloring, probably due to its reduced state. The combined activity of Mg, Ca, and Fe elements in this sample produced the nucleation and growth of dendritic pyroxene crystals from the melt, with the simultaneous presence of diopside and augite; the relative abundance of the two phases depends on the substitution that occurs in the pyroxene structure. The high contents of Fe are related to the presence of metal inclusions as coloring agent, as attested by the presence of Cu-Fe-S inclusions enriched in Pb, Ni and Sb.

In contrast with the Salina samples, the HMG glasses of the FBA from Lipari are colored exclusively by copper. The presence of HMG glasses in the Final Bronze Age is a new evidence; in fact, soda-rich glasses are not present in the Italian peninsula during this phase, while they are widespread in the coeval New Eastern/Egyptian productions (Henderson 1989, 2000; Tite et al. 2003). They are very similar in their alkali contents and in line with the typical HMG compositions (Na = 15.30÷20 wt%, K = 2÷3.60 wt%, Mg = 5.75÷8 wt%, Ca = 4.52÷9.54 wt%). They are colored by low contents of Cu (0.85÷0.58 wt%) with no other element associated to copper, making it difficult to identify the coloring source. However, in one sample a Cu drop was found, which may suggest the use of metallic copper as a coloring source. They have a homogeneous texture except for two glasses characterized by a few diopside and Ca-Na crystals as seen for HMG glasses from Salina. At the same time, one sample (L311SPA) presents differences in the chemical distribution of copper in the glass matrix, due to the coloring technique.

The blue LMHK glasses from Lipari are all dated to the Final Bronze Age, consistently with the glass production of the period in the Italian peninsula and in Central Europe. Most of them are Cu-colored with high contents of Cu (CuO = 2.8 ÷5 wt%), while thirteen are colored by Co (CoO = 0.07÷0.25 wt%) and Cu (CuO = 0.3÷2 wt%). Both Cu- and Co-colored glasses have similar monovalent (Na and K) and bivalent (Ca and Mg) alkali contents.
The K_2O *vs* MgO diagram (Fig. 6.1a), used to characterize the different compositional glass classes, highlights that the Lipari glasses have values of K (K_2O = 6.12÷12.38 wt%) and Mg (MgO = 0.47÷1.30 wt%) characteristic of mixed alkali glasses. This is true also when

comparing, in the same diagram, the Lipari glasses with coeval data from the literature of blue glass beads from north-eastern Italy (Angelini et al. 2004, 2010a; Brill 1999; Santopadre and Verità 2000; Towle et al. 2001) and Central Europe, in particular Switzerland (Henderson 1993), France (Croutsch et al. 2011; Gratuze et al. 1998; Séguier et al. 2010) and Bohemia (Venclová et al. 2011). All samples show similar K and Mg amounts, except for some glasses with higher Mg levels, and testify the use of the same alkali source. This is confirmed also considering the Na_2O/K_2O ratio that ranges from 0.36 to 1.35 in Lipari glasses, as well as in the north-eastern and central European glasses in which it varies from 0.35 to 1.47 (fig. 6.1b). Na and K are strongly negative correlated, suggesting the same provenance for the two elements (the alkali source). However, two Lipari samples (L312AA2 and L18AA1) have a particularly low Na_2O/K_2O ratio (0.04 and 0.18, respectively), indicating a K-rich source of alkali as flux. These characteristics were also found in one crucible, one annular bead and one vessel from Frattesina (Rovigo) and in one annular bead from Narde (Rovigo) (Angelini et al. 2010a; Towle et al. 2001); in the European glasses there seems to be no use of K-rich flux, except for one fusiform Cu-colored bead with a white spirals decoration from Bohemia (empty star, fig. 6.1b) (Venclová et al. 2011). The blue annular bead L312AA2 is more similar to two of the glasses from Frattesina (Na_2O/K_2O = 0.05 and 0.07, Towle et al. 2001), while sample L18AA1 is similar to the other samples from Frattesina, Narde and Bohemia (Na_2O/K_2O = 0.11÷0.12, Angelini et al. 2010a; Towle et al. 2001; Venclová et al. 2011). The presence at Lipari – Piazza Monfalcone cemetery of the K class subgroup associated to other LMHK glasses (same graves and necklace), suggests that the two types probably travelled together and, therefore, that the LMHK – K class was typical of the Frattesina or more generally of the north Italian vitreous productions.

Comparing Al and Fe values (fig. 6.2a), it is evident that Al contents are quite high in all samples (Al_2O_3 = 1÷2.50 wt%) and probably related to the feldspar minerals present in the sand (source of silica), while Fe contents are variable. In the Cu-colored samples Fe is low (FeO = 0.37÷0.68 wt%) and due to impurity imported by the sand; moreover, with respect to the Al and Fe contents, the Cu-colored glasses are closer together than the Co-colored glasses, indicating similar values of the two elements (fig. 6.2a dotted line). Conversely, in the Co-colored samples the iron content is higher (FeO = 0.73÷1.25 wt%) and its concentration is not

only related to the sand but possibly also to other raw materials, as the coloring agent source. This is in line with literature data, too, where Co-colored glasses present higher amounts of Fe with respect to the Cu-colored ones. In particular, similar high levels of Fe are attested in cobalt blue beads from Mariconda, Narde and Frattesina (Rovigo) (Angelini et al. 2010a; Brill 1992; Towle et al. 2001) and also in two beads from Eirstein (France) (Croutsch et al. 2011) and in one barrel bead from Hauterive-Champréveyre (Switzerland) (Henderson 1993). The difference between the two material classes (Co- and Cu-colored glasses) is more evident when considering the trace elements associated to the coloring source.

Most of the Lipari samples are Cu-colored with high copper concentrations (CuO = 2.8 ÷5 wt%) as in the considered samples from north-eastern Italy (Angelini et al. 2004, 2010a; Brill 1999; Santopadre et al. 2000; Towle et al. 2001) and central Europe (Croutsch et al. 2011; Gratuze et al. 1998; Henderson 1993; Séguier et al. 2010; Venclová et al. 2011). In all the analyzed samples there are low levels of Sb (Sb_2O_3 = 0.04÷0.14 wt%) and both of Sb and Sn in half of them (Sn_2O = 0.04÷ 0.35 wt%). The presence of Sn could be related to the use of bronze slags as a source of Cu, as testified in one sample (L311AA2) by the presence of Sn oxides inclusions (fig. 6f, Ch. 5), as in some samples from Frattesina (Santopadre et al. 2000, Angelini et al. 2004) and Narde (Angelini et al. 2010). Considering the literature data, generally Cu is related to Sn but rarely to Sb only or to both Sn and Sb. In particular, copper is associated to Sn (Sn_2O = 0.07 ÷ 0.90 wt%) in the glasses from Le Theil, Sein-et-Marne and Eirstein (France) (Croutsch et al. 2011; Gratuzeet al. 1998; Séguier et al. 2010) and from Frattesina (Rovigo) (Angelini et al. 2004, 2010a; Brill 1999; Santopadre et al. 2000; Towle et al. 2001). In the samples from Narde (Rovigo) (Angelini et al. 2010) and Hauterive-Champréveyre (Switzerland) (Henderson 1993) Cu is related in some cases exclusively to Sn and in fewer cases to both Sn and Sb. Considering both Sb and Sn in the Cu-colored samples (fig. 6.3) we clearly distinguish the glasses from Lipari containing both Sb and Sn from those containing only Sb (with Sn under the detection limit). Interestingly, in the Cu-colored glasses from Lipari, copper is never related only to Sn as occurs in the other coeval glasses instead. The presence of both Sn and Sb is attested only in some samples from Narde (Rovigo) (Angelini et al. 2010a) and in one sample from Hauterive-Champréveyre (Switzerland) (Henderson 1993) while copper related exclusively to Sb is present in a few beads from Mariconda and Narde (Rovigo) (dotted circle in fig. 6.3).

Therefore it seems that the Cu-colored Lipari samples probably have two different copper sources: in one case Cu-Sb ores and in the other case Cu-Sn-Sb- ores or metal scraps containing these elements.

In the Co-Cu colored LMHK glasses from Lipari traces of Ni together with As and Sb were found. Nickel is correlated, even if not systematically, to Co (fig. 6.4a) as in some glasses from Frattesina, Narde, Mariconda (Rovigo) (Angelini et al. 2004, 2010a; Brill 1999; Santopadre et al. 2000; Towle et al. 2001), Switzerland (Henderson 1993) and France (Croutsch et al. 2011; Gratuze et al. 1998; Séguier et al. 2010). Considering Co *vs* Sb_2O_3, the situation is variable. Some Lipari glasses have a higher concentration of Sb (Sb_2O_3 = 0.38÷0.6 wt%) rarely found in coeval glasses, except for one glass from Bohemia (dotted circle fig. 6.4b) (Venclová et al. 2011). The other samples have a lower Sb content (Sb_2O_3 = 0.1÷0.2 wt%) as samples from Marconda, Narde (Rovigo) (Angelini et al. 2010a; Towle et al. 2001) and Switzerland (Henderson 1993).
Essentially, in the coeval cobalt blue samples from north-eastern Italy and central Europe considered, Co is always associated to Cu and Ni but not systematically to As and Sb. Concerning the Lipari samples, the cobalt source seems to contain a Cu-As-Ni-Sb ores that is difficult to identify. Samples L314AN1-AN2-CO1 also show significant Zn traces while only sample L18DA has no As but Pb, suggesting a different Co source or possibly a variability in the composition of the same Co source.

Beyond the chemical differences linked to the different coloring sources, both Cu and Co LMHK glasses show numerous crystals of tridymite, often grouped in large aggregates. In all the analyzed glasses, tridymite is the only phase identified both in the elongated crystals and in the rectangular ones (often grouped in large aggregates). The tridymite ↔ quartz transition starts around 870°C and is stable between 870 and 1470°C (Stevens et al. 1997).
In the Lipari glasses the presence of tridymite as a unique phase testifies that all the quartz reacted into tridymite and the lamellar morphology of the crystals indicates crystallization from the melt at high temperature (Artioli et al. 2008). During the cooling a volume contraction

occurred, producing circular cracks around the crystals. However the fractures are present only around the large aggregates and not on the lamellar crystals.

The coloring techniques seem to be characterized first by the production of the colorless glass and then by adding the coloring agent, which sometimes did not mix well, causing the formation of bands with different amounts of copper, as observed at the SEM. This has been verified both for Co- and Cu-colored HMG and LMHK glasses.

No white beads are present in the finds from the Aeolian Islands and white glass is used only for the bead decorations.
The white glasses analyzed in this study belong to some decorations of blue beads. One glass is dated to the Middle Bronze Age 3, while the other eight white samples are dated to the Final Bronze Age.
The MBA3 glass is a HMG glass and comes from Salina – Villaggio di Portella and is part of a blue fragment (SALCFR4B). As the blue body, the white decoration is characterized by higher levels of Al (Al_2O_3 = 2.10 wt%) with respect to the other blue HMG blue glasses from Salina. The glass phase also has high amounts of Sb (Sb_2O_3 = 2.86 wt%), which is consistent with the presence of numerous small (a few µm) Ca antimonate crystals, finely dispersed in the matrix. The use of Ca antimonates as coloring /opacifier agent is not attested in Italy during the Middle Bronze Age 3, while it is known in the same period in the Egyptian glass productions (Shortland 2002). Small particles (~5 µm) of calcium antimonate within the glass were also found in some HMG white glasses from Malkata (near Thebes) and Amarna in Middle Egypt, dated to the 18th Dynasty, 1570–1292 B.C. (Shortland 2002). The Ca antimonate in these glasses is in the orthorhombic phase, $Ca_2Sb_2O_7$, like in those from Salina, with similar Sb contents in the glass phase (Sb_2O_3 = 2.50 wt%). Some differences occur in the Al content, which is higher in the Salina glass (Al_2O_3 = 3.10 wt%) with respect to the Egyptian ones (Al_2O_3 = 0.8 wt%). In the glasses from Malkata and Amarna the glass matrix of the calcium antimonate glasses is on average lower in lime than its calcium antimonate-free counterpart. This implies that antimony (or a simple antimony compound, such as an oxide or sulphide) was added to the glass batch or to the raw glass to generate the color. Consequently, the lower values of lime in the glass phase probably result from the calcium antimonate crystals forming as the glass

cools and drawing lime out of the glass matrix (*in situ* crystallization). This aspect does not occur in the Salina glass; in fact, the white glass has a higher amount of lime (CaO = 6.98 wt%) with respect to the blue body (CaO = 5.37 wt%). Moreover, also considering the other translucent blue glasses form Salina, the Ca content is variable, in some cases it is lower and in others it is higher than in the calcium antimonate white glass. Nevertheless, for Egyptian glasses recent studies seem to support an *extra situ* crystallization and an intentional addition of the synthesized $Ca_2Sb_2O_7$ crystals to translucent glass (Lahlil et al. 2010a). Indeed, the experimental study highlights that in the *in situ* crystallization the nucleation of the crystals occurs randomly or at preferential nucleation sites in the vitreous matrix, producing isolated crystals or crystals around bubbles. The very compact and widespread crystals observed in the Salina glass, are not compatible with *in situ* crystallization. Moreover, it was proved that $Ca_2Sb_2O_7$ is thermodynamically stable and grows at the expense of $CaSb_2O_6$, which is kinetically favored. Consequently, the *in situ* process implies that when $Ca_2Sb_2O_7$ is the major phase obtained, crystals are not nano-metric, as they are in the Salina glass instead. The hypothesis of the *extra situ* crystallization is also compatible with the higher amounts of Ca in the white glass with respect to the blue body, since the calcium is also introduced by the opacifier and not only by the sand.

The technology used to obtain the white LMHK glasses form Lipari is completely different. They all have similar contents of Na, K and Mg comparable with the other glass colors and in line with the mixed alkali glasses composition. Indeed, based on the calcium contents and on the types of inclusions present, it is possible to distinguish two different technologies that were identified also in coeval northern Italian LMHK glasses (Angelini et al. 2010a). Actually, in the first one the opacity is produced by abundant SiO_2 inclusions identified as tridymite. The glass phase in these samples is unfortunately weathered, but in the only two samples preserved the amount of SiO_2 in the amorphous phase is about 75 wt%. Most of the white glasses analyzed were opacified in this way.

In the second one, the opacity is produced by the presence of Ca silicates dispersed in the matrix. The Lipari glasses opacified with this technology are characterized by higher amounts of Ca (CaO = 8÷12 wt%) in the glass phase than the other glasses (CaO = 1.63÷1.92 wt%), and by lower Si contents (SiO_2 ~ 70 wt%). This suggests that calcium was intentionally added

to the glass batch and the nucleation of the Ca silicates occurred during the glass cooling. The Ca silicates are made of wollastonite ($CaSiO_3$) even though some differences are present inside this group. Sample L31CB2B is characterized by wollastonite inclusions with irregular shapes, finely dispersed, and with a few tridymite and quartz inclusions. Instead, samples L31CGB and L31CB1B are characterized only by wollastonite with euhedral morphology and the inclusions seem more isolated. Interestingly, all the white decorations belong to Cu-colored blue beads, but those opacified by SiO_2 inclusions are applied to beads with eyes decorations, while those opacified by wollastonite inclusions are associated to globular or barrel beads with spiral decorations. It may be possible that the two different technologies were used for specific typologies, but the analyzed white glasses of the Final Bronze Age are still scarce and do not give significant information about the texture. The only data available are those from Narde, Rovigo (Angelini et al. 2010) where two white decorations glasses were analyzed. The study highlights the presence of both technologies in the glasses from Lipari, even though in the glasses from Narde the use of a specific technology seems to be more related to the color of the bead body (Co- or Cu-colored) than to its typology.

Among the analyzed glasses there are four transparent yellow/brown glasses and one black sample, all with HMG compositions.

The yellow samples Lβ5AG and LC21M come from the Lipari Acropolis and are dated to the Final Bronze Age 2-3 and to the Middle Bronze Age 1-2, respectively. Samples L31CCR and L311GM1 are from grave 31 of the Piazza Monfalcone cemetery and are dated to the Final Bronze Age 1-2. They all have comparable alkali contents and low amounts of Fe and Al suggesting the use of a pure sand. As there are no other coloring elements, the color may have been produced by an iron sulphide complex producing this shade in a reducing atmosphere (Jackson et al. 2006; Nenna et al. 1997). The Fe contents ranges from 0.22 and 0.36 wt% in the yellow shades (Lβ5AG, LC21M, L31CCR) and is 0.57 wt% in the transparent brown one (L311GM1). The latter presents also manganese (MnO = 0.83 wt%).

Coeval transparent yellow/brown beads in the Italian peninsula are scarcely present. The only transparent HMG yellow bead dated to the MBA3-RBA is from Sardinia (Angelini et al. 2012) even though the contents of Al and Fe is lower than in those from Lipari. During the MBA3-RBA in north-central Italy particular brown glasses were produced (HMBG glasses) but with

a completely different composition, characterized by high levels of Al, Fe and K and with numerous inclusions of augite, diopside and copper sulphides (Angelini et al. 2005; Artioli et al. 2008; Angelini 2011). Instead, the Lipari glasses have a very similar composition to that of some Egyptian samples, where the production of transparent yellow/brown glasses is well attested (Shortland et al. 2006).

Concerning the Final Bronze Age in Italy, the production of transparent yellow/brown glasses is not attested, except for some amber glasses from Sardinia dated to the RBA-EIA, but having LMG compositions (Angelini et al. 2012).

The only black HMG glass is from grave 31 of the Piazza Monfalcone cemetery and is very similar to the transparent/brown glasses for the composition of the main elements. It only presents high contents of Fe (FeO = 0.73 wt%), S (SO_3 = 0.60 wt%) and Al (Al_2O_3 = 1.30%). The dark coloring and opacity are probably due also to Cu-Fe sulfides enriched of Ni, rarely found in the glass matrix. Similar black beads are not attested in the coeval literature; dark blue beads are also present but colored by Co and sometimes traces of Cu. The first black glasses in Italy are attested in some Early Iron Age beads from Bologna, but have an LMG composition (Polla et al. 2011).

Fig. 6.1. a) MgO *vs* K_2O and b) Na_2O *vs* K_2O contents of the glass phase in the analyzed blue samples (pink) of the FBA from Lipari in comparison with coeval literature data (black and gray). Grey and black symbols = provenances of the literature data; empty symbols = Cu blue beads; full symbols = Co blue beads (References: [1] Towle et al. 2001; [2] Angelini et al. 2010; [3] Angelini et al. 2004; [4] Brill 1992; [5] Santopadre et al. 2000; [6] Henderson 1993; [7] Croutsch et al. 2011; [8] Gratuze et al. 1998; [9] Séguier et al. 2010; [10] Venclová et al. 2011).

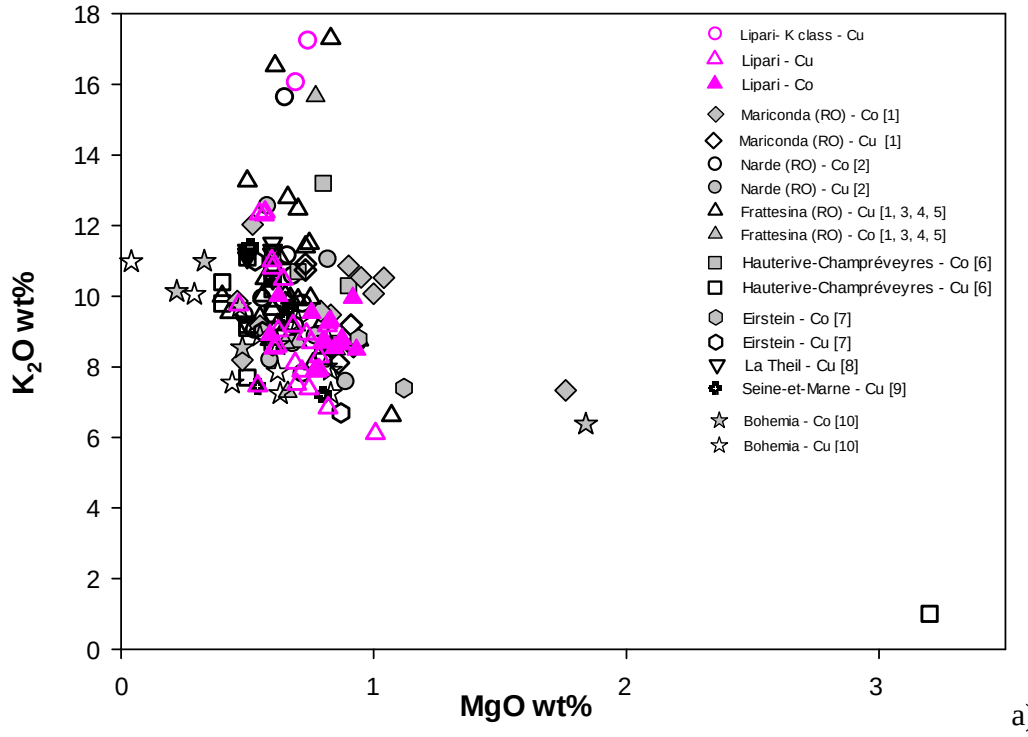
Lipari- K class - Cu
Lipari - Cu
Lipari - Co
Mariconda (RO) - Co [1]
Mariconda (RO) - Cu [1]
Narde (RO) - Co [2]
Narde (RO) - Cu [2]
Frattesina (RO) - Cu [1, 3, 4, 5]
Frattesina (RO) - Co [1, 3, 4, 5]
Hauterive-Champréveyres - Co [6]
Hauterive-Champréveyres - Cu [6]
Eirstein - Co [7]
Eirstein - Cu [7]
La Theil - Cu [8]
Seine-et-Marne - Cu [9]
Bohemia - Co [10]
Bohemia - Cu [10]
K2O wt%
MgO wt%
0
1
2
3
0
2
4
6
8
10
12
14
16
18

a)

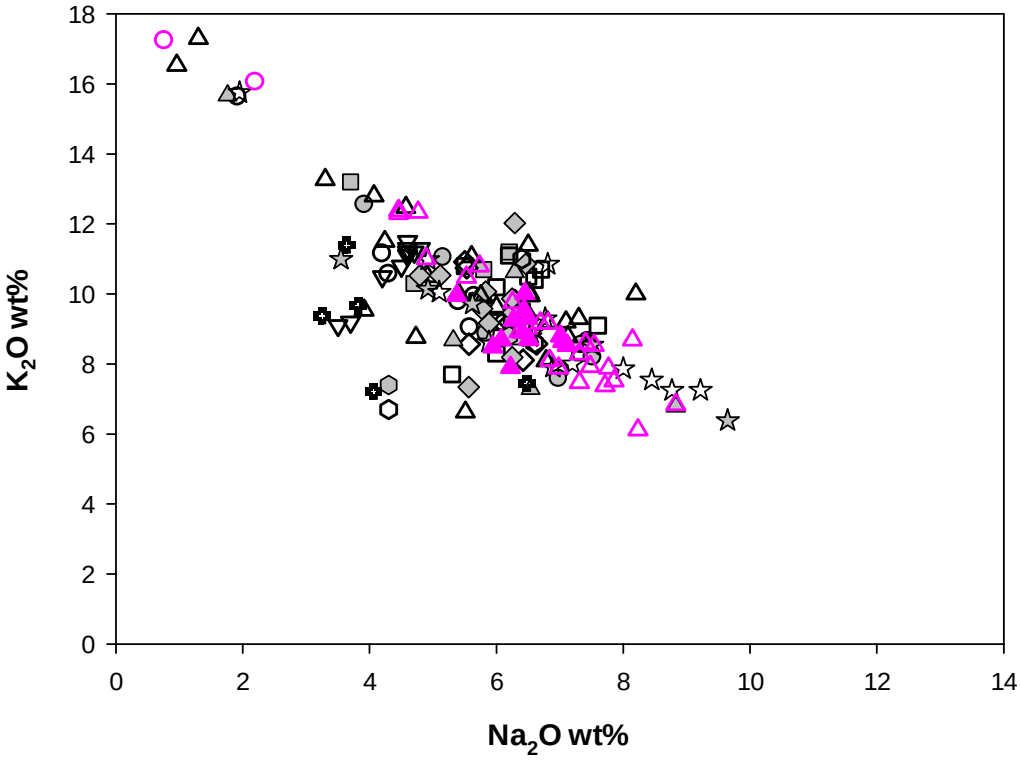
K2O wt%
Na2O wt%
0
2
4
6
8
10
12
14
16
18

b)

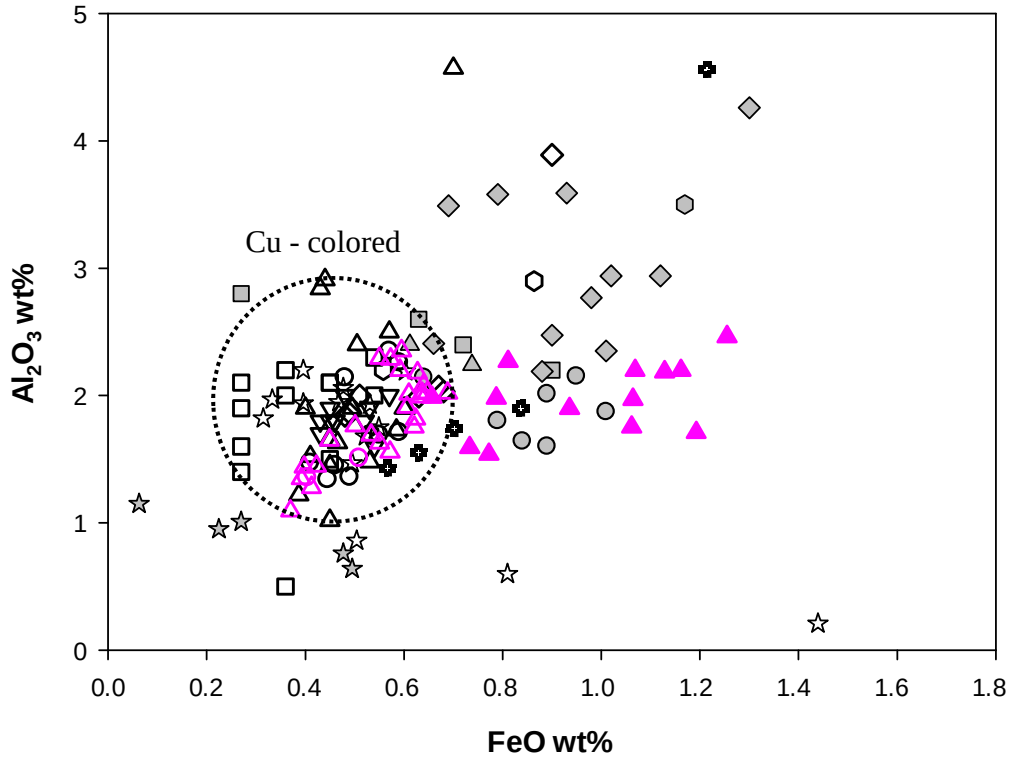

Fig. 6.2. FeO *vs* Al_2O_3 contents of the glass phase in the analyzed blue samples (pink) of the FBA from Lipari in comparison with some coeval literature data (black and gray). Geometric shapes = provenances for literature data; empty symbols = Cu blue beads; full symbols = Co blue beads (References: see fig. 6.1).

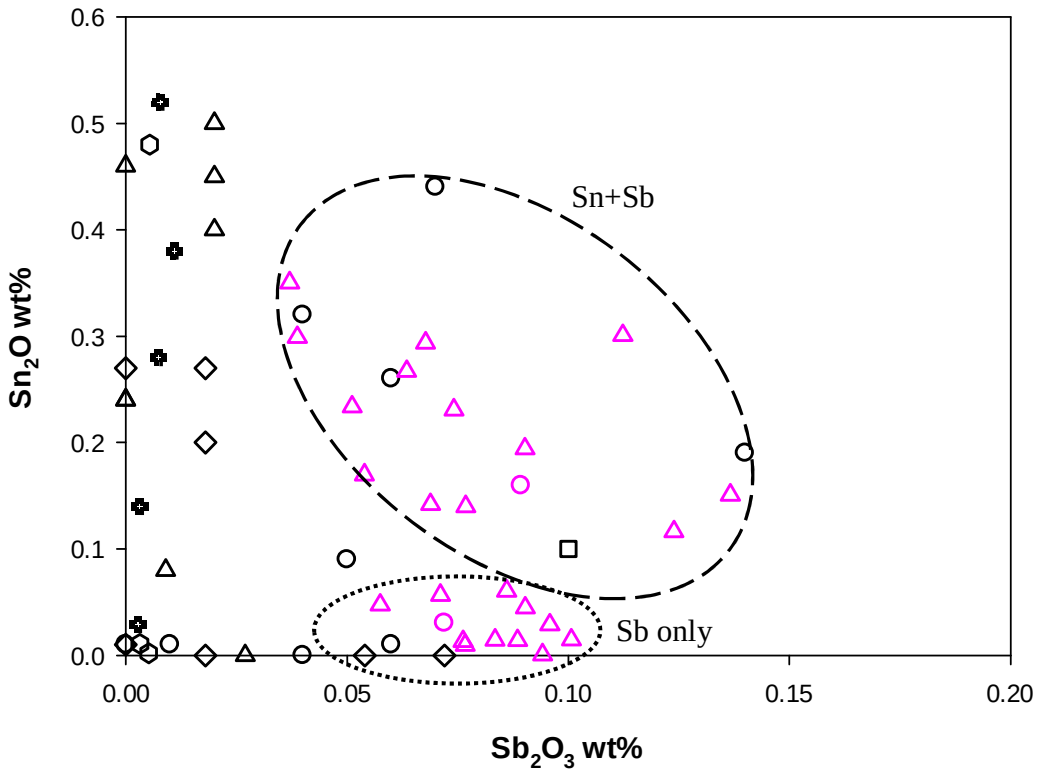

Fig. 6.3. Sb_2O_3 *vs* Sn_2O contents of the glass phase in the analyzed Cu blue samples (pink) of the FBA from Lipari in comparison with some coeval literature data (black and gray). Geometric shapes = provenances for literature data (References: see fig. 6.1).

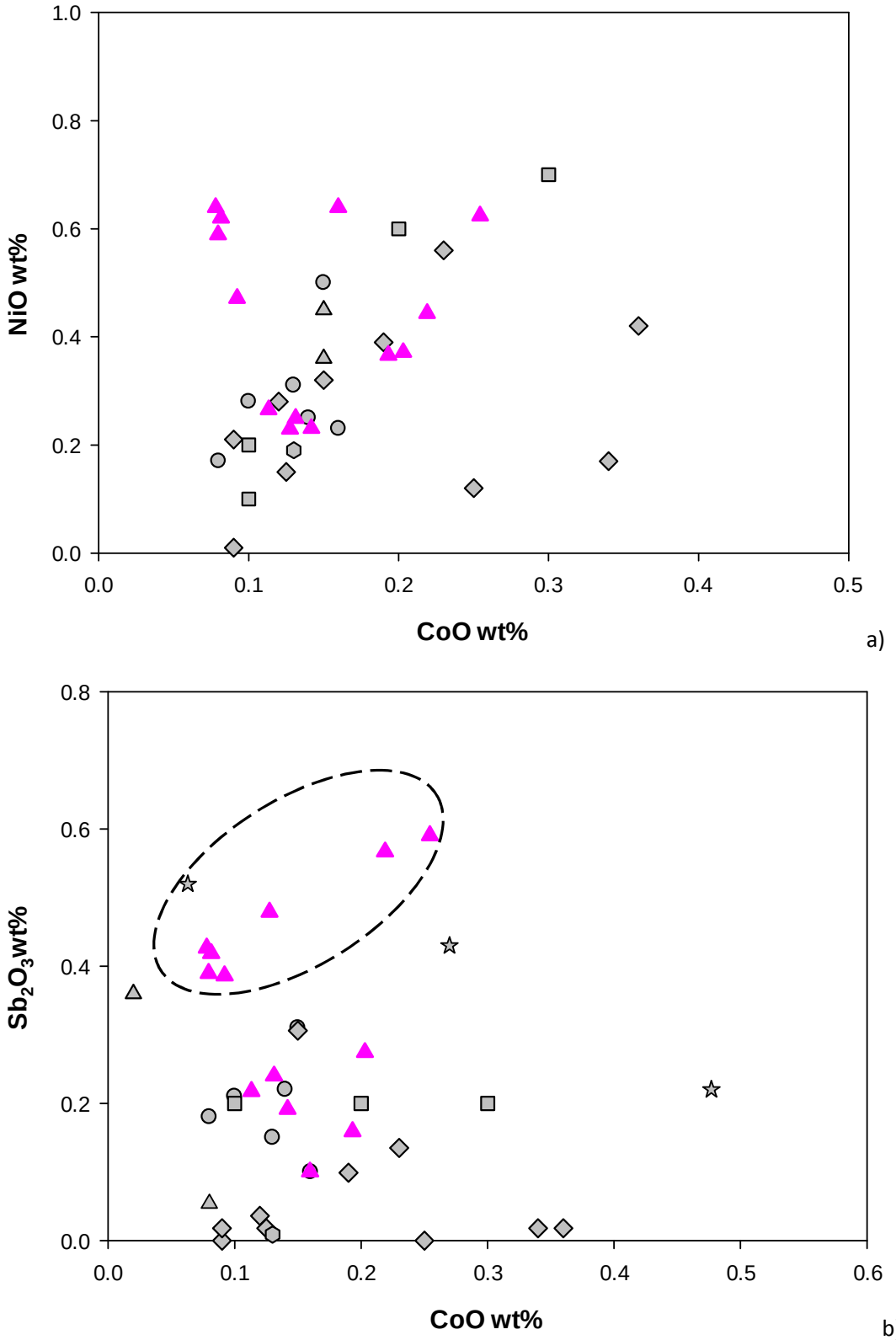

Fig. 6.4. a. CoO *vs* NiO and b) CoO *vs* Sb_2O_3 contents of the glass phase in the analyzed Co blue samples (pink) of the FBA from Lipari in comparison with some coeval literature data (black and gray). Geometric shapes = provenances for literature data (References: see fig. 6.1).

6.2 Piovego cemetery

The EPMA chemical analysis of the analyzed glasses (Tab. 5.2.1) show that all, but one, are soda lime silica glasses obtained using *natron* as flux and are classify Low Magnesium Glasses (LMG). Only sample PG-FUA, coming from grave 14 and dated to the Este IIIC phase (575-525 B.C.), is produced using soda – rich plant ashes as flux and is a High Magnesium Glass (HMG). It has an undefined typology, is Cu – colored (CuO = 1.01 wt%) and has a composition perfectly comparable with those of typical HMG glasses dated to the MBA 3- RBA (Angelini 2009; Angelini et al. 2010), and with those of the HMG glasses that still persist during the Early Iron Age (Angelini et al. 2011; Arletti et al. 2010a; Polla et al. 2011). Interestingly, in the Piovego cemetery there are not mixed alkali glasses LMHK typical of the Final Bronze Age (Angelini 2009; Angelini et al. 2010) and found, rarely, also in the Early Iron Age, specifically in some beads from Lombardy dated to the 9th century B.C. (Angelini et al. 2011) and from Bologna dated to the 8th century B.C. (Arletti et al. 2011).

Most of the Iron Age analyzed vitreous materials, independently to their typology and colors, are LMG glasses. The use of *natron* - evaporitic mineral deposits of sodium carbonate- is testified since the Final Bronze Age – Early Iron Age (EIA) in a few beads from Sardinia (Angelini et al. 2012). In the continental Italy this compositional class is present only since the EIA in some beads from the Villanovian necropolies near Bologna (Polla et al. 2011) and, outside Italy, in some coeval European ornaments from France (Gratuze and Billaud 2003). However, it was during the second Iron Age and throughout the Roman Empire that LMG glasses became widespread, both in European and Mediterranean contexts (Angelini et al. 2010a; Arletti et al. 2010, 2011a; Artioli and Angelini 2013; Hartmann et al. 1997; Freestone et al. 2000; Gratuze et al. 2006, 2007; Polla et al. 2011; Read et al. 2009; Purowski 2012, 2014; Shortland et al. 2009; Towle et al. 2001, 2007). The *natron* lakes of the Wadi el-Natrun in Egypt have long been favoured as the most likely source of these evaporites in antiquity (Forbes 1957; Henderson 1985; Nenna 2000; Shortland 2004). It is conceivable, however, that other sources of evaporitic sodium carbonates had been exploited (Shortland et al. 2005).

During the Iron Age, variations in typology and, in particular, important chemical changes occurred in the glass composition, testifying the introduction of new technologies in the glass production. At present, the few analytical studies on Italian EIA vitreous materials were

performed to on samples from Lombardy and dated to the 9th – 7th century B.C. (Angelini et al., 2011) and from the Villanovian cemetery of Bologna (Polla et al., 2011). The analyses show that both LMG and HGM glasses are present, although is evident a remarkable change in the raw material used, especially in the coloring techniques, and the introduction of new recipes. Since the 6th century B.C. both glass beads and core-forming vessels *natron* – based are present in the Etruscan centers of Adria and Spina and analyzed by different authors (Arletti et al. 2010, 2011a and b; Panighello et al. 2012; Towle et al. 2001; Towle and Henderson, 2007). Coeval LMG glass ornaments are also attested at Mozia, south Italy, and dated to the 6th – 4th century B.C. (Arletti et al. 2012). No other data are available in the literature for pre-Roman Iron Age glasses.

It is therefore clear that only a few archaeometrical data are available for Italian ornamental vitreous material belonging to the Iron Age and in particular there are no data on north-eastern Italian glasses. In this line, the study of the Piovego cemetery beads is particularly interesting to shed light on the different raw materials and technologies used during the Iron Age in the Italian peninsula.

- *Sand and flux composition*

The Piovego glasses, dated between the second half of the 6th century and the end of the 5th century B.C., are soda lime silica glasses produced using *natron* as flux (LMG glasses), according to the few data of the coeval Italian glasses present in the literature. Only samples PG-FUA is produced using soda – rich plant ashes as flux (HMG). Considering the MgO *vs* K_2O contents (fig. 6.2.1), commonly used to define the compositional classes of protohistoric vitreous materials, and comparing the Piovego glasses with those from the literature for Italian ornaments, we can note a variation of the chemical composition during the time.

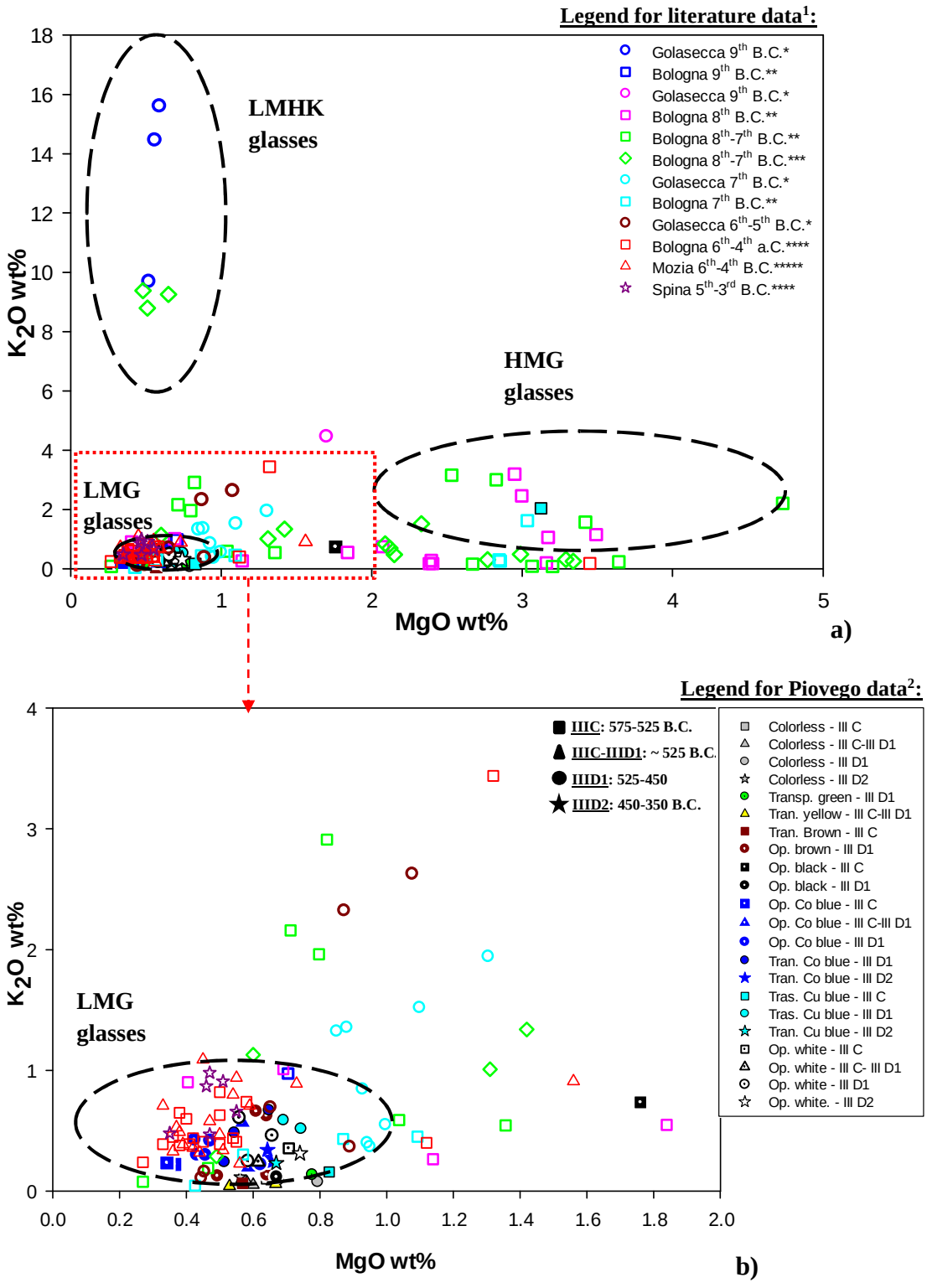

*Fig. 6.2.1: a) MgO vs K_2O contents of the analyzed glasses from the Piovego cemetery in comparison with Italian coeval materials from the 9th century to the 3rd century B.C. b) detail in the red square of fig. a. [1]Legend for the literature data: color = age; symbols = provenance. [2]Legend for the Piovego data: color = color of the glass; symbols = ages referred to the Este chronology. [references data: *Angelini et al. 2011; ** Polla et al. 2011; ***Arletti et al. 2011; ****Arletti et al. 2010a; *****Arletti et al. 2012].*

The Early Iron Age glasses from Bologna and Golasecca (Angelini et al. 2011; Arletti et al. 2011; Polla et al. 2011) have both HMG and LMG glasses and a few LMHK dated to the 9th century B.C. are also persist. However, the MgO *vs* K_2O contents are variable and numerous samples result outside of the conventional LMG class (fig. 6.2.1). The only HMG glass from the Piovego cemetery is the sample PG-FUA, dated to the Este IIIC phase (575-525 B.C.), and is perfectly comparable to the Early Iron Age HMG glasses from Bologna (Polla et al. 2011; Arletti et al. 2010a). Since the 6th century B.C. the *natron* – based glasses are predominant and the chemical composition became more uniform. The Piovego glasses present a MgO *vs* K_2O contents similar to the coeval samples from Golasecca, Bologna, Mozia and Spina (Angelini et al. 2011; Arletti et al. 2010a; Arletti et al. 2012) (fig. 6.2.1b). However, the K contents is variable, ranging from 0.08 wt% to 1 wt%; the different content of K_2O in glasses made using natural soda may be due to *natron* having a variable composition (Henderson 1985). Moreover, in some cases K_2O could have got into the glass even with the sand and therefore may be related to a variation in the raw material used as source of silica (Tite et al. 2008c). Consequently, even though the Na_2O content in the considered literature data is about 10÷20 wt%, the Na_2O/K_2O is extremely variable, ranging from 14 to 180, as the Piovego glasses. The CaO contents is more homogeneous, 5÷10 wt%, comparable with the Piovego samples and in line with the typical *natron* – based glass.

Considering the coeval European productions, during the Iron Age is attested the same variability in the glass production. In fact, in the Early Iron Age, beside the first LMG glasses, persist the presence of compositional classes typical of the period from the Middle Bronze Age to the Final Bronze Age. In particular, HMG and LMHK glasses are still present in two glasses dated to the 9th – 7th century B.C. from lower Saxony (Hartman et al. 1997) and LMHK composition characterize also some glasses from Rathgall (Ireland) dated to the 9th – 6th century B.C. (Henderson 1988). Interestingly, some glasses from Polonia (Purowski et al. 2012) dated to Hallstatt C period (7th – 6th century B.C.) have LMMK composition (Low Magnesium Medium Potassium).

The European *natron* – based glasses of the second Iron Age (6th – 4th century B.C.) have monovalent and bivalent alkali contents comparable with those of the Piovego ones, and generally with the other Italian material considered (Gratuze et al. 2006, 2007; Hartmann et al.

1997; Haevernick 1983; Henderson 1994, 1995; Henderson et al. 1981; Purowski et al. 2012, 2014).

The FeO *vs* Al_2O_3 contents (fig. 6.2.2) is extremely variable. The highest Fe contents (FeO = 6.09÷14.64 wt%) are attested in the opaque blue and brown glasses and are related not only to the sand as source of silica but especially to the source used as coloring agent. In the other Italian contexts here considered the Fe amounts is generally higher than in the Piovego one (FeO = 2.78÷6.90 wt%) and in general the highest values are attested in the glasses dated to the 8^{th} – 7^{th} century B.C. from Bologna and Golasecca (Angelini et al. 2011; Arletti et al. 2011; Polla et al. 2011) even though several beads interestingly registered also the lower amounts of Fe and Al (fig. 6.2.2b, green, blue and turquoise symbols). The Al contents in the Piovego glasses is present in significant amounts (Al_2O_3 = 0.40÷2.60 wt%) as well as for the other coeval samples. The highest amounts of Al (Al_2O_3 = 4.02÷8.06 wt%) are in some samples dated to the 8^{th} – 7^{th} century B.C. from Bologna and Golasecca (Angelini et al. 2011; Arletti et al. 2011; Polla et al. 2011) and in one sample (Al_2O_3 = 3.44 wt%) date to the 6^{th} – 4^{th} century B.C. from Bologna (Arletti et al. 2010a). Considering the coeval European glasses, the iron content is totally comparable with the Piovego production and strictly related to the color of the glass. Generally, in the considered European glasses alumina content is largely variable; in particular, comparable levels of Al with the Piovego ornaments are attested in glasses from France (Gratuze et al. 2006, 2007; Gratuze 2009), lower Saxony (Hartmann et al. 1997), England (Henderson 1995) and Slovenia (Haevernick 1983) in which Al_2O_3 ranging from 0.40÷4.9 wt%. Interestingly, alumina contents are particularly high in some vitreous materials from Polonia (Purowski 2011, 2014) and dated to Hallstatt C and D period (7^{th} – 5^{th} century B.C.) in which Al_2O_3 is up to 8.13 wt% similarly to some samples from Bologna dated to the 8^{th} – 7^{th} century B.C. (Polla et al. 2011).

These data clearly show that in the majority of the case sand was used as source of silica rather than quartzite. Moreover generally the sand is not particularly “pure”.

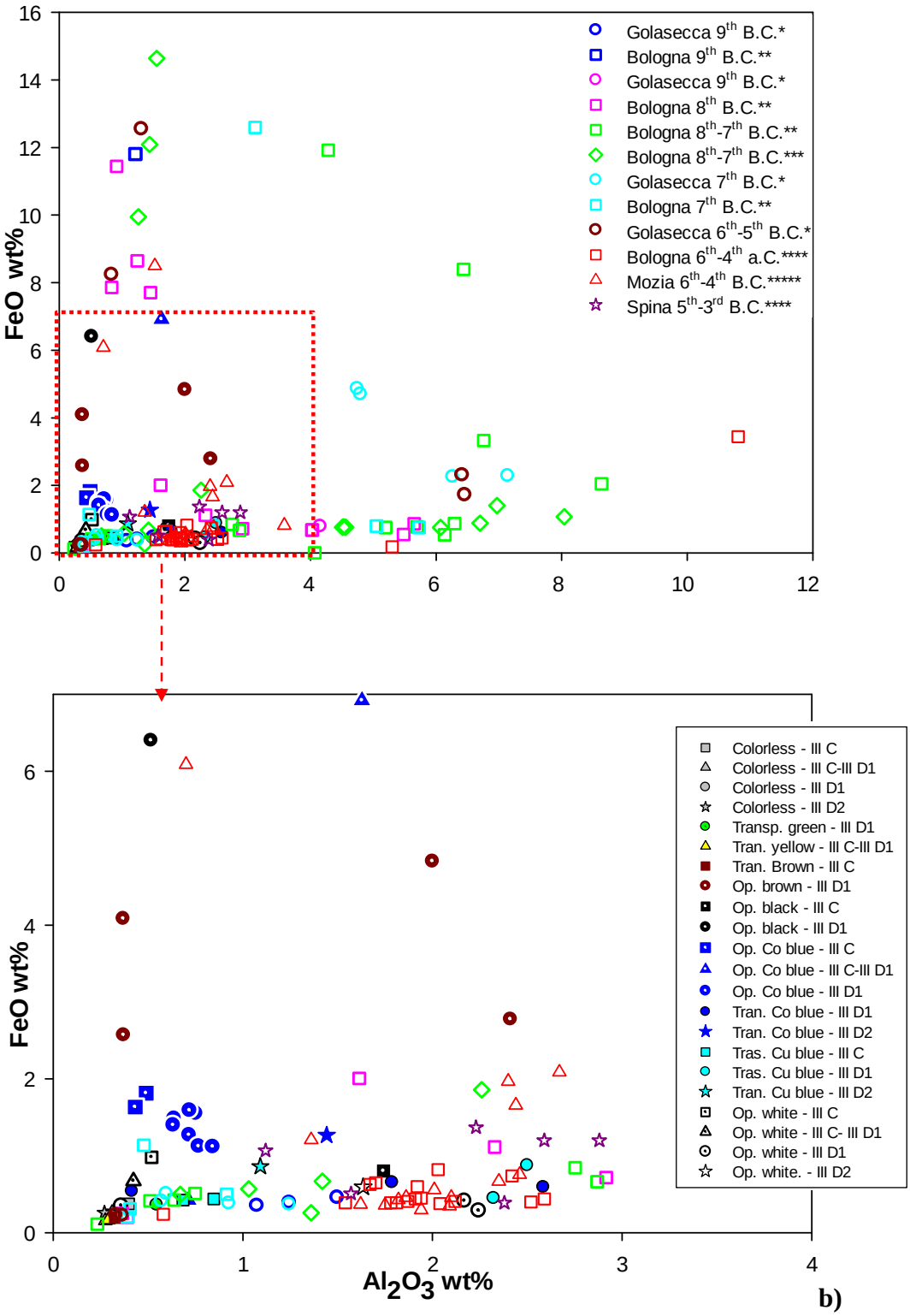

Fig. 6.2.2: a) Al_2O_3 vs FeO contents of the analyzed glasses from the Piovego cemetery in comparison with Italian coeval materials from the 9th century to the 3rd century B.C. b) detail in the red square of fig. a. Legend is the same used in fig. 6.2.1 as well as the reference data.

- *Coloring and opacifiers*

Different colors characterized the Piovego glasses. The most representative color is blue (19 beads), while the other colors are transparent pale blue/green (9 beads and fragments), transparent yellow (1 bead and 1 fragment), transparent/opaque brown (5 beads and fragments), opaque black (2 beads), white (6 eyes decorations).

The blue beads are mostly colored by cobalt (CoO = 0.04÷0.47 wt%) associated to copper (CuO = 0.08÷1.07 wt%). Among these, 7 small annular beads (PG-AB8, PG-AB9a/b/c/d and PG-ABOa/b), 2 annular beads (PG-AB and PG-AB1_2) and the 5 horned bead (PG-SB) present a texture more similar to a *glassy faïence* than an actual glass (see below). The small annular beads, belong to the grave 127 and dated to the Este IIID1 phase (525-450 B.C.), present traces of Ni, As, Sb and in two samples also of Pb. Cobalt associated to Cu, Ni, As and Sb was previously found in some blue beads from the Final Bronze Age site of Frattesina (Angelini et al. 2004; Angelini et al. 2010; Towle et al. 2001). In the Iron Age glasses it is difficult to find the compresence of all these elements associate to cobalt, even though nickel and arsenic are not measured in the most of the literature works. However, cobalt associated to nickel and antimony or to arsenic and/or antimony is present in some blue beads from Golasecca culture and dated to the 7^{th} – 5^{th} century B.C. (Angelini et al. 2011). Copper and nickel are presents in a few Co blue beads from Bologna, in two cases associated also to antimony and lead, dated to the 8^{th} – 7^{th} B.C. (Arletti et al. 2011). Considering the coeval European production, the compresence of Ni, As, Sb and P are interestingly present in numerous vitreous materials from Polonia dated to the Hallstatt C period (Purowski et al. 2014). In particular, considering the CoO *vs* NiO contents of the cobalt blue beads from Piovego compared with those from Golasecca culture in Lombardy (Angelini et al. 2011), Bologna (Arletti et al. 2011) and Polonia (Purowski et al. 2014), is evident a general trend of some samples (fig. 6.2.3, inside the dotted line). Inside this general tendency, we can note a similarity in the Ni and Co amounts of Piovego samples with some glasses from Golasecca culture and Polonia (fig. 6.2.3, inside the continuous line).

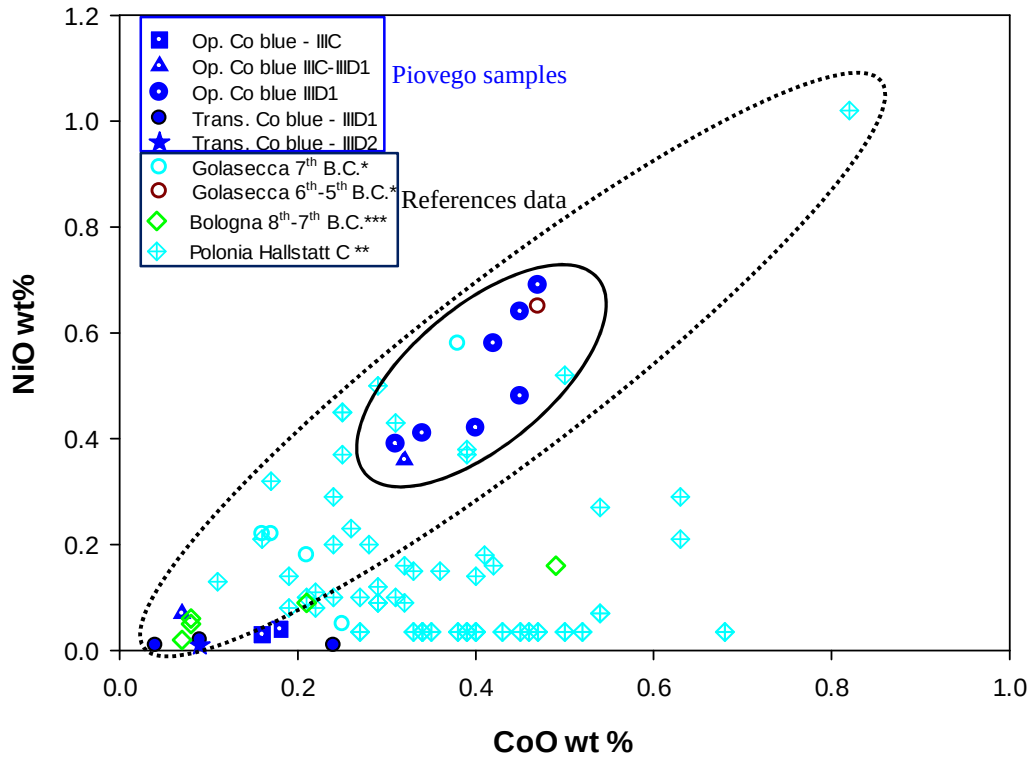

Fig. 6.2.3: CoO vs *NiO contents of the analyzed glasses from the Piovego cemetery in comparison with Italian and European coeval materials from the 8th century to the 5th century B.C. In the Piovego samples, symbols are referred to ages and colors to the glass colors. The chronological phases IIIC, IIIC-IIID1, IIID1 and IIID2 are the same used in fig. 6.2.1. In the references data, symbols are referred to provenance and colors to ages. [references data: *Angelini et al. 2011; **Purowski et al. 2014; ***Arletti et al. 2011].*

Interestingly, the vitreous materials from Polonia and Lombardy present a texture very similar to a *glassy faïence* as in the Piovego ones, characterized by numerous SiO_2 crystals and inclusions rich in metal elements. Inclusions in the cobalt blue Piovego samples are particularly interesting. They are very small, mostly round and sometimes irregular shaped, and made up of sulfides with chalcocite composition (Cu_2S) and characterized by segregation of Ni, As, Ag and in some cases also of Sb and Fe. Their presence in the raw material may be due to poly - metallic ores possibly associated to the source of Co added to the glass melt for color effect. During the cooling process the alloys crystallized, forming characteristics intergrowths depending on the composition of the specific drop. Same composition characterized metals inclusions in several vitreous materials from Polonia (Purowski et al. 2014); considering also

the close correlation Co-Ni between the small annular beads and some Polonia samples, we can hypothesizes the same cobalt source (fig. 6.2.3, dotted line).

Numerous studies have been carried out on the source of cobalt in glasses (i.e.: Henderson 1985, 2000; Shortland and Tite 2000, Reheren 2001; Gratuze 2009). Generally, Piovego glasses have not significant levels of Al and Mg as found in some cobalt blue glass from France in the Iron Age (Gratuze 2009). Furthermore, cobalt is not related to Mn as in the Mediterranean Group II date to the Iron Age (Arletti et al. 2011). Similarly, Piovego glasses are not comparable with the Egyptian/ Near Eastern cobalt blue vitreous production in which the cobalt source is due to cobaltiferous alum salts (Shortland 2000; Shortland et al. 2000; Reheren 2001; Tite et al. 2008b). However, even if the sources of Co for the Piovego glasses are not identify at the moment, we cannot exclude that the cobalt source originate from Europe, as cobalt minerals are common in modern Germany, Austria, Switzerland, Czech Republic and Slovakia (Henderson 1985).

Beyond the metals inclusions, the heterogeneous texture of these glasses is due to numerous unreacted quartz grain related to the use of sand as source of silica, together with traces of albite/anorthoclase and K-feldspars. The presence of silicates relicts and the absence of the quartz polymorphs tridymite/cristobalite (except for one inclusion) testify a temperature not particularly high reached in the melting process. Interestingly, some newly formed Ca-Na phosphates were identify. The raman spectra of these inclusions is similar to the apatite one, with the stoichiometry very close to the buckwaldite ($NaCaPO_4$). The presence of Ca phosphates testify that low quantity of bones were present in the mix of the raw materials.

The two cobalt annular beads PG-AB and PG-AB1_2 and the 5 horned bead PG-SB have a similar texture of the small annular beads even though different association to Co are present. In fact, PG-SB, dated to the Este IIIC-IIID1 phase (about 525 B.C.), presents only Cu and Ni in the glass matrix, with a good correspondence between Co and Ni (fig. 6.2.3, full blue triangle). The metal inclusions in the glass phase have the same composition of those in the small annular beads, composed of chalcocite (Cu_2S) enriched in Ni, As and Ag. Instead, PG-AB and PG-AB1_2 present Cu, Sb and Pb but not Ni and As, as found in other coeval glasses from Adria (Towle et al. 2001), Bologna (Arletti et al. 2010a) and Mozia (Arletti et al. 2012). Similar elements in cobalt blue glasses were observed in coeval European glasses from Polonia

(Puroeski et al. 2012) and France (Gratuze et al. 2006, 2007). For these glasses, we can hypotheses a different cobalt ore as source of coloring agent with respect to the previous discussed Co – colored glasses from the Piovego cemetery. Same trace elements are observed in the blue body PG-GO3B, even though Pb is slightly lower and it not presents any inclusions in the glass phase.

Homogeneous texture characterized also the blue body PG-GOB and the annular bead PG-AAB, but the first one presents in the glass phase Cu and significant amounts of Sb, while the second one has only traces of Cu. Very different from all the other are samples PG-FA and PG-GOB8. The first one has the highest Sb level (Sb_2O_3 = 2.77 wt%) with respect to other cobalt blue glasses and presents high amounts of Pb (PbO = 6.70 wt%) that improve the fluidity of the melt. The high Sb is in accordance with presence of very small Ca antimonates finely dispersed in the glass phase, and crystallized in their orthorhombic phase, $Ca_2Sb_2O_7$. Sample PG-GOB8 has cobalt associated to traces of Cu, Ni As and Sb as in the small annular beads. However it has a particularly high Pb content in the glass phase (PbO = 18.50 wt%) and a particularly texture as well as in the sample PG-CM and will be discuss together below.

It is evident that the Co-Cu colored glasses of the Piovego cemetery have difference both in the trace elements and texture. For these glasses we can hypnotizes different cobalt ores sources and also different production techniques. Totally, considering the elements association, we can identify 4 different association possibly related to the cobalt source:

a) Co, Cu, As, Ni, Sb and Pb; b) Co, Cu, As Ni, Sb (traces of Zn); c) Co, Cu, Sb, Pb, (traces of Zn); d) Cu, Sb. However, some elements, such as Pb or Sb, can be voluntary added or related to other raw materials.

The Cu coloring is poorly present in the Piovego glasses and observed only in four glass with low Cu contents (CuO = 0.09÷1 wt%). Sample PG-FUA is the only HMG glass, with a composition comparable with both HMG glasses dated to MBA3-BR (Angelini et al. 2009, 2010b) and those that persist in the EIA (Angelini et al. 2011; Arletti et al. 2010a; Polla et al. 2011) even though the Cu content in the Piovego glass and in those of the EIA is lower than the MBA3-RBA glasses. It has a homogenous texture and no trace elements associate to copper.

The three LMG copper colored glasses have low Cu contents (CuO = 0.46÷0.90 wt%) except for sample PG-GO6B in which copper is particularly low (CuO = 0.09 wt%). Different are the trace elements observed in the glass phase. Sample PG-GAT1 presents significant amount of Mn (MnO = 0.92 wt%). Values of MnO ≤ 0,3 wt% are due to impurities in the raw materials, since at least 1 wt% of MnO is required to ensure glass is decolorized (Brems et al. 2012) and, in any case, a $MnO/(Fe_2O_3)_{TOT}$ ratio > 2 (Silvestri et al. 2008). As regards sample PG-GAT1, the quantity of manganese is too high to come from sand alone, and too low to have been added deliberately. It may be due to both the sand and to the recycling of decolored glass, even though at the Piovego cemetery are not present Mn decolorized glasses.

The blue bodies PG-GO6B and PG-GOA present Sb that is in low amount in the first one (Sb_2O_3 = 0.52wt%) and in significant amounts in the second one (Sb_2O_3 = 1.92 wt%). In sample PG-GOA the higher contents of Sb are in accordance to the presence of Ca antimonates finely dispersed in the glass matrix, crystallized in their orthorhombic phase, $Ca_2Sb_2O_7$. Moreover are present also small amounts of Pb (PbO = 0.17wt%).

In coeval Italian vitreous materials copper is usually observed as coloring agent in turquoise glasses, associated to the presence of Ca antimonates (i.e.: Arletti et al. 2010a, 2012). In the Piovego glasses Ca antimonates are present only in one opaque turquoise sample (PG-GOA) while the other glasses have only low amounts of Cu, are transparent with darker shades and a homogenous texture as well as the HMG glass PG-FUA.

Yellow coloring is present only in two transparent glass fragments. They have a homogenous texture and are both obtained using a very pure sand with very low Al and Fe contents (both ≤ 0.30 wt% of the oxides). Consequently, in absence of any other coloring elements, the color is due to Fe associated to S (SO_3 = 0.10÷0.15 wt%).

Similar composition characterized the amber glasses produced by an iron sulphide complex in a reducing atmosphere (Jackson et al. 2006; Nenna et al. 1997). Amber glasses with similar characteristics were also found in some samples from France and dated to the Iron Age (Gratuze 2009). At present, the only yellow glasses from Italy are attested in Sardinia (Angelini et al. 2012). Interestingly, in the Piovego cemetery are not attested opaque yellow glasses with Pb antimonates, a technology present in the Italian glass beads since the Early Iron Age (Angelini et al. 2011, 2012; Arletti et al. 2010a, 2011, 2012; Polla et al. 2011).

Brown glasses in the Piovego cemetery are both transparent and opaque, homogeneous and heterogeneous. However, the only chromophore element is iron, possibly in its oxidized status, that ranging from 0.20 to 4.83 wt% (FeO content) and give different shades to the glass. Despite the Fe contents, samples PG-FM14, PG-GONM and PG-FM89 have a very similar chemical composition and a homogeneous texture and they are obtained with a very pure sand, poor in feldspar minerals. Sample PG-FM14 have a particular low content of Fe (FeO = 0.20 wt%). The other two samples, PG-FM83 and PG-CM, have higher contents of Al and K and testify the use of a more impure sand rich in feldspar minerals. However, if sample PG-FM83 has a homogenous texture, sample PG-CM has a very heterogeneous texture due to the presence of numerous crystalline inclusions with different nature. Moreover, it has high contents of (PbO = 25.23 wt%), Fe (FeO = 4.83 wt%) and Mn (MnO = 0.87 wt%). Same characteristics are observed in the blue sample PG-GOB8. They both have a texture very close to a *glassy faïance*, characterized by comparable concentrations of crystalline inclusions and glass phase (Angelini et al. 2002). They both have a lower Na contents (Na_2O = 6.98 and 9.54 wt% in PG-CM and PG-GOB8, respectively) and high Pb amounts (PbO = 25.23 wt% and 18.50 wt% respectively), that facility the fluidity of the glass melt. Similar chemical and textural characteristics were found only in some glasses and *glassy faïance* from Lombardy dated to 9^{th} – 7^{th} century B.C. (Angelini et al. 2011). The typologies of these beads are similar in the case of PG-GOB8, even though with yellow eyes, while no typology comparison are available for the biconical bead PG-CM. The few data available to date, do not allow to define specific areas or production centers fro these particular glasses / *glassy faïance.*

The crystalline inclusions present in samples PG-CM and PG-GOB8 are mainly residual quartz crystals. Wollastonite and Na-Ca silicate phases are also present, due to the devitrification of the glass that normally occur in silica – soda – lime glasses at temperature between 750 to 1200 °C (Morey 1930; Simmons et al. 1981). In addiction, sample PG-CM presents some diopside/augite crystals with irregular or sub-rounded morphologies and Ca phosphates. The high Fe contents could be due to the insertion of metal slags as coloring materials, as indicated by the presence of inclusions rich in metal (Cu, Fe, As, Ag) and dispersed in the glass phase. Furthermore, elongated crystals with a peculiar composition made of Pb-As-Ca-Fe-P-O, characterized sample PG-GOB8.

These glasses seems to be obtained with a very impure sand rich in silicates and produced using low firing temperature.

Two black glasses are present in the Piovego cemetery. The annular bead PG-AN has a homogenous texture and is obtained with a pure sand, poor in feldspar minerals, and colored by high amounts of Fe (FeO = 6.40 wt%). These characteristics are present also in some black glasses from France, even if they contain also traces of Ni, Co and Zn, not observed in the Piovego one, and an Egyptian origin is supposed for the French materials (Gratuze 2009). In the coeval Italian materials, black coloring is only attested in a few Early Iron Age glasses from Bologna (Polla et al. 2011).
The large globular black bead PG-GO5B is different both for its major and minor elements. It has higher Mg and K with respect to the other *natron* – based glasses (Fig. 5.2.1 and tab. 5.2.1). It has higher contents of Al than sample PG-AN and has traces of Mn, Sb and Pb. The coloring is due to low Fe contents (FeO = 0.80 wt%) possibly in association with copper sulfides (chalcocite, Cu_2S) enriched in Fe, Pb and occasionally Ni; these inclusions are finely dispersed in the glass phase and the coloring is probably due by the absorbent effect of the copper sulifdes. Therefore, different raw materials were used in the production of these black glasses.

The white glasses in the Piovego cemetery are all colored and opacified by Ca antimonates. The use of Ca antimonates as opacifier is attested in Egypt since the 18th Dynasty, 1570–1292 B.C. (Shortland 2002), while in Italy this production technique appear during the Early Iron Age (Angelini et al. 2011; Arletti et al 2010a; Polla et al. 2011) and is attested also in Europe (Henderson 1995; Gratuze et al. 2007; Purowski et al. 2011). However, as previously discussed (par. 6.2.1), the early use of calcium antimonates as opacifier is attested by the research of this thesis in one white glass from Salina –Villaggio di Portella, dated to the MBA3.
The white glasses belong to the eyes decorations of the beads. Samples PG-GO3Bi and PG-GOBi are applied on Co – colored blue body; PG-GO6Bi is applied on a Cu – colored globular bead; PG-GONBi is applied on a brown globular bead; PG-GO5Bi and PG-AOBi are applied on black bodies. Sample PG-GO5Bi is particularly interesting because presents high Pb contents in the glass matrix (PbO = 15.92 wt%) even though it is white colored and opacified by Ca antimonates. Moreover, the black body (PG-GO5N) on which is applied the white glass,

has a different glass composition without Pb. It is possible that Pb was added to give brilliance and to improve the fluidity of the white glass during the working process.

Calcium antimonate has two different phases: *hexagonal*, $CaSb_2O_6$, and *orthorhombic*, $Ca_2Sb_2O_7$. Except for sample PG-GO5Bi that present only the *hexagonal* phase, $CaSb_2O_6$, the other glasses have both *hexagonal* and *orthorhombic* phases. The ratio amounts of Ca antimonate phases $CaSb_2O_6/Ca_2Sb_2O_7$ may provide information on the temperature range used to produce opaque glass. The synthesis of pure crystals of Ca antimonate shows that $CaSb_2O_6$ crystallizes from 927 °C at the expense of $Ca_2Sb_2O_7$, which forms at lower temperatures, and becomes the only phase from 1094°C (Butler et al. 1950; Lahlil et al. 2008). However, a recent experimental study by Lahlil et al. (2010a) on syntheses of *in situ* opacified glass carried out at 1100°C from periods ranging from 30 min to 13 days, highlights that $CaSb_2O_6$ is kinetically favored, whereas $Ca_2Sb_2O_7$ is thermodynamically stable. Therefore, both time of fire and temperature play an important role in the crystallization of the two different Ca antimonates phases. In the Piovego white glasses, sample PG-GO5Bi seems to have only the *hexagonal* phase, $CaSb_2O_6$ and, interestingly, it has high Pb content (PbO = 15.92 wt%) in the glass matrix indicating a particular recipe in the production of this glass. The only presence of the hexagonal phase allow us to hypothesize a high melting temperature for the production of this glass and/or short firing time. The same is for sample PG-GONBi in which the *hexagonal* phase is the major phase identified. Instead, in samples PG-GO3Bi, GO6Bi and AOBi, the *orthorhombic* phase is predominant suggesting possibly lower melting temperature or longer firing time. Sample PG-GOBi seems presents an equal distribution of the two phases indicating a favorable temperature and time conditions for both the phases.

Considering the morphologies of the crystals, they are finely and homogeneously dispersed in the glass matrix. The very small dimensions of the particles (a few microns) suggest that they are newly formed crystals (*in situ* growth). The inclusions show in several cases euhedral habits and sometimes they are grouped in larger aggregates (up to 20÷30 µm) with very irregular shapes. Except for sample PG-GO3BBi, the Sb amounts in the glass phase are very high, ranging from 4.65 to 8.62 wt% (Sb_2O_3), even though we have to note that the Ca antimonite crystals are finely dispersed in the glass matrix and the spot size of the microprobe (~1µm) could have involuntary detected also some nano-crystals. However, the high levels of antimony and the euhedral morphologies of the inclusions allow us to hypotheses an *in situ* crystallization

for these samples, with the precipitation of Ca antimonates from soda – lime glass melt by intentional adding of antimony, possibly Sb_2O_3 (Lahlil et al. 2008; Mass et al. 1998; Shortland 2002).
As regards the decoration techniques, the marked line between the blue body and the white decoration observed for several glasses at the SEM, suggests that the white eyes were applied secondarily on the cooled or partially cooled bead body, according to the bubbles aligned on the boundary line.

Nine samples are colorless, transparent with very pale blue or green shades. They are produced with particularly poor sand and, except for sample PG-FVA67, are decolorized by antimony. Sample PG-FVA67 has manganese (MnO = 0.42 wt%) even if is not enough to decolorize the glass (Brems et al. 2012; Silvestri et al. 2008) and it is probably due both to the sand and to the recycling of decolorized glass. Samples decolored by antimony have a homogeneous texture except the globular bead PG-GVA97 that has numerous Ca antimonite crystals dispersed in the glass matrix in its *hexagonal* phase, $CaSb_2O_6$, and the glass appear semi – transparent.
Colorless glasses decolored by antimony are typical of the Iron Age and are attested in several glasses from Golasecca culture and Bologna (Angelini et al. 2011; Polla et al. 2011) and also in some samples from France (Gratuze 2009).

6.3 Villa di Villa site

Annular beads

The two annular blue beads were produced using two different fluxing agents. Sample VV-AB6 is a LMHK glass as shown by the MgO *vs* K_2O and Na_2O *vs* K_2O contents (Fig. 5.3.1a and b). Mixed alkali glasses were widespread during the Final Bronze Age in northern Italy and central Europe. Interestingly, the only known working/production centers of the period were all in the Veneto region and, among these, Frattesina is surely the most important and best known (Angelini et al. 2004, 2010; Henderson 1988; Towle et al. 2001). LMHK glasses were occasionally found in several Early Iron Age beads from a tomb dated to the 9th century B.C. belonging to the Golasecca culture (Lombardy) (Angelini et al. 2011) and in Villanovian beads of the 8th century B.C. (Arletti et al. 2010). By contrast, sample VV-AB is a typical LMG glass obtained with *natro*n as flux, in accordance with its contents of SO_3 and Cl_2O - 0.19 and 1.73 wt%, respectively. The use of *natron* is testified since the Early Iron Age in some beads from the Villanovian necropoleis near Bologna (Polla et al. 2011) and occasionally in some coeval European ornaments from France (Gratuze et al. 2003). However, it was during the second Iron Age and throughout the Roman Age that LMG glasses became widespread, both in European and Mediterranean contexts (Angelini et al. 2010; Arletti et al. 2010, 2011a; Artioli et al. 2013; Hartmann et al. 1997; Freestone et al. 2000; Gratuze et al. 2006; Polla et al. 2011; Read et al. 2009; Shortland et al. 2009; Towle et al. 2007).

The alumina in VV-AB is slightly high (Al_2O_3=1.78 wt%) suggesting use of impure sand made of feldspar minerals, calcite and traces of heavy metals, in accordance with CaO and FeO levels - 7 and 1 wt%, respectively. The same may be said of sample VV-AB6, which has greater alumina content (2.97 wt%), slightly lower FeO (0.6 wt%) and CaO (1.57 wt%), typical features of LMHK glass (Angelini et al. 2004, 2010; Brill 1992; Henderson 1988; Towle et al. 2001; Santopadre and Verità. 2000).

The blue color of VV-AB and VV-AB6 is due to Co (CoO 0.04 and 0.15 wt%, respectively). Both of the samples present also Cu (CuO 0.12 and 0.15 wt%, respectively). In addition, cobalt in the LMHK bead is associated with low Sb content (Sb_2O_3 = 0.12 wt%), like in the Co–colored mixed alkali glasses from Frattesina, although in that case the Cu level is higher (CuO

= 0.37÷0.9 wt%) and cobalt is also associated with nickel (Angelini et al. 2010; Brill 1992). Cobalt is not associated with any other element in VV-AB, which makes identification of its cobalt source difficult. In any case, results suggest different provenances of the cobalt ores for the two annular blue beads.

SEM-EDS analysis shows that in contrast with sample VV-AB, which has a homogeneous texture, sample VV-AB6 has large numbers of SiO_2 inclusions with lamellar or rectangular morphologies, often grouped in large aggregates. The biggest grains are often surrounded by large fractures due to changes in volume during glass cooling, especially when phase transitions from quartz to tridymite and/or cristobalite occur (Angelini et al. 2004; Artioli et al. 2008). However, these inclusions are more properly considered relicts of initial raw material, as testified by the recrystallization of lamellar inclusions on the edges of the biggest grains. The large aggregates of SiO_2 - analyzed through µ-Raman spectroscopy - are made up of cristobalite and quartz, while the lamellar crystals are tridymite. The presence of cristobalite is indicative, since it is one of the high-temperature polymorphs of silica. Pure quartz starts converting into cristobalite above 1300°C, depending on the heating path and kinetics, with fast transformation rates above 1470 °C (Artioli et al. 2008; Sosmans 1995; Stevens et al. 1997). However, both cristobalite and tridymite are stabilized by alkali ions, such as Na and K, and research shows that cristobalite crystallization in alkali environments starts as a cristobalite/tridymite inter-growth, evolving towards cristobalite or tridymite depending on temperature, time and alkali concentration (Artioli et al. 2008; Stevens 1997). Therefore, the temperature reached during the production of sample VV-AB 6 might have been lower than 1300°C, but nonetheless quite high, possibly 1000-1200°C.

Bracelet fragments

The three blue bracelet fragments belong to different typologies: VV-BRB9 is plain with a D-shaped section and corresponds to group 3a of Haevernick 1960, while VV-BRB5 and VV-BRB2 are decorated by ribbing similar to group 8a and c of Haevernick 1960. The different typologies are associated with different glass classes. VV-BRB9 is a typical LMG *natron*-based glass, with 0.64 wt% MgO and 0.54 wt% K_2O, in accordance with the contents of Cl_2O (1.15 wt%) and SO_3 (0.24 wt%). VV-BRB5 and VV-BRB2 have higher levels of MgO (0.94

and 0.92 wt%, respectively) and especially K_2O (1.80 and 1.84 wt%) which usually never exceed 1.5 wt% in typical *natron*–based glasses. However, the flux is probably *natron* due to the Na_2O/K_2O ratio (about 7.5 in both arm rings) and the presence of Cl (Cl_2O about 0.9 wt%), while the high K content is associated with sand type (see below). On the other hand, it is worth noting that the low S amount (SO_3 about 0.05 wt%) and P traces (P_2O_5 about 0.19 wt%) are compatible with the use of plant ash. Similar alkali contents were found in a few *natron*–based bracelets from Brittany, some samples of which have K_2O = 1.5÷3 wt% with P_2O_5 ~ 2 wt% (Dinard 2009).

The levels of Al_2O_3 and FeO are similar in all three samples and range between 2.38 and 2.41 wt%, and between 0.60 to 0.80 wt%, respectively. Two groups are clearly identified by comparing the contents of Al_2O_3 *vs* FeO of the three samples with those of arm rings in the literature (Fig. 6.3.1a and b): the first one with high amounts of Al_2O_3 varying between 1.91 to 2.96 wt% (symbols in the dotted line) and the second one with low Al_2O_3 levels (0.7-1.46 wt% (symbols in the circled line). In both groups FeO content is low (0.14-0.9 wt%), except for several green and yellow glasses in which iron is the principal chromophore (Fig. 6.3.1a and b, symbols outside the lines). The two groups suggest two different sand sources and the 3 samples from Villa di Villa belong to the group with the highest alumina content. The data suggest that different raw materials are apparently more closely associated with bracelet typology (Fig. 6.3.1b) rather than color (Fig. 6.3.1a).

The three glasses are colored by Co (CoO = 0.11÷0.16 wt%) and they also present Cu (CuO = 0.20÷0.24 wt%) (Fig. 6.3.2). As regards the contents of Co and Cu, the three samples from Villa di Villa are very similar to some blue bracelets from Austria (Karwowski 2004), and sample VV-BRB9 to some samples from Brittany (Dinard 2009) and Slovakia (Brezinova et al. 2013). There appears to be no correlation between the CoO *vs* CuO contents and the typologies of bracelets from Villa di Villa and the European sites examined.

All the Villa di Villa arm rings contain Mn in similar low concentrations (MnO = 0.41÷0.79 wt%). These quantities are not sufficient to obtain decoloration, and were therefore probably introduced as impurities from the raw materials used (possibly the coloring agent).

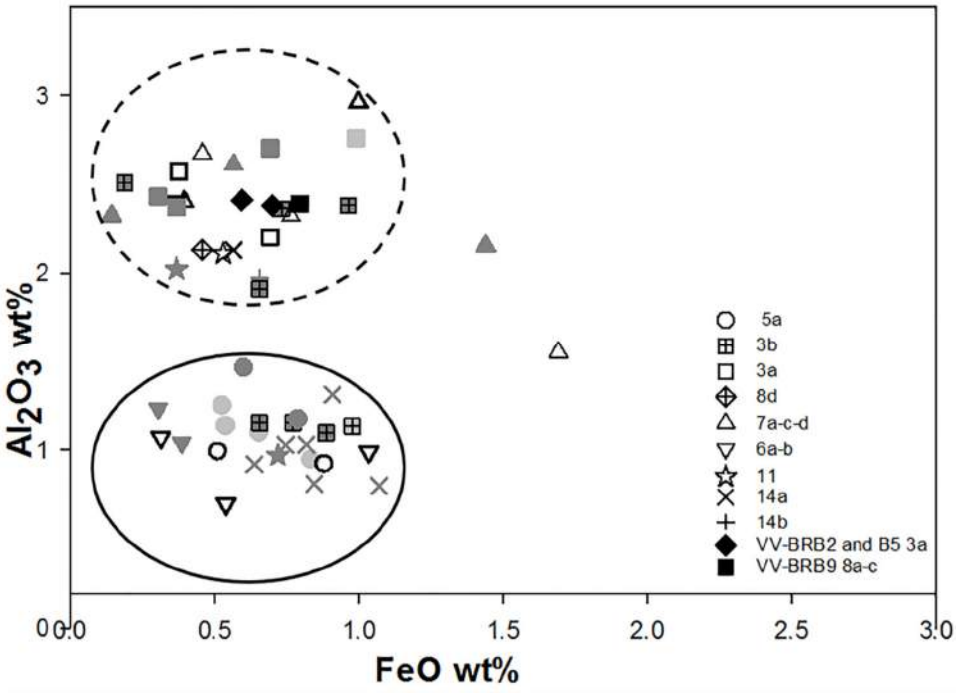

a)

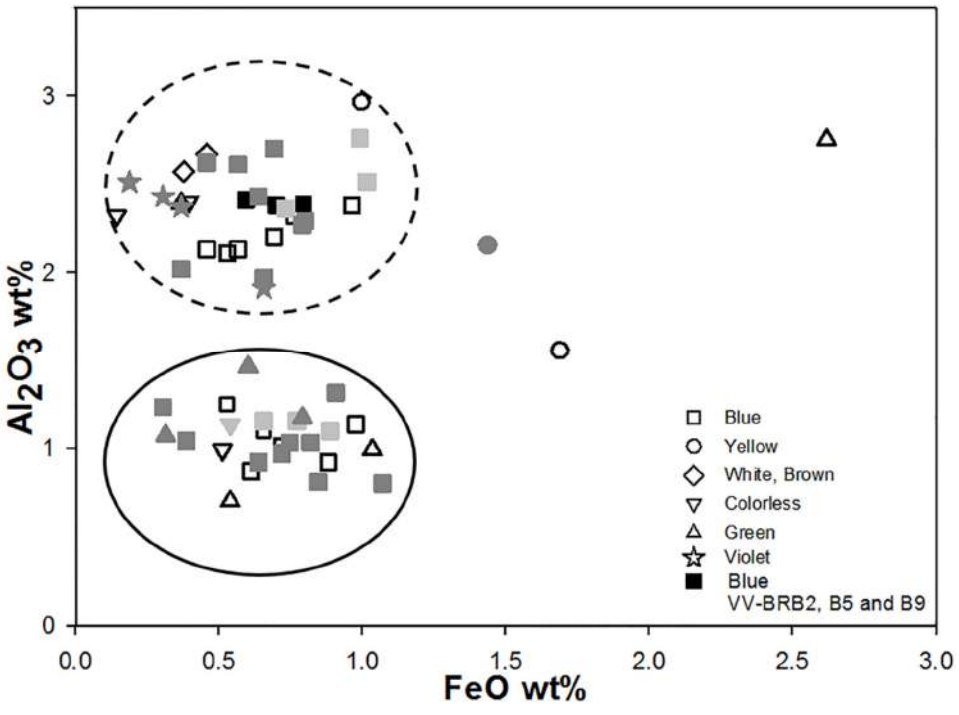

b)

Fig. 6.3.1a and b: FeO vs *Al_2O_3 contents of the 3 blue arm rings grouped by typology (a) (Haevernick 1960) and color (b). Reference data are also reported (Gray= Brezinova et al. 2013; Dark gray= Venclova et al. 2009; Empty= Dinard 2009).*

Similar interesting Mn contents were found in other cobalt blue bracelets from Austria (Karwowski 2004), France (Dinard et al. 2009), Slovakia (Brezinova et al. 2013) and the Czech Republic (Venclova 2009). Henderson (2000) reports that around the 2nd century B.C., the source of cobalt used in European blue glasses changed from an antimony-rich to a manganese-rich source, at the same time as industrial and social centralization changes occurred. By contrast, other authors argue that the association of cobalt with manganese or antimony could also be due to the recycling of manganese- and antimony-bearing glass in different periods, and not only to the changes in the minerals employed as cobalt-bearing phases (Arletti et al. 2011b).

Considering the total chemical characteristics of the bracelets from Villa di Villa, we can conclude that samples VV-BRB2 and B5 are very similar in both major and minor elements, and were perhaps produced in the same center. Instead, the arm ring VV-BRB9 differs for the type of flux and/or sand used in its manufacture.

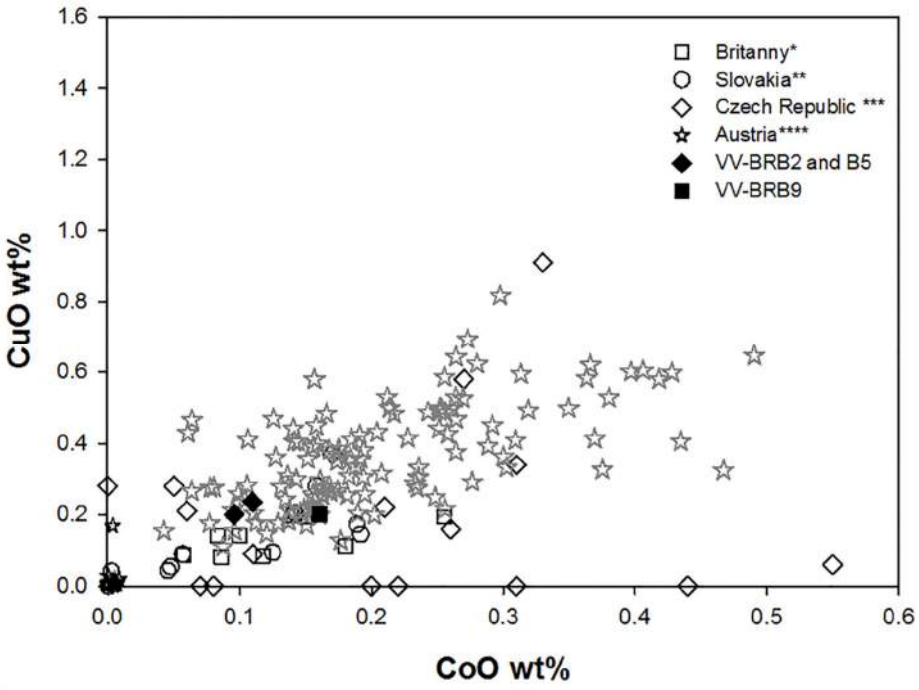

Fig. 6.3.2: CoO vs *CuO contents of the 3 blue arm rings. Reference data of blue arm rings are also reported and grouped according to their provenance (*Dinard 2009; **Brezinova et al. 2013; ***Venclova et al. 2009; ****Karwowski 2004).*

Globular bead with eyes decoration

The globular yellow bead VV-GGi was produced using *natron* as flux, as suggested by its levels of MgO and K_2O <1 wt%, Cl_2O (1.23 wt%) and SO_3 (0.07 wt%). The glass phase of the bead body shows PbO and Sb_2O_3 of 10.71 and 1.05 wt%, respectively, with Na_2O lower than the other *natron*-based glasses from Villa di Villa. This is consistent with numerous crystals rich in Pb and Sb in the glass matrix, as observed by SEM-EDS. Although this bead typology was common between the 6th and 3rd century B.C. in northern Italy (Gambacurta 1987; Towle et al. 2001), as of today no chemical analyses have been performed on the same typology, and data are only available for some opaque yellow beads from Bologna (Polla et al. 2011; Arletti et sl. 2010) and for opaque yellow decorations from several sites in northern Italy (Angelini et al. 2011; Arletti et al. 2010; Polla et al. 2011). As shown in Fig. 6.3.3, PbO contents are variable and the highest value is about 37 wt% for some opaque yellow decorations from Bologna dated to the Early Iron Age (Polla et al. 2011). Other opaque yellow decorations of Early Iron Age beads belonging to the Golasecca culture (Angelini et al. 2011) have a particular glass matrix composition without Na_2O and with PbO up to 17 wt%. The yellow bead from Villa has 10.71 wt% PbO content in the glass matrix and, in particular, a PbO/Na_2O ratio very similar to some samples from Bologna and Spina (Arletti et al. 2010) dated to the 6th-4th century B.C. This similarity is also found in the value of Sb_2O_3, which is 1.05 wt% in the Villa di Villa bead and 0.8–1.3 wt% in the samples from Bologna and Spina.

BSE images show a heterogeneous glass texture rich in Pb antimonates and SiO_2 crystals. The Pb antimonates are have a dimension of a few microns and are grouped in aggregates of 25-30 µm with irregular shapes. Silica inclusions have lamellar or rectangular morphologies 20 to 50 µm in size and sometimes are grouped in larger aggregates. As in sample VV-AB6, lamellar inclusions on the edges of the biggest grains show recrystallization of silica from the sand used as raw material. XRD characterization of the mineral phases on the whole object identified quartz, tridymite, cristobalite and bindheimite. Raman spectroscopy identified Pb antimonates as bindheimite phases ($Pb_2Sb_2O_7$).

As regards the distribution of silica phases, the µ-Raman data show that the bigger aggregates are characterized in the center by cristobalite and in the edges by lamellar crystals of tridymite plus cristobalite. As mentioned above, the presence of both cristobalite and tridymite is

indicative of the temperature reached during the melting process. The quartz identified by X-ray diffraction is not confirmed by Raman spectroscopy in the yellow glass, and is probably associated with the blue and white eyes.

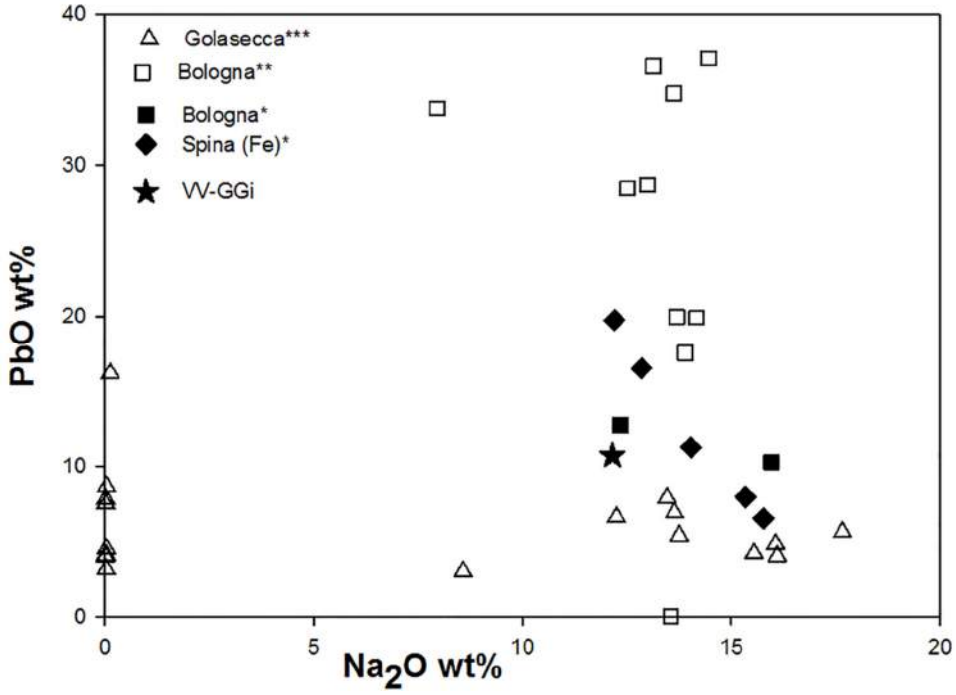

*Fig. 6.3.3: Na_2O vs PbO contents of yellow bead VV-GGi. Reference data are also reported and grouped according to age and provenance (Age in centuries: Empty= 8th-7th B.C.; Black=6th-4th B.C.; *Arletti et al. 2010; **Polla et al. 2011; ***Angelini et al. 2011).*

Rod fragment

The rod fragment with semicircular section has a transparent body (VV-FBT) decorated with yellow (VV-FBGi), blue (VV-FBB) and white (VV-FBBi) spirals. The four glasses are all *natron* based, with levels of MgO and K_2O < 1 wt% and in line with Cl_2O (0.77÷1.46 wt%) and SO_3 (0.14÷0.43 wt%). This is consistent with the composition of Early Roman glass production (Silvestri et al. 2008) and the estimated archaeological dating. MnO and FeO contents in samples VV-FBT, B and Bi range between 0.32 to 0.58 wt% and between 0.37 and 0.91 wt%, respectively. Values of MnO ≤ 0,3 wt% are due to impurities in the raw materials,

since at least 1 wt% of MnO is required to ensure glass is decolorized (Brems et al. 2012) and, in any case, a $MnO/(Fe_2O_3)_{TOT}$ ratio > 2 (Silvestri et al. 2008). As regards samples VV-FBT, B and Bi, the quantity of manganese is too high to come from sand alone, and too low to have been added deliberately. It may be due to both the sand and to the recycling of decolorized cullet, which was very common in the Roman period (Silvestri et al. 2008). The transparent yellow spiral, VV-FBGi, has a lower content of FeO (0.26 wt%) than the other 3 glasses analyzed, suggesting use of a purer sand. As there are no other coloring elements, the color may have been produced by an iron sulphide complex producing this shade in a reducing atmosphere (Jackson et al. 2006; Nenna et al. 1997; Schreurs and Brill 1984).

The blue spiral is colored by Fe (FeO = 0,91 wt%), probably in a bivalent oxidation state traces, and presents also traces of Cu (CuO = 0,09 wt%).

The white glass is colored and opacified by finely dispersed Ca antimonates in the glass matrix (Sb_2O_3 in the glass phase = 8,86 wt%, Tab. 2). The Ca-antimonate crystals have particularly small (1- 30 µm) irregular morphologies, apparently elongated and oriented like the bubbles. Micro Raman analysis on the Ca antimonates shows they are all composed by the orthorhombic phase $Ca_2Sb_2O_7$.

The identified types of coloring agents are typical of the glass production techniques used in the Early Roman Age, and consistent with the age of the find.

Melon bead

The glass phase of the blue melon bead VV-MB is made up of K_2O = 2.45 wt%, MgO = 1.01 wt% and CaO = 3.56 wt%. The Na content is associated with *natron* as flux (Na_2O = 13 wt%), although levels of K and Mg are slightly high. However, as the last 2 elements partially derive from the particular type of sand used (see below), we can assume that the glass phase is a LMG type.

The high content of both alumina (Al_2O_3 = 3.29 wt%) and K suggest the sand used was rich in feldspar minerals with traces of heavy metals, as shown by FeO (0.77 wt%) and TiO_2 (0.16 wt%) (Freestone et al. 2002). The blue color is due to high concentrations of Cu (CuO = 3.78 wt%), and traces of Sn (SnO_2 in the glass matrix = 0.11 wt%), and dispersed cassiterite inclusions suggest that Cu could derive from bronze.

The heterogeneous texture is typical of *faïence*, in which there are greater concentrations of crystalline inclusions (i.e., quartz, feldspar and metals) than glass matrix (Angelini et al. 2002). The melon bead of Villa di Villa does not preserve the glaze phase, except for a small weathered relict 120 µm thick. The glass phase in the core is well preserved and the texture is scarcely porous with bubbles up to 50 µm in diameter. The mineral grain sizes range between 30 and 150 µm, showing both round and rectangular shapes, so no accurate grinding and dimensional selection of the sand was carried out when producing the bead. XRD and SEM-EDS data show that the inclusions are mostly made up of quartz and by relict K-feldspars cassiterite, titanite and iron oxides.

Although coeval melon beads are largely attested in Italy (Tori et al. 2006), analytical data are only available for one turquoise melon bead from Mozia dated to the 6th-4th c B.C. (Arletti et al. 2012) and 4 blue melon beads from Tebtynis dated to the Late Roman Age (Bettineschi 2014, unpublished data). As regards glass composition, the melon bead from Villa di Villa is more similar to those from Tebtynis, which have comparable values of K_2O, Al_2O_3, CaO and CuO associated with traces of SnO_2. Conversely, the melon bead from Mozia has a typical *natron*–based composition (K_2O and MgO < 0.6 wt%), with fewer K- feldspar minerals, higher CaO and very low Cu in its sand composition.

CHAPTER 7

CONCLUSIONS

A combined approach, involving chemical, mineralogical and textural analyses, was carried on in the present research to study the evolution of the materials and technologies adopted in the production of vitreous material ornaments in Italy, during several chronological phases: from the Middle Bronze Age to the second Iron Age. The thesis involved the study of 112 different glass ornaments found in important archaeological sites: Padova and Villa di Villa (Veneto region, north east Italy) and Lipari and Salina islands (Aeolian archipelago, south Italy).

In particular, 130 glass fragments were sampled from the body and the decoration of the beads and underwent SEM-EDS and EPMA whereas non – invasive X-Ray Diffraction was performed on the beads. Some samples were also studied by means of Single Crystal X-Ray Diffraction and Micro – Raman Spectroscopy to identify crystalline inclusions dispersed in the glass phase.

§ Lipari and Salina §

The analyzed glasses from Lipari and Salina, dated from the Middle Bronze Age (MBA) to the Final Bronze Age (FBA), were obtained using two different fluxes: soda – rich plant ashes (HMG glasses) and mixed alkali plant ashes (LMHK glasses).

- The only bead dated to the MBA 1-2 is from Lipari Acropolis and has a HMG composition. Chemically, it is comparable to the coeval vitreous materials of central and south Italy, even though is brown colored and not blue as commonly attested in this phase. It was obtained with a particularly pure sand or quartzite and the coloring is probably due to an iron sulfide complex produced in a reducing atmosphere.

- The glasses dated to the MBA 3 are all from Salina – Villaggio di Portella and have HMG composition. They are blue colored and also a white glass from a bead fragment decoration is present.

Blue glasses

Most of the samples are colored by Co associated to Cu. In the analyzed blue samples from Salina, 3 different cobalt sources seems to be used:

1. two samples present cobalt associated to Ni, Zn, Fe and have high contents of Al and Mn typical of the Egyptian cobaltiferous alum salts;
2. four samples show cobalt associated to Sb and in two cases also to Pb similarly to some coeval *faïence* from central Italy (Santopadre et al. 2000; Angelini et al. 2005) and to a few Mycenaean *faïence/glassy faïence* from Crete and Psara (Tite et al. 2008a). However, the ratio amounts of the elements in these vitreous materials is not the same and the use of a different cobalt source cannot be excluded for the glasses from Salina;
3. one sample is characterized by rarely Cu-Pb-S inclusions in the glass phase possibly related to the use of a source of cobalt containing copper sulfides.

The different cobalt sources suggest therefore the use of different raw materials and, probable, provenance from different production centers.

Several blue samples present crystals of diopside and/or devitrite due to the devitrification that can occur in the glass between 750°C and 1200°C, allowing to evidence the glass furnace treatments (Lahlil et al. 2010).

Two blue beads from Salina have Fe as only chromophore element. In one case the Fe amount is very high and the glass phase is characterized by newly formed crystals very close to augite. Instead, the other one is homogeneous and with low Fe content. In these glasses the color is probably due to Fe in its bivalent oxidation state.

The blue glasses from Salina present in several cases bands with different chemical composition due to a heterogeneous distribution of the chromophore agent (Cu-Co or Fe) suggesting that first the beads were obtained by a heterogeneous mixing of a strongly colored glass with the colorless matrix.

White glasses

At Salina are not present white beads and the only white glass belong to a bead fragment decoration. It is colored and opacified by Ca antimonate crystals present in the *orthorombic* phase, $Ca_2Sb_2O_7$. The technology to produce this glass is probably due to *extra situ* crystallization with an intentional addition of synthesized $Ca_2Sb_2O_7$ crystals. Interestingly, it seems to be the early presence in Italy of Ca antimonates to obtain an opaque white glass, since this technology is not attested during the Bronze Age while is well known in the same period in Egypt (Shortland 2002), therefore it may suggests the Egyptian or Near Eastern provenance for this HMG white glass.

The HMG glasses are attested in Italy since the MBA1-2 and in that period were present only in south and central Italy. Widespread presence of HMG in the Italian peninsula starts only since the MBA3 – RBA. The presence of this glass type starting from south Italy suggests that they were probably treaded from the Near East as well as the HMG glasses from Salina.

- The only studied RBA bead is from Lipari Acropolis but, unfortunately, the glass is weathered and no information can be inferred on the production technology of this object.

- The beads dated to the FBA come mostly from Lipari Piazza Monfalcone cemetery and only three from the Lipari Acropolis. The three glasses from the Acropolis have a HMG composition. The glasses from the cemetery have mostly a LMHK composition even though a group of 15 samples are HMG glasses. Moreover, two glasses are obtained with a K – rich flux as a particular sub group (LMHK – K class) found at the moment mainly in the Frattesina productions and in one other glass from north Italy (Angelini et al. 2010).

  In this light, we can highlight three important evidences:

  1. the presence of soda – rich glasses during the FBA is particularly interesting since this composition is not attested in the Italian peninsula in this period but only in the Mediterranean islands (one samples comes from Sardinia, Angelini et al. 2012)

while is typical in the coeval Near East/Egyptian productions and therefore we can hypothesize an exotic provenance for these glasses;

2. the presence of LMHK glasses is coherent with the coeval production of the Italian peninsula, in particular of north Italy, and attest a circulation of these objects from north to south. Moreover, the presence at Lipari – Piazza Monfalcone cemetery of the K class subgroup associated to other LMHK glasses suggests that the two types probably travelled together and, therefore, that the LMHK – K class was typical of the Frattesina vitreous productions, even though the evidences are numerically scarce.
3. The presence in the grave 31 of the Lipari cemetery of both LMHK and HMG glass beads, testify that materials of different provenances were imported and used at the same time.

As regards the glass coloring in the FBA glasses from Lipari we can summarize as following.

Blue glasses

- The blue HMG glasses are all colored by low amount of copper and probably iron involuntary introduced through the sand used as source of silica. No any other minor element is associated to copper and no information can be inferred on the copper source but we can exclude the use of bronze as source of Cu, as verified the LMHK FBA beads (Angelini et al. 2004, 2010a; Towle et al. 2001; Santopadre and Verità 2000). Moreover, they present a homogeneous texture with rarely devetrification phases (e.g.: diopside, devitrite etc.) or residual inclusions rich in metal elements;
- the blue LMHK glasses are mostly colored by copper and only thirteen by cobalt associated to copper. The copper colored glasses have higher amounts of Cu with respect to the HMG ones and have a heterogeneous texture due to numerous crystals of tridymite. In particular, the lamellar crystals observed, testify a crystallization from the melt at high temperature (Artioli et al. 2008). Two different ores, Cu-Sb and Cu-Sn-Sb, seem to be used as raw material for the coloring agent. Interestingly,

in the copper colored glasses from Lipari, copper is never associated only to Sn as occur in the most coeval north Italian and European glasses (Angelini et al. 2004, 2010a; Brill 1999; Croutsch et al. 2011; Gratuze 1998; Santopadre et al. 2000; Séguier et al. 2010; Towle et al. 2001).

- The cobalt blue beads present cobalt associated to Cu, Ni, As and Sb. In the coeval glasses from north Italy (Angelini et al. 2004, 2010a; Brill 1999; Santopadre and Verità 2000; Towle et al. 2001) and Europe (Croutsch et al. 2011; Gratuze 1998; Seguiér et al. 2010; Venclová et al. 2011) cobalt is systematically associated to Cu and Ni and, in some glasses, with a good correlation between Ni and Co. We can therefore hypothesize the same cobalt sources even though not all the literature data have associated also As and Sb because of the volatility of these elements and because in some publications these elements are not measured.

  Similarly to the HMG Salina glasses, several LMHK blue glasses present bands with different chemical composition due to a heterogeneous distribution of the chromophore agent (Cu-Co or Cu) suggesting that first the beads were obtained by a heterogeneous mixing of a strongly colored glass with the colorless matrix.

Yellow glasses

No opaque yellow beads with Pb antimonates are attested at Lipari but only transparent yellow/brown glasses, even though this color is present only in 4 glasses. They show all homogeneous texture and HMG composition and the color is to ascribe to the iron sulfide complex obtained in a reducing atmosphere (Shreurs and Brill 1984). In one brown glass the darker shade is due also to the presence of significant amounts of Mn. Interestingly, the beads have different ages and provenance: two of them come from the Acropolis and are dated to the MBA 1-2 and to the FBA 2-3; two are from the grave 31 of the Piazza Monfalcone cemetery and are dated to FBA 1-2. No comparison are known in Italy for the MBA1-2 amber glasses, but only for one HMG amber glass dated to the MBA3-RBA and four LMG amber glasses dated to the FBA-EIA from Sardinia (Angelini et al. 2012).

Black glasses

Black color is present only in one annular bead dated to FBA 1-2. It is homogenous with a HMG composition. Interestingly, the Fe and S contents are slightly higher than in the yellow/brown glasses. In absence of any other chromophore element, is possible that the color is due to the Fe-S chromophore traditionally used to produce amber glass and which in sufficiently high concentrations appears black.

White glasses

As observed at Salina, no white beads are present at Lipari but white glasses are attested only as decoration in globular and barrel – shaped beads. They all are applied to LMHK glasses colored by copper and they are LMHK glasses.

Two opacifying technologies are attested, as identified in coeval north Italian LMHK glasses (Angelini et al. 2010a): (i) in the first one, the glass is opacified by the presence of SiO_2 crystals possibly added trough the sand used as raw materials. The SiO_2 inclusions are all of tridymite, indicating that all quartz reacted into tridymite, a transition that starts around 870°C. The passage between the blue body and the white decoration is marked suggesting the application of the eye to the cooled or partially cooled body. Most of the white glasses are opacified in this way; (ii) in the second one, which characterized 3 samples, the glasses are opacified by Ca silicates. Inside this group we can distinguish one sample characterized by amorphous Ca silicate crystals (close to wollastonite) with variable stoichiometry and finely dispersed in the glass phase, plus quartz and tridymite inclusions. In the other two samples we have euhedral crystals of wollastonite and the inclusions seems more isolated each other.

Considering the morphologies of the crystals and the high contents of Ca in the glass phase, we can hypothesizes that calcium was intentionally added to the glass batch and the nucleation of the Ca silicates occurred during the glass cooling. The passage from the blue body is not marked suggesting the application of the decoration on the not totally cooled body.

Interestingly, the glasses opacified trough Ca silicates are all spiral decorations applied to globular or barrel – shaped beads, while the glasses opacified trough tridymite are all eyes decorations applied to globular beads. It may be possible that the two

technologies were used for specific decoration typologies or that were produced into different production centers. However the analyses on the texture of the LMHK white glasses are still scarce and do not allow sure hypothesizes. Nevertheless, the available analyses of FBA LMHK glasses from Hauterive-Champréveyeres (Switzerland, Henderson 1993) support what observed at Lipari. In fact, even though the crystalline phases are not determined, in the Swiss glasses the white spiral decorations are obtained with Ca silicates while the eyes decorations are composed of SiO_2 inclusions. Similarly, the only analyzed white glass from Greece is an eyes decoration and show SiO_2 inclusions (Nikita and Henderson 2006).

The data show a large variability of colors and production techniques especially at Lipari. The presence of both LMHK and HMG glasses in the grave 31 of the Piazza Monfalcone cemetery is particularly interesting because highlight the important role of Lipari as trade center in which circulated materials coming both from North Italy and Near East/Egypt.

§ Piovego cemetery §

The archaeometric study of the glass beads from the Piovego cemetery can be considered the first, very representative, analyses on northeast Italian vitreous materials dated to the second Iron Age (second half of the 6th century-end of the 5th century B.C.).
The chemical data show that:

- all but one glasses are obtained using *natron* as flux and are classified as LMG glasses;
- only one sample is a HMG glass produced with soda rich plants ashes as flux as typical of the Italian glasses during the MBA3 – RBA, generally interpreted as imported Near Eastern, Aegean or Egyptian materials and also similar to the HMG glasses that still persist during the Early Iron Age;
- interestingly, no mixed alkali glasses are present in the analyzed Iron Age samples, even if LMHK glasses have been found, although rarely, in the Early Iron Age materials, specifically in some beads from Golasecca (9th century B.C., Angelini et al. 2011) and Bologna (8th century B.C., Polla et al. 2011). Therefore, we can considered completely

disused the mixed plant ashes as flux and *natron* seems to be essentially the only flux used in the Italian vitreous materials in this period. Actually, also the HMG glasses are extremely rare, only one sample at the Piovego cemetery is present;

- the Al and Fe contents are extremely variable as attested in the coeval European objects (Gratuze 2009). In some Piovego samples (in particular semitransparent or colorless glasses), Al and Fe contents are very low, testyfing the selection and use of "pure" sand depending on the colors of the objects. In fact, the Fe content is also related to the coloring agent especially in the dark blue and opaque brown/black beads.

Except for the flux, the other elements show a high chemical variability related both to the different raw materials used and to the wide range of production techniques used (especially for the glass color). This variability is not apparently related to the different chronological phases identified (Este phases), but rather, in some cases, to the beads typologies as well as, obviously, to the specific colors. This may suggest or a production based on different raw materials depending on the colors/typologies of the beads, or the presence of different production centers "specialized" in the use of specific raw materials and/or beads production.

Different colors are present at the Piovego cemetery: colorless/transparent (very pale blue and very pale green), transparent yellow, opaque/transparent brown, opaque/transparent blue, black and opaque white.

Blue glasses

The blue coloring is the predominant one; most of the beads are colored by Co associated to Cu while three beads are only Cu colored.

- The identified minor elements associated to Co are different testifying possible different cobalt sources. The seven small annular beads belong to the grave 127 and dated to the Este IIID1 phase (524-450 B.C.) all present the Cu, Ni, As and Sb association in the glass phase suggesting the use of the same raw material as cobalt source. In particular the raw material used for the cobalt source seems to contain copper sulfides particularly enriched in Ni, As, Sb and Ag as testified by the metal inclusions

present in the glass phase. Three of the seven small annular beads show also low amounts of Pb (PbO = 0.30÷0.50 wt%) in the glass phase and a lower NiO/As_2O_3 ratio. Interestingly, same characteristics were found in some vitreous materials from Poland dated to Hallstatt C period (Purowski et al. 2014).

- Two annular beads belong to the grave 121 and dated to the Este IIIC phase (525-450 B.C.) present the same inclusions of the small annular ones, even though they have in the glass phase only Cu, Sb and significant amounts of Pb (PbO = 2.81÷2.57 wt%) suggesting the use of a different poly-metallic ores.

  At present the cobalt source for these Piovego glasses has not been identified, but we can suppose a European origin since the Egyptian and Near East glasses have a different composition.
- The other cobalt colored glasses are different from the annular and small annular beads both for texture and chemical composition; the elements related to cobalt varying from sample to sample in particular as regards the amounts. The main identified association of elements are: (i) Cu, Ni, As, Sb, Zn; (ii) Cu, Sb, Pb, Zn; (iii) Cu, Sb. However some elements, such Sb or Pb, when presents in significant amounts are to be related not only to the coloring agent, but they are also due to voluntary adding or introduced by other raw materials. In particular, the Sb content could be related to the use decoloring agent or to the recycling of decolored glasses, while Pb could be add in some cases to improve the fluidity or the brilliance of the materials.
- The Cu coloring is poorly present and due to low amounts of copper (CuO = 0.90÷1.01 wt%) and in one case very low (CuO = 0.09 wt%). The texture is homogeneous without any inclusions. Among these, there is the only HMG glass found in the Piovego cemetery.

Yellow glasses

The transparent yellow glasses have a homogeneous texture and are obtained by a very pure sand or quartzite and colored by a iron sulfide complex as typical in the amber glasses. Interestingly, at the Piovego cemetery the opaque yellow coloring is not attested even though is very common in the coeval Italian glass materials.

Black glasses

A particular coloring technique was observed in one opaque black glass in which the iron amount is not particularly high (FeO = 0.98 wt%) and the very dark coloring an the opacity are due to the absorbent effects of the numerous small metal inclusions (Cu_2S) finely dispersed in the glass phase.

White glasses

The white glasses are present in the Piovego cemetery only related to the decorations of the beads (blue, black and brown bodies), while white beads are not attested. They are colored and opacified by Ca antimonates finely dispersed in the glass phase. In all but one of the samples both the orthorombic and hexagonal phases of the Ca antimonate were identified. The euhedral morphologies and small size of the crystals and the high Sb contents in the glass phase, allow us to hypothesize for these glasses an *in situ* crystallization by adding antimony oxides to a lime – rich glass batch. The decoration was applied to the cooled body of the bead as testify by the marked line between the two different colors.

Interestingly, three beads (PG-CM, PG-GOB8 and PG-GO5Bi) present very high amounts of Pb in the glass matrix (15÷25 wt%) as observed only is some Early Iron Age glasses from Lombardy (Angelini et al. 2011). However, these glasses have different colors (brown, blue and white) and texture and belong to different beads typologies, so it is no possible at present to identify a specific compositional class.

The texture observed in the Piovego glasses is particularly interesting. The annular and small annular beads and the 5 horned bead are characterized by a texture very close to a *glassy faience*, due to numerous residual quartz crystals and minor other minerals (e.g.: albite/anorthoclase, K-feldspar) or metals inclusions related to the coloring agent. A similar texture characterized also the opaque brown sample PG-CM and the opaque blue one PG-GOB8. In addiction the last two samples also present newly formed crystals such as wollastonite, diopside and augite.

The presence in these glasses of unreacted raw materials testify the use of melting temperature not particularly high and considering also the chemical variability testify a period of experimentation using different production techniques.

In conclusion, it is clear that this period is characterized by new experimentation using different raw materials (especially for the coloring agents) and receipts. This variability seems to suggest that the samples were produced in different production centers and/or geographic areas.
The data in the literature for this chronological phase (half of the 6th and the end of the 5th century B.C.) and for similar bead typologies are numerically scarce and do not allow to identify possible production areas of the ornaments.

§ Villa di Villa site §

The ornaments from Villa di Villa are different in both type and age, cover a time span ranging from the Final Bronze Age to the Late Roman Age, and show great variations in the glass production techniques involved.
All but one of the samples are LMG glasses produced using *natron* as flux. In addition to homogeneous glasses, there are also heterogeneous glasses and *faïence*.
Considering the different typologies of the ornaments we can summarize as following:

- although most of the samples are LMG glasses, one show a LMHK composition which is typical of northern Italian production in the Final Bronze Age;
- archaeometric analyses identified the ages of two annular beads belonging to the same SU. The LMHK one was produced in the Final Bronze Age, whereas the LMG one certainly dates back to the Iron Age;
- the 3 dark blue glass arm rings were colored using cobalt related to copper and traces of manganese, typical of other coeval European bracelets (Karwowski 2004; Dinard et al. 2009; Brezinova et al. 2013; Venclova 2009). Interestingly, all the arm rings from Villa di Villa have high Al content like other European bracelets of the same typology. Moreover, the 2 decorated bracelets were probably produced at the same site, whereas the chemical signature suggests a different origin for the undecorated one.

- Opaque white and yellow glasses are opacified and colored by calcium and lead antimonates, respectively;
- the color of the transparent yellow glass of the Late Roman rod is due to an iron sulfide complex obtained in a reducing atmosphere;
- the *faïence* melon bead is pale blue due to copper, which was introduced in the glass using bronze scraps. In addition, the mineralogical and chemical compositions of the bead are interestingly similar to some analyzed Egyptian melon beads dated to the Late Roman Age (Bettineschi 2014, unpublished data).

Archaeometric analysis on the ornaments from Villa di Villa provides a fascinating case study because it enables us to distinguish the different compositions and textures of each find, and to verify correlations between raw materials and glass production techniques during the great time span examined. Moreover, in the case of materials found in secondary deposition and/or dated to a wider time range, the analytical data provide more detailed information about the ages of the ornaments.

****

Final remarks

The study of a great number of vitreous material ornaments belonging to different periods between the Middle Bronze Age to the second Iron Age, allow us to highlight some aspects on the evolution of the flux and coloring/opacifying techniques used.

Flux

- The first HMG glasses appeared in the 19th century B.C. in the Near East and since the 16th-14th centuries B.C. they start to be massively produced also in Egypt and in the Eastern Mediterranean (Henderson 1989, 2000; Tite et al. 2003, 2008b). The presence of HMG glasses in Italy is attested since the MBA 1-2 in central and southern Italy (Angelini et al. 2003, 2005; Bellintani et al. 2006) and during the MBA 3 – RBA only

HMG vitreous materials, widespread in the entire Italian peninsula and in Sardinia, were present (Angelini et al. 2002, 2005, 2012; Bellintani et al. 2006).

Therefore, considering that HMG glasses:

i. first appeared in the Near East, Egypt and Eastern Mediterranean;
ii. in the Italian peninsula they are attested later and in a lower number;
iii. in the Italian peninsula their circulation started since the south/central Italy during the MBA1-2 when in the meantime LMHK vitreous materials were attested in north Italy (Angelini et al. 2005);

we can conclude that HMG Italian glasses were traded from the Near East or Egyptian/Mediterranean area as well as the HMG glasses from the Aeolian Islands.

- During the FBA both LMHK (plus LMHK-K class) and HMG glasses are present at Lipari while HMG glasses are not attested in the Italian peninsula in the same period. This testify the important role of Lipari as trade center in which circulated materials coming from both North Italy and Near East/Egypt.

- The few Italian EIA glasses analyzed to date are from central and north – west Italy (Angelini et al. 2011; Arletti et al. 2011; Polla et al. 2011) and have essentially LMG and HMG compositions, although they show a remarkable degree of compositional variation in the raw material used, especially in the coloring techniques, and the introduction of new recipes.

- During the second Iron Age HMG glasses seems to disappear from the Italian peninsula (but not in Sardinia, Angelini et al. 2012) with the exception of one glass at the Piovego cemetery. The LMG *natron* – based glasses are essentially the only glass type that circulated in Italy in this period, even though coeval data are still scarce at present making difficult to know the production areas of these glasses.

Coloring/opacifying

- The HMG glasses dated to the MBA are mostly blue Co – colored even though a few amber glasses and one white glass are present. Different cobalt sources were hypothesized suggesting the use of different raw materials and, probable, provenance from different production centers. Interestingly, no blue Cu – colored glasses are present in the HMG MBA glasses but only in the HMG FBA ones (see below).
  Interestingly, the only analyzed white glass seems to be the early presence in Italy of Ca antimonates to obtain an opaque white glass.

- Similarly, the FBA glasses are mainly blue colored due to (i) cobalt associated to copper or (ii) copper. Beside the blue glasses, also a few amber, black and white glasses are present.
  Cu – colored glasses show both LMHK and HMG composition but they differ both in the amounts of copper, that is very high to obtain the blue LMHK glasses and very low in the HMG ones, and in the texture, that is heterogeneous in the mixed alkali glasses and homogeneous in the soda – rich ones.
  Co – colored LMHK glasses seems to be colored using the same cobalt source comparable with that used for the coeval north Italian cobalt blue LMHK glasses.
  The analyzed white glasses are opacified not by Ca antimonates but by SiO_2 or Ca silicate inclsuions.

- During the Iron Age new components are used in glass production, including: (1) lead antimonate as yellow colorant; (2) Ca antimonate in the white opaque glass; (3) high amounts of Fe, and sometimes Mn, in the dark blue/black glass; (4) Pb in opaque dark blue/black glass objects which show numerous crystals and inclusions rich in heavy metal elements.
  The compositional variability of the glass is likely to be related both to different origins of the materials and to the glass recycling process.

REFERENCES

ANGELINI I. 2009, *Indagini archeometriche dei vaghi in vetro,* in *Il ripostiglio del Monte Cavanero di Chiusa di Pesio (Cuneo),* in M. VENTURINO GAMBARI, a cura di, *Il ripostiglio del Monte Cavanero di Chiusa di Pesio,* Alessandria, pp. 185-192.

ANGELINI I., ARTIOLI G., BELLINTANI P., DIELLA V., GEMMI M., POLLA A., ROSSI A. 2004, *Chemical analyses of Bronze Age glasses from Frattesina di Rovigo, Northern Italy,* in J. of Arch. Sci. 31, pp. 1175-1184.

ANGELINI I., ARTIOLI G., BELLINTANI P., DIELLA V., POLLA A., RECCHIA G., RESIDORI G. 2003, *Materiali vetrosi da Grotta Manaccora e Coppa Nevigata: inquadramento archeologico, archeometrico nell'ambito dell'età del Bronzo italiana*. In: Atti II Convegno Multidisciplinare "Il vetro in Italia meridionale e insulare", Napoli 5-7 dicembre 2001, Ed. Studio 22, Napoli.

ANGELINI I., ARTIOLI G., BELLINTANI P., DIELLA V., POLLA A., RESIDORI G. 2002, *Glass materials in the protohistory of North Italy: a first summary,* in C. D'Amico, edit by, *Atti del II Congresso Nazionale AIAr*, Bologna, pp. 581-595.

ANGELINI I., ARTIOLI G., BELLINTANI P., POLLA A. 2005, *Protohistoric vitreous materials of Italy: from early faience to final bronze age glasses*, in Proceedings 16e Congrès AIHV, London, pp. 32-36

ANGELINI I., CUPITÒ M., BETTINESCHI C., LEONARDI G., MOLIN G. 2010b, *Chronological investigation of prehistoric vitreous materials from Veneto by archaeometric analysis*, in *Riflessioni e Trasparenze. Diagnosi e conservazione di opere e manufatti vetrosi*, Atti del Congresso Nazionale di Archeometria, Ravenna 24-26 Febbraio 2009.

ANGELINI I., NICOLA C., ARTIOLI G. 2006, *Studio analitico dei materiali vetrosi,* in Venturino Gambari M., edit by, *Navigando lungo l'Eridano. La necropoli Golasecchiana di Morano Po,* Casale Monferrato, pp. 77-82.

ANGELINI I., NICOLA C., ARTIOLI G. 2012, *Materiali vetrosi protostorici della Sardegna: indagini archeometriche e confronto analitico con reperti coevi,* XLIV Riunione Scientifica dell'IIPP, La preistoria e la protostoria della Sardegna, pp. 1131-1150.

ANGELINI I., NICOLA C., ARTIOLI G., DEMARINIS R., RAPI M., UBOLDI M. 2011, *Chemical, Mineralogical and Textural Characterisation of Early Iron Age Vitreous Materials*

from the Golasecca Culture (Northern Italy), in TURBANTI-MEMMI I. (edit by), *Proceedings of the 37th International Symposium on Archaeometry*, Berlin, pp. 25-32.

ANGELINI I., POLLA A. ARTIOLI G. 2007, *I vaghi in vetro provenienti dalla necropoli di Ponte Nuovo (Gazzo Veronese): indagini archeometriche e confronto con materiali coevi*, Notizie Archeologiche Bergomensi, 13, 2005, pp. 141-152.

ANGELINI I., POLLA A., MOLIN G. 2010a, *Studio analitico dei vaghi in vetro provenienti dalla necropoli di Narde*, in SALZANI L., COLONNA C., edit by, *La fragilità dell'urna, I recenti scavi a Narde Necropoli di Frattesina (XII-IX sec. a. C.)*, Catalogo della mostra, Rovigo, pp. 105-134.

ARLETTI R., BERTONI E., VEZZALINI G., MENGOLI D. 2011a, *Glass beads from Villanovian excavations in Bologna (Italy): an archaeometrical investigation*, Euro J. Mineral., 23, pp. 959-968.

ARLETTI R., FERRARI D., VEZZALINI G. 2012, *Pre-Roman glass from Mozia (Sicily-Italy): the first archaeometrical data*, Journal of Archaeological Science, 39, pp. 3396-3401.

ARLETTI R., MAIORANO C., FERRARI D., VEZZALINI G., QUARTIERI S. 2010, *The first archaeometric data on polychrome Iron Age glass from sites located in northern Italy*, Journal of Archaeological Science, 37, pp. 703-712.

ARLETTI R., RIVI L., FERRARI D., VEZZALINI G. 2011b, *The Mediterranean Group II: analyses of vessels from Etruscan contexts in northern Italy*, Journal of Archaeological Science, 38, pp. 2094-2100.

ARTIOLI G., ANGELINI I. 2013, *Evolution of vitreous materials in Bronze Age Italy*, in Janssens K.H.A., a cura di, Modern Methods for Analysing Archaeological and Historical Glass

ARTIOLI G., ANGELINI I., POLLA A. 2008, *Crystals and phase transitions in protohistoric glass materials*, in Phase Transitions 81, pp. 233-252.

BARBET A. 1981, Les décors à matériaux mixtes à l'époque romaine, in Revue Archéologique, 1, pp. 67-70.

BELLINTANI P., ANGELINI I., ARTIOLI G., POLLA A. 2006, *Origini dei materiali vetrosi italiani: esotismi e localismi*, Atti IIPP XXXIX, III, pp. 1495-1531.

BERNABÒ BREA L. 1958, *La Sicilia prima dei Greci*, Milano 1958.

BERNABÒ BREA L., CAVALIER M. 1960, *Meligunìs Lipàra*, vol. I, *La stazione preistorica della contrada Diana e* la *necropoli protostorica di Lipari*, Palermo 1960.

BERNABÒ BREA L., CAVALIER M. 1968, *Meligunìs Lipàra*, vol. III, *Stazioni preistoriche delle isole Panarea, Salina e Stromboli*, Palermo 1968.

BERNABÒ BREA L., CAVALIER M. 1980, *Meligunìs Lipàra*, vol. IV, *L'acropoli di Lipari nella preistoria*, Palermo 1980.

BIAVATI A. AND VERITÀ M. 1989, *The glass from Frattesina, aglass making center in the late bronze age*, in "Rivistadella stazione sperimentale del vetro", 4, pp. 295-303.

BREMS D., DEGRYSE P., HASENDONCKS F., GIMENO D., SILVESTRI A., VASSILEVA E., LUYPAERS S., HONINGS J. 2012, *Western Mediterranean sand deposits as a raw material for Roman glass production*, 39, 9: 2897–2907.

BŘEZINOVÁ G., VENCLOVÁ N., FRÁNA J., FIKRLE M. 2013, *Early blue glass bracelets in the middle danube region*, SlovenSká archeológia lXi−1, pp. 107−142.

BRILL R.H. 1992, *Chemical analyses of some glasses from Frattesina*, Journal of Glass Studies 34, pp. 11-22.

CALZAVARA CAPUIS L., LEONARDI G.1979, *Padova, località S. Gregorio: necropoli paleo veneta del Piovego*, Rivista di Archeologia, 3, pp. 137-141.

CARANCINI G.L., CARDARELLI A., PACCIARELLI M., PERONI R. 1996, *L'Italia*, in *The Bronze Age in Europe and the Mediterranean*, Colloquia of XIII UISPP 11, Forlì 1996, Forlì, pp. 75-86.

CAVADA E. (edit by) 1986, *Archeologia a Mezzocorona. Documenti per la storia del popolamento rustico di età romana nell'area atesina.*

CHIECO BIANCHI A.M. 1987, *Dati preliminari su nuove tombe di III secolo da Este*, in VITALI D., edit by, *Celti ed Etruschi nell'Italia centro-settentrionale dal V sec. a.C. alla romanizzazione*, Atti del colloquio internazionale, Bologna, pp. 196-236.

CROUTSCH, C., TEGEL W., NICOLAS T., LOGEL T., PUTELAT O. 2011, *Les sites protohistoriques d'Erstein « Grasweg-PAE » (Alsace, Bas-Rhin) : L'occupation Rhin-Suisse-France-Orientale,* Revue Archéologique de l'Est, t. 60-2011, p. 83-146.

CUPITÒ M. 1996-1997, Thesis.

CUPITÒ M. 2013, *Tomba CUS Piovego 2*, in GAMBA M., GAMBACURTA G., RUTA SERAFINI M., TINÈ V., VERONESE F., edit by, *Venetkens. Viaggio nella terra dei Veneti antichi*, Catalogo della mostra, Padova 6 aprile -17 novembre 2013, pp. 353-355.

DAMIANI I., MAGGIANI A., PELLEGRINI E., SALTINI A.C., SERGES A. 1992, *L'età del ferro nel reggiano. I materiali delle collezioni dei civici Musei di Reggio Emilia*, Reggio Emilia.

DE MARINIS R.C., RAPI M. 2005, a cura di, *L'abitato etrusco del Forcello di Bagnolo San Vito (Mantova): le fasi arcaiche*, Firenze.

ESTE I – CHIECO BIANCHI A.M., CALZAVARA CAPUIS L. 1985, *Este. Le necropoli Casa di Ricovero, Casa Muletti Prosdocimi e Casa Alfonsi*, Roma.

ESTE II – CAPUIS L., CHIECO BIANCHI A.M. 2006, *Este. La necropoli di Villa Benvenuti*, Roma.

FORBES, R. J., 1957, *Glass*, Studies in Ancient Technology 5, E. J. Brill, Leiden.

FREESTONE I., PONTING M., M.J. HUGHES 2002, *The origins of Byzantine glass from Maroni Petrera, Cyprus*, Archaeometry, 44: 257–272.

FREESTONE, I.C., GORIN-ROSEN, Y. & HUGHES, M.J. 2000, *Primary glass from Israel and the production of glass in late antiquity and the early Islamic period*, Travaux de la Maison de l'Orient méditerranéen, 33:65–83.

GABROVEC S. 2006, a cura di, *Stična. Gomile starejše železne dobe (Grabhügel aus der ältern Eisenzeit). II/1 Katalog*, Ljubljana.

GAMBA M., GAMBACURTA G., RUTA SERAFINI A., TINÉ V., VERONESE F. 2013, edit by, *Venetkens. Viaggio nella terra dei Veneti antichi*, Catalogo della mostra, Venezia.

GAMBACURTA G. 1986, *Prime osservazioni sulle perle in pasta vitrea di età protostorica, provenienti da Altino (Ve)*, Aquileia Nostra LVII, coll. 165-184.

GAMBACURTA G. 1987, *Perle in pasta vitrea da Altino: proposta di una tipologia e analisi della distribuzione areale*, QAV III, pp. 192-214.

GRATUZE B., BILLAUD Y. 2003, *La circulation des perles en verre dans le basin méditerranéen de l'Âge du Bronze moyen jusqu'au Hallstatt*. In: Foy D., Nenna M.D. (edit by), *Echanges et commerce du verre dans le monde antique*. Actes du colloque de l'AFAV, Aix-en-Provence et Marseille, Montagnac 2003, pp. 11-16.

GRATUZE B., LORENZI F. 2006, *Les éléments de parure en verre du site de Lumaca (Age du Fer, Centuri, Haute-Corse) compositions et typo-chronologie, Bulletin de la Société préhistorique française*, T. 103, 2, pp. 379-384.

GRATUZE, B., LOUBOUTIN, C. AND BILLAUD, Y. 1998, *Les perles protohistoriques en verre du Mus´ees des Antiquit´es nationales*, Antiquit´es Nationales 30, pp. 11–24.

HAEVERNICK 1960, *Die Glasarmringe und Ringperlen der Mittel- und Spätlatènezeit auf dem europäischen Festland*, Rudolf Habelt Verlag, Bonn.

HARTMANN G., KAPPELB I., GROTEC K., ARNDTD B. 1997, *Chemistry and Technology of Prehistoric Glass from Lower Saxony and Hesse*, Journal of Archaeological Science, 24, pp. 547–559.

HENDERSON J. 1988, *Glass production and Bronze Age Europe*, Antiquity 62, pp. 435-451.

HENDERSON J. 1993, *Chemical analysis of the glass and faience from Hauterive-Champréveyeres, Switzerland*, in RychnerFaraggi A.M., a cura di, Hauterive-Champréveyeres, 9: Mètal et Parure au Bronze Final, Neuchatel, pp. 111-117.

HENDERSON J. 2000, *The Science and Archaeology of Materials*, London and New York.

HENDERSON, J. 1989, *The scientific analysis of ancient glass and its archaeological interpretation, Scientific analysis in archaeology and its interpretation* (ed. J. Henderson), Oxford University Committee on Archaeology Monograph no. 19, UCLA Institute of Archaeology Research Tools 5, Oxford: Oxbow Books, pp. 30–62.

HENDERSON, J. 2006, *Medieval and post-medieval glass finewares from Lincoln: An investigation of the relationships between technology, chemical compositions, typology and value*, The Archaeological Journal 162, pp. 256–322

HENDERSON, J., 1985, *The raw-materials of early glass production*, Oxford Journal of Archaeology, 4, 267–91.

JACKSON C., PRICE J., LEMKE C. 2006, *Glass production in the 1st century A.D.: insights into glass technology*, Annales 17th Congress AIHV, pp. 150-155.

JACKSON C.M., NICHOLSON P.T. 2010, *The provenience of some ingots from Uluburun shipwreck*, Journal of Archaeological Science 37, pp. 295-301.

KARWOWSKI, M. 2004, *Latènezeitlicher Glasringschmuck ausOstösterreich*, Mitteilungen der Prähistorischen Kommission, 55, Vienne.

LAHLIL S., BIRON I., COTTE M., SUSINI J., MENGURY N. 2010a, *Synthesis of calcium antimonate nano-crystals by the 18th dynasty Egyptian glassmakers*, Appl Phys A, 98, pp. 1–8.

LEONARDI G. (edit by) 2004, *La tomba bisoma di uomo e di cavallo nella necropoli del Piovego-Padova*, Venezia 2004.

LEONARDI G., BALISTA C., VANZETTI A. 1989, *Padova, via J. Corrado, impianti sportivi del C.U.S.: l'area archeologica del Piovego*, Quaderni di archeologia del Veneto, 5, pp. 40-63.

LEONARDI G., LOTTO D., BOARO S. 2009, *Le evidenze strutturali del santuario di Villa di Villa, in G. Cresci Marrone, M. Tirelli* (edit by), *ALTNOI. Il santuario altinate: strutture del sacro a confronto e i luoghi di culto lungo la via Annia*, Atti del Convegno (Venezia, 4-6 dicembre 2006), Studi e ricerche sulla Gallia Cisalpina, 23, Roma, pp. 213-227.

MACELLARI R. 2002, *Il sepolcreto etrusco nel terreno Arnoaldi di Bologna (550-350 a.C.)*, Bologna.

MANDRUZZATO L. (edit by) 2008, *Vetri antichi del museo archeologico nazionale di Aquileia. Ornamenti e oggettistica e vetro pre- e post-romano*, Comitato Nazionale Italiano per l'AIHV, Corpus delle Collezioni del vetro in Friuli Venezia Giulia, Vol. 4.

MANESSI P, NASCIMBENE A. 2003, *Montebelluna: sepolture preromane dalle necropoli di Santa Maria in Colle e Posmon*, Quaderni del Museo di Storia Naturale e Archeologia di Montebelluna, Montebelluna.

MARINETTI A. 2013, *Ciottoloni fluviali iscritti degli Andeti*, in GAMBA M., GAMBACURTA G., RUTA SERAFINI M., TINÈ V., VERONESE F., edit by, *Venetkens. Viaggio nella terra dei Veneti antichi*, Catalogo della mostra, Padova 6 aprile -17 novembre 2013, pp. 256-257.

MARTINELLI M.C. (edit by) 2005, *Il villaggio dell'età del Bronzo medio di Portella a Salina nelle Isole Eolie*, Firenze 2005.

MARTINELLI M.C., PROCELLI E., PACCIARELLI M., CAVALIER M. 2012, *L'età del Bronzo antica e media nella Sicilia orientale e nella zona dello Stretto di Messina*, in Atti XLI Riunione Scientifica I.I.P.P., 2006, pp. 157-184.

MOREY G.W. 1930, *J. Am. Ceram. Soc.* 13(10), pg. 683.

NENNA M.D., VICHY M., PICON M. 1997, *L'Atelier del Verrier de Lyon, duier siécle après J.-C., et l'origine del verres "romains"*, Revue d'Archeometrie, 21, pp. 81-87.

NENNA M.D., VICHY M., PICON M. 1997, *L'Atelier del Verrier de Lyon, duier siécle après J.-C., et l'origine del verres "romains"*, Revue d'Archeometrie, 21:81-87.

NENNA, M.D., 2000, *La route du verre: ateliers primaires et secondaires du second millénaire av. J.-C. au Moyen Age,* Travaux de la Maison de l'Orient Méditerranéen, Maison de l'Orient Méditerranéen-Jean Pouilloux, Lyon.

NIGHTINGALE G. 1996*, Perlen aus Glas un Fayence aus der mykenischen Nekropole Elateia-Alonaki,* in LORENZ T., EARTH G., LEHNER M., SCHWARZ G. (edit by), *Akten des 6. Österreichischen Archäologentages, Vienna,* pp. 141-148.

NIKITA K., HENDERSON J. 2006, *Glass analyses from Mycenaean Thebes and Elateia: compositional evidence for a Mycenaean glass industry,* Journal of Glass Studies 48, pp. 71-120.

PACCIARELLI M. 2001, *Dal villaggio alla città. La svolta protourbana del 1000 a.C. nell'Italia tirrenica,* in *Grandi Contesti e Problemi della Protostoria Italiana,* 3, Firenze.

PALTINERI S. 2013, *Tomba CUS-Piovego 97,* in GAMBA M., GAMBACURTA G., RUTA SERAFINI M., TINÈ V., VERONESE F., edit by, *Venetkens. Viaggio nella terra dei Veneti antichi,* Catalogo della mostra, Padova 6 aprile -17 novembre 2013, pp. 355-356.

PERONI R., CARANCINI L.G., IRDI CORETTI P., *Studi sulla cronologia delle civiltà di Este e Golasecca,* Sansoni, Firenze.

PIZZIRANI C. 2009*, Il sepolcreto etrusco della Galassina di Castelvetro (Modena),* Bologna.

POLLA A., ANGELINI I., ARTIOLI G., BELLINTANI P., DORE A. 2011, *Archaeometric Investigation of Early Iron Age Glasses from Bologna,* in TURBANTI-MEMMI I. (ed.), *Proceedings of the 37th International Symposium on Archaeometry,* Berlin, pp. 139-144.

REHREN T. 2001, Aspects of production of cobalt-blue glass in Egypt, Archaeometry 43,pp. 483-489.

ROFFIA E. 1993, *I vetri antichi delle Civiche raccolte archeologiche di Milano,* Milano.

SANTOPADRE P., VERITÀ, M. 2000, *Analyses of production technologies of Italian vitreous materials of the Bronze Age,* Journal of Glass Studies 42, pp. 25-40.

SAYRE, E.V. AND SMITH R.W. 1963, *The intentional use of antimony and manganese in ancient glasses,* in Proceedings of the VI International Congress on Glass. Advances in Glass Technology, pt. 2 (eds. F.R. Matson and G.E. Rindone), *History papers and discussion of the technical papers*, New York: Plenum Press, pp. 263–82.

SEAR F. 1975, *The earliest wall mosaics in Italy*, in *Papers of the British School at Rome*, 43, pp. 83-97.

SÉGUIER J.M., DELATTRE V.,GRATUZE B.,PEAKE R., VIAND A. *2010, Nécropoles protohistoriques de "La Haute Grève" à Gouaix , Seine-et-Marne (Les): contribution à l'étude des pratiques funéraires au cours de l'étape moyenne du Bronze final (XIIe-XIe siècle av. J.-C.) et au début du second âge du Fer (Ve-IIIe siè le av; J;-C.) dans le sud du Bassin parisien*, Edité par FERACF. Tours (Indre-et-Loire), 2010.

SHORTLAND A.J. 2000, Vitreous materials at Amarna, BAR S827, Oxford.

SHORTLAND A.J. 2002, *The use and origin of antimonate colorants in early Egyptian glass, Archaeometry* 44, pp. 517-530.

SHORTLAND A.J., EREMIN K. 2006, *The analysis of second millennium glass from Egypt and Mesopotamia*, part 1: new WDS analyses, Archaeometry 48, pp. 581-603.

SHORTLAND, A. J., 2004, *Evaporites of the Wadi Natrun: seasonal and annual variation and its implication for ancient exploitation*, Archaeometry, 46, 497–516.

SHORTLAND, A. J., SCHACHNER, L., FREESTONE, I. C., AND TITE, M. S., 2005, *Natron as a flux in the early vitreous materials industry: sources, beginnings and reasons for decline*, Journal of Archaeological Science, 33, 1–10.

SHORTLAND, A. J., SCHROEDER H. 2009, *Analysis of first millennium BC glass vessels and beads from the Pichvnari necropolis, Georgia*, Archaeometry 51, 6, pp. 947–965.

SHORTLOAND A.J., TITE M.S. 2000, *Raw materials of glass from Amarna and implications for the origins of Egyptian glass*, Archaeometry 42, pp. 141-151.

SILVESTRI A., MOLIN G., SALVIULO G. 2008, *The colourless glass of* Iulia Felix, Journal of Archaeological Science, 35, pp. 331-341.

SIMMONS J.H., UHLMANN D.R., BEALL G.H. 1981 (edit by), *Advances in Ceramics, Nucleation and Crystallization in Glasses*, vol. 4 (The American Ceramic Society, Ohio, 1981).

TARPINI R. 2007. *Braccialetti vitrei di tipo celtico dalla necropoli di Spina: inquadramento tipologico ed analisi dei contesti,* in *Il Vetro nell'Alto Adriatico*, Atti delle IX Giornate Nazionali di Studio (Ferrara, 13-14 dicembre 2003), AIHV Comitato Nazionale Italiano, pp. 9-18.

TECCHIATI U., ANGELINI I., ARTIOLI G., BELLINTANI P., POLLA A., 2006, *Vetri dal sito del Bronzo finale di Salorno – Cava Girardi (BZ)*, in *Materie prime e scambi nella protostoria*

Italiana, Atti della XXXIX Riunione Scientifica dell'Istituto Italiano di Preistoria e Protostoria, Firenze, Italy, 25-27 Novembre 2004, Vol III, pp 1627-1631.

TECCO-HVALA S., DULAR J, KOKUVAN E., 2004, *Zeleznodobne gomile na Magdalenski gori (Eisenzeitliche Grabhugel auf der Magdalenska Gora)*, Ljubljana.

TERŽAN B., LO SCHIAVO F., TRAMPUZ-OREL N. 1985, *Most na Soči II*, Ljubljana.

TITE M.S., SHORTLAND A.J. 2003, *Production Technology for Copper- and Cobalt-Blue Vitreous Materials from the New Kingdom Site of Amarna—A Reappraisal*, Archaeometry, 45, 2, pp. 285-312.

TITE M.S., SHORTLAND A.J., BOUQUILLON A., KACZMARCZYK A., VANDIVER P.B. 2008c, *Faience production in the Near East and the Indus Valley*, in *Production technology*, pp. 93107.

TITE M.S., SHORTLAND A.J., HATTON G., MANATIS Y., KAVOUSSANAKI D., PYRLI M., PANAGIOTAKI M. 2008a, *The scientific examination of Aegean Vitreous Materials - Problems and Potential*, in JACKSON C.M., WAGER E.C., edit by, *Vitreous Materials in the Late Bronze Age Aegean*, London, pp.103-125.

TITE M.S., SHORTLAND A.J., VANDIVER P.B. 2008b, *Raw materials and fabrication methods used in the production of faience*, in *Production technology*, pp. 37-56.

TITE M.S.,HATTON G.D.,SHORTLAND A.J.,MANIATIS Y., KAVOUSSANAKI D., PANAGIOTAKI M. 2005, *Raw materials used to produce Aegean Bronze Age glass and related vitreous materials*, in Annales de l'Association Internationale pour l'Histoire du Verre, London 2003, Nottingham, England: AIHV, pp .10–13.

TITE, M.S., SHORTLAND, A., MANIATIS, Y., KAVOUSSANAKI, D. AND HARRIS, S.A. 2006, *The composition of the soda-rich and mixed alkali plant ashes used in the production of glass*, Journal of Archaeological Science 33: 1284–92.

TORI L., CARLEVARO E., DELLA CASA P., PERNET L., SCHMIDT-SIKIMC B., VIETTI G. 2006, *La necropoli di Giubiasco (TI). Vol. II: Les tombes de La Tène finale et d'époque romaine, Zurich*, pg. 128.

TOWLE A., HENDERSON J. 2007, *The glass Bead Game: Archaeometric evidences for the existence of an Etruscan glass industry*, in *Etruscan Studies, 10.*

TOWLE A., HENDERSON J., BELLINTANI P., GAMBACURTA G. 2001, *Frattesina and Adria: report of scientific analyses of early glass from the Veneto*, Padusa NS XXXVII, pp. 7-68.

VELLANI S. 1996, *Per un corpus dei bracciali lateniani in vetro dell'Italia, in Il vetro dall'antichità all'età contemporanea*, Atti della I Giornata nazionale di studio (Venezia, 2 dicembre 1995), AIHV Comitato nazionale Italiano, pp. 17-23.

VELLANI S. 1997, *La Téne Glass Bracelets from Emilia Romagna*, in *The prehistory & history of glassmaking technology*, Annales du XIII Congrès de l'Association internationale pour l'histoire du verre (Paesi Bassi, 28 agosto – 1 settembre 1995), pp. 33-46.

VENCLOVÁ N. 1989, *La Parure celtique en verre en Europe centrale*, in Feugère M. (edit by). *Le Verre préromain en Europe Occidentale*, pp. 85-97.

VENCLOVÁ N., HULÍNSKÝ V., FRÁNA J, FIKRLE M. 2009, *Němčice a zpracování skla v laténské Evropě*, Archeologické rozhledy LXI, pp. 383-426.

VENCLOVÁ, N., HULÍNSKÝ V., HENDERSON, J, CHENERY, S., SULOVA, L. AND HLOZEK, J. 2011, *Late Bronze Age mixed-alkali glasses from Bohemia*, Archeologick´e rozhledyLXIII, pp. 559–85.

VITRI S., GAMBACURTA G., ANGELINI A., GIACOMELLO R., MICHELINI P., SANGHERO T., DE CECCOC., PASSERA L., *Polcenigo (PN), San Giovanni, località Sottocolle, "Necropoli di S. Floriano". Scavi 2006*, Notiziario della Soprintendenza per i Beni Archeologici del Friuli Venezia Giulia, 1, pp. 24-32.

WALTON M.S., SHORTLAND A., KIRK S., DEGRYSE P. 2009, *Evidence for the trade of Mesopotamian glass to Mycenaean Greece*, Journal of Archaeological Science 36, pp. 1496-1503.

ACKNOWLEDGMENT

It is a great pleasure to thank Prof. Gianmario Molin and Dr. Ivana Angelini for their scientific and thoughtful guidance during the doctoral years.
I wish to thank the Museo Archeologico di Lipari, Istituto Italiano di Preistoria and Protostoria and the Soprintendenza per I Beni Archeologici del Veneto to support and allow me to study and analyze the vitreous materials.
I am particularly grateful to Prof. Giovanni Leonardi and Prof. Michele Cupitò for allowing me to study the materials of the Villa di Villa site and of the Piovego cemetery and to support me in the writing of the archaeological contexts chapters.
I extend thanks to Paolo Bellintani (Soprintendenza per i Beni Librari Archivistici e Archeologici della Provincia Autonoma di Trento) for the collaboration in the archaeological study of the vitreous materials from Lipari and Salina.
Thanks to the Fondazione Ing. Aldo Gini to support my research at the Department of Scientific Research of the Metropolitan Museum of Art (New York City, NY).
I wish to thanks Stefano Castelli, Leonardo Tauro, Federico Zorzi and Raul Carampin of the Department of Geoscience of Padova University for their help and support during the analyses.
Thanks also to Agostino Rizzi of the Earth Science Department of Milano for his helps in the SEM-EDS analyses.
I am grateful to Prof. Fabrizio Nestola of the Geiscience Department of Padova University to help me in the analyses but, above all, for his support in my (numerous) difficult moments.
Particularly thanks to Dr. Marco Leona, Dr. Federico Carò, Dr. Adriana Rizzo and Dr. Silvia Centeno of the Department of Scientific Research of the Metropolitan Museum of Art for their help and support during my research activity at the Museum.

Thanks to my family (mamma, papà e Raffaele) for allowing me to do this Ph.D. and for all their love.

Giulia